



City Research Online

City, University of London Institutional Repository

Citation: Dhunput, A. (2009). Oil Transport in Piston Ring Assemblies. (Unpublished Doctoral thesis, City University London)

This is the accepted version of the paper.

This version of the publication may differ from the final published version.

Permanent repository link: <https://openaccess.city.ac.uk/id/eprint/11916/>

Link to published version:

Copyright: City Research Online aims to make research outputs of City, University of London available to a wider audience. Copyright and Moral Rights remain with the author(s) and/or copyright holders. URLs from City Research Online may be freely distributed and linked to.

Reuse: Copies of full items can be used for personal research or study, educational, or not-for-profit purposes without prior permission or charge. Provided that the authors, title and full bibliographic details are credited, a hyperlink and/or URL is given for the original metadata page and the content is not changed in any way.



**CITY UNIVERSITY
LONDON**

School of Engineering & Mathematical Sciences

**Oil Transport in Piston Ring
Assemblies**

Ashvin Dhunput (BEng)

Thesis submitted in partial fulfilment of the requirements for the degree of
Doctor of Philosophy

June 2009

“The fact that a little grease will enable almost any surface to slide for a time has tended doubtless to obscure the action of the revolving journal to maintain the oil between the surfaces at the point of pressure. And yet, although only now understood, it is this action that has alone rendered our machines and even our carriages possible.”

Osborne Reynolds, 1886

TABLE OF CONTENTS

TABLE OF CONTENTS	3
LIST OF FIGURES	6
LIST OF TABLES	12
ACKNOWLEDGEMENTS	13
DECLARATION	14
ABSTRACT	15
NOMENCLATURE	16
CHAPTER 1 INTRODUCTION	19
1.1 MOTIVATION	19
1.2 HISTORICAL BACKGROUND	21
1.3 OPERATING PRINCIPLE OF A PISTON RING	22
1.4 THE STRIBECK DIAGRAM.....	24
1.5 FUNDAMENTALS OF LUBRICANTS	27
1.5.1 Functions of a lubricant	27
1.6 LUBRICANT CHEMISTRY	28
1.6.1 Base stocks	29
1.6.2 Mineral oils.....	30
1.6.3 Synthetic oil.....	32
1.6.4 Additives.....	33
1.7 LUBRICANT AND EMISSIONS	36
1.7.1 Nitrogen oxides (no _x).....	39
1.7.2 Particulates.....	39
1.7.3 Hydrocarbons.....	40
1.8 THESIS OUTLINE.....	41
CHAPTER 2 LITERATURE REVIEW	43
2.1 INTRODUCTION	43
2.2 OIL FILM THICKNESS MEASUREMENT TECHNIQUES	43
2.2.1 Electrical Techniques	44

2.2.2 Acoustic Techniques.....	49
2.2.3 Optical Techniques	49
2.3 CAVITATION IN PISTON RING LUBRICATION	56
2.4 OIL FILM PRESSURE.....	61
2.5 PREVIOUS WORK	63
2.6 SUMMARY	65
CHAPTER 3 EXPERIMENTAL SYSTEMS & TECHNIQUES.....	66
3.1 INTRODUCTION	66
3.2 EXPERIMENTAL SET-UP: TEST RIG	66
3.3 TEST RIG INSTRUMENTATION	69
3.3.1 Capacitance Transducer.....	69
3.3.2 Friction Transducer.....	72
3.3.3 Laser Induced Fluorescence Technique	74
3.3.4 Pressure Transducer.....	88
3.3.5 Data Acquisition System for Test Rig.....	96
3.3.6 Shaft Encoder for Test Rig	96
3.4 OIL FILM VISUALISATION	96
3.4.1 Glass liner	97
3.4.2 CCD Imaging Technique for Test Rig	98
3.4.3 High Speed Digital Video Technique for Test Rig	100
3.5 ENGINE EXPERIMENT.....	102
3.5.1 Engine Characteristics	102
3.5.2 Engine Cylinder Head Pressure Transducer.....	104
3.5.3 Data Acquisition System and Shaft Encoder.....	104
3.5.4 Modified Engine Block and Optical Access.....	106
3.5.5 Modified Engine Block for Current Work	109
3.5.6 Oil Film Pressure Transducer.	112
3.5.7 High Speed Digital Video Technique for Engine.....	113
3.5.8 Piston Ring pack	115
3.6 SUMMARY OF EQUIPMENT AND TECHNIQUES	116
CHAPTER 4 CHARACTERISATION OF OIL FILM IN THE IDEALISED TEST-RIG	117

4.1	RESULTS: QUANTITATIVE MEASUREMENTS	117
4.1.1	Oil Film Thickness (Capacitance Method) Measurements	119
4.1.2	Friction measurement	121
4.1.3	Oil Film Pressure and LIF measurements	125
4.2	BASE FLUID RHEOLOGY CHARACTERISTICS OF MONOGRADE MARINE ENGINE OILS.....	132
4.2.1	Discussion of Lubricant Film Thickness Study Results.....	134
4.2.2	Discussion of Friction Measurement Results	146
4.2.3	Discussion of Oil Film Pressure Study Results	158
4.2.4	Discussion of LIF Results.....	170
4.3	SUMMARY	180
CHAPTER 5 VISUALISATION OF OIL FILM IN TEST-RIG AND DIESEL ENGINE		182
5.1	TEST RIG VISUALISATION.....	182
5.1.1	High Speed Video Imaging	182
5.1.2	Visualisation of Cavities and Oil Film Pressure Distribution	192
5.1.3	Load and Speed Tests	198
5.1.4	Cavitation in Monograde Marine Engine Oils	199
5.2	DIESEL ENGINE VISUALISATION	208
5.2.1	Oil Consumption Sources and Oil Transport Mechanisms in Piston-Rings Assemblies.....	208
5.2.2	High Speed video Imaging in Diesel Engine.....	212
5.2.3	Oil Film Pressure measurements in Diesel Engine	217
5.2.4	Visualisation Experiments: Cavitation inception	219
5.2.5	Oil Film Visualisation: Lower Window	225
5.3	SUMMARY	228
CHAPTER 6 CONCLUSIONS AND FUTURE WORK.....		229
6.1	CONCLUSIONS.....	229
6.2	FUTURE WORK	233
REFERENCE LIST		237
APPENDIX: THEORY OF FLUORESCENCE.....		247

LIST OF FIGURES

Figure 1.1: Schematic representation of piston ring assembly for an internal combustion engine	23
Figure 1.2: Stribeck diagram.....	24
Figure 1.3: (a) Surface roughness, (b) Variation of friction coefficient with film thickness (Hamrock <i>et al.</i> , 2004).....	26
Figure 1.4: a) straight paraffin, b) branch paraffin, c) naphthene, d) aromatic (Stachowiak and Batchelor, 2000)	31
Figure 1.5: Chronology of the development of lubricant additives (Liskiewicz <i>et al.</i> , 2008).....	33
Figure 1.6: Effects of temperature on viscosity (The Technical Committee of Petroleum Additive Manufacturers (ATC)).....	36
Figure 1.7: Main parameters affecting particulate formation	40
Figure 2.1 Hydrodynamic pressure profile and film shape with alternative cavitation models (Priest et al, 2000).....	58
Figure 2.2: Speed and load effect on effective piston ring width (Dellis, 2005)	62
Figure 3.1: Test rig (a) Schematic (b) Photographic overview	67
Figure 3.2: Schematic of test ring with capacitance probe	69
Figure 3.3: Calibration setup for capacitance probe	70
Figure 3.4: Calibration of capacitance probe	71
Figure 3.5: Capacitance output for dry lubrication	71
Figure 3.6: Friction transducer	72
Figure 3.7: Friction calibration setup	73
Figure 3.8: Calibration curve for friction transducer (a) hung weight (b) release weight	73
Figure 3.9: Jablonski diagram (Haugland, 1999).....	74
Figure 3.10: Excitation of a fluorophore at three different wavelengths	76
Figure 3.11 Fluorescence of fluid element.....	77
Figure 3.12: Schematic of laser induced fluorescence optical setup	79
Figure 3.13: Methods of calibration (Sanda <i>et al.</i> , 1993)	82
Figure 3.14: The static calibration micrometer	83

Figure 3.15: Specimen ring with groove (a) picture (b) drawing	86
Figure 3.16: Profile measurement around the area of laser path.....	87
Figure 3.17: Matching groove data against average LIF data.....	87
Figure 3.18: Calibration coefficient as a function of oil temperature	87
Figure 3.19: Pressure transducer mounting.....	89
Figure 3.20: Kulite pressure transducer with (a) screen (b) screen removed and filled with RTV	89
Figure 3.21: Pressure transducer measuring approach.....	91
Figure 3.22: In situ pressure calibration setup	93
Figure 3.23: (a) pressure reading (b) schematic of diaphragm gauge.....	94
Figure 3.24: Calibration curve for Entran pressure transducer	95
Figure 3.25: Metal to glass liner	97
Figure 3.26: Schematic of glass liner	98
Figure 3.27: Schematic of CCD imaging experimental setup.....	99
Figure 3.28: Schematic of high speed video camera experimental setup	100
Figure 3.29: Plint dynamometer coupled to engine	103
Figure 3.30: Power envelope for dynamometer, TE 46	103
Figure 3.31: AVL pressure transducer calibration curve	104
Figure 3.32: Oscilloscope trace for shaft encoder calibration.....	105
Figure 3.33: Signal processor box - input and output signals	106
Figure 3.34: Dimensions and positions of the quartz window slots	107
Figure 3.35: Quartz windows dimensions.....	108
Figure 3.36: Engine block	108
Figure 3.37: Details of pressure transducer holes	110
Figure 3.38: Seal plate for engine liner.....	110
Figure 3.39: Crack around middle pressure hole	111
Figure 3.40: Oil film pressure calibration setup.....	112
Figure 3.41: Kulite pressure transducer calibration curve	113
Figure 3.42: (a) Schematic of video imaging system (b) Engine visualisation set-up..	114
Figure 4.1: Liner movement.....	118
Figure 4.2: Specimen ring profile	118
Figure 4.3: Variation of oil film thickness with CA at different loads for oil 2A	119
Figure 4.4: Variation of oil film thickness with CA at different speeds for oil 2A	120

Figure 4.5: Possible lubricant regimes encountered during downstroke at 300 rpm with 1868 N/m.....	121
Figure 4.6: Relationship between oil film thickness and friction	123
Figure 4.7: Variation of friction with CA at different loads for oil 2A	123
Figure 4.8: Variation of friction with CA at different speeds for oil 2A	124
Figure 4.9: Variation of oil film pressure with CA at different loads for oil 2A.....	126
Figure 4.10: Variation of oil film pressure with CA at different speeds for oil 2A.....	127
Figure 4.11: Pressure measurements over 20 consecutive cycles for 500 rpm - 2841 N/m	128
Figure 4.12: Average pressure reading and error bars based on 20 cycles	128
Figure 4.13: Variation of LIF measurements with CA at different loads for oil 2A	129
Figure 4.14: Variation of LIF measurements with CA at different speeds for oil 2A ..	130
Figure 4.15: Downstroke and Upstroke LIF measurement.....	131
Figure 4.16: Oil film pressure and corresponding oil film thickness.....	132
Figure 4.17: Variation of oil film thickness with CA at different loads for oil 026A ..	134
Figure 4.18: Variation of oil film thickness with CA at different speeds for oil 026A	135
Figure 4.19: Variation of oil film thickness with CA at different loads for oil 001C...	136
Figure 4.20: Variation of oil film thickness with CA at different speeds for oil 001C	136
Figure 4.21: Variation of oil film thickness with CA at different loads for oil 004B...	137
Figure 4.22: Variation of oil film thickness with CA at different speeds for oil 004B	138
Figure 4.23: Variation of oil film thickness with CA at different loads for oil AW004	138
Figure 4.24: Variation of oil film thickness with CA at different speeds for oil AW004	139
Figure 4.25: Variation of oil film thickness with CA at different loads for oil 097A ..	140
Figure 4.26: Variation of oil film thickness with CA at different speeds for oil 097A	140
Figure 4.27: Variation of oil film thickness with CA at different loads for oil 001A ..	141
Figure 4.28: Variation of oil film thickness with CA at different speeds for oil 001A	142
Figure 4.29: Oil Film Thickness- Oil Comparison, Speed 600rpm – Load effect.....	143
Figure 4.30: Oil Film Thickness- Oil Comparison, Load 977 N/m – Speed effect	143
Figure 4.31: Oil film thickness- temperature effect, 600rpm - 2354 N/m.....	144
Figure 4.32: Oil film thickness (oil comparison) - temperature effect, 600 rpm – 2354 N	145

Figure 4.33: Relationship between temperature and viscosity.....	145
Figure 4.34: Variation of friction with CA at different loads for oil 026A	147
Figure 4.35: Variation of friction with CA at different speeds for oil 026A	147
Figure 4.36: Variation of friction with CA at different loads for oil 001C.....	148
Figure 4.37: Variation of friction with CA at different speeds for oil 001C	149
Figure 4.38: Variation of friction with CA at different loads for oil 004B.....	149
Figure 4.39: Variation of friction as with CA at different speeds for oil 004B	150
Figure 4.40: Variation of friction with CA at different loads for oil AW004.....	151
Figure 4.41: Variation of friction with CA at different speeds for oil AW004	151
Figure 4.42: Variation of friction with CA at different loads for oil 097A	152
Figure 4.43: Variation of friction with CA at different speeds for oil 097A	153
Figure 4.44: Variation of friction with CA at different loads for oil 001A	153
Figure 4.45: Variation of friction with CA at different speeds for oil 001A	154
Figure 4.46: Friction measurement -oil comparison, 977 N/m - speed effect	155
Figure 4.47: Friction measurement -oil comparison, 600 rpm – load effect.....	156
Figure 4.48: Friction measurements - temperature effect, 600rpm - 2354 N/m	157
Figure 4.49: Friction measurement (oil comparison) - temperature effect, 600 rpm – 2354 N	158
Figure 4.50: Variation of oil film pressure with CA at different loads for oil 026A....	160
Figure 4.51: Variation of oil film pressure with CA at different speeds for oil 026A..	160
Figure 4.52: Variation of oil film pressure with CA at different loads for oil 001C	161
Figure 4.53: Variation of oil film pressure with CA at different speeds for oil 001C..	162
Figure 4.54: Variation of oil film pressure with CA at different loads for oil 004B	162
Figure 4.55: Variation of oil film pressure with CA at different speeds for oil 004B..	163
Figure 4.56: Variation of oil film pressure with CA at different loads for oil AW004	164
Figure 4.57: Variation of oil film pressure with CA at different speeds for oil AW004	164
Figure 4.58: Variation of oil film pressure with CA at different loads for oil 097A....	165
Figure 4.59: Variation of oil film pressure with CA at different speeds for oil 097A..	166
Figure 4.60: Variation of oil film pressure with CA at different loads for oil 001A	166
Figure 4.61: Variation of oil film pressure with CA at different speeds for oil 001A..	167
Figure 4.62: Oil film pressure - oil comparison, 977N/m - speed effect	168
Figure 4.63: Oil film pressure - oil comparison, 600 rpm - load effect.....	168

Figure 4.64: Oil film pressure - temperature effect, 600rpm - 2354 N/m.....	169
Figure 4.65: Oil film pressure (oil comparison) - temperature effect, at 600 rpm – 2354 N	170
Figure 4.66: Variation of LIF measurement with CA at different loads for oil 026A..	172
Figure 4.67: Variation of LIF measurement with CA at different speeds for oil 026A	172
Figure 4.68: Variation of LIF measurement with CA at different loads for oil 001C ..	173
Figure 4.69: Variation of LIF measurement with CA at different speeds for oil 001C	174
Figure 4.70: Variation of LIF measurement with CA at different loads for oil 004B ..	174
Figure 4.71: Variation of LIF measurement with CA at different speeds for oil 004B	175
Figure 4.72: Variation of LIF measurement with CA at different loads for oil AW004	176
Figure 4.73: Variation of LIF measurement with CA at different speeds for oil AW004	176
Figure 4.74: Variation of LIF measurement with CA at different loads for oil 097A..	177
Figure 4.75: Variation of LIF measurement with CA at different speeds for oil 097A	178
Figure 4.76: Variation of LIF measurement with CA at different loads for oil 001A..	178
Figure 4.77: Variation of LIF measurement with CA at different speeds for oil 001A	179
Figure 4.78: LIF measurements - temperature effect, 600rpm - 2354 N/m.....	180
Figure 5.1: Viewing window for high speed video imaging in the idealised test rig ...	183
Figure 5.2: High speed video photographs of oil film ruptures at 300 rpm and 977 N/m	189
Figure 5.3: Development of cavities as they appear on the surface on the ring	191
Figure 5.4: Development of internal cavities and corresponding pressure measurements at 300 rpm.....	194
Figure 5.5: Still imaging at random cycles	195
Figure 5.6: LIF measurements over 20 cycles at 300 rpm.....	196
Figure 5.7: Laser beam path with respect to string cavities at random cycles.....	197
Figure 5.8: Initiation of fern cavities for different loads and speeds	198
Figure 5.9: The number of string cavities per mm at mid-stroke.....	199
Figure 5.10: High speed video images of film rupture for oil 001A	202
Figure 5.11: Fern shape number and size for marine oils at 600rpm.....	204
Figure 5.12: Development of cavitation strings along the stroke at 600 rpm	204
Figure 5.13: Temperature effect on oil AW004.....	205

Figure 5.14: Temperature effect on oil 001A.....	206
Figure 5.15: Temperature effect on oil 097A.....	207
Figure 5.16: Number of string cavities per mm at mid-stroke for marine oils	207
Figure 5.17:Schematic of oil consumption sources (Yilmaz <i>et al.</i> , 2004).....	209
Figure 5.18: High speed video imaging window for diesel engine.....	212
Figure 5.19: Cycle oil distribution around piston-rings and land at 600 rpm	216
Figure 5.20: Cylinder and oil film pressure distribution in engine	218
Figure 5.21: Oil film visualisation for compression rings	223
Figure 5.22: Possible cavitation pattern and hydrodynamic pressure in diesel engine.	224
Figure 5.23: Oil film visualisation on lower window	225
Figure 5.24: Oil mist moving towards combustion chamber in the power stroke	226
Figure 5.25: String cavities(Dellis, 2005)	227
Figure 5.26: Image of first compression ring when piston stationary.....	227

LIST OF TABLES

Table 1.1: European emission standards for passenger cars (g/km)	38
Table 2.1: Oil Film Thickness Measurement using Electrical Method.	48
Table 2.2: Oil Film Thickness Measurements using Optical Methods.....	55
Table 3.1: Results for Calibration factors	88
Table 3.2: Specifications of Entran and Kulite pressure transducers.....	92
Table 3.3: Lister-Petter engine characteristics	102
Table 3.4: Piston ring pack.....	115
Table 4.1: Tested oil properties.....	118
Table 4.2: Ring and liner surface characteristics	118
Table 4.3: Properties of tested marine oils.....	133

ACKNOWLEDGEMENTS

Firstly, I would like to thank Professor Constantine (Dinos) Arcoumanis as my main supervisor for his continuous professional and priceless support during the time towards completion of my PhD. Furthermore I am very grateful to him for not only giving me an opportunity to pursue this research work but also found the funding to make this project richer in experiences. I would also like to express my gratitude to Dr Jamshid Nouri, my co-supervisor, and Dr Youyou Yan for the continuous help and the helpful discussions over the years. Also I would like to thank Castrol/BP/ BP Marine and, in particular, to Mr Hugh Preston, Dr Tabitha Rawlinson, Dr Samir Chachine and Mrs Tracey Veitch for some technical and financial support towards the project.

Special thanks to Mr Tom Flemming, Mr J. Kenny, Mr Ian Wright, Mr Jim Ford and Mr Jim Hooker for providing technical assistance, re-installing, modifying and repairing the test rig and where needed as well as the Lister-Petter engine. I would also like to thank my colleagues at City University, Dr Talal Ous, Mr Lucas Liverani, Mr Andrea Marchi, Dr Nikos Mitroglou, Dr Kevin Wang, Mr M. Chester, Mr Oliver Pierce and Mr Diego Guerrato.

Finally, I would like to express my special thanks to all members of my family. This thesis would not have been completed without their unconditional support. I am very grateful to my father, mother, brothers (Vischal and Sandip) and fiancée Kiran for their continuous encouragement and support.

London, June 2009

DECLARATION

I hereby declare that the presented work in this thesis is my own or was developed in a joint effort with other members of the research group as it is stated and referenced in the text accordingly!

I grant powers of discretion to the University Librarian to allow this thesis to be copied in whole or in part without further reference to me. This permission covers only single copies made for study purposes, subject to normal conditions of acknowledgement.

London

(Ashvin Dhunput)

ABSTRACT

The interface between the piston, piston-rings and the cylinder liner represents one of the most hostile environments the crankcase lubricant experiences in reciprocating engines. The role of piston rings is also becoming more complex in line with the increasing requirements for lower oil consumption and friction. A test rig has been developed to simulate under idealised conditions the lubrication action between the piston-ring and the cylinder-liner in reciprocating engines. This approach attempts to separate the tribological conditions from some of the fundamental and unsteady conditions occurring in production engine piston assemblies such as lubricant starvation, ring and piston dynamics, thermal and elastic deformations and blow by, thus allowing the lubricant film characteristics to be examined in isolation. The current work proposes a methodology in assessing the rheological behaviour of various base oils and their additive chemistry with a view to establishing the likely field performance in formulated lubricating oil. The experiment comprised of testing different types of engine oils where the lubricant film thickness, oil film pressure and friction were simultaneously measured throughout the stroke as a function of speed, load and temperature. Furthermore, laser induced fluorescence (LIF) was used to identify the onset of cavitation occurring in the diverging part of the lubricant film between the piston ring specimen and the liner wall. Recognition that lubricant films under certain condition may cavitate opens up a new area for research, focusing on possible links between cavitation, oil consumption, friction and wear. Oil flow visualisation in the test rig using a high speed video camera allowed observation of cavitation in the diverging part of the ring through an optical liner. The high recording framing rates of the camera have permitted the initiation, development and disintegration of the cavities throughout the stroke to be revealed. An attempt was made to extend the oil film visualisation to a motored diesel engine, with parts of the liner cut and fitted with quartz windows, to confirm the presence of cavitation in the piston-rings interface. Moreover the identification of sub-atmospheric pressure in the rings provided additional support to the visualisation of cavitation found in the engine, albeit of much inferior resolution to that of the idealised piston-ring assembly.

NOMENCLATURE

ABBREVIATIONS

2-D	Two-dimensional
3-D	Three-dimensional
A/D	Analogue to digital
AFR	Air to fuel ratio
BDC	Bottom dead centre
CCD	Charge coupled device
CF	High magnification lenses for CCD camera
CI	Compression ignition
CO/CO₂	Carbon monoxide/dioxide
DAQ	Data acquisition
DELIF	Dual Emission Laser Induced Fluorescence
DI	Direct injection
DISI	Direct injection spark ignition
DWF	Dual wavelength fluorescence
EGR	Exhaust gas recirculation
EHL	Elasto-hydrodynamic lubrication
GDI	Gasoline direct injection
HC	Hydro carbons
IDI	Indirect injection
LED	Light emitting diode
LIF	Laser induced fluorescence
MOFT	Minimum oil film thickness
NO_x	Nitrogen oxides
OCR	Oil control ring
OFT	Oil film thickness
PM	Particulate matter
PMT	Photomultiplier tube
ppm	Parts per million
ppr	Pulses per revolution
Psia	Pounds per square inch absolute
RMS	Root mean square
SI	Spark ignition
TDC	Top dead centre
TML	Transducer Measurement Limit
TTL	Transistor-transistor logic
UV	Ultraviolet

ROMAN SYMBOLS

A_{MAX}	Fibre acceptance angle
$ATDC$	After top dead centre
b	Ring width
B	Bearing length
CA	Crank angle
d_{ns}	Number of molecules
F	Friction force
g	gravity acceleration
h_{ex}	Excitation energy
h	Path length
$HTHS$	High temperature high shear viscosity
I_a	Intensity of absorbed light
I_o	Intensity
k	constant
m_h	Mass applied at the weight hanging point
NA	Numerical aperture
n	Refractive index
n_s	Molecular density
P	Oil film pressure
P_{MAX}	Maximum pressure at combustion chamber
P_{back}	Back pressure, pressure at the diverging wedge of ring
P_{comp}	Combustion chamber pressure at the converging wedge of the ring
P_{atm}	Atmospheric pressure
P_{vapour}	Vapour pressure of working liquid
P_{VL}	Spectral fluorescence power yield
R_a	Average roughness
R_q	RMS roughness
R_{crank}	Crank radius
S^*	Excited electronic singlet-state energy
S_p	Relaxed singlet excited state
S_o	Ground state
T	Temperature
U	Axial piston velocity
v_{ex}	Wavelength of excitation
V	Sample volume
VI	Viscosity index
$W(\theta)$	Load acting on the ring
x	Molar concentration of fluorescing species

GREEK SYMBOLS

ϵ	Molar absorptivity
λ	Beam wavelength
ν	Kinematic viscosity
ν_{40}	Kinematic viscosity at 40°C

ν_{100}	Kinematic viscosity at 100°C
ρ	Lubricant density
σ	Standard deviation
σ_{κ}	Standard deviation for K_{mean}
Φ_A	Radiant power of absorbed energy
Φ_F	Fluorescence efficiency
Φ_L	Quantum yield of fluorescence
$\omega(\theta)$	crank angular velocity

Chapter 1

INTRODUCTION

1.1 MOTIVATION

The interface between the piston, piston-rings and the cylinder liner represents one of the most hostile environments the crankcase lubricant experiences in reciprocating engines. The role of piston rings is also becoming more complex and stringent in line with the recent requirements for lower oil consumption and friction. At the same time the importance of piston rings is increasing in terms of engine performance, durability and wear. On the other hand, piston-ring lubrication in reciprocating engines is becoming a topic of attention as regulations of fuel consumption and exhaust emissions become more stringent. The higher the engine friction, the more fuel must be burnt to achieve the same brake power output. When an oil film is too thin, surface interaction can lead to wear. On the other hand, thicker films may lead to greater oil consumption, which is a direct contributor to exhaust hydrocarbon and particulate emissions.

As mentioned by Wakuri *et al.* (1995) an effective way to accomplish this is to reduce the piston-liner friction losses as the overall piston assembly is a substantial contributor to friction losses in the engine. The exact proportion depends upon the type of engine and operating conditions, but it has been estimated that typical figures lie in the range of 20-60 % (Dowson 1992; Jeng 1992; Priest and Dowson 1999; Taylor 1992, 1998), particularly at the interfaces between the liner and the piston rings and skirt. Most of the mechanical friction losses in the internal combustion engine are generated on lubricated surfaces around the piston ring and skirt (Harigaya *et al.*, 1996). In order for a vehicle to maximize fuel efficiency, mechanical losses in the engine must be reduced to a minimum; these include oil film resistance between moving parts. Factors that affect these lubrication characteristics in the piston ring are the oil film thickness and the oil

viscosity between the piston ring and the cylinder liner. Higher viscosity oils provide adequate wear protection but create increased resistance to movement and high frictional losses. Lower viscosity oils, on the other hand, reduce frictional losses and thus increase fuel efficiency. However, lower viscosity oils exhibit have an increased volatility which consequently increases hydrocarbon emissions. In the light of current and future emissions legislation, more research is needed to explore any possibilities for further reduction of engine friction and oil consumption.

In the conjunction between the piston ring and cylinder liner, similarly to other engineering applications such as journal bearing, hydraulic pump devices, high pressure nozzle injectors and naval impellers, one encounters two-phase fluid flows where the occurrence of gas or vapour bubbles representing the second phase in the flow can have a considerable influence on the liquid flow itself. This formation of gas or vapour bubbles is known as cavitation. This development of a two-phase mixture of gas/vapour and liquid occurs at the point where the local pressure of the liquid drops below a threshold value, a value usually considered equal to the vapour pressure. Cavitation has long been recognised to degrade performances in most engineering applications and this phenomenon is definitely not desirable in piston-ring assemblies. The formation of gas cavities in the lubricant film between a piston-ring and cylinder liner, influences the shape of the hydrodynamic pressure profile in the entrainment direction and, as a result, this has an effect on the load-carrying capacity of the interface, which is the integral of the pressure distribution, the lubricant film thickness, the friction force and the lubricant flow rate, as discussed by Priest *et al.*(2000). From an engineer's point of view, it is desirable to identify, understand, predict and control the physical mechanisms leading to cavitation inception. In the open literature, many workers have focused their attention towards theoretical modelling, analytical/numerical prediction of cavitation in piston rings and the numerous published papers have provided limited consensus on the nature of cavitation in the piston ring/cylinder wall interface. This is perhaps due to the lack of detailed experimental data to validate these predictive models. Therefore, it is imperative that future advancements must be based upon collective theoretical and experimental approaches to this problem. Experimentally, there may be few ways of studying cavitation but direct observation remains the most satisfactory method (Swales, 1974).

1.2 HISTORICAL BACKGROUND

A piston ring is defined by Webster's Dictionary as "*A springy split metal ring for sealing the gap between a piston and the cylinder wall.*" That is a very good description of exactly what a piston ring looks like; how a ring performs and its function is much more important. The modern form of piston-ring assemblies owes much to its development to the era of steam engines rather than to internal combustion engines and its development to the stage of achieving a satisfactory seal has a long history. These seals, leather discs or rings, were probably used in hydraulic devices such as water-pumps, where they were found to be adequate for this kind of operation. In 1650 flax or hemp were filled in a circumferential groove of a piston which acted as a seal in the famous demonstration of atmospheric pressure by Ottonis de Guericke, Burgomaster of Magdeburg. The seal was sufficient to hold a pressure difference when air was drawn out of the cylinder and thus overcome the pulling force of over twenty men. In 1667 Robert Boyle constructed a comparable mechanism which used leather seals on the piston. In the latter part of the seventeen century efforts were made in developing devices driven by the explosion of gunpowder within cylinders, or by subsequent condensation of the products of combustion, but they were very unproductive. It has been speculated that the unsuccessful attempts were due to insufficient sealing of the piston in such machines (Dowson, 1979).

During the early eighteen century the thermal efficiency in steam engines was still below one percent and one of its major problems was the leakage of steam past the piston. At first, those engines used as a sealing material rope or hemp (Dowson, 1979). Ramsbottom (1854, 1855) and Miller (1862) were among the pioneers to investigate the behaviour of the piston rings in steam engines. Ramsbottom, in 1854, constructed a single-piece, metallic piston ring. The free diameter of the ring was 10 per cent larger than the diameter of the cylinder bore. When fitted into a groove in a piston, the ring was pressed against the cylinder bore by its own elasticity and found that this oversize diameter was quite adequate to keep the rings steam tight. Previous piston rings had consisted of multiple pieces and used springs to provide an adequate sealing force against the cylinder bore. Miller, in 1862, introduced a modification to the Ramsbottom ring; this modification consisted of allowing the steam pressure to act on the backside of the ring, hence providing a higher sealing force. This new solution enabled the use of

more flexible rings, which conformed better to the cylinder bore circumference (Priest and Taylor, 2000).

1.3 OPERATING PRINCIPLE OF A PISTON RING

The piston assembly plays a vital role in the efficient operation of the internal combustion engine. The principal function of the piston rings is to form a dynamic seal, a schematic diagram of which is depicted in Figure 1.1, between the working fluid in the combustion chamber and the crankcase of the engine. The goal is to prevent combustion gases from passing downwards into the crankcase and oil from passing upwards into the combustion chamber. During the compression and power strokes, the compression ring seals the combustion gases and prevents blow-by. Dowson (1979) showed that although blow-by is not completely eliminated, it is kept to an acceptable level. If the sealing action is poor, pressure in the combustion chamber will be reduced during the compression, combustion and expansion stages of the engine cycle, thus leading to a reduction in power output and efficiency and a rapid deterioration of the lubricant in the crankcase. In a combustion process a large amount of heat is produced and most of it is conducted and convected into piston. The secondary role of the piston ring pack is to dissipate this thermal energy from the piston to the adjacent component to the cylinder wall and from there into the engine coolant. The final function of the piston ring pack takes place during the compression and exhaust strokes where the cylinder walls are lubricated with oil thrown off from the connecting rod bearings; any excess oil is wiped off by the piston rings. Not only does the oil ring have the responsibility of wiping the excess oil off the cylinder walls, but this function is also shared by all the rings, leaving a fine layer of oil on the wall to provide lubrication for the following ring.

Modern pistons employ three to four rings and can be classified as follows:

- (a) Top compression ring; it is located in the first groove and has the primary function, as mentioned above, of providing a seal. It is also the means by which heat is transferred from the piston to the liner, the wall of the cylinder.
- (b) Second or intermediate ring; this ring has a dual purpose. It assists the top compression ring in sealing and heat transfer. The ring is also used in oil control by shearing the layer of the oil left by the oil ring so that the top compression ring has enough lubrication.

- (c) Oil control ring; it is there just to control the oil that is splashed onto the wall of the cylinder from the connecting rod bearing throw off. The rings scrape the cylinder walls returning the oil back to the crankcase. Oil control rings can let oil pass between the face of the ring and the cylinder, pass through the ring gap or pass around behind the ring.

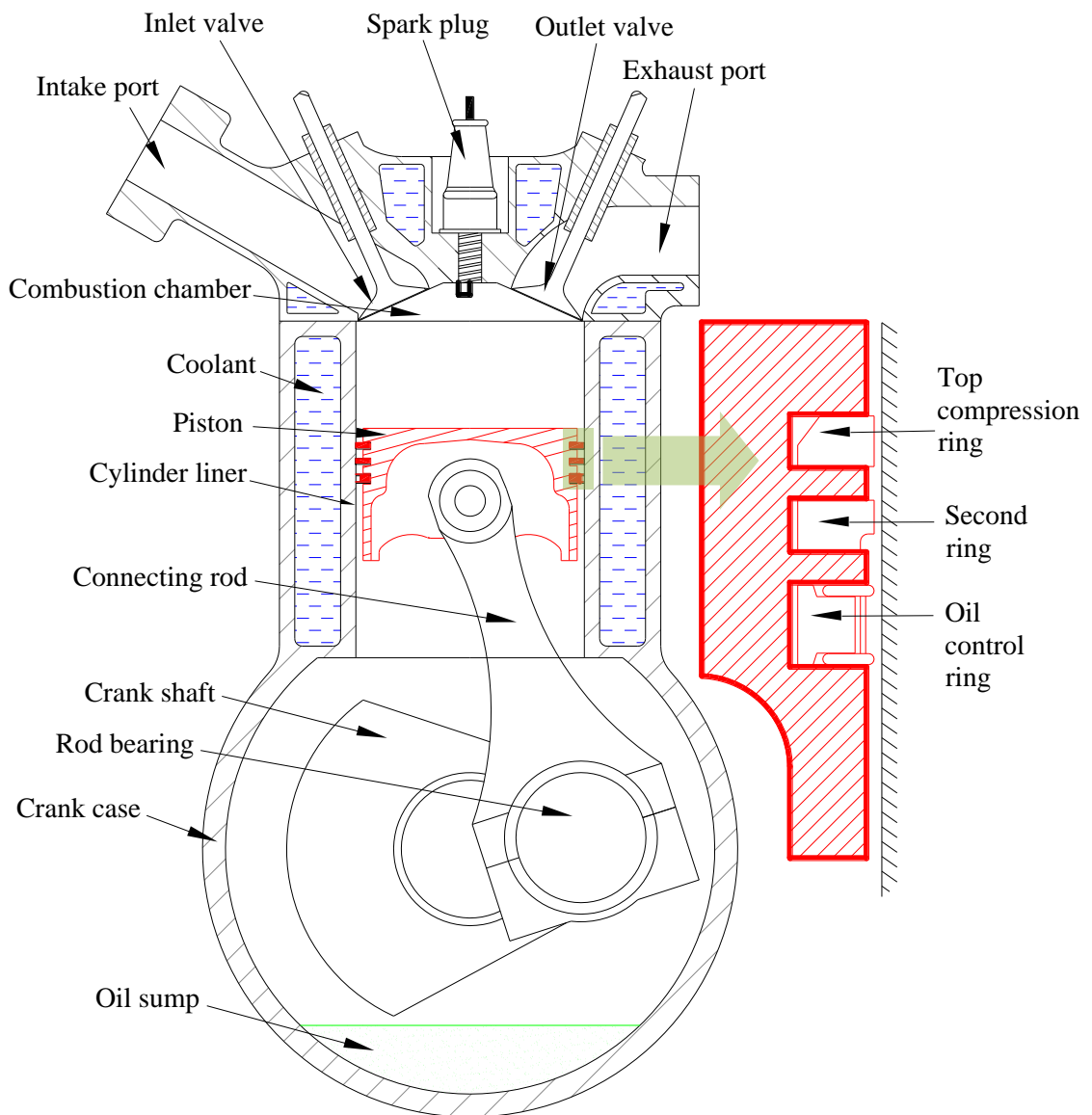


Figure 1.1: Schematic representation of piston ring assembly for an internal combustion engine

1.4 THE STRIBECK DIAGRAM

The Stribeck diagram or otherwise known as Reynolds-Sommerfeld curve (Meyer, 1998) illustrated in Figure 1.2, is frequently used as a tool to analyse the lubrication and wear performance. The concept has initially been developed for journal bearings, but it has been later on adapted for various situations in which the friction involves two fluid lubricated sliding surfaces such as the piston ring/liner interface.

The curve correlates two non-dimensional groups. The ordinate is the coefficient of friction (μ) under steady-state condition and the abscissa is a variation of a dimensionless number, sometimes referred to as Sommerfeld number (Luengo *et al.*, 1996; Priest and Taylor, 2000), given as

$$S_o = \frac{\eta U}{p} \quad (1.1)$$

where η is the dynamic viscosity, p is the normal stress per unit length and U is the sliding velocity (for piston rings, the instantaneous speed may be used instead (Ting, 1993a, b)). This diagram can be divided into four regions, which correspond to the four main important tribological regimes: boundary, mixed (partial), elastohydrodynamic and hydrodynamic; they are illustrated on the top part of Figure 1.2

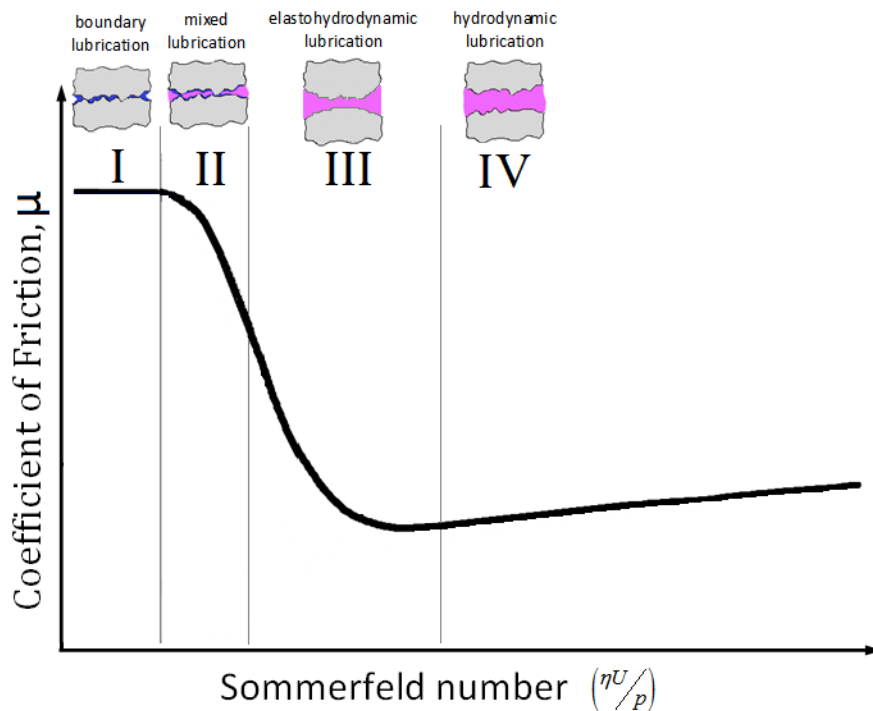


Figure 1.2: Stribeck diagram

In the first region of the Stribeck diagram (I), the friction regime is boundary lubrication is essentially constant. In this regime the solid is not separated by the lubricant, fluid effects are negligible and the friction is mainly caused by metal-to-metal contact between surface asperities. The contact lubrication is characterised by the chemical and physical properties of thin films of molecular proportions.

In the second region (II) the regime is mixed lubrication. In this area the influence of the oil trapped between the sliding surfaces becomes appreciable, but the effect of the surface asperities interaction contact is still an important factor. The friction coefficient decreases with an increase of the Sommerfeld number.

In the third region (III) the regime is elastohydrodynamic lubrication (EHL) where there is also full fluid lubrication with surface separation, but it is a more concentrated mechanism where elastic deformation of the surfaces and the effect of pressure on viscosity are imperative.

In the last region (IV) of the Stribeck curve the lubrication regime is hydrodynamic where the surfaces are completely separated by a fluid film. The friction force is given by the viscous shear of the oil film where the dynamic viscosity of the lubricant is its most important property. In this area, an increase in the Sommerfeld number leads to an increase of the friction coefficient as well.

The progress of understanding the lubrication regimes has led to the appreciation of the occurrence of surface interaction in a range of lubricated machine elements and an acknowledgment that surface topography can have a considerable role in the performance and robustness of such components. The Stribeck diagram has been modified (Hamrock *et al.*, 2004; Priest and Taylor, 2000; Taylor, 1998) to include the film parameter, Lamda (λ) ratio, on the abscissa as depicted in figure 1.3(b). The Lamda (λ) is defined as the ratio of film thickness (taking the surfaces to be smooth) to the composite surface roughness (Dowson, 1993). The relationship between the dimensionless film parameter λ and the minimum film thickness h_{\min} is

$$\lambda = \frac{h_{\min}}{\sqrt{R_{q,a}^2 + R_{q,b}^2}} \quad (1.2)$$

where (Figure 1.3(a))

$R_{q,a}$ = rms surface finish of surface a

$R_{q,b}$ = rms surface finish of surface b

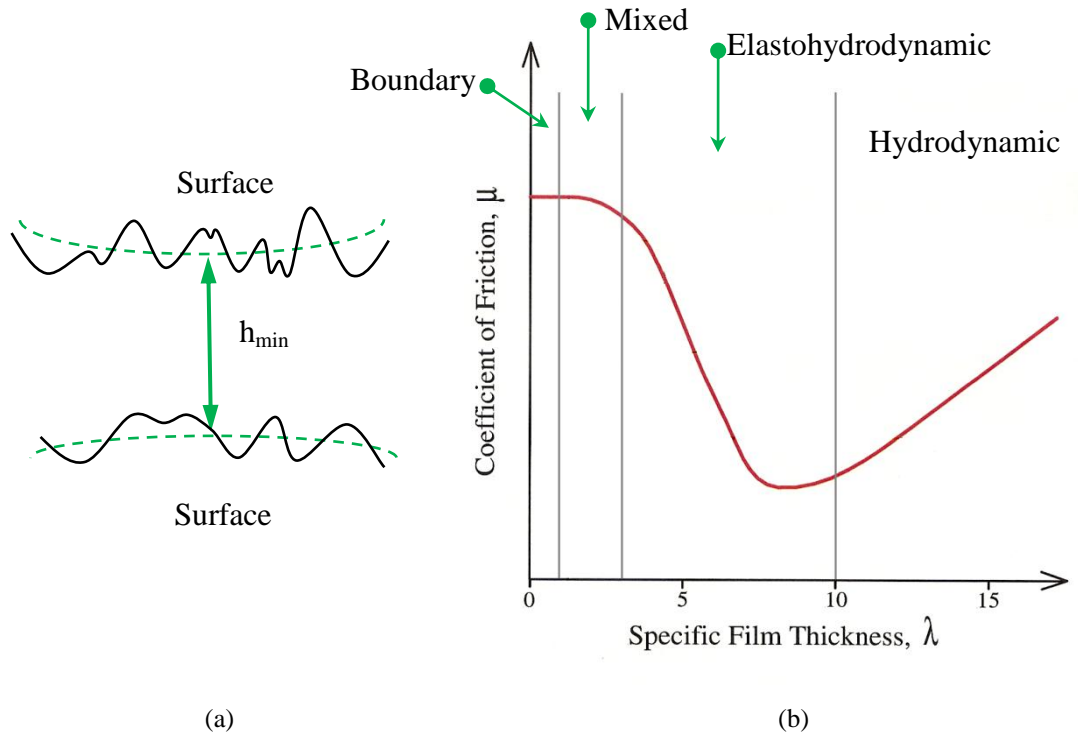


Figure 1.3: (a) Surface roughness, (b) Variation of friction coefficient with film thickness (Hamrock *et al.*, 2004)

The film thickness is used to define the four important lubrication regimes as described above. The range of λ for these four regimes is described below and these values are considered rough estimates (Hamrock *et al.*, 2004), i.e.

1. Hydrodynamic lubrication, $5 < \lambda < 100$
2. Elastohydrodynamic lubrication, $3 < \lambda < 10$
3. Mixed lubrication, $1 < \lambda < 5$
4. Boundary lubrication, $\lambda < 1$

1.5 FUNDAMENTALS OF LUBRICANTS

A lubricant can be defined as a substance introduced between two surfaces in relative motion in order to reduce friction between them (Caines and Haycock, 1996). It is not known precisely when lubricants were first deliberately and consciously used, but various forms of primitive bearings were known in the Middle East several thousands of years B.C. It is reasonable to assume that if the concept of a bearing had been developed, then the use of a lubricant with that bearing could have been highly likely even if only water. As industrial revolution started, lubricants were used in a wide variety of applications from light to heavy machinery. Today the automotive industry is one of the major consumers of lubricants and friction has been characterised as one of the key mechanisms capable of improving further the fuel efficiency of advanced passenger car engines.

1.5.1 FUNCTIONS OF A LUBRICANT

The primary purpose of lubrication is to reduce wear and heat between contacting surfaces in relative motion. While wear and heat cannot be completely eliminated, they can be reduced to negligible or acceptable levels. Because heat and wear are associated with friction, both effects can be minimized by reducing the coefficient of friction between the contacting surfaces. Lubrication is also used to reduce oxidation and prevent rust; to provide insulation in transformer applications; to transmit mechanical power in hydraulic fluid power applications; and to seal against dust, dirt, and water.

In practice, lubricants are called upon to fulfil other functions, some of which are equally vital to the operation of the equipment in which they are employed. The desired properties can have positive aspects or negative aspects. The ability of oil to meet any particular requirement is usually a matter of degree, rather than an absolute fact, and therefore questions of testing and test limits and the acceptance of limitations of both lubricants and machine have to be taken into account. A simplified list of the positive properties particularly applicable to motor oil can be given as follows:

1. *Friction reduction*- This reduces the energy requirements to operate the mechanism and reduces local heat generation

2. *Wear reduction*- An obvious need for keeping the equipment operating for a longer period and in an efficient manner.
3. *Cooling*- In an engine the lubricant is an initial heat transfer agent between some parts heated by combustion (e.g., piston), and the heat dissipating systems (sump, cooling jacket, etc.). In addition, and in other systems, the lubricant dissipates heat generated by friction or through the mechanical work performed.
4. *Anti-corrosion*- Either from its own degradation or by combustion contamination the oil could become acidic and corrode metals. Moist environments and lack of use can also cause rusting of ferrous components; the lubricant should counter all of these effects.
5. *Cleaning Action*-The oil should prevent fouling of mechanical parts from its own degradation products or from combustion contamination. Deposits, classified usually by descriptive terms such as “solid carbon,” “varnish” or “sludge,” can interfere with the correct and efficient operation of the equipment. In extreme cases, piston rings may become stuck, and oil passages blocked, if the oil does prevent these effects.
6. *Sealing*-The oil should assist in forming the seals between pistons and cylinders to avoid leakage and ground contamination (piston to rings, and rings to cylinder walls).

1.6 LUBRICANT CHEMISTRY

The lubricant used in an internal combustion engine must operate under extremely aggressive conditions, such as high temperatures or even very low temperatures and in contact with compounds that can cause it to degrade. Therefore under such vigorous conditions it must perform all its roles, as mentioned in section 1.5.1, efficiently and consistently over the prescribed period.

Until the 1930s crankcase engine oils contained no additives, comprising base oils. Oil drain intervals were necessarily very short (1500 km or less) to ensure adequate lubrication and the existing oil classification system, first adopted in America in 1911 by SAE, was related only to oil viscosity and not performance. However, due to increasing consumer demands and economic pressures, internal engines were becoming

more sophisticated. Engine oils were becoming more stressed, giving rise to a need for additives (see section 1.6.4). The reduction of wear and friction losses in an internal combustion engine is largely a function of improved lubrication (Masjuki *et al.*, 1999). Therefore, advanced lubricants are now being formulated to reduce the wear and friction of the various tribological components. The development of modern lubricants and their proper use are of great importance for the national economy, individual drivers and environment. Lubricants, optimally adjusted to a given task, can save billions of pounds in the case of an industrialized nation, reduce wear, reduce maintenance requirements and reduce the problem of local and global air pollution (Klamann and Rost, 1984).

1.6.1 BASE STOCKS

The basic fluid that constitutes the major part of a lubricating oil is almost invariably made from mixture of two or more components, generally referred to as base stock (Caines and Haycock, 1996); base stock is the term used to describe plain mineral oil. The physical properties of an oil depend on its base stock; in most cases it is chemically inert. There are three sources of base stock: biological, mineral and synthetic. The oils manufactured from these sources exhibit different properties and they are suitable for different applications. For example:

- biological oils are suitable in applications where the risk of contamination must be reduced to a minimum as, for example, in the food or pharmaceutical industry. There can be two sources of this type of oil: vegetable and animal. Examples of vegetable oils are: castor, palm and rape-seed oils while examples of animal oils are: sperm, fish and wool oils from sheep (lanolin).
- mineral oils are the most commonly used lubricants throughout industry. They are petroleum-based and are used in applications where temperature requirements are moderate. Typical applications of mineral oils are to gears, bearings, engines, turbines, etc.
- synthetic oils are artificially-developed substitutes for mineral oils. They are specifically developed to provide lubricants with superior properties than mineral oils. For example, temperature resistant synthetic oils are used in high performance machinery operating at high temperatures; synthetic oils for very low temperature applications are also available.

1.6.2 MINERAL OILS

Mineral oils are obtained through the refining of crude oil which contains impurities, petroleum gas and water when it is first recovered. Mineral oils are the most commonly used lubricants. Complex hydrocarbons are the basic constituents of crude oil and a detailed analysis has revealed 125 different compounds of which only 45 have been analysed (Dorinson and Ludema, 1985). The impure nature of mineral oils results in a range of useful and harmful properties (Stachowiak and Batchelor, 2000) such as, for example, trace compounds that provide anti-oxidants and boundary lubrication properties but also cause deposits which can impede lubrication. There are also many other compounds present in mineral oil such as waxes which are virtually useless and can easily be oxidized. Depending on the source of crude oil and the refining process, the fundamental differences between mineral oils are based on:

- chemical form,
- sulphur content,
- viscosity.

Chemical forms

There are three basic chemical forms of mineral oil:

- paraffinic,
- naphthenic,
- aromatic.

They have originated from crudes from different sources and correspond to an exact chemical type. As shown in Figure 1.4, paraffinic implies a straight chain hydrocarbon, naphthenic means cyclic carbon molecules with no unsaturated bonds and aromatic oils contain benzene type compounds. Oils are distinguished based on the relative proportions of paraffinic, naphthenic and aromatic components present.

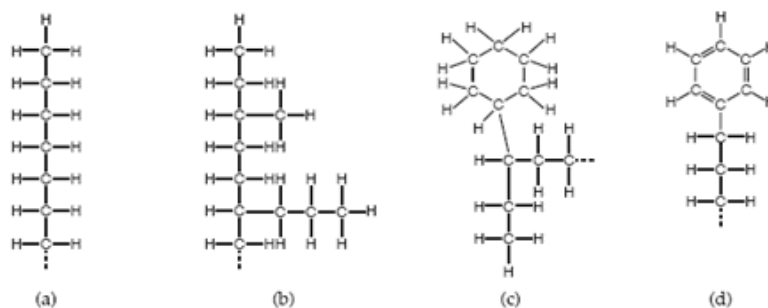


Figure 1.4: a) straight paraffin, b) branch paraffin, c) naphthene, d) aromatic (Stachowiak and Batchelor, 2000)

Sulphur content

Sulphur content in mineral oils varies depending on the source of the crude oil and the refining process. Small amounts of sulphur in the oil are desirable to give good lubrication and oxidation properties. It has been demonstrated, for example, that between 0.1% to 1% of natural sulphur content ensures reduced wear (Benchaita *et al.*, 1990). On the other hand, too much sulphur is detrimental to the performance of the engine, e.g. it may accelerate the corrosion of seals. Excess sulphur can be removed from oil by refining, but this can be expensive. The sulphur content varies with the source of crude oil and its range of concentration lies between 0% and 8%. For example, sulphur content of Pennsylvanian oil is <0.25%, Venezuelan ~2%, Middle East ~1% and Mexican 5%.

Viscosity

Viscosity is a measure of the resistance of a fluid when it is deformed by either shear stress or extensional stress. A simplistic definition of viscosity is the resistance of a liquid to flow. Mineral oils can also be classified by viscosity, which depends on the degree of refining. For commonly used mineral oils, viscosity varies from about 5 cS to 700 cS. For example, the viscosity of a typical spindle oil is about 20 cS, engine oil is between 30 - 300 cS and bright stock is about 600 cS. (Stachowiak and Batchelor, 2000).

1.6.3 SYNTHETIC OIL

The development of synthetic oil originally began in the early part of last century by countries lacking a reliable supply of mineral oil. These lubricants had high manufacturing cost and did not gain general acceptance. The use of synthetic oil became commercially significant after World War II and increased especially in more specialised applications for which mineral oils were inadequate. Many types of fluid can be used as synthetic base stocks, and some of the major ones include synthetic hydrocarbons, polyalphaolefins, polybutenes and esters.

Synthetic lubricants can generally be divided into two groups:

- fluids intended to provide superior lubrication at ambient or elevated temperatures, and
- lubricants for extremes of temperature or chemical attack.

There is also a clear distinction between exotic lubricants with high performance but high cost and more economical moderate performance lubricants. There are three basic types of synthetic lubricant currently in use:

- synthetic hydrocarbon lubricants,
- silicon analogues of hydrocarbons, and
- organohalogens.

All of the hundred or more specific types of synthetic lubricant available on the market conform to one of these broad categories. Phosphates, as in polyphenyl phosphate, deviate from the pattern as they are generally associated with simple hydrocarbons. These three groups of synthetic lubricants have distinct characteristics which sustain the usefulness of this form of classification. These are:

- synthetic hydrocarbons which provide a lubricant that is similar in price to mineral oil but has superior performance,
- silicon analogues or silicones which are resistant to extremes of temperature and vacuum but do not provide good adsorption or extreme pressure lubrication (sometimes known as ‘boundary characteristics’) and are also expensive,
- organohalogens which can offer effective lubrication by adsorption and extreme pressure lubrication mechanisms while resisting extremes of temperature or chemical attack, but are also expensive.

1.6.4 ADDITIVES

An essential part of a modern automotive lubricant is its additive package. This is the combination of chemicals added to the lubricant to improve its properties. Modern oils, and particularly motor oils, contain considerable quantities of additives as well as several base stocks. An additive may introduce a new property to the base oil which it does not have naturally or merely strengthen an existing property that is desirable. Interestingly, the first additives could be considered to be mineral oil addition to vegetable or animal oils which were employed to extend the quantity and render these natural lubricants somewhat cheaper. When mineral oils began to be used in large quantities as lubricants, the situation was reversed and the first additives for mineral oils were in fact natural vegetable and animal oils which provide “lubricity” to the mineral oils, that were considered to be lacking in this rather ill-defined property. Figure 1.5 gives a chronological view of the development of the main additive families and the main crankcase lubricant classifications and specifications. Some of the main types of additives used in lubricants indented for automotive applications are reviewed in the following sections.

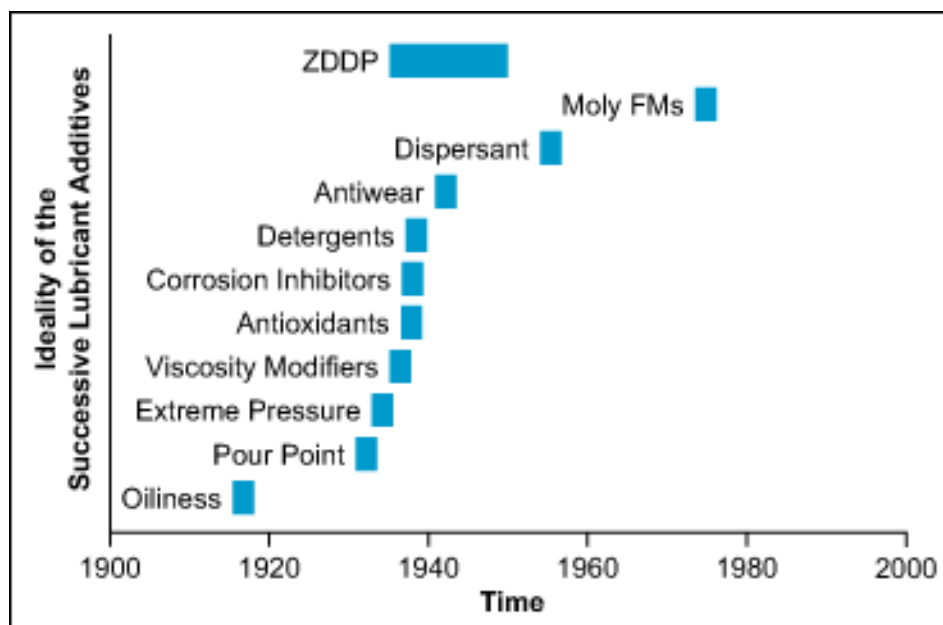


Figure 1.5: Chronology of the development of lubricant additives (Liskiewicz *et al.*, 2008)

Friction modifiers

Friction modifying additives are included in the lubricants to reduce friction under boundary lubrication conditions. By definition, the base fluid itself is the primary friction modifier. And it is the need for fuel economy that required additional friction modifiers. These are surface active agents closely related to extreme pressure additives in structure and mode of action (boundary lubrication). The additives in current use are mostly the fatty acids and the esters and amines of the same fatty acids. Sulphurised fatty acid derivatives are commonly used as friction modifiers in modern engine lubricants. They usually have a polar group (-OH) at one end of the molecule and react with the contacting surfaces through the mechanism; however they are effective only at relatively low temperatures and loads (Stachowiak and Batchelor, 2000).

Anti-wear additives

Hydrodynamic lubrication is maintained by a multimolecular film of lubricant between the surfaces involved. If the surfaces do not touch, there is no wear. However, hydrodynamic lubrication is not always possible. When points of asperities cause metal to metal contact between lubricated surfaces, boundary lubrication occurs. In order to protect contacting surfaces at higher temperatures above the range of effectiveness of adsorption or boundary agents, anti-wear additives were designed and manufactured. There are several different types of anti-wear additives that are currently used in oil formulations. For example, in engine oils the most commonly used anti-wear additive is zinc dialkyldithiophosphate (ZnDDP or ZDDP) (Hamrock *et al.*, 2004), while in gas turbine oils tricresylphosphate or other phosphate esters are used. Phosphorous additives are used where anti-wear protection at relatively low loads is required. These additives react with the surfaces through the mechanism of chemisorption, and the protective surface layer produced is much more durable than that generated by adsorption or boundary agents.

Pour point depressant

These additives act in order to lower the pour point of oil which is the lowest temperature at which an oil will pour or flow when cooled. A low pour point is particularly important for proper performance of lubricants in cold climates. The most

common chemical types are the polyacrylates and polymethacrylates. At low temperatures, the wax left in the lubricant base stock comes out from the solution as wax crystals, producing a gel like structure which impedes the flow of the lubricant to critical engine parts. Pour point depressants are added not to reduce the amount of wax but to inhibit the formation of interlocking crystal networks.

Viscosity Index improvers

These are additives which hold the decline in oil viscosity with temperature and they are commonly known as viscosity index improvers. By suitable formulation, it is possible to make an engine lubricant which satisfies both the low and high temperature requirements of the SAE Viscosity Classification System, J300. This entails meeting, simultaneously, the limits for low-temperature W-grades (determined with a Cold Cranking Simulator (CCS) and Mini Rotary Viscometer (MRV)) and high-temperature grades (kinematic viscosity at 100°C). High molecular weight polymers, known as viscosity modifiers or viscosity index improvers, are commonly used for this purpose. Such oils are referred to as multigrade oils (e.g. SAE 10W-40). Their viscosity is less sensitive to temperature than that of monograde oils having the same high temperature viscosity (e.g. SAE40). As a consequence, multigrade oils allow acceptable engine operation over a much wider temperature range. Multigrade oils have a lower viscosity at low temperatures, allowing easier cranking and starting than the corresponding monograde oil and resulting in improved fuel consumption and higher viscosity at lower temperatures. These effects are shown schematically in Figure 1.6.

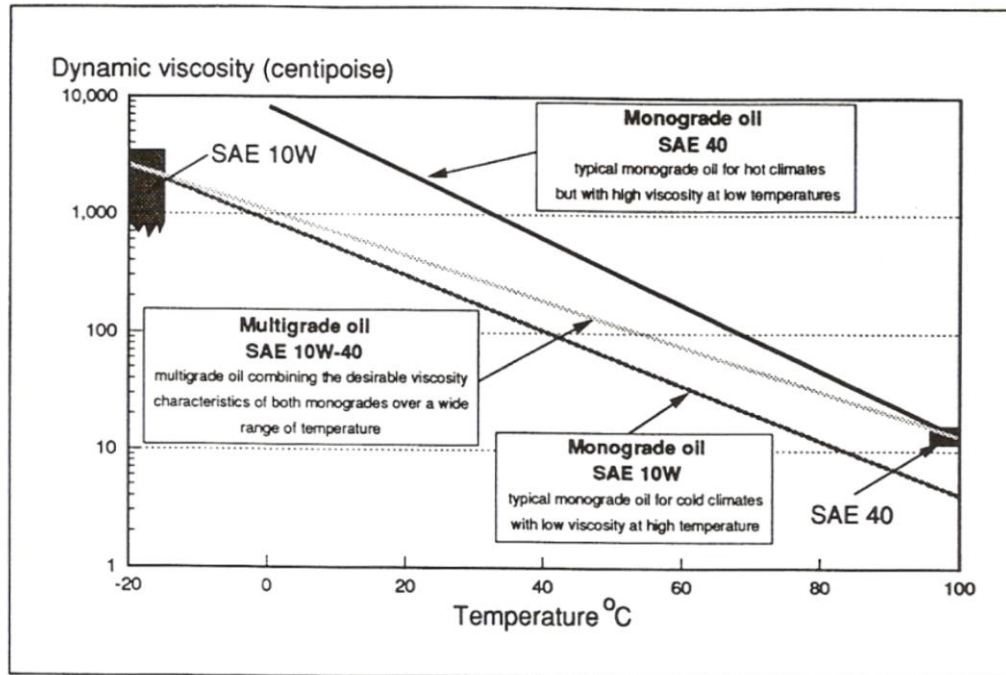


Figure 1.6: Effects of temperature on viscosity (The Technical Committee of Petroleum Additive Manufacturers (ATC))

Anti-oxidant

Mineral oils inevitably oxidize during service and this causes significant increases in friction and wear which affects the performance of the machinery. The main effect of oxidation is a gradual rise in the viscosity and acidity of an oil. A highly oxidized oil needs to be replaced since it causes power losses due to increased viscous drag and difficulties in pumping through the lubricant feed lines. It should be mentioned, however, that oxidation is not the only cause of viscosity increase in lubricating oils.

Another cause is diesel soot. Elevated oil acidity can cause concentrated corrosion of certain machinery components such as seals and bearings. For example, lead, copper and cadmium are used in the bearing alloys of an internal combustion engine and they are particularly prone to corrosion.

1.7 LUBRICANT AND EMISSIONS

Fuel exhausts have an impact on air quality and human health, especially in urban areas where traffic is dense. To reduce this impact, the EU is preparing to impose stricter emission limits on both diesel and petrol cars, limiting in particular the concentration of

nitrogen oxides (NO_x) and particulate matter (PM) which pose the most serious health problems. With the next generation of standards for cars (known as Euro 5) recently drafted and set to enter into operation in 2009, some member states including France and Germany are already pressing ahead with measures of their own. While the combustion of the fuel has perhaps the greatest impact on emissions, the influence of the lubricating oil has been gradually receiving more attention since crankcase lubrication plays an important role in internal combustion engines. Wear protection, deposit formation inhibition, and heat transportation are amongst the most important functions of the lubricant. Some part of the lubricant, however, will be unintentionally sacrificed in the combustion process (Van Dam and Klelser, 1995). Lubricant can enter the combustion chamber via:

- (a) the piston ring pack
- (b) the valve guides, and
- (c) the positive crankcase ventilation system.

The combustion products of the consumed oil might contribute to the exhaust gas emissions (Cooke, 1990) and with the emission legislation becoming more stringent, it is important that oil consumption is reduced to the lowest possible level. Oil consumption increases when the oil which fails to be scraped off the piston rings and remains in the combustion chamber evaporates and burns as it is exposed to the high temperatures during the combustion phase. Therefore, one way to reduce the oil consumption is to improve the piston and piston ring designs to improve the oil scraping effect off the rings so that the evaporation can be eliminated (Dellis, 2005). The physical characteristics of oils can influence the mechanical efficiency of the internal combustion engine and, as a result the specific fuel consumption. The variation in the quantity of fuel consumed at constant power output can influence the combustion process thus affecting the exhaust emissions of NO_x , HC, CO and particulate matter (Laurence *et al.*, 1996; Schiemann *et al.*, 1995).

Tier	CO	HC	HC+NO _x	NO _x	PM
Diesel					
Euro1 (1992)	2.7	-	0.97	-	0.14
Euro2 (1996)	1.0	-	0.7(DI: 0.9)	-	0.08(DI: 0.10)
Euro3 (2000)	0.64	-	0.56	0.50	0.05
Euro4 (2005)	0.50	-	0.30	0.25	0.025
Euro5 (2009)	0.50	-	0.23	0.18	0.005
Euro6 (2014)	0.50	-	0.17	0.08	0.005
Petrol (Gasoline)					
Euro1 (1992)	2.72	-	0.97	-	-
Euro2 (1996)	2.2	-	0.5	-	-
Euro3 (2000)	2.30	0.20	-	0.15	-
Euro4 (2005)	1.0	0.10	-	0.08	-
Euro5 (2009)	1.0	0.10	-	0.06	DI: 0.005
Euro6 (2014)	1.0	0.10	-	0.06	DI: 0.005

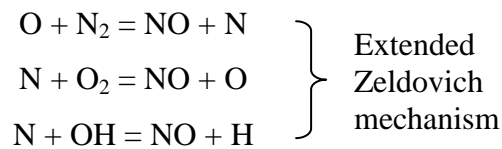
Table 1.1: European emission standards for passenger cars (g/km)

Emissions of NO_x and particulate matter (PM) from diesel engines are higher than for petrol engines and are thus, considered to pose the most serious environmental and health problems. New findings about the harmful health effects of particulates have called for significant reductions in the emission limits from diesel vehicles. The draft Euro 5 limits would reduce emissions of particulates from diesel cars by 80% compared to Euro 4.

To prepare for these changes, car makers are working on technologies to optimise diesel engines for higher fuel economy and reduced NO_x and PM emissions. The quantity and composition of emissions vary depending on several technical factors including: the quality of diesel fuel and oil used; the type of engine and the engine tuning; the workload demand on the engine. Table 1.1 shows the European emission standards for both diesel and petrol passenger cars, where the limits are given in mass per driven kilometre during the stringent test cycles including cold start. Note that the planned introduction of EURO6 is not fixed yet, but will most likely be in effect from 2014.

1.7.1 NITROGEN OXIDES (NO_x)

The principal source of oxides of Nitrogen (NO_x) is oxidation of atmospheric N₂ at high temperatures (>1800K, thermal NO). If fuel contains nitrogen, the oxidation of fuel N containing compounds is an additional source of NO (fuel NO). There is also prompt NO but has a small contribution since it is formed at the flame front. The mechanism of NO formation from atmospheric nitrogen is being described by the Zeldovich mechanism. In combustion of near stoichiometric fuel-air mixtures the principal reactions governing the formation of NO from molecular nitrogen are:



NO forms in both the flame front and the postflame gases; the latter mechanism dominates. It also depends on the maximum cylinder gas temperature.

1.7.2 PARTICULATES

The achievement and maintenance of low level of oil consumption is considered an essential part of most OEMs (original equipment manufacturers) strategy for meeting the ever more stringent vehicle emissions limits. In the heavy diesel engine sector particulates emissions are of primary importance (Burnett, 1989). It is generally accepted that the lubricating oil can make a substantial contribution to the particulates formation (Wong and Hault, 1991), although the published literature indicates that this contribution can vary significantly depending upon engine, oil and measuring procedures (Furuhama, 1985, 1987; Ruddy *et al.*, 1982).

The formation of particulates is based on unoxidised or partially-oxidised fuel molecules at the high temperatures (above 1800K) present in fuel rich zones. The principal mechanism is imperfect mixing, locally over-lean or locally over-rich, and flame quenching at the combustion chamber walls. Their composition is unburned hydrocarbons, lubricating oil sulphates and various aromatic compounds. The morphology of the particulates is spheres of 0.01 µm diameter for the case of the primary particulates and 0.1 µm for the secondary particulates which are agglomerates

of the primary ones have varying shapes. Figure 1.7 depicts the main parameters leading to the formation of particulates.

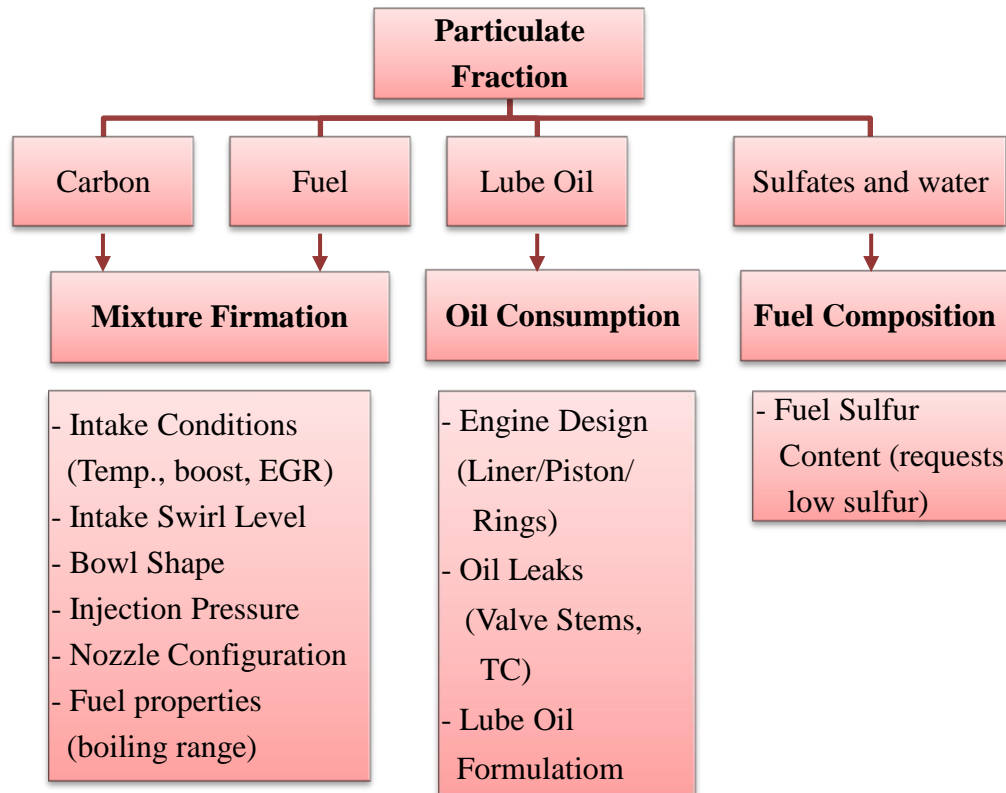


Figure 1.7: Main parameters affecting particulate formation

1.7.3 HYDROCARBONS

At temperatures of 300°C or more in the absence of air, oils may decompose to produce low molecular weight fragments from the large molecular weight species typically found in mineral oils. The fragmented or ‘cracked’ hydrocarbon molecules either recombine to form tarry deposits (asphaltenes) or are released to the atmosphere as volatile components (Woods and Trowbridge, 1955); these deposits are undesirable in almost all cases. Hydrocarbon (HC) emissions are not only caused by lubricating oil that becomes entrained in the combustion gases flowing into and out of the ring-pack area, but also result from incomplete fuel combustion and from fuel evaporation. Measuring the fuel content in the oil film is important to the auto industry for several reasons. Yu and Min (2002) developed a model to assess the absorption and desorption of fuel in oil films. This was investigated in a parametric study according to engine speed, load and oil film temperature. Under warm-up conditions, engine speed had little

influence on the amount of fuel absorbed/desorbed, but when the oil film temperature was low, the quantity of fuel absorbed/desorbed decreased with increasing engine speed. Liquid fuel on the oil film and piston head caused higher HC emissions and, under base conditions (a simulated cold engine), the amount of fuel vaporized from fuel film and desorbed from wetted oil film was 24.5% of the stoichiometric fuel mass. The effect of oil film with liquid fuel was 5.3 times larger than that of oil film without liquid fuel. The amount of fuel that escaped from the piston crevice was 1.3 times larger than that of fuel in the oil film. However, the fuel trapped in the oil film desorbed into the combustion chamber more slowly than the fuel that escaped from the piston crevices under cold engine conditions. Parks *et al* (1998) used LIF spectroscopy to investigate possible hydrocarbon emission sources within the engine. In particular, an effort was made to quantify the concentration of the fuel absorbed in the oil on the cylinder wall of a small engine. Fluorescence provides an ideal spectrometric method for distinguishing the concentration of individual chemical components in a simple mixture. Because unburned fuel in the cylinder-wall oil film is a suspected major emission source during engine start-up (cold start), the amount of fuel in oil is of particular interest for determining hydrocarbon emission sources and the relevant detailed mechanism (Dellis, 2005).

1.8 THESIS OUTLINE

The present thesis consists of 6 chapters including the introductory *Chapter 1*, where the motivation for this research work is outlined and a brief history of the development of piston rings is given. Moreover, the functions of lubrication are highlighted and the basic lubrication chemistry is described followed by a summarised description of the emission regulations aspect pertaining in lubrication.

Chapter 2 reviews relevant publications in the area of measurement techniques. The different methods for measuring the oil film thickness have been summarised and the presence of cavitation in the lubricant of piston rings has also been discussed. Finally the previous work carried out within the research group has been summarised.

The equipment and the various experimental techniques used for investigating the oil film in the test rig and diesel engine are described in *Chapter 3*.

Chapter 4 and *Chapter 5* present the experimental results obtained in the test rig and the diesel engine, respectively.

Chapter 6 concludes the thesis with the summary of the major findings, in addition to the brief summaries contained in *Chapter 2* through *Chapter 5*. Recommendations for further work are also included in *Chapter 6*.

A list of the relevant publications, which were reviewed and referenced in this thesis, is given in the references section.

Chapter 2

LITERATURE REVIEW

2.1 INTRODUCTION

This section is devoted to the discussion of published research on various topics that are relevant to the area of the current work. The purpose of this section is to obtain an insight into the different approaches for investigating the piston-ring cylinder liner conjunction in order to provide the foundation for the understanding and analysis of the subsequent results. A number of experimental techniques have been developed to examine the characteristics of the oil film quantitatively on the liner and within the ring pack. Furthermore to the quantitative analysis, oil film visualisation techniques have been also put into practice in order to understand the transient behaviour of the oil transportation mechanism. This overview will highlight a large variety of methods presently in use and allow the importance of the current study to be put into perspective.

2.2 OIL FILM THICKNESS MEASUREMENT TECHNIQUES

A wide range of experimental techniques have been developed over the years to examine the distribution, both quantitatively and qualitatively, of the oil film thickness within contact of the liner and ring pack. In addition to motored and firing engines, simplified test rigs have been used to identify the characteristics of the oil film under idealised conditions. Here this research is reviewed and the main conclusions and techniques are identified and summarised in the following tables below.

As discussed by Sherrington and Söchting (2006), these techniques may be divided into three categories: electrical techniques, acoustic techniques and optical techniques.

2.2.1 ELECTRICAL TECHNIQUES

Specially designed electrical transducers have been made to measure the oil film thickness between piston rings and cylinder liner. These can be broken down into four groups according to the principle of operation: resistance methods, inductive methods, eddy current methods and capacitance methods.

Resistance methods

The resistance method determines the thickness of the oil film from the resistance between two electrodes. In this case, one electrode can be the piston ring. The piston ring is electrically insulated, the whole or part of the piston-ring, from the rest of the piston and current passes through the ring to the liner. Eventually, changes in the resistance of the ring/liner junction during operation would correlate with changes in the thickness of the prevailing oil-film. The absence of smooth changes in the resistance prevented the determination of values or trends in the oil film thickness. This method of measurement did not prove useful in measuring the oil film thickness due to numerous short circuits occurring between the ring and liner. However, to certain extent the resistance measurements reveal the degree of contact between the ring and liner that is metal to metal contact. In this case, a greater level of breakdown is detected around TDC than at BDC, pointing out to the increasing asperity contact characteristic of boundary lubrication (Sherrington and Smith, 1985).

An enhanced resistance technique was developed by Furuham and Sumi (1961) where one end of the piston ring is fixed to the piston, and by attaching the other end to the anode of a movable anode vane it was made possible to measure the variation in the piston ring gap width. After first measuring the static ring gap throughout the stroke and then deducting the variation from the dynamic results (variations in the bore circumference necessitated this step), the average oil film thickness could be deduced from geometrical considerations. The authors compared their film measurement with the model of Furuham (1959) and found the results to be qualitatively similar.

Inductance methods

Inductance is fundamentally related to the number of magnetic field line loops around a conductor, per Ampere current through it. The inductance transducer is based on the theory that the inductance of a wire coil changes as its separation from the magnetic material alters.

An indirect method, self-inductance, was employed by Wing and Saunders (1972) to measure the oil film thickness between the piston rings and cylinder liner. It was not possible to fit the transducers on the rings themselves owing to their large dimensions. Instead, two of them were mounted at the back of the piston ring grooves at opposite locations. The variation in the gap behind the ring was assumed to be similar to that of the variation in oil film thickness.

However, using inductance transducers as a measuring technique causes some difficulties and two particular problems were identified by Sherrington and Smith (1985). To begin with, the output of the transducer is non-linear and in addition thermal instability renders calibration in the combustion chamber of the firing engines unreliable. Furthermore, due to improvements in spatial resolution of other measuring techniques such as the capacitance and laser induced fluorescence methods, the inductance method has been largely discarded.

Capacitance methods

In the open literature capacitance the methods have been the most popular and widely used and has proven to be the most enduring and useful electrical technique. The principle of this method is based on the capacitance of two parallel metal plates where the variation of the later is inversely proportional to their separation. Capacitance measurements are widely used in industry as proximity sensors but commercially available sensors are not suitable to use for measuring oil film thickness between piston ring and cylinder liner. Their large dimensions make it difficult to mount on the piston ring and their spatial resolution is reduced and may be inadequate.

Hamilton and Moore (1974) designed special capacitance transducers to measure the oil film thickness over the whole stroke in a firing diesel engine. The authors were able to

measure oil film thickness up to about 10 μm but beyond this any changes in capacitance were insensitive for determining the oil film thickness. The capacitance method is also used in this current research and will be described in more detail in subsequent chapters.

Eddy current methods

Eddy current sensors work on the principle of the eddy current effect in conductive metal where the clearance between the transducer and the ring is changed into an electric property which can be measured. This method has the same advantages as the inductance methods, i.e the measurements are independent of the medium between the transducers and the rings. Literature suggests that this method is unpopular may be due to its poor spatial resolution as the eddy current sensors are large in dimensions.

<i>Reference</i>	<i>Experimental Set-up</i>	<i>Technique(s)</i>	<i>Major Findings</i>
Furuhama and Sumi (1961)	Reciprocating cylinder over a stationary ring	<ul style="list-style-type: none"> • Resistance. • Entire ring acts as electrode • Minimum oil film thickness calculated from ring gap size. 	<ul style="list-style-type: none"> • Thin oil film occurs at TDC and BDC and thick film around mid-stroke. • Oil film thickness values are similar to theoretical calculations. • The oil film thickness increases with speed or reduction in load.
Wing and Saunders (1972)	Piston assembly of a firing engine	<ul style="list-style-type: none"> • Inductance 	<ul style="list-style-type: none"> • First oil film thickness measurements.
Hamilton and Moore (1974)	Single cylinder four stroke small diesel engine. Firing condition.	<ul style="list-style-type: none"> • Three capacitance transducers mounted on the side of the liner. • Calibration using slip gauges 	<ul style="list-style-type: none"> • Lubrication found to be hydrodynamic and oil film in the range of 0.4-2.5 μm. • Error could occur if the ring/liner conjunction was not filled with oil as dielectric constant of the capacitance probe would vary
Hamilton and Moore (1974)	Motored condition. Single fixed ring.	<ul style="list-style-type: none"> • Capacitance 	<ul style="list-style-type: none"> • Measured results are in disagreement with predicted ones.

Parker <i>et al.</i> (1975)	Test rig, straight section of piston ring reciprocating over a flat plate. Firing engine.	<ul style="list-style-type: none"> • Capacitance transducer in test rig. • Capacitance, inductance and resistance transducers in firing engine. 	<ul style="list-style-type: none"> • Good agreement between theory and measured results in test rig. • In firing engine the oil film varies within the stroke and decreases with increased speed. • Film thickness is smaller after top dead centre than predicted by theory due to the squeeze action.
Moore and Hamilton (1978)	Four stroke single indirect injection diesel engine, Peter AV1. The engine was couple to a standard Heenan and Froude water brake.	<ul style="list-style-type: none"> • Capacitance 	<ul style="list-style-type: none"> • Over a majority of stroke, the piston rings usually operate under conditions of starved lubrication.
Moore and Hamilton (1980)	Normally aspirated four stroke single indirect injection diesel engine, Peter AV1, and AVB version supercharged engine	<ul style="list-style-type: none"> • Capacitance 	<ul style="list-style-type: none"> • Considerable variation of the ring profile around the circumference was measured after removal. • Effect of starvation on capacitance signal by ring profile fitting was identified. • Generally oil film was much thinner in the turbocharged engine.
Sanda and Someya (1987)	Test rig with a flat reciprocating liner over a fix specimen ring	<ul style="list-style-type: none"> • Eddy current 	<ul style="list-style-type: none"> • Relative displacement between reciprocating liner and stationary ring specimen was measured and the film thickness was calculated.
Myers <i>et al.</i> (1990)	A TACOM-LABECO single cylinder diesel research engine.	<ul style="list-style-type: none"> • Capacitance 	<ul style="list-style-type: none"> • Changes of oil film thickness on top ring are mainly due to engine factors than oil characteristics. • Large deviation of oil film thickness was recorded over long running period. • Capacitance gauges were able to detect oil film break down and metal to metal contact.

			<ul style="list-style-type: none"> • The mechanical condition of the engine was believed to be crucial.
Grice and Sherrington (1993)	Single cylinder Peter AV1L firing diesel engine. Motored test carried out as well	<ul style="list-style-type: none"> • Capacitance • inductance 	<ul style="list-style-type: none"> • Oil film thickness varies a lot on the top compression ring especially during firing. • The inductance probe displayed problems with its signal to noise ratio and spatial resolution. • Low repeatability in motored tests.
Shenghua <i>et al.</i> (1996)	Four stokes Diesel Engine with splash lubrication system. Motored test performed. Three transducers were installed at TDC, Mid-Stroke and BDC respectively	<ul style="list-style-type: none"> • Eddy Current 	<ul style="list-style-type: none"> • Hydrodynamic compression lubrication is formed at mid-stroke at high speed. • Oil viscosity is more significant than engine speed at TDC and BDC. • Profile of the rings has a significant effect on the lubrication. Plain rings cut down the film thickness and thus reduce oil consumption. • Eddy Current Sensors were proved to be successful for the measurement.
Takiguchi <i>et al.</i> (2000)	A direct-injection, naturally aspirated four stroke six cylinder diesel engine. Fourth cylinder used for oil film thickness measurement.	<ul style="list-style-type: none"> • Capacitance 	<ul style="list-style-type: none"> • Oil film thickness measured on the top ring is in agreement with calculated values but much thicker film is found in expansion stroke than predicted values. • Thinner oil film on top ring than other subsequent rings. • Piston slap motion affects the variation of oil film thickness in a cycle. • Thicker oil film on top and second ring in expansion stroke may be due to lower pressure working on the back of the ring than the gas pressure working on the sliding surface.

Table 2.1: Oil Film Thickness Measurement using Electrical Method.

2.2.2 ACOUSTIC TECHNIQUES

Acoustic methods employ the reflection of ultrasonic signals from interface surfaces to measure the oil film thickness. Traditionally acoustic techniques have been used to spot defects in materials and to monitor incipient fatigue growth cracks in critical structures (Boness and Hawthorne, 1995; Boness *et al.*, 1990; Kustas *et al.*, 1994). However, this method for measuring the oil film thickness in piston rings has been scarcely seen in the open literature. Drinkwater *et al.* (1997) used ultrasonic waves to investigate the surface roughness of solid-rubber surfaces. Green *et al.* (2006) employed ultrasonic waves to calculate the contact pressure at two automotive components: a cam/follower interface and a valve tip contact. Shuster *et al.* (2000) measured different levels of scuffing damage between piston ring and cylinder liner using acoustic emission and this method provided more information regarding this phenomenon in comparison with friction measurement. Sun *et al.* (2006) utilised the same method as aforementioned authors to monitor the various phases of wear generated within a sliding bearing steel contact under boundary lubrication and oil starved conditions. Dwyer-Joyce *et al.* (2004) used ultrasonic waves, based on reflection, as a method to measure oil film thickness. This method was first evaluated between two flat plates separated by an oil film. Then it was applied to a journal bearing to measure the oil film thickness over a range of loads and speeds. The measured values were found to be similar to those predicted by the classical hydrodynamic theory. The advantages in using this method are that no major modification is needed and the oil film is not obstructed.

2.2.3 OPTICAL TECHNIQUES

Another way of quantifying or qualifying the oil film distribution is by optical techniques. This can be classified further into three categories: interferometric methods, two dimensional examination of the oil distribution (visualisation) and finally single point measurements using laser induced fluorescence (LIF). Each method will be described in detail below.

Interferometric Methods

The principle of the interferometric technique is based on the interference pattern generated by the path difference between two light beams. Wakuri *et al.* (1979) used thin film interferometry to measure the oil film thickness between a ring specimen and a glass plate, substituting for a cylinder surface, to investigate cavitation. The optical arrangement consisted of a monochromatic laser as light source and a beam splitter was used to illuminate the underside of the oil wedge through the optical plate. The measured oil film thickness was found to be in relatively good agreement with theoretical predictions. The researchers (Wakuri *et al.*, 1981) have used the same apparatus in measuring simultaneously the squeeze velocity and the separation boundary of the oil film which enabled them to validate their theoretical studies of piston ring/cylinder wall interface.

Visualisation

The second optical technique consists of a transparent glass cylinder, replacing the conventional liner, a camera and appropriate illumination to enable the visualisation of the lubricant film. Greene (1969) manufactured a transparent Perspex cylinder with a surface roughness matching the original liner. Photographic techniques for recording, under motored circumstances, were developed and results at different operating conditions were obtained and presented quantitatively. Inagaki *et al* (1995) developed a two-dimensional system for measuring the oil film distribution which was implemented to a single cylinder diesel engine. A flash lamp was used as a light source and a pulse laser was used to measure the oil distribution. The tests were carried out at different engine operation conditions and ring configurations. Several oil transport mechanisms were identified and the results were used to configure their theoretical models. Thirouard *et al* (1998) employed a two-dimensional Laser Induced Fluorescence (LIF) system to visualise the oil distribution and study the oil transport mechanisms in a single cylinder diesel engine through an optical window on the liner. The experiment was carried out at different engine conditions and the oil flow around the ring pack was primarily due to inertia of the oil in the axial direction and oil dragging by gas flow in the circumferential direction.

Point measurements using Laser Induced Fluorescence (LIF)

Laser Induced Fluorescence is renowned as one of the most advanced techniques in investigating oil film behaviour in piston ring assemblies (Arcoumanis *et al.*, 1998a; Arcoumanis *et al.*, 1998b; Hout and Takiguchi, 1991; Myers *et al.*, 1990; Richardson and Borman, 1992; Sanda, 1998). The principle of LIF (a brief description of the theory is given in Chapter 3) is that when laser light impacts onto an oil film, sometimes containing a fluorescent dye, the film emits fluorescence light whose intensity is proportional to its thickness. The concept of LIF was first employed by Smart and Ford (1974). This technique has become more sophisticated with the advancement of laser light applications, although the basic concept of LIF remains the same. Moreover, the use of laser light and fibre optics to carry the light to and from the oil film has rendered this method more accessible to various applications. The data provided by LIF can be even used to identify cavitation or oil starvation (Sherrington and Smith, 1985). However, the main drawback for this method is the calibration as fluorescence is temperature dependant (Lux *et al.*, 1990; Phen *et al.*, 1993; Sherrington and Smith, 1985).

<i>Reference</i>	<i>Experimental Set-up</i>	<i>Technique(s)</i>	<i>Major Findings</i>
Greene (1969)	Single cylinder spark ignition engine with a transparent liner. Motored test only.	<ul style="list-style-type: none"> • Visual and photographic studies by two methods: ultraviolet and scattered light. 	<ul style="list-style-type: none"> • The piston skirt was observed to have abundant of lubricant. • Scattered light technique could only detect the lubricant adhered to the surface of the cylinder liner. • A continuous oil film separated the liner and the piston ring. • The ultraviolet technique detected all the oil film between the liner and piston ring but unable to identify which surface the lubricant was stayed on.
Wakuri <i>et al.</i> (1979)	Single test rig which the reciprocating ring sample had a circular profile. Liner made of glass.	<ul style="list-style-type: none"> • Interferometry 	<ul style="list-style-type: none"> • A disturbance in the fringes was taken to be the point of film disruption. • Good agreement between theoretical and experimental results regarding oil film thickness.

Lux <i>et al.</i> (1990)	Single cylinder four stroke diesel engine with quartz windows. Motoring and firing conditions.	<ul style="list-style-type: none"> • Laser Induced Fluorescence (14 mW HeCd laser) • Tool marks on piston skirts used for calibration 	<ul style="list-style-type: none"> • The top rail of the oil control ring cavitates on both upstroke and downstroke. • Statically and dynamically obtained calibration coefficients for the LIF have large discrepancies. • The oil transport characteristics are influenced by speed and oil transport results indicate local flows 35 to 500 times larger than nominal oil consumption of the engine.
Wong and Hoult (1991)	Single cylinder four stroke indirect injection diesel engine. Liner is fitted with quartz window for optical access. Firing conditions. Monogrades and multigrades oil tested.	<ul style="list-style-type: none"> • Laser Induced Fluorescence (14-17mW HeCd laser) • Oil flow and consumption by measured by radioactive tritium tracer technique 	<ul style="list-style-type: none"> • Single grades oils were found to wet the top ring to a greater extent than multigrades ones. • The authors conclude that the crown land do not contribute to oil consumption significantly as the later run virtually dry. • No correlation could be found between measured oil flows and oil consumption.
Shaw <i>et al.</i> (1992)	Single cylinder diesel engine. Firing engine with optical access made of quartz window.	<ul style="list-style-type: none"> • Laser Induced Fluorescence, single point measurement made through quartz windows 	<ul style="list-style-type: none"> • The calibration coefficients obtained using optical fibre optics were an order of magnitude greater than those obtained using conventional optical train.
Brown <i>et al.</i> (1993)	Caterpillar single cylinder diesel engine with fused silica window.	<ul style="list-style-type: none"> • Laser Induced Fluorescence (20 mW air cooled Argon Ion laser) 	<ul style="list-style-type: none"> • Fluorescence intensity decreases as oil degrades and different quantum yield for different lubricants. • The effect of oil film pressure on fluorescence quantum yield was negligible.
Phen <i>et al.</i> (1993)	Four-stroke single cylinder direct injection diesel engine. (Cummins L-10). Motored test only.	<ul style="list-style-type: none"> • Laser Induced Fluorescence (He-Cd laser of 40mW). Multimode fibres used. 	<ul style="list-style-type: none"> • The reflectivity of the surfaces had an important effect on the LIF measurements. • OFT increases with engine speed and thus validating hydrodynamic lubrication.

			<ul style="list-style-type: none"> • OFT does not vary much with effect of intake pressure effect. However, it did at lower speed. • Trends predicted by theory match well with that observed in the measurements. • Oil film thickness was found to be approximately proportional to the square root of the kinematic viscosity.
Sanda <i>et al.</i> (1993)	<p>Four stroke single cylinder spark ignition engine.</p> <p>Transparent cylinder made of fused silica used for motored tests.</p> <p>Normal cylinder with quartz window used for firing tests</p>	<ul style="list-style-type: none"> • Scanning Laser Induced Fluorescence using rotating polygonal mirror. 	<ul style="list-style-type: none"> • Thinner OFT and oil starvation were observed on top ring in firing than in motoring condition. • A reduced tangential force on oil control ring increased the oil volume on the piston third land thus affecting oil consumption. • Oil film rupture was observed just before compression top dead centre. • Oil movement towards the combustion chamber was observed just after immediate closing of throttle. An increase in oil consumption is expected.
Inagaki <i>et al.</i> (1995)	<p>Four stroke single cylinder spark ignition engine.</p> <p>For motoring tests a whole transparent liner made was used.</p> <p>For firing tests, cast iron liner fitted with two sapphire glass windows was used.</p> <p>Coumarin 6 was used as a fluorescent dye and this gave</p>	<ul style="list-style-type: none"> • Laser Induced Fluorescence. The system consists of a xenon flash lamp and a CCD video camera. 	<ul style="list-style-type: none"> • During motoring test, film thickness distribution of less than 5 μm was observed on the piston ring surface. • Large amount of oil consumption was observed around the first compression ring gap. • During firing test, a decrease in manifold pressure (engine load) increased the oil splashes in the combustion chamber • At high speed of over 3000 rpm oil spouts increased when the piston is in exhaust stroke. • The oil film thickness

	high solubility, sufficient fluorescence intensity and thermal stability		measurement at the spouting area is closely related to the oil consumption.
Nakashima and Ishihara (1995)	Modified four stroke, four cylinder gasoline engine with one transparent cylinder. Motoring test only.	<ul style="list-style-type: none"> • Visualisation with a video camera 	<ul style="list-style-type: none"> • Investigation of effect on oil flow of ring gap size, shape and phase difference. • Oil flow was reduced to 26% by reducing oil ring upper rail gap
Frølund <i>et al.</i> (1997)	4 cylinders spark ignition four stroke engine fitted with quartz silica window and thermocouple. 25 L of coolant is used to steady the warm-up process.	<ul style="list-style-type: none"> • Laser Induced Fluorescence (a He-Cd laser of 40mW output) 	<ul style="list-style-type: none"> • The liner is heated much faster than the coolant and oil. • The MOFT of the compression ring decreases exponentially with temperature due to viscosity-temperature dependency for the engine oils. • The liner OFT is half the compression ring MOFT.
Arcoumanis <i>et al.</i> (1998a)	Firing single cylinder direct injection diesel engine. Fiber optics were placed at TDC, midstroke and BDC.	<ul style="list-style-type: none"> • Laser Induced Fluorescence (air cooled argon ion laser) 	<ul style="list-style-type: none"> • The lubricant film thickness under the piston rings proved to be very repeatable but much more random in front and behind the rings. • At TDC, the OFT under the top compression ring was always less than 5µm. • The TDC OFT decreases with engine load and speed • The effect of oil additive chemistry on the TDC lubricant film thickness appears more significant than the viscometrics effects.
Arcoumanis <i>et al.</i> (1998b)	Firing single cylinder direct injection diesel engine.	<ul style="list-style-type: none"> • Laser Induced Fluorescence (air cooled argon ion laser) 	<ul style="list-style-type: none"> • Development of oil film in a cylinder liner is complicated and highly unsteady due to different oil transport mechanisms.
Takiguchi <i>et al.</i> (1998)	Single cylinder diesel engine	<ul style="list-style-type: none"> • Laser Induced Fluorescence (multipoint 	<ul style="list-style-type: none"> • The OFT on the ring increased noticeably in the expansion and intake strokes

		measurement)	<p>on the thrust side and in intake stroke on the anti-thrust side.</p> <ul style="list-style-type: none"> • OFT on the piston ring is more affecting by lubricant availability than the engine speed or load.
Thirouard <i>et al.</i> (1998)	Firing single diesel engine with wide quartz windows on the cylinder liner.	<ul style="list-style-type: none"> • Laser Induced Fluorescence (Nd YAG laser). CCD camera for acquiring signal. 	<ul style="list-style-type: none"> • The top ring up-scraping was responsible to some degree for oil accumulation on the crown land at certain engine operation and is believed that more piston dynamic tilt at higher engine speed is a contribution for this mechanism. • The oil flow around the ring pack was primarily due to inertia of the oil in the axial direction and oil dragging by gas flow in the circumferential direction.
Wong <i>et al.</i> (1999)	Modified single cylinder spark ignition engine with six silica windows. Motoring and firing test carried out.	<ul style="list-style-type: none"> • Laser Induced Fluorescence. 	<ul style="list-style-type: none"> • The measured OFT increases in general with viscosity and found to be in good agreement with simulated results. • OFT increases with the square root of the sliding speed. • Ring dynamics and gas can affect oil distribution for various speeds and loads.
Seki <i>et al.</i> (2000)	Small single diesel engine.	<ul style="list-style-type: none"> • Laser Induced fluorescence. Multipoint measurements. 	<ul style="list-style-type: none"> • Oil control ring OFT increases significantly in comparison with theoretical value in the early stage of downstroke. • Reduction in ring tangential tension increases OFT and decreases where the ring width increases. • A reduction in engine load increases amount of lubricating oil around each ring. Effect of OFT is small.

Table 2.2: Oil Film Thickness Measurements using Optical Methods.

2.3 CAVITATION IN PISTON RING LUBRICATION

Cavitation and boiling may be classified as similar phenomena; they essentially represent a phase change process except that their thermodynamic paths occur differently to each other. That is, cavitation is caused by pressure drop at constant temperature whereas boiling is caused by temperature increase at constant pressure (Brennen, 1995). In the present context cavitation is a naturally occurring phenomenon in the diverging section of the lubricant film in a converging-diverging wedge, such as that between the interface of the piston ring and the liner (Priest *et al.*, 2000). As the fluid film tries to occupy the clearance space with increasing volume in the diverging region, the pressure drops below the saturation pressure in the piston-ring/liner. Owing to the inability of the fluid to sustain large and continuous negative pressure (Cameron, 1971), air/gas cavities or vapor appears. According to Dowson *et al.* (1980) these phenomena can be classified into two types: gaseous or vaporous. Vaporous cavitation will occur when the pressure of the liquid lubricant is reduced to its vapour pressure, at which point evaporation or boiling will ensue. Gaseous cavitation can result when the lubricant pressure falls to the saturation pressure and dissolved gases are emitted from the solution, as mineral oil normally has about 8-15 % by volume of dissolved air (Dellis and Arcoumanis, 2004; Swales, 1974). A pressure reduction below ambient conditions may either encourage suspended bubbles of gas to grow or draw gas into the lubricating film from an external source such as the atmosphere; this form of gaseous cavitation is called ventilation.

The most important physical sub-process of phase change is nucleation, namely the creation of precursors of the new phase in the old one. In an effort to understand nucleation physics, a necessary distinction should be made regarding the condition of the liquid undergoing the aforementioned process and the containing system. In pure liquids contained in ideal environments, the nuclei that can initiate phase change are microscopic voids caused by thermal motion within the liquid. This kind of nucleation is termed homogeneous. Contrary to this, in most engineering systems phase transition occurs due to contamination associated with the presence of other types of nuclei which are unrelated to the thermal motion of the liquid but occur as a result of the existence of weaknesses between the liquid and a solid interface. This solid interface can be either

the wall of the container or small impurities suspended in the liquid. It is for this reason that this kind of nucleation is termed heterogeneous.

The phenomenon of cavitation was first observed by Newton in 1669 (Arcoumanis *et al.*, 1995). It was rediscovered independently by Skinner (1903) where its occurrence was observed in an experiment determining the refractive index of a liquid, and investigated in depth. Newton's observation was that the inflow of the liquid to fill the vacuous space must depend in some way on its viscosity; the higher the viscosity, the larger is the vacuous space. The author thought that cavitation was an advantage because spaces formerly filled with viscous material were then filled with something having small viscosity. This will reduce friction due to viscous shear and this might have been the case for perfectly smooth surfaces. However, for imperfectly smooth surfaces this could be detrimental, for it would result in direct contact and would enhance friction due to surface asperities.

Taylor (1963) pointed out that two physically diverse forms of cavitation can take place. One of them is bubble cavitation where surface tension plays no role in it and the other, which is akin to hydrodynamic separation, relies essentially on surface tension. Castleman (1936) was the first to extend and to give a hydrodynamical explanation of Reynolds' theory to the lubrication of piston rings in an engine. He made the assumption that oil cannot withstand absolute tension. Due to the existence of cavitation, there are two problems in solving the Reynolds equation governing film lubrication. The first problem is specifying the pressure at the cavitation boundary; the second is locating its position. Although there is consensus about the pressure at the cavitating interface, locating the cavitation boundary requires an extra condition; it is the choice of this extra condition that has resulted in the historical divergence of the approach followed by many researchers in this field. Boundary conditions such as separation (including Coyne and Elrod) and Floberg are considered to be the preferred methods for low load cases where Reynolds cavitation and fluid reformation may be applicable. Arcoumanis *et al.* (1997), Richardson and Borman (1992) and Priest *et al.* (2000) have demonstrated that the boundary conditions applied when solving Reynolds equation for the piston ring/liner wall can have different results on the analysis and thus the prediction of hydrodynamic pressure profiles, lubricant film boundaries, lubricant

film thickness, oil flow and friction could vary significantly. Hydrodynamic profile and film shape with alternative cavitation models is shown in Figure 2.1.

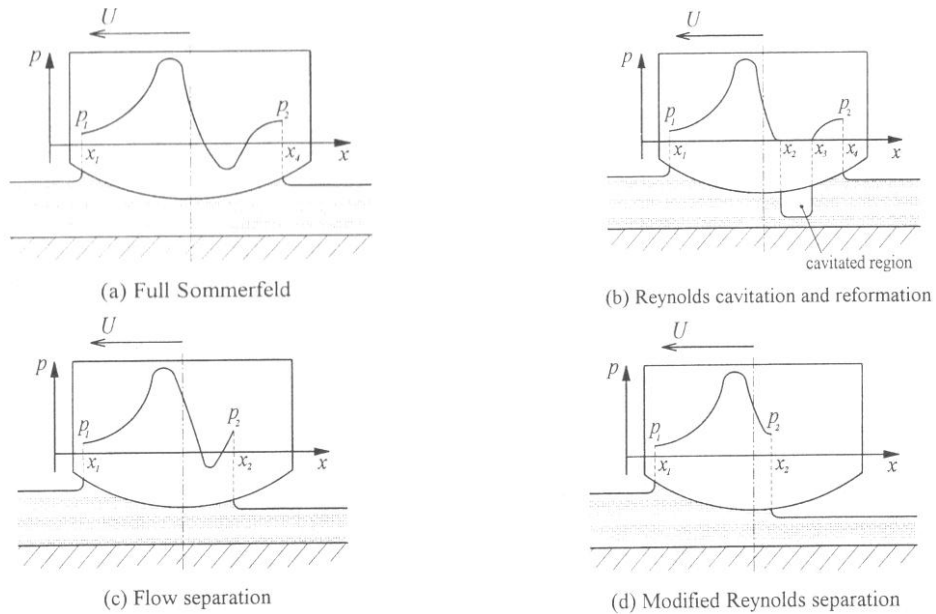


Figure 2.1 Hydrodynamic pressure profile and film shape with alternative cavitation models (Priest et al, 2000)

Sommerfeld proposed a simple solution of Reynolds equation, often referred to as ‘Full Sommerfeld’ condition, in a journal bearing. When the lubricating equation is solved the oil builds up a positive hydrodynamic pressure in the converging section of the ring where as in the diverging one a negative or sub atmospheric pressure is developed. However, it is well known and has been agreed by many researchers (Cameron, 1971) that fluid is unable to sustain this large and momentary negative pressures and thus it will eventually rupture or cavitate. Gümble (1921) recognized this and truncated the negative pressure in the Full Sommerfeld condition to zero gauge thus producing a cavitating region. This modification is also known as ‘Half Sommerfeld’ condition. Unfortunately, this boundary condition does not satisfy the law of mass continuity. Swift (1932) and Stieber (1933) independently arrived at the formulation of the Reynolds cavitation condition (figure 2.1b) whereby the boundary condition is considered at the liquid rupture due to flow stability and flow continuity, respectively. The lubricant is assumed to flow between the air cavities but the details pertaining to the cavity-fluid interface are ignored. They suggested that at the cavitation boundary the pressure gradient in the direction of the flow is zero and the pressure is equal to that of the cavity. Another form of the Reynolds equation has been proposed by Dowson *et al.*

(1979) whereby flow separation occurs instead of cavitation. An alternative model used in piston ring lubrication which is referred to as modified Reynolds cavitation (Priest *et al.*, 2000) has been proposed which relies upon the saturation pressure of the dissolved gas in the lubricant being equal to the outlet.

Hamilton *et al.* (1966b) conducted an experiment in an optically flat rotor seal to allow the visualization of the interfacial film under the influence of various speeds and loads. It was observed that the film was interrupted and was broken into several long and narrow cavitation streamers. The authors found that the locations at which some streamers appeared to initiate and end unexpectedly corresponded to micro-irregularities on the stator surface and hence concluded that the streamers are linked to surface roughness. They also argued that the pressure is isobaric in the region of a cavity and cannot be lower than the fluid vapour pressure. Moreover, their results from theoretical analysis have shown reasonable qualitative agreement with the experiment.

In order to clarify the behaviour of an oil film between a piston ring and a cylinder liner, Kim *et al.* (1995) used a simulation rig where pressure measurement and visualization were carried out simultaneously. Negative pressures were found in the cavitating region and a maximum tension of 350 kPa was recorded. Based on photographic results the authors grouped the cavities into four periods; (a) a period for generating and developing internal cavities, (b) a period for generating external cavities and coalescence of two series of cavities, (c) a stable period and (d) a decay period. They also noted that at higher revolution speeds internal cavities occur earlier, the number of cavities decreases and the width of the cavities increases. The researchers concluded that a negative pressure involving tension develops before the oil film ruptures. The tension is released with the generation of internal cavities but the negative pressure is still maintained. External cavities are generated by suction from the rear side of the ring. Washio *et al.* (2003) investigated cavitation at the point of separation on a smooth cylindrical wall in a hydraulic oil flow and found that cavitation starts with a microcavity and the tensile force working on the point of separation increases with fluid velocity. It was observed that the newly born cavity does not stay on the wall but grows, splits and vanishes within a short period after generation.

Dellis and Arcoumanis (2004) used an idealised test rig that simulates the lubrication condition between a piston-ring and the cylinder liner in reciprocating engines which was subsequently modified to allow oil film visualization with a charged-coupled device (CCD) camera. The authors identified four types of cavities that may develop under the piston ring throughout the stroke:

- (a) fern cavities,
- (b) fissure cavities,
- (c) String cavities,
- (d) Bubbles.

The formation of strings begins as the lubricant oil inside the ferns is divided into several small liquid fingers separated by air or oil vapour which grow in length as the axial velocity of the liner increases. It was observed that load affects the initiation of the cavities at the beginning of the stroke; the higher the load, the earlier in the stroke the fern cavities appear. Contrary to Kim *et al.* (1995), the present authors found out that the higher the speed, the later in the stroke the fern cavities appear and the larger their size; these findings are similar to the work of Skinner (1903).

To control the physical mechanisms leading to cavitation inception, it is important to first classify and understand them. A wealth of literature has been reported for the theoretical modelling and experimental verification of cavitation in journal bearings (Cameron, 1971; Elrod, 1979; Floberg, 1973). In contrast, little attention has been paid specifically to the nature of cavitation in the piston-rings conjunction (Arcoumanis *et al.*, 1995; Dellis and Arcoumanis, 2004; Priest *et al.*, 2000). Although the basic principle of cavitation formation is very similar for both cases, there are several important differences. The large majority of journal bearings (used in engineering applications) have a continuous rotating motion. This encourages the film formation, diminishing friction losses and protecting the two sides of the lubricated conjunction from direct interaction and consequent wear. On the other hand, during engine operation, the piston reciprocates from one dead centre to the other and consequently, the entrainment velocity of the oil in the lubricated conjunction fluctuates over a broad range. It is zero at the dead centres and it reaches a maximum between the two positions. The load applied on the ring-liner conjunction is directly proportional to the pressure behind the ring. This is usually a fraction of the pressure in the combustion

chamber, and therefore, it varies extensively during the engine cycle, reaching a maximum near the top dead centre. Additionally, during the reciprocating motion of the piston, a very thin film of oil is left behind the rings. Near top dead centre, the film is subjected to very high temperatures as it is exposed to the combustion gases. Therefore, it is expected that localised oil degradation can take place. During the following cycle, the degraded oil mixes with fresh oil and this can have a dramatic influence over the lubrication regime. Thus, the ring-liner conjunction operates in inherently transient lubricating conditions, and therefore, the importance of understanding the mechanisms that govern oil film formation/cavitation cannot be underestimated.

2.4 OIL FILM PRESSURE

Pressure measurements are even more important when combined with oil film thickness measurements to characterise the lubrication process. It has been demonstrated (Dellis and Arcoumanis, 2004; Kim *et al.*, 1995) that they can be used together to identify cavitation in the lubricant film. The measurement of pressure within cavities presents particular problem especially when measured with conventional manometers where vapour locking can take place. The use of modern transducers has made pressure measurements in piston ring/liner assemblies possible and, on top of that they provide sufficient resolution for accurate characterisation of the film. However, there are very few papers in the open literature describing the measurement of pressure between the piston rings and the liner conjunction. One of the main reasons for this is the hostile nature of engines which render its application quite difficult.

Brown *et al.* (1975) have demonstrated that it is feasible to measure the hydrodynamic pressure under the ring surface with a miniature piezoelectric transducer. Pressure measurements and oil film thickness were recorded simultaneously. From their results has been possible to detect the occurrence of oil starvation and the pressures postulated by Castleman (1936) have been observed directly. Brown and Hamilton (1977) measured the oil pressure in the ring pack alongside the oil film thickness in a motored diesel engine. Discrepancies between the theoretical and experimental pressure measurements were found and the authors argued that oil starvation at the inlet of the ring could be responsible for this. In a further experiment (Brown and Hamilton, 1978)

the authors recorded a peak value of -780 kPa in the diverging section of the ring, after top dead centre, which is far in excess of the values normally assumed to be needed to produce cavitation. The observed cavitation was quite reproducible and an outlet pressure of -100 kPa was measured, corresponding to the oil vapour pressure. It is noted that oil film thickness continued to fall in the cavitating region.

Dellis and Arcoumanis (2004) have successfully implemented a silicon chip miniature transducer to record pressure measurements of the oil films in their idealised test rig. They found out that the lubricant film thickness has a major influence on the cavitation behaviour, which in turn affects the shape of the hydrodynamic pressure profile in the entrainment direction and consequently the ring pack's load carrying capacity. Also the use of the transducer has provided both qualitative and quantitative pressure data which proved to support the flow visualization results, while its robustness and good repeatability offer promise for its application to the piston-ring pack of production engines. Dellis (2005) in this experimental work on the piston ring, he pointed out that the pressure level in the oil film varies in relation to changes in the effective width of the ring. Han and Lee (1998) mentioned that in their experimental research they discovered that not all the entire surface of the ring is soaked with oil and estimated that the mean effective width is between 30-40 % (Brown and Hamilton, 1977; Richardson and Borman, 1992) of the whole ring width. Figure 2.2 provides an insight of the effective piston ring width and how it changes with varying speed and load.

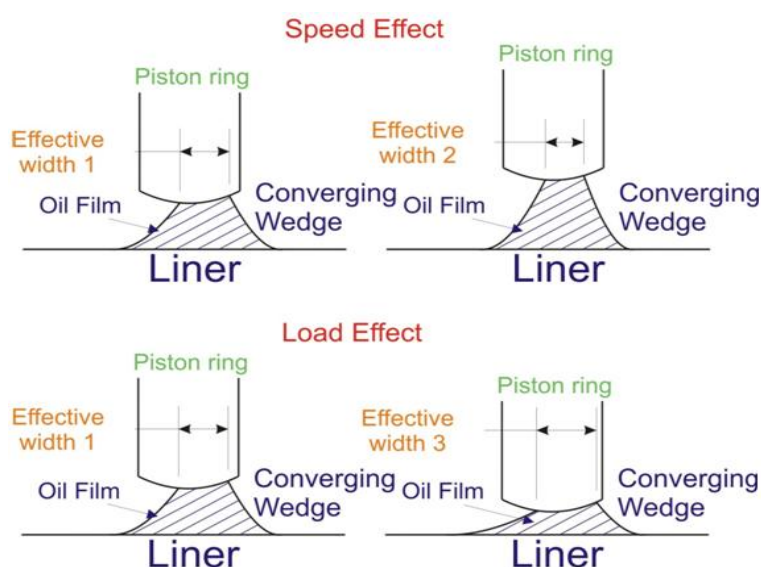


Figure 2.2: Speed and load effect on effective piston ring width (Dellis, 2005)

2.5 PREVIOUS WORK

In this section, the previous work carried out within City's research group, previously based at Imperial College, is highlighted. Ostovar (1996) developed a single-ring test rig to simulate under idealised conditions the lubrication action between the piston ring and the cylinder liner in a reciprocating engine. The test rig allowed the measurement of oil film thickness, using the capacitance method, and friction measurement between the ring and liner to be recorded simultaneously. A numerical method had been proposed for the prediction of the lubricant film parameters which allows the Swift-Stieber, separation, Coyne and Elrod and Floberg boundary conditions to be employed by simply changing a in the equation set; the model was assessed against the results obtained in the test rig. A cavitation delay mechanism was found to be responsible for the thinner film, after reversal points of reciprocation, than that predicted by the Reynolds boundary condition. Furthermore, the surface roughness models were found to be very sensitive to the roughness parameters used. A dual Laser Induced Fluorescence and interferometric technique had also been developed which, in theory could permit the dynamic calibration of the oil film thickness in an engine.

Duszynski (1999) employed the Laser Induced Fluorescence technique developed by Ostovar (1996) in a firing four-stroke diesel engine but the interferometric technique proved to be inadequately accurate to be used for this application. Optical fibres were installed in the liner and a static calibration method was developed. He performed a quantitative study of the temperature effect on the calibration coefficients of all the engine oils tested with a custom made calibration apparatus. It consists of 20 x 20 x 100 mm block of fused silica on which the calibration standard was in the form of grooves of known depth. The selection of the material was made on the base of its physical properties and, in particular, its low thermal expansion. The grooves etched into the surface of the block were intended to be incremental in depth between 2 and 10 μm , in steps of 2 μm . From the early engine tests, it was found that the oil film thickness under the piston rings varied within that range. Various oils were examined, varying in additive concentration and viscosity. At top dead centre, chemistry-related effects were found to be more significant than those related to viscosity. The Laser Induced Fluorescence technique was later applied to a two stroke engine and the results showed higher oiling rates associated with thicker films.

Pyke (2000) carried out experiments to characterise piston ring lubrication in both a firing diesel engine and in an idealised test rig. Oil film thickness was measured on the liner by employing the LIF technique. Sets of experiment were carried out in the engine at different operating conditions. Repetitive measurements of oil film thickness on the liner did not prove to be satisfactory except on the ring where results were found to be more consistent. Complications have arisen in comparing lubricants due to issues related to the calibration of the LIF technique. Despite the difficulty in some cases to decouple the various parameters, the expected trends in the film thickness variation with engine conditions were confirmed. Experiments at engine start up were also conducted where the behaviour of the oil film thickness was analysed. The build up of the oil film was identified to be a four- stage process and the effects of cylinder pressure, engine speed, liner temperature and lubricant availability on the film thickness were all visible during the first two hundred cycles. The test rig built by Ostovar (1996) was modified by inserting an optical fibre where the LIF technique was used to identify cavitation under the ring for a range of lubricants. However, uncertainty in the variation of cavitation along the ring has made comparison difficult. An investigation about the surface roughness orientation and its effect on friction was also carried out. The results clearly show that transversely orientated roughness produces a reduction in friction when the lubricant is mixed and while for hydrodynamic conditions the opposite is true.

Dellis (2005) utilised the purpose built test rig to measure the oil film thickness using both the capacitance and the LIF techniques. Various methods for calibrating the LIF technique were employed. A dynamic technique has been proposed whereby a groove of known depth on a piston ring specimen is used to provide in-situ dynamic calibration, circumventing the uncertainties in static calibration of oil film temperature and properties variation during the cycle. A micrometer-based static calibration method has been compared directly to the dynamic one. The power output of the fibres had been taken into account as well as the background noise and resident voltage on the fluorescence detector. However, none of the above mentioned methods proved to be satisfactory in comparison with the capacitance's results. Therefore, a ring profile fitting was being used as the standard calibration method. Parametric studies on oil have been conducted where the oil film thickness, friction and oil film pressure measurements were measured and compared for different speed, load, temperature, lubricant type and

piston-ring geometry. The test rig has been modified in order to provide optical access, between the specimen ring and the liner, to visualise the onset and development of cavitation with a CCD camera. Different types of cavities had been identified which already have been discussed above in section 2.3. The single cylinder diesel engine used by Pyke (2000) has been modified to incorporate quartz windows for visualisation experiments. The tests were run at motored conditions where similar forms of cavity to that of the test rig were identified and an approach towards their formation has been suggested. On the other hand, the lack of pressure measurements in the engine does not allow confirmation of the presence of cavity provided by the imaging results alone and this raises some important questions. Although the top compression ring operates under starved lubrication conditions, oil droplets were captured by the camera emerging from the ring side clearances that contribute to oil transport. Higher magnification images provided further evidence and these were compared with previous engine research on oil transport by other investigators.

2.6 SUMMARY

In this chapter, an attempt has been made to provide an extensive literature review in order to provide the foundation for the understanding and analysis of the subsequent results. An overview of the different techniques that have been developed, by different investigators, to measure the oil film thickness between the piston rings and cylinder liner of reciprocating engines has been presented. Some of the techniques and results have been tabled in order to get a coherent insight of the lubrication process. Subsequently, the phenomena related to cavitation in the lubricant have been addressed and their effects in the oil film thickness, albeit brief, have been analysed. It has been argued that pressure measurements in the oil film do provide evidence of cavitation and hence deemed to be an important task in this current research.

Finally, the past research carried out within the research group has been summarised and their results have been discussed in brief. It should be clear from the above summary that despite the wealth of material concerning the subject of piston ring lubrication, there is much that remains uncertain due to the quite complex nature of the process.

Chapter 3

EXPERIMENTAL SYSTEMS & TECHNIQUES

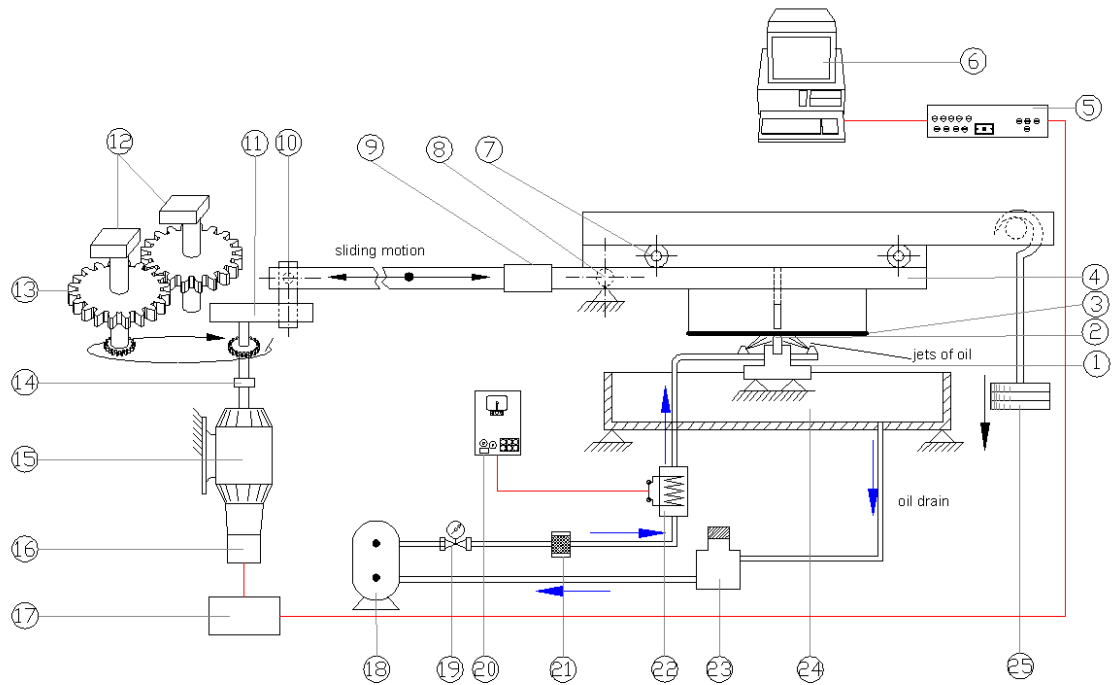
3.1 INTRODUCTION

The experimental programme is divided in two parts. The first part considers an idealised test rig which simulates the lubricating conditions between the piston rings and the cylinder liner in a reciprocating engine. The advantage of this approach is that the tribological conditions can be isolated from the plethora of physical phenomena occurring in the piston-liner assembly under firing conditions such as ring and piston dynamics, thermal and elastic deformations of the rings, circumferential ring variations, lubricant degradation and blow by. Additionally, a test rig approach allows easy access to the ring-liner interface and, therefore, a better understanding of the lubricant characteristics. The second part consists a of modified single cylinder diesel engine where quartz windows have been inserted to visualise the lubricant film characteristics between the piston-ring liner interactions. Moreover, pressure measurement stations have been implemented at TDC, mid-stroke and BDC.

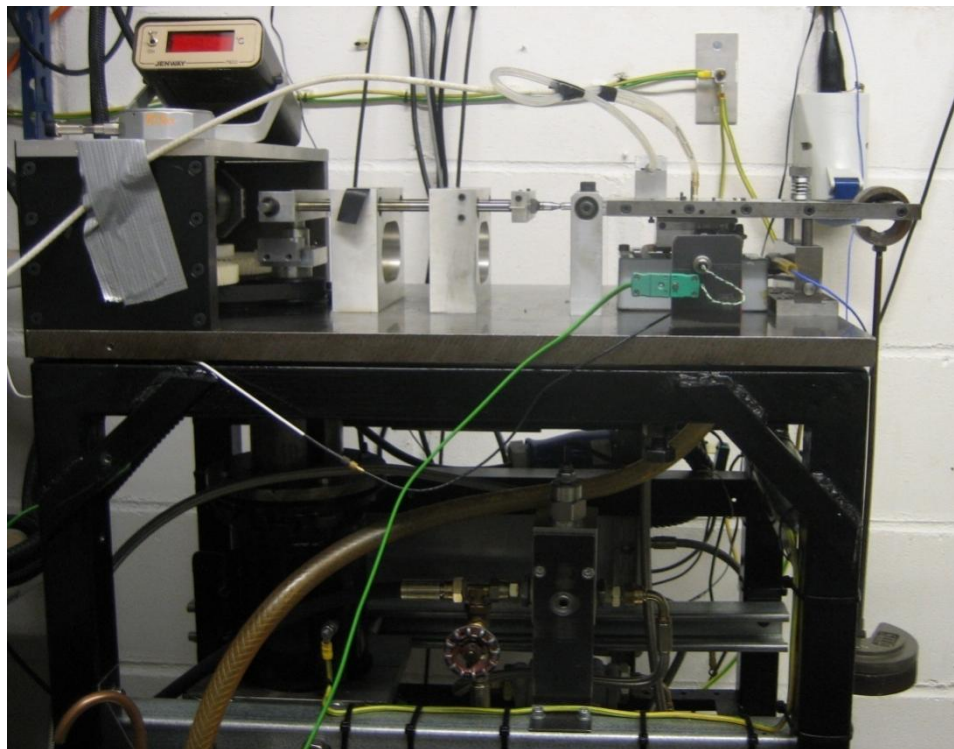
3.2 EXPERIMENTAL SET-UP: TEST RIG

Figures 3.1a and b show a schematic representation and photographic overview of the test rig respectively. A flat horizontal plate (No: 3 in Figure 3.1a) reciprocates above a stationary ring specimen (2). The liner is made up of heat treated gauge steel, representative of the cylinder liner, and secured in an aluminium block (4). Controlled load (25) is applied on the ring-liner contact by a loading arm. Low friction between the loading arm and the liner specimen is ensured by a set of high precision low friction roller bearings (7). The reciprocating motion of the liner is obtained using a variable speed DC electric motor (15), which is mechanically isolated from the rig to minimize any vibrations. The motor is coupled to the “crank guide linear bearing” (10), through a

crank mechanism (11). This arrangement converts the rotation of the crank mechanism into the reciprocating motion of the liner.



(a)



(b)

Figure 3.1: Test rig (a) Schematic (b) Photographic overview

Isolation of the shaft is achieved by a flexible neoprene coupling (14). In order to maximize the speed stability of the system and reduce vibrations, provision is made to increase and adjust the system's inertia using a pair of contra-rotating weights (12) driven from the shaft and coupled together by a pair of low noise nylon helical gears (13). To improve the measurement accuracy, the electric motor's angular velocity is monitored by a shaft encoder (16) and the corresponding linear sliding motion of the liner is computed by considering the mechanism geometry. The shaft encoder, with a resolution of 2000 pulses per revolution from the process unit (17), allows measurements every 0.18 degrees. The liner holder is connected to the drive mechanism by a removable connecting joint (9). Access to the ring specimen is allowed by removing the joint and rocking the liner around the pivot (8). The ring specimen is fixed in the ring holder which is further placed in the ring assembly (1), that is attached to the base. The ring holder sits on a knife edge which allows it to tilt in the transverse direction ensuring good conformity between the ring and the liner. An electric pump (18) circulates the oil firstly through a Parker oil filter (21), secondly through a heat exchanger (22) and then feeds it to the ring/liner interface by eight jets located on both sides of the ring, ensuring a fully flooded area. The oil which is stored in a tank (23) is collected in a bath which is then drained back to the tank (23); its flow is controlled by a pressure regulator (19). A K-type thermocouple monitors the temperature oil sprayed onto the ring-liner interface. The oil temperature can be increased from room temperature to 80°C via a controlled box (20); during operation the oil temperature exhibits a variation of $\pm 0.5^\circ\text{C}$.

To investigate the effect of contact load on the specimen ring, the applied weights (25) can be changed. Arcoumanis *et al.*(2000) showed that the load on the ring can be expressed as a function of speed as:

$$W(\theta) = \frac{0.1830g + 0.25gm_h + 0.5024g(0.089 - R_{crank} \cos \theta) + 5.78 \times 10^3 R_{crank} \cos \theta \omega^2(\theta)}{(0.088 + 0.5b)B} \quad (3.1)$$

where $W(\theta)$ is the normal force per metre on the ring, g is the acceleration due to gravity, m_h is the mass applied on the hanger, R_{crank} is the crank radius, $\omega(\theta)$ is the crank angular velocity, b is the ring width and B is the ring length.

3.3 TEST RIG INSTRUMENTATION

3.3.1 CAPACITANCE TRANSDUCER

The capacitance transducer is used to measure the oil film thickness. The probe contains a central metal core surrounded by a plastic insulation cylinder. This in turn is surrounded by a metal cylinder acting as one of the electrodes. A further layer of insulation surrounds the outer electrode and, for protection, the whole probe is wrapped in a steel cylinder. The capacitance is measured by a Capacitec unit 3101-SP; this device converts the signal and outputs a voltage that is being recorded by the data acquisition system.

Figure 3.2 shows a schematic representation of the capacitance probe setup. The probe holder, made of high tensile steel, is bolted on a powerful Eclipse E909 magnet. This overcomes the influence of the constant and strong vibrations coming from the electric motor. The probe is placed parallel to the specimen ring at approximately 30 microns just below the flat plate attached to the liner, as shown in the schematic below.

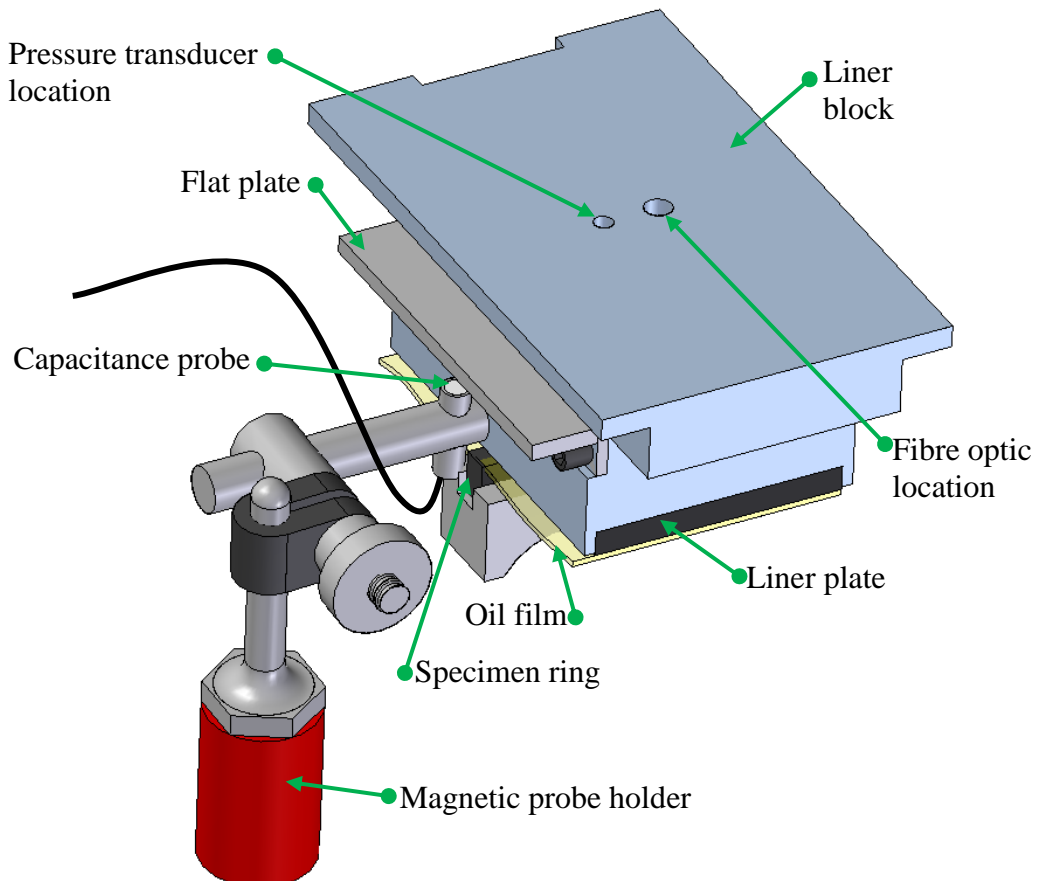


Figure 3.2: Schematic of test ring with capacitance probe

Calibration of capacitance probe

The calibration method of the capacitance described by Pyke (2000) and Dellis (2005) was carefully considered and adapted. The liner was set at mid stroke and a dial gauge, providing reading in μm , was placed just under the middle of the liner next to the ring specimen as shown in Figure 3.2 and Figure 3.3 . A flat gauge that provided a flat surface was positioned under the calibration screw that lifts the liner. The screw is then slowly adjusted to raise the liner into $2 \mu\text{m}$ increments which is the resolution of the dial gauge. The data was fitted in a quadratic curve and adjusted until the best correlation is obtained. The calibration curve is the same for all the parametric oils studied. Figure 3.4 shows the calibration curve.

Hence the oil film thickness (OFT) for all the oils tested can be calculated from equation (3.2):

$$\text{OFT}(\text{microns}) = 0.0000031273(\text{mV})^2 + 0.0260702325(\text{mV}) \quad (3.2)$$

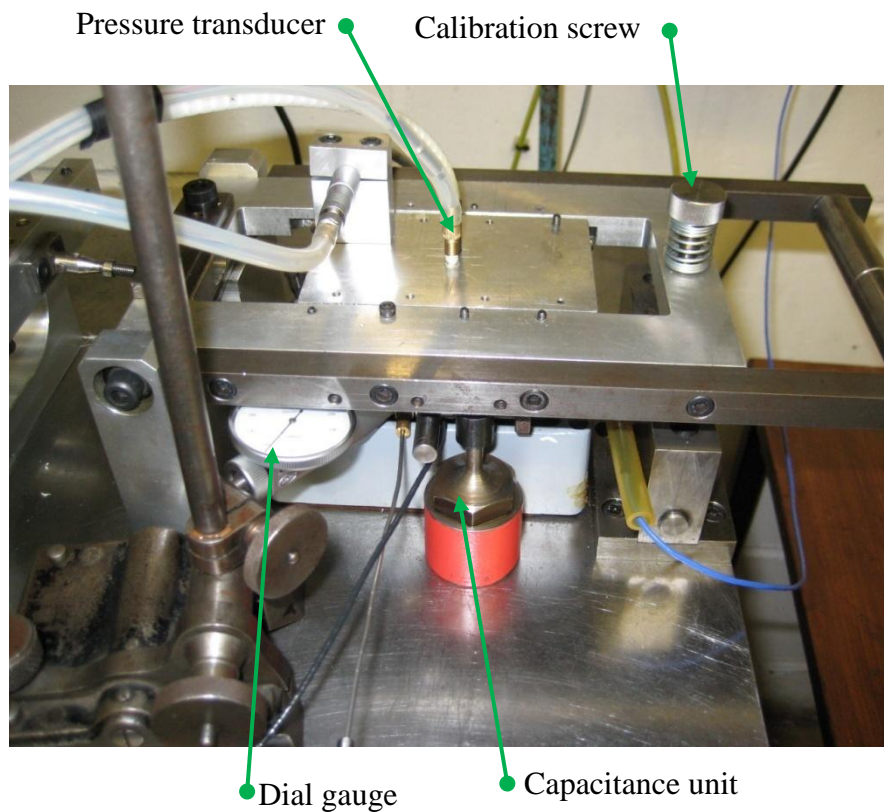


Figure 3.3: Calibration setup for capacitance probe

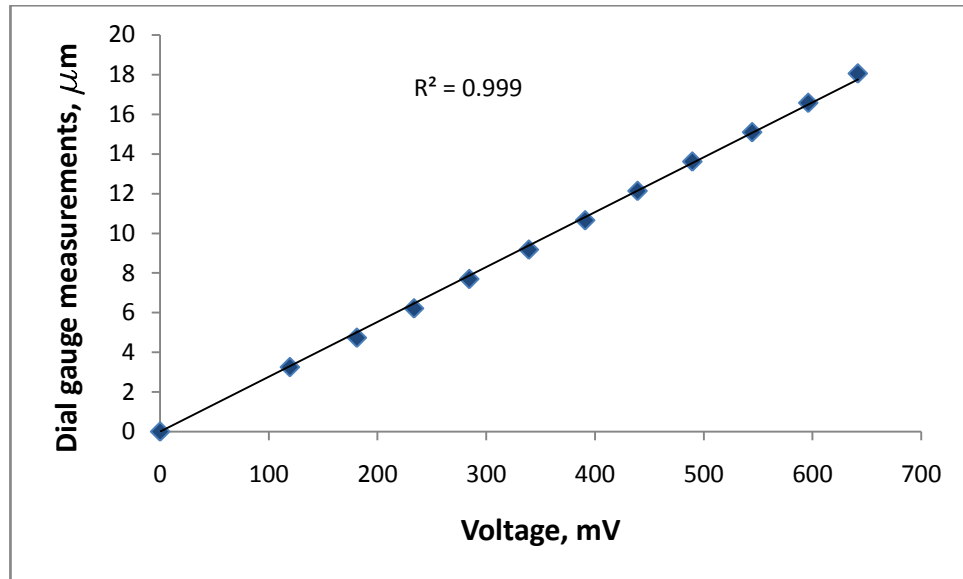


Figure 3.4: Calibration of capacitance probe

The test rig is run at a low speed of around 20 rpm without any oil. A load of 3 lbs is imposed at the edge of the liner holder to squeeze out any remaining oil as far as possible thus ensuring dry lubrication between the liner and specimen ring (the load applied is assumed to cause negligible distortion). Figure 3.5 shows the average output of the capacitance for dry lubrication (the voltmeter has not been initialised to zero prior to taking the readings). Clearly it can be seen that there is some variation over the cycle owing to the offset of the probe to the flat plate. To eliminate this effect from the results, the variation is subtracted from each measurement. This also eliminates any imperfection in the manufacturing of the flat plate or in the flatness of the liner.

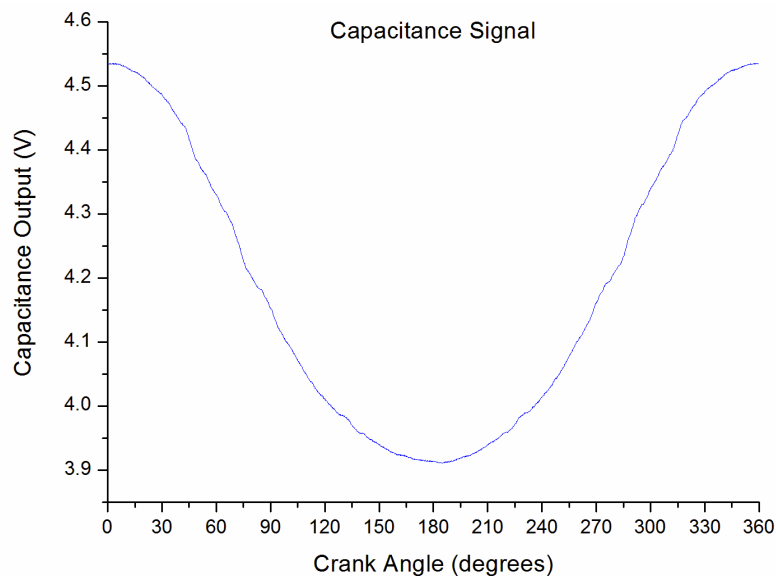


Figure 3.5: Capacitance output for dry lubrication

3.3.2 FRICTION TRANSDUCER

The device used to measure friction is a piezoelectric force transducer, model PCB 208, and a PCB F482A unit amplifies its signal. It is very sensitive to small displacement of the ring assembly caused by the axial friction of the moving liner which resulted in tension or compression of the quartz. Figure 3.6 shows the location of the transducer.

Calibration method

The friction transducer was recalibrated to make sure the device is working properly. The calibration method was adopted to that described by Ostovar (1996). Specially designed pulleys were screwed to both oil feed and oil drainage fittings. Nylon strings were placed in their position as shown in Figure 3.7. Then the ring assembly was either put in compression or tension by placing a calibrated weight on the string on either side (right hand side in compression and left hand side in tension).

Two methods were used for comparison:

- 1) Weight is hung on the lower side of the string and, at the time that is placed on the hanger, the voltage reading is obtained on the multimeter simultaneously.
- 2) This time the voltage on the multimeter is allowed to zero while the weight is still on the hanger, which is the same reading when no weight is hung. This is due to the property of the piezoelectric material of the transducer itself. Then the weight is removed quickly in one movement and the reading is taken simultaneously. This time the reading will indicate the effect of the balancing force.

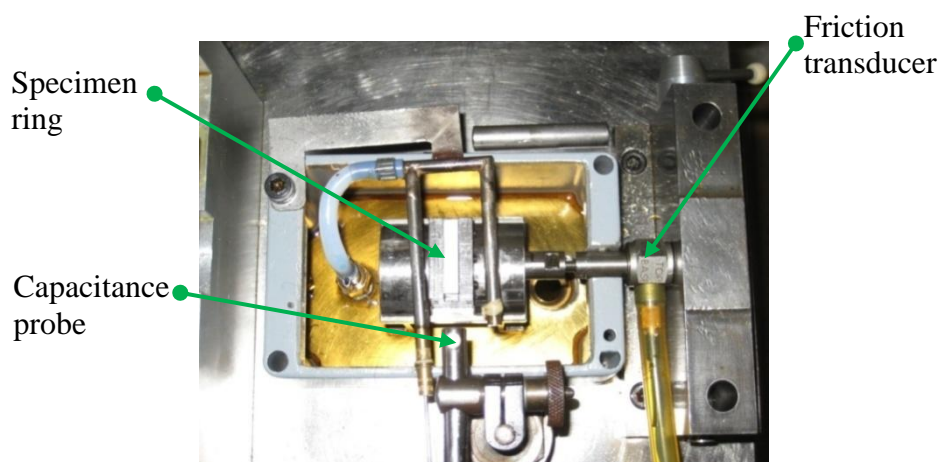


Figure 3.6: Friction transducer

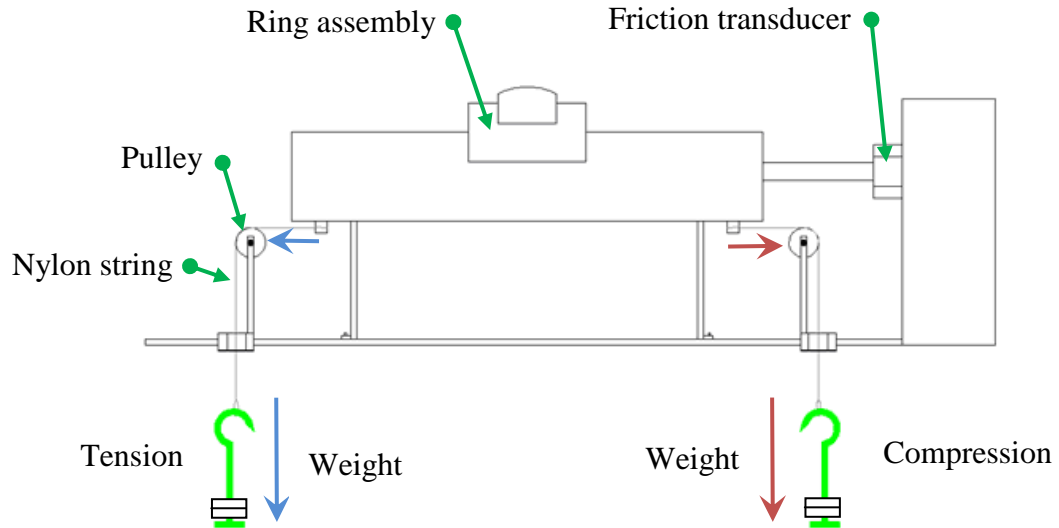


Figure 3.7: Friction calibration setup

To increase the accuracy each method was repeated twice and the graphs in figure 3.8 show the average. The calibration coefficients vary slightly. Both coefficients have been used and then averaged for the experiments.

$$\text{For hung weight: } F(\text{N}) = 30.08V(\text{volts}) + 0.225 \quad (3.3)$$

$$\text{For release weight: } F(\text{N}) = 29.87V(\text{volts}) - 0.350 \quad (3.4)$$

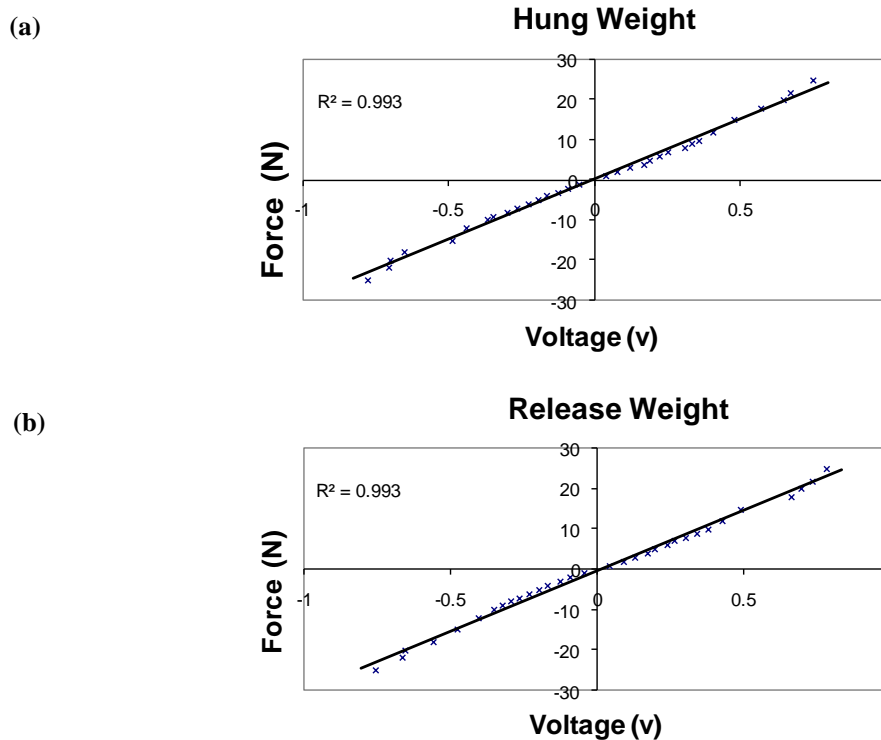


Figure 3.8: Calibration curve for friction transducer (a) hung weight (b) release weight

3.3.3 LASER INDUCED FLUORESCENCE TECHNIQUE

Brief Description

Laser induced fluorescence (LIF) is a process whereby molecules or atoms are excited to a higher electronic energy state via laser absorption and subsequently fluoresce; the intensity of this fluorescence is, in general, a function of the species concentration (number density), and the gas temperature and pressure. Among other things, this fluorescence is linearly dependent on the absorber number density. By virtue of the fact that the energy states of the molecules or atoms are quantized, the spectral absorption regions are discrete; however, for large molecules, the spacing of discrete absorption regions are not observed (only absorption bands are observed). Typically, fluorescence occurs at wavelengths greater than or equal to the laser wavelength.

Fluorescence Techniques

As stated by Haugland (1999) fluorescence is the result of a three-stage process that occurs in certain molecules (generally polyaromatic hydrocarbons or heterocycles) called fluorophores or fluorescent dyes. A fluorescent probe is a fluorophore designed to localize within a specific region of a biological specimen or to respond to a specific stimulus. The process responsible for the fluorescence of fluorescent probes and other fluorophores is illustrated by the simple electronic-state diagram shown in Figure 3.9.

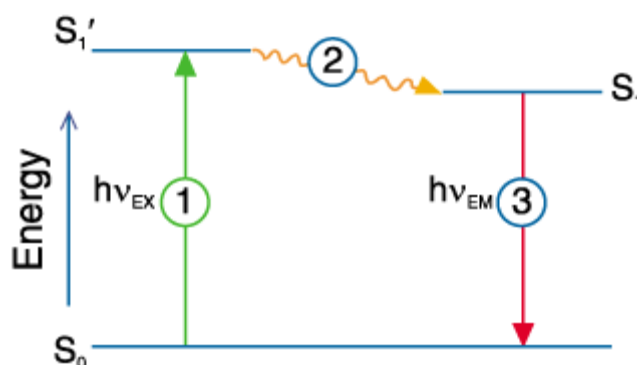


Figure 3.9: Jablonski diagram (Haugland, 1999)

Stage 1: Excitation

A photon of energy $h\nu_{\text{EX}}$ is supplied by an external source such as an incandescent lamp or a laser and absorbed by the fluorophore, creating an excited electronic singlet state (S_1'). This process distinguishes fluorescence from chemiluminescence, in which the excited state is populated by a chemical reaction.

Stage 2: Excited-State Lifetime

The excited state exists for a finite time (typically 1–10 ns). During this time, the fluorophore undergoes conformational changes and is also subject to a multitude of possible interactions with its molecular environment. These processes have two important consequences. First, the energy of S_1' is partially dissipated, yielding a relaxed singlet excited state (S_1) from which fluorescence emission originates. Second, not all the molecules initially excited by absorption (Stage 1) return to the ground state (S_0) by fluorescence emission. Other processes such as collisional quenching, fluorescence resonance energy transfer (FRET) and intersystem crossing may also depopulate S_1 . The fluorescence quantum yield, which is the ratio of the number of fluorescence photons emitted (Stage 3) to the number of photons absorbed (Stage 1), is a measure of the relative extent to which these processes occur.

Stage 3: Fluorescence Emission

A photon of energy $h\nu_{\text{EM}}$ is emitted, returning the fluorophore to its ground state S_0 . Due to energy dissipation during the excited-state lifetime, the energy of this photon is lower and, therefore, of longer wavelength than the excitation photon $h\nu_{\text{EX}}$. The difference in energy or wavelength represented by $(h\nu_{\text{EX}} - h\nu_{\text{EM}})$ is called the Stokes shift. The Stokes shift is fundamental to the sensitivity of the fluorescence techniques because it allows emitted photons to be detected against a low background, isolated from the excitation photons. In contrast, absorption spectrophotometry requires measurement of the transmitted light relative to the high incident light levels at the same wavelength.

Fluorescence Spectra

The entire fluorescence process is cyclical. Unless the fluorophore is irreversibly destroyed in the excited state, the same fluorophore can be repeatedly excited and detected. The fact that a single fluorophore can generate many thousands of detectable photons is fundamental to the high sensitivity of the fluorescence detection techniques. For polyatomic molecules in solution, the discrete electronic transitions represented by $h\nu_{\text{EX}}$ and $h\nu_{\text{EM}}$ in Figure 3.9 are replaced by rather broad energy spectra called the fluorescence excitation spectrum and fluorescence emission spectrum, respectively. The bandwidths of these spectra are parameters of particular importance for applications in which two or more different fluorophores are simultaneously detected. With few exceptions, the fluorescence excitation spectrum of a single fluorophore species in dilute solution is identical to its absorption spectrum. Under the same conditions, the fluorescence emission spectrum is independent of the excitation wavelength, due to the partial dissipation of excitation energy during the excited-state lifetime, as illustrated in Figure 3.10. The emission intensity is proportional to the amplitude of the fluorescence excitation spectrum at the excitation wavelength (Figure 3.10).

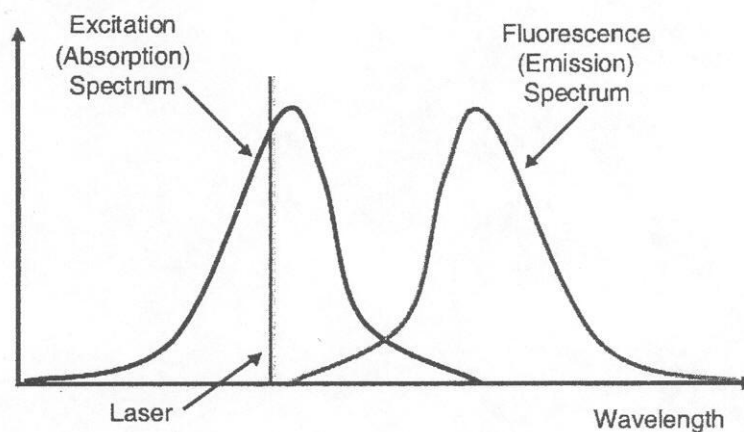


Figure 3.10: Excitation of a fluorophore at three different wavelengths

Theory: Basic LIF

Consider a rectangular differential volume of fluid (oil) with a cross-sectional area A and length Δx irradiated by light (laser) normal to area A with uniform intensity I_e . The total fluorescence (F), emitted by this differential volume is given by:

$$F = I_e \varepsilon(\lambda_{\text{laser}}) \Phi \Delta V \quad (3.5)$$

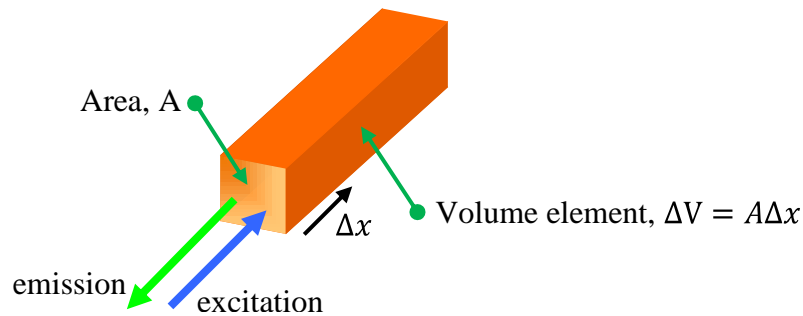


Figure 3.11 Fluorescence of fluid element

From equation 3.5, it is evident that the fluorescence intensity is dependent on:

- (1) the amount of exciting light available to produce molecular transitions to the higher excited levels,
- (2) molar absorpsivity ($\varepsilon(\lambda)$), which determines how much of the incident light per molecule produces actual molecular transitions,
- (3) fluid concentration, which is a measure of the number of molecules present,
- (4) quantum efficiency (Φ), which is the ratio of the energy emitted to the energy absorbed, and is a measure of how much of the energy stored in the higher electronic states is emitted as fluorescence light, when the molecules return to their ground state, and,
- (5) the volume of the element, which is the control volume over which excitation and fluorescence take place.

Dividing equation (3.5) by the area A , the fluorescence intensity normal to the area A is obtained by:

$$I_f = I_e \varepsilon(\lambda_{\text{laser}}) \Phi \Delta x \quad (3.6)$$

If the area A is assumed to be the projected area of a fibre optic cable, it is apparent that this fibre area intensity is proportional to the excitation intensity and the thickness of the fluid element. For very thin film thickness, this representation is quite accurate (Haugland, 1999). If the excitation intensity is known, the fluid film thickness can be directly inferred from the fluorescence intensity. A more accurate representation of the fluorescence phenomena can be obtained from Beer Lambert's law of absorption as shown in the appendix.

LASER INDUCED FLUORESCENCE MEASURING TECHNIQUE

The oil film thickness is measured using a Laser Induced Fluorescence (LIF) technique as used by Pyke (2000) and Dellis (2005). An optical fibre is installed in the middle of the liner surface in order to provide the measurement of the oil film thickness. Figure 3.12 depicts a schematic drawing of the basic concept of the fluorescence technique with fibre optics. A fibre is used to transmit laser light through the liner to the ring specimen. The type of optical fibre used was an Oxford Electronics graded index multimode fibre with a high purity silica core of 1.457 refractive index, doped silica cladding and aluminium coating. The fibre can operate up to the maximum temperature of 400°C. The oil between the ring specimen and the liner wall is illuminated with "blue light" laser ($\lambda = 488$ nm). The illuminated oil then naturally fluoresces in the green spectrum region (around $\lambda = 500$ nm). The fluorescence light is transmitted out of the liner with the same multi-mode fibre. The fibre core diameter is 44 ± 2 μm , which is consequently the spatial resolution of the technique; the outer diameter of the aluminium cladding is 167 ± 5 μm .

Figure 3.12 also illustrates the instrumentation for measuring the oil film thickness in the test rig and the paths of the laser beam and the fluorescent light as they pass through the optical components. The fluorescence light intensity is related to the oil film thickness by the theory mentioned above. The illuminating laser beam is provided by an Argon-ion air-cooled laser with an operating wavelength of 488 nm and an output power of 30 mW. The laser light travels through the optical fibre to the liner; it is emitted from the end of the fibre and illuminates the oil film (bottom of Figure 3.12). The laser beam causes the oil to fluoresce at a different wavelength to the incident one. Then this light travels back through the fibre along with the reflected laser light.

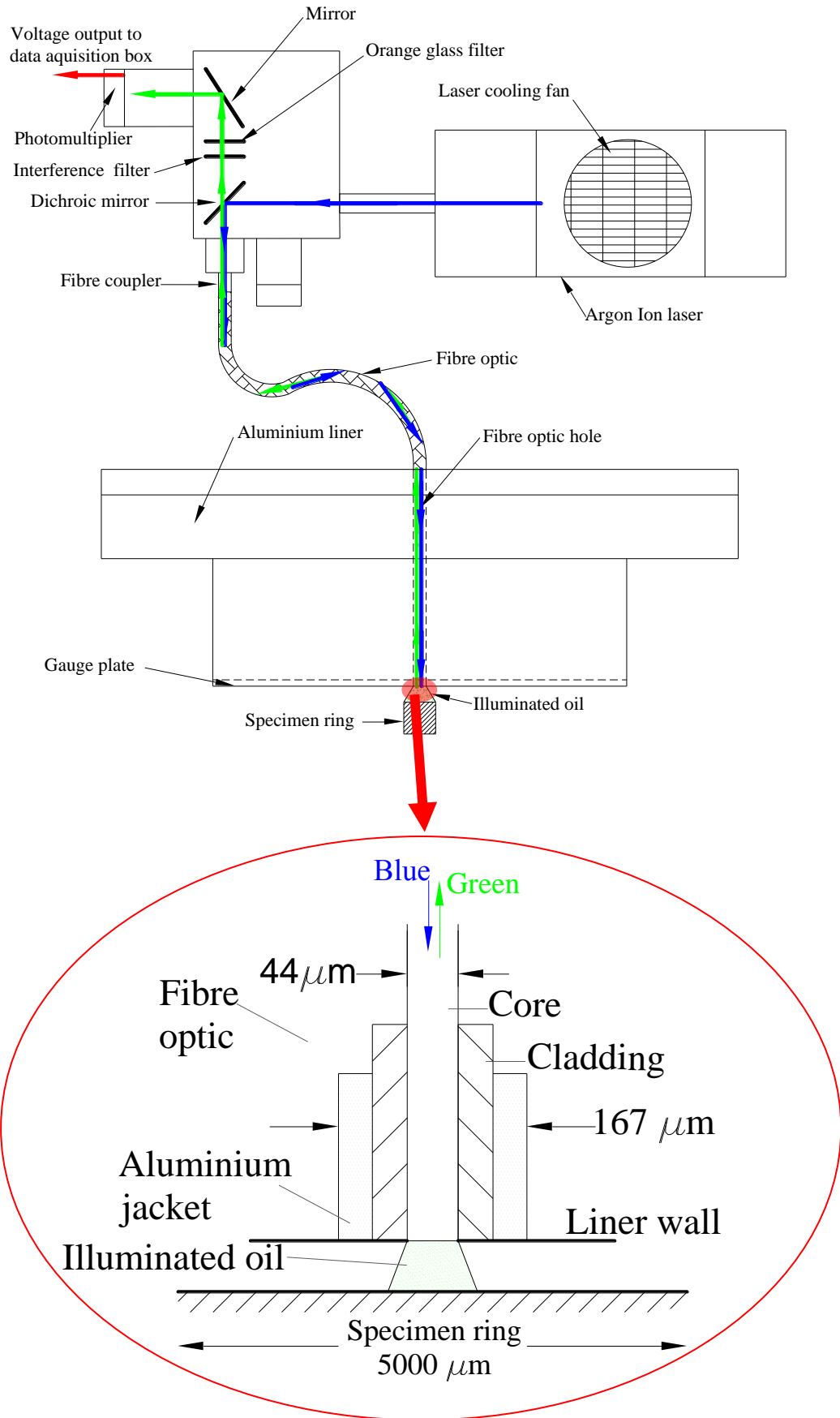


Figure 3.12: Schematic of laser induced fluorescence optical setup

The dichroic mirror is transparent to the green fluorescent light, but blocks the blue laser light and hence removes most of the reflected laser light from the fluorescent signal. However, some of the excitation light does pass through, necessitating its removal by using two further filters. Initially a single OG530 orange glass filter was utilized but, although efficient enough to remove the blue laser light, it has the adverse characteristic of itself fluorescing. To curtail this effect, an interference filter was inserted in front of the orange glass to lessen the intensity of the blue beam reaching the orange filter. Finally the light intensity is converted into a low current output by a photo-multiplier. A DA type socket amplifier converts the current into an amplified voltage signal. The voltage output is stored using the data acquisition system which is described in section 3.3.5. The output voltage from the photomultiplier (PMT) is finally converted into lubricant film thickness using the calibration technique mentioned below.

Calibration of LIF signal

Calculating the oil film thickness directly from the output voltage of the photomultiplier is theoretically possible. However, in practice it is rather complicated since detailed information concerning the optical efficiency of the system and the lubricant fluorescence efficiency are required. Therefore it is imperative to devise a calibration method. One of the major weaknesses using the fluorescence technique has been the calibration process (Hoult *et al.*, 1988; Sherrington and Smith, 1985) since the latter varies with lubricant temperature and composition. It may be useful to examine the methods employed by various researchers in calibrating the fluorescence signal before investigating the current approach. In this section several strategies for calibrating the oil fluorescence measurements are presented and discussed.

Hoult *et al.* (1988) used two independent calibration methods. A bench calibration was performed using lubricant films of constant, known thickness created by inserting shims between optically flat microscope slides. Lubricant was drawn between the slides by capillary action and the slides were clamped and edges sealed. The thickness of the oil film was determined by subtracting the thickness of each microscope slide from the overall thickness of the slide and oil combination. However, the authors recognised the importance of investigating the potential effects of oil temperature and the fluorescence photobleaching phenomena (irreversible photochemical changes undergone by the oil

sample under investigation when exposed to high light intensities) in this calibration method. In a more detailed study Hoult and Takiguchi (1991) demonstrated that the fluorescence quantum yield of a given oil decreased with increasing temperature. Therefore, it is important that the temperature of the oil film at the measurement point must be known if accurate film thickness is to be determined in conjunction with the calibration procedure. The next method, in-situ dynamic calibration, involves discerning a ring contour from the fluorescent intensity measured as voltage versus time during engine operation, as the ring passes through the beam. This voltage profile contour is compared to the ring measured beforehand. The piston-ring profiles were measured, before installation, with a Talysurf profilometer. However, it has been reported by other researchers (Froelund *et al.*, 2001; Phen *et al.*, 1993; Takiguchi *et al.*, 1998) that it is difficult or impossible to follow such an approach owing to oil starvation and ring twist. Nevertheless, Hoult and co-workers found that the in-situ dynamic calibration result was in good agreement to that of the bench static calibration, which validates the overall calibration procedure.

Wong and Hoult (1991) employed an in-situ calibration where three chemically etched marks of known depths were created on the piston to provide distinguishing marks for calibration, in addition to the scraper ring profile. Two grooves were etched on the piston skirt and one on the piston land. The calibration marks were made to provide a dynamic reference for converting the photomultiplier voltage output to oil film thickness. For this procedure the researchers assumed that the grooves are always completely filled with lubricant; then any changes in fluorescence characteristics emitted by the groove sample will be a consequence of changes in the conditions experienced by the oil. The etched marks on the piston skirt would provide almost the same calibration and their repeatability and consistency is checked by comparing the two local calibration coefficients.

Brown *et al.* (1993) carried out an in-situ calibration, similar to the aforementioned authors, by preparing grooves in the piston skirt and top compression ring with depths that have been spark eroded. During the engine running they observed that the oil filling behaviour was random in nature and that usually there was inadequate oil in the contact to support complete filling of the grooves. Thus, when time averaged, the intensity of

the fluorescent signal suggested that the grooves were repeatedly under-filled. They concluded that this procedure was unsuitable for calibration purposes and in order to properly quantify the relationship between the oil film fluorescence intensities and the film thickness they had to opt for a bench-top calibration procedure. The bench-top calibration device has been a modified micrometer consisting of a slot such that when filled with oil it mimicked the wall/piston interface in the engine. The micrometer had a nominal resolution of $1\ \mu\text{m}$ and to replicate the effect of oil temperature on the fluorescence intensity a heating coil was fitted. To prevent the photobleaching effect, the interrogation zone was ensured that it was continuously supplied with fresh oil.

A ring profile fitting for calibration was utilised by Phen *et al.* (1993) but it was subjected to a serious error due to variation of the reflectance over the ring surface and twisting of the ring. Instead a static test rig was used consisting of two lapped steel plates and seven gage blocks of different thicknesses. In this setup, clearances from 5 to $25\ \mu\text{m}$ were produced and fresh oil was supplied into them. The static test rig showed that the calibration was linear. Sanda *et al.* (1993) built two devices for calibration as shown in Figure 3.13. A special gauge made with faced gaps as stairs with four steps by Nickel-plating, each with a height of around $2.2\ \mu\text{m}$, was used to investigate the relationship between the oil film thickness and the PMT output in the range $2\text{-}10\ \mu\text{m}$. For higher film thicknesses $10\text{-}100\ \mu\text{m}$ a micrometer gauge head and an optical flat were used. In general, the authors argued that the fluorescence intensity in both devices was found to have exceptionally good linearity with the oil film thickness.

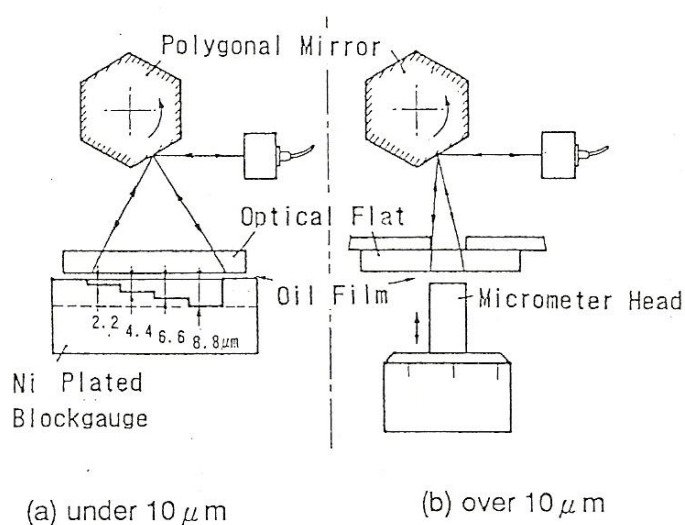


Figure 3.13: Methods of calibration (Sanda *et al.*, 1993)

Inagaki *et al.* (1995) developed a calibration method which measures the oil film thickness distribution between a cylindrical-shaped surface and an optical flat glass. The calibration was found to be in agreement with the theoretical considerations. To calibrate films thinner than $5\ \mu\text{m}$ the authors used a similar device, a special gauge with stepped-plane face, to that of Sanda and co-workers (1993). The system was demonstrated to be capable of measuring thin film thicknesses with an adequate resolution of sub-micron order.

To calibrate the LIF signal, Duszynsky (1999) and Pyke (2000) used a micrometer of high resolution ($1\ \mu\text{m}$). Their static calibration rig (Figure 3.14) consists of an optical fibre mounted flush with the anvil of the micrometer enabling a continuous variation of the oil film thickness. Alongside a hypodermic needle was inserted through which a constant oil supply could be fed. This was considered vital to ensure that the effect of photobleaching is eradicated. To investigate the temperature dependence on the fluorescence light, the micrometer was equipped with a line heater for adjusting the temperature of the oil flowing into the interrogation zone between the anvil and the micrometer.

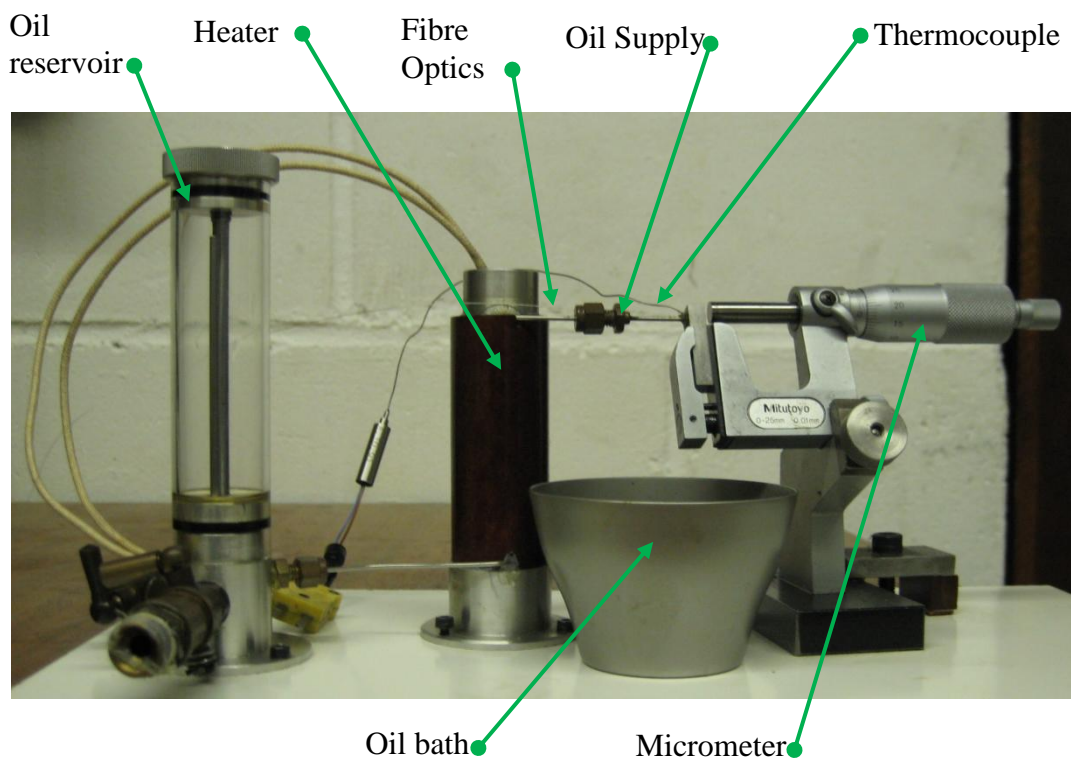


Figure 3.14: The static calibration micrometer

Nevertheless, the calibration of the oil film thickness below 10 μm did prove to be problematic due to the signal being non-linear. It was thought that either the zero position of the micrometer was not set correctly or there was some protrusion of the fibre optic. However, Duszynski (1999) reported that a Talysurf trace showed no protrusion and therefore the former explanation has been assumed. Pyke (2000) suggested that this could have occurred due to the difficulty of squeezing out oil from the small gap and also possibly due to photobleaching. Another possible reason for this occurrence is the one assumed by Takiguchi *et al.* (1998) who also used a micrometer test bench similar to the former researchers. In their experiments they also encountered the difficulty of calibrating oil film thicknesses of smaller magnitude and found that the PMT output plummeted markedly against the continuous oil film when there was an air layer in the oil film, even if the oil film thickness remained practically the same. Therefore it was concluded that the oil film thickness could not be measured accurately if there were some bubbles or an air layer in the oil film. To accurately calibrate the oil film thickness below 10 μm , Duszynski (1999) resorted to another bench-top calibration set-up. A series of grooves 5 mm wide, 5 mm apart with an incremental depth from 2-10 μm in 2 μm steps was etched on a surface fused silica.

Dellis (2005) employed the same static LIF calibration method, a micrometer test rig, as used by Duszynski (1999) and Pyke (2000). In his attempt, calibration of oil film thicknesses less than 5 μm proved to be impossible. The latter thus opted for a dynamic calibration technique. A new specimen ring was produced for use in an experimental set-up in the test rig previously described in section 3.2. A groove of known depth was etched on the surface of the ring where the optical fibre travels above. The dynamic LIF calibration attempt was accomplished with the matching of the groove data, provided by a Talysurf measurement, versus the LIF data acquired during a run-in experimental setup. Dellis (2005) compared the calibration coefficients from the static and dynamic calibration methods and found out a large discrepancy between the two calibration factors. The above comparisons had given ground to the author of the present thesis to speculate on possible reasons behind the large differences between the calibration techniques. Potential reasons include optical efficiency variation for each setup (the one on the liner surface and the one on the micrometer test bench) and temperature variation. Since different fibres were used for each calibration method, Dellis (2005)

investigated the laser power output and his measurements revealed that they differed by 125% at 50 mW laser power and 90% for 30 mW laser power. In the latter case the oil film thickness was also being measured by using the capacitance method. It was found that the dynamic LIF calibration results differ significantly from those acquired by the capacitance method. Hence the calibration of the signal was carried out by using the post-processed data obtained from the capacitance signal (i.e. error - free series of data) the ring profile is fitted to the LIF signal at maximum speed (90° and 270°). The minimum point of the ring is assumed to be that given by the capacitance probe and the calibration coefficient was then adjusted to give a good fit. In order to have more accuracy for the calibration, after the LIF curve is fitted in the best way possible to the ring profile, the distance between the LIF curve edge and the ring profile was measured and recorded. When the calibrated LIF data were used for the graphs, the curves were shifted by the recorded offset. However, this method gave a negative signal in the cavitation region which questioned the integrity of this calibration method.

Dynamic LIF Calibration

To calibrate the LIF signals used for the test rig experiments, the dynamic calibration method proposed by Dellis (2005) has been adopted. This technique consists of a specimen ring where an etched groove of known depth was spark eroded on the surface in a way so that the optical fibre travels above. The drawing of the piston ring specimen with the groove can be seen in Figure 3.15(b). The groove data was acquired using Talysurf surface profilometry around the area of the laser path as depicted in Figure 3.16. The groove has a width of 1.525 mm, a depth of around 15 µm and an R_a value of 1.23 µm. The calibration is carried out by matching the groove data against the LIF data acquired during a purpose made experimental set-up. Before carrying out any LIF calibration, the Argon-ion laser equipment was serviced and the end fibre optics thoroughly polished. Then the fibre was aligned in a way to capture maximum light beam from the laser so as to optimize the laser power output.

The stroke length in the test rig was set at 22 mm for the current experiments. A continuous supply of oil to the specimen ring was always ensured. Then, results were acquired with a 38°C oil temperature at the low speed of 20 rpm; every experiment was repeated for 20 cycles. Subsequently, the LIF data were averaged and a mean LIF curve

from the data was obtained and loaded in an interface written in LabView with the unit of the signal in volts. To convert the signal into units of μm , a calibration constant has to be found in units $\mu\text{m} / \text{volt}$. In the calibration interface the mean LIF curve, from the same specimen ring, is superimposed on the groove data. If the depth of the groove corresponds to the same depth as the LIF signal, the right calibration has been found assuming the groove is fully flooded with oil. The calibration coefficient derived is graphically illustrated in Figure 3.17. To investigate the effect of temperature on the LIF signal, the matching was repeated for every experimental temperature condition that was chosen from the beginning of the tests and in the end the calibration coefficient was taken as the statistical average of each individual matching measurement (Table 3.1). It is clear that LIF signal decreases exponentially with increasing temperature. Therefore, the calibration factor increases exponentially with temperature according to the dependency shown in Figure 3.18.

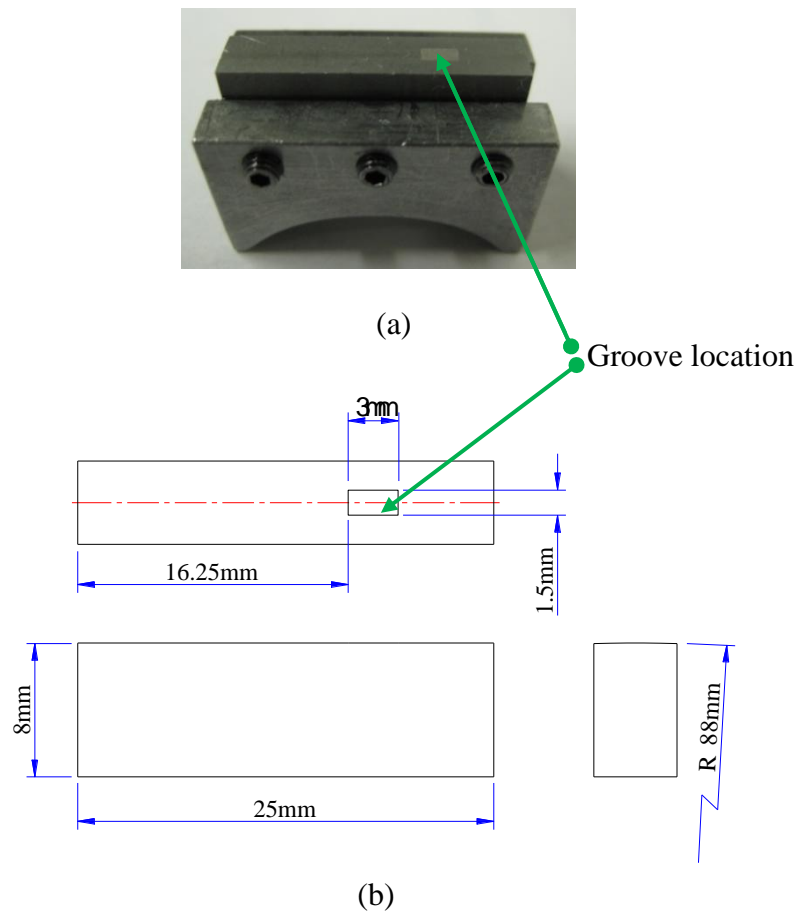


Figure 3.15: Specimen ring with groove (a) picture (b) drawing

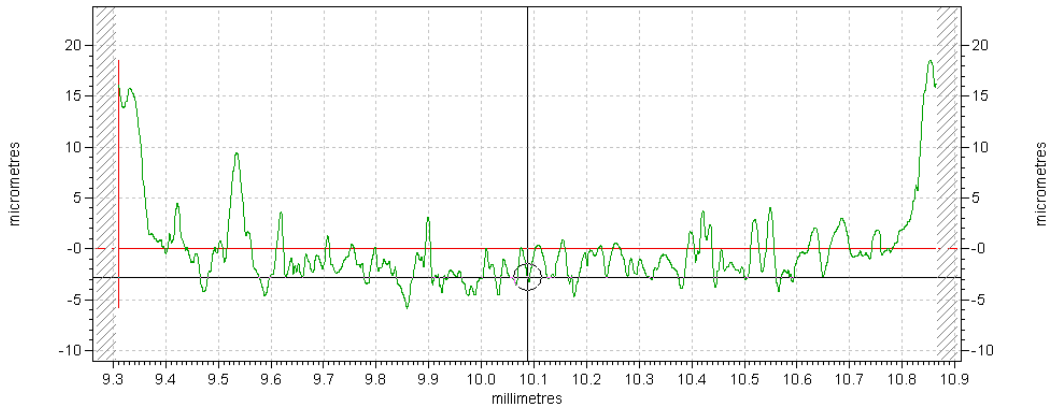


Figure 3.16: Profile measurement around the area of laser path

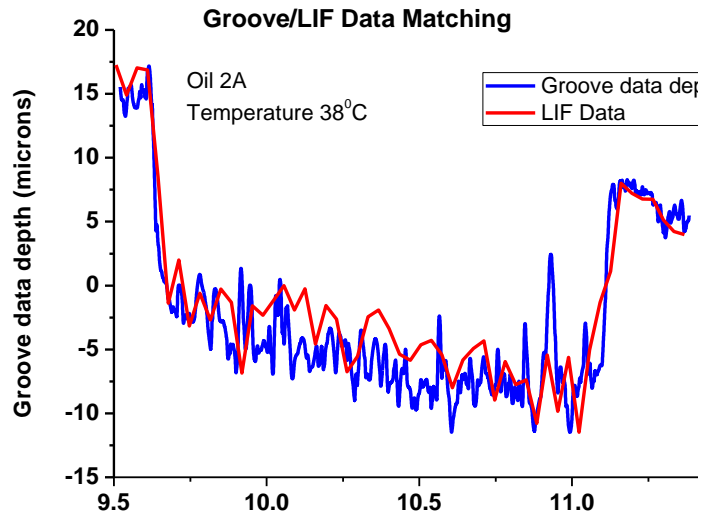


Figure 3.17: Matching groove data against average LIF data

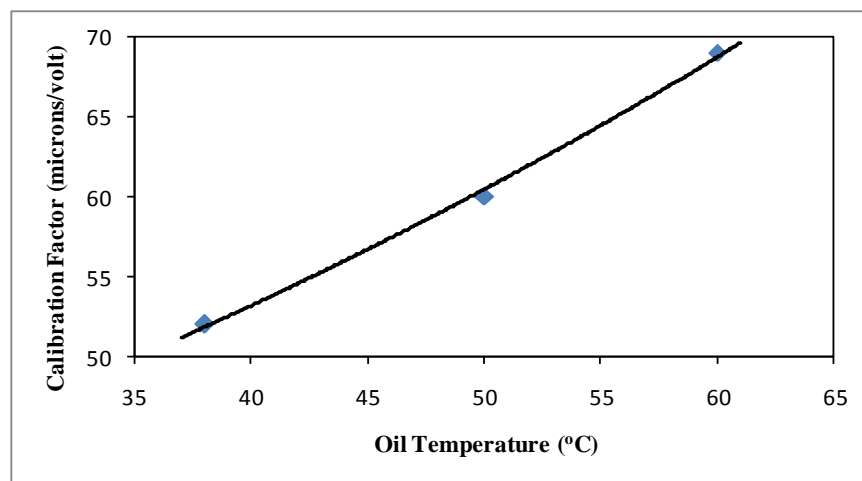


Figure 3.18: Calibration coefficient as a function of oil temperature

Temperature (°C)	Calibration Coefficient (microns/volt)	Standard deviation (microns/volt)	Error (%)
38	52	1.26	2.3
50	60	5.37	8.9
60	69	5.69	8.2

Table 3.1: Results for Calibration factors

3.3.4 PRESSURE TRANSDUCER

To measure the oil film pressure the technique described by Dellis and Arcoumanis (2004) was carefully adapted. A miniature silicon diaphragm pressure transducer manufactured by Kulite, model XCQ-080-500, was mounted in the aluminium liner specimen (Figure 3.4) and used to measure the temporal pressure variation in the oil film. Figure 3.19 shows the details of the transducer mounting. The pressure transducer is connected to a Wheatstone bridge conditioner and its signal is amplified by a FYLDE amplifier. The value measured by the sensor represents an average over the measurement window. Therefore, the size of the measuring window (in crank angle degrees) is one of the most critical parameters of the experimental investigation. To further improve the measurement resolution, the pressure sensor and the oil film were linked through a narrow slit of 0.1mm (section A-A in Figure 3.19), which runs parallel to the ring-liner contact line.

Unfortunately the pressure transducer failed and was replaced by another one of the same model. The screen of the latter was removed and its cavity was filled with a special silicone compound (RTV – Room Temperature Vulcanising) as seen in the schematic diagram shown in Figure 3.20. This step was proposed by Kulite to Dellis (2005) due to the air cavity affecting the pressure measurements.

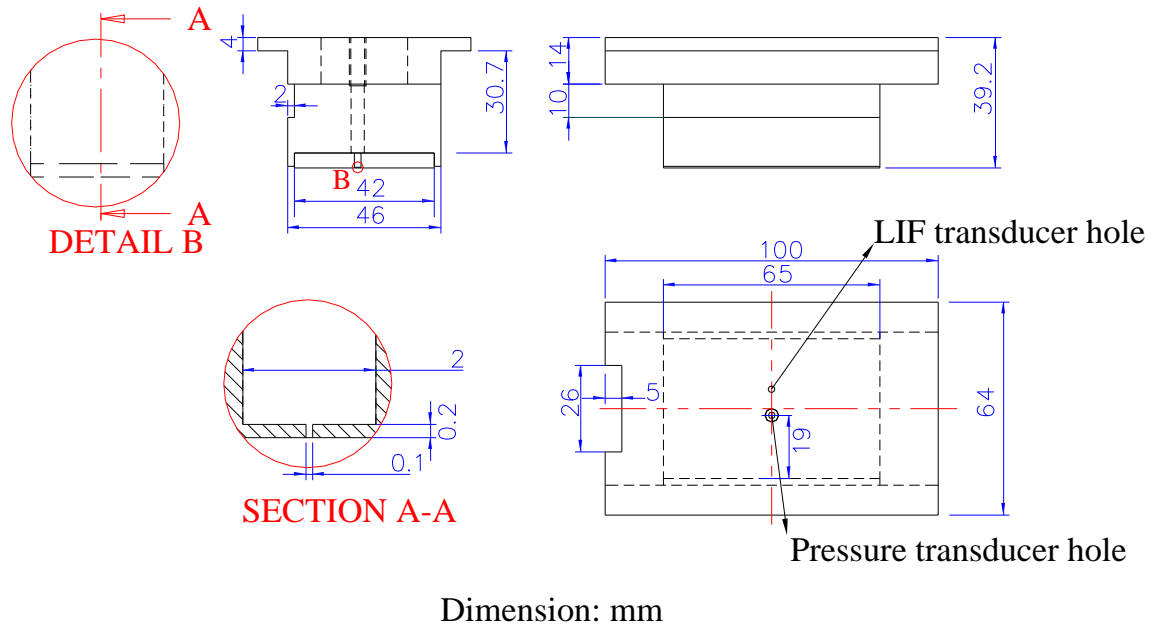


Figure 3.19: Pressure transducer mounting

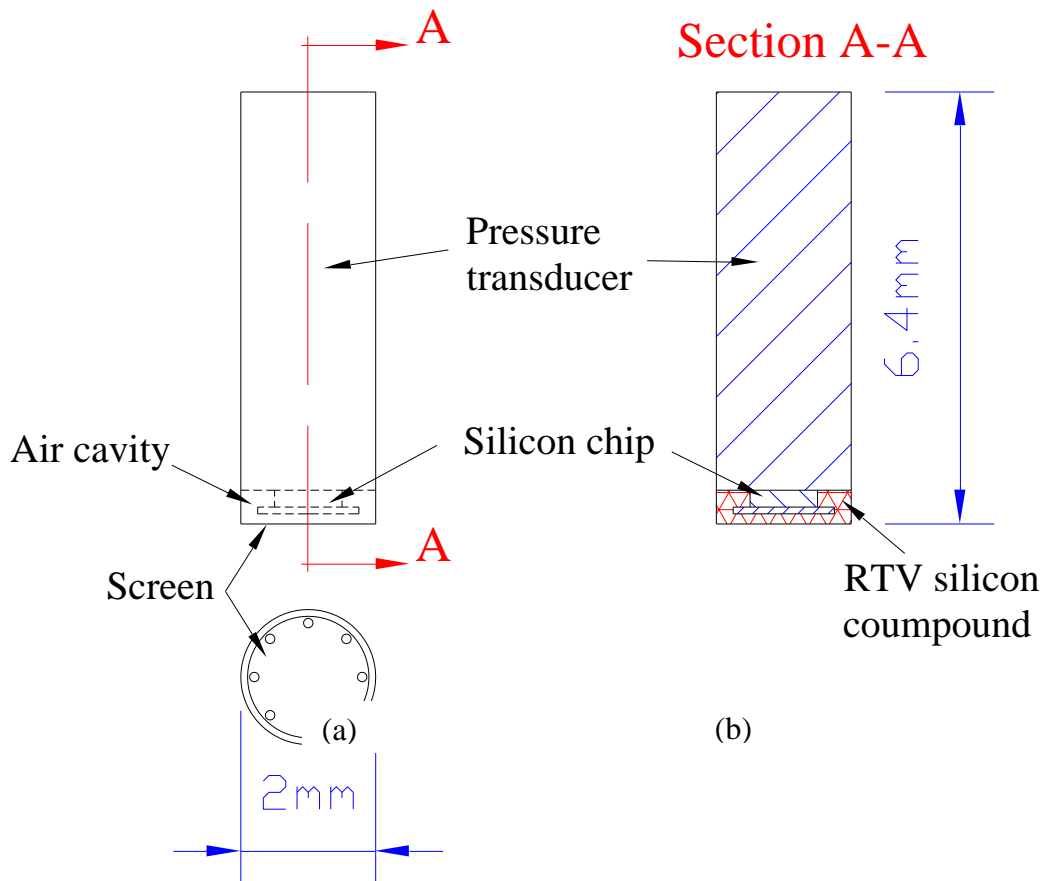


Figure 3.20: Kulite pressure transducer with (a) screen (b) screen removed and filled with RTV

This silicone compound is in principle able to take out most of the air pockets in the silicon chip cavity as it will be filling it under a certain angle pushing any air out of the cavity; this protects the transducer and leaves the signal unaffected. The main arguments for this modification were the successful implementation of this method to other customers who, in turn, found difficulties in measuring air pressures in wind tunnels. In many cases, small particles were accelerated by the air flow and by hitting the silicon chip, they affected the real air pressure measurement. In the worst case they were able to damage the transducer. Filling the cavity with silicon compound eliminated these problems.

The calibration of the new Kulite pressure transducer was done by employing a dead weight tester method and a calibration coefficient of 200 kPa/volt was found. After the calibration of the new pressure sensor, oil film pressure measurements were acquired and found to be very low compared to the one acquired with the old transducer for the same test configuration. An investigation has been carried out and the following conclusion has been reached. Despite the high precision required for the manufacturing of the pressure transducer, as well as the liner specimen, there is a narrow gap between the active face of the sensor and the surface of the liner wall. This dead volume, together with the additional volume of the narrow slit, can potentially lead to measurement errors. During the suction phase, represented in Figure 3.21 by the negative pressure, some of the oil present in this constant volume is expected to drain and replaced by a small amount of gas which is convected towards the sensor's surface. Consequently, during the following high peak pressure phase this gas is trapped and it is compressed by the oil pressure, resulting in alteration of the true pressure reading. Furthermore, since in the proximity of the measuring sensor the liner incorporates a narrow slit, the validity of the assumption of a laminar lubricant flow with the film on solid walls (as required by Reynolds equation) is questionable.

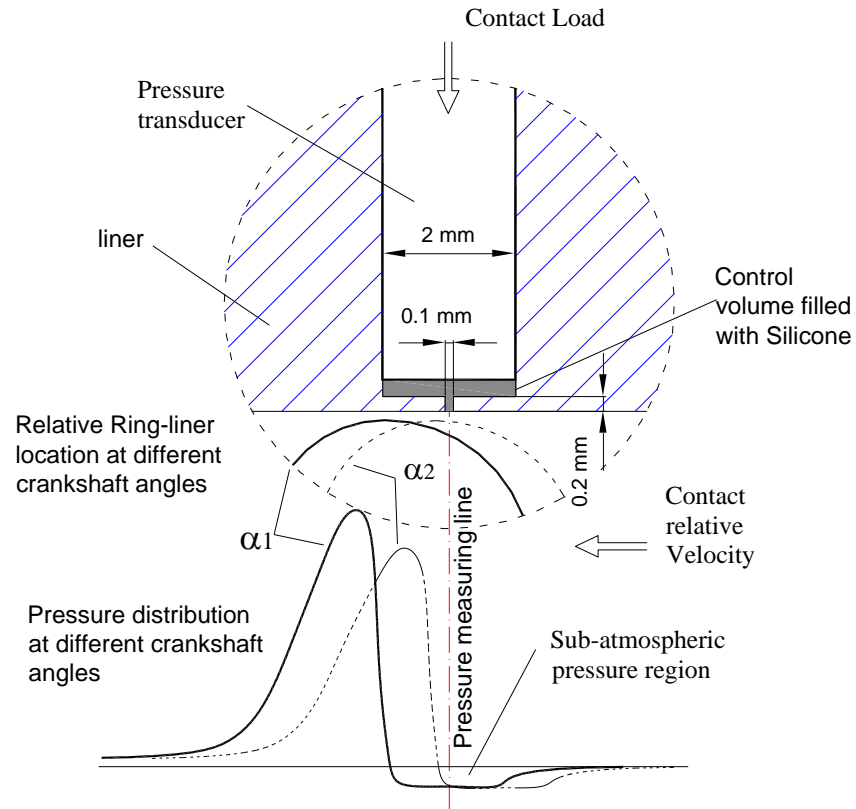


Figure 3.21: Pressure transducer measuring approach

To compensate for these possible sources of error, a small amount of DC4 (Silicone electrical compound) was initially added to the surface of the pressure sensor before inserting it into the liner. In this arrangement, the DC4 compound is assumed to fill and remove the air in the control volume completely where it acts as a medium between the oil pressure and the surface of the pressure sensor. After a few progressive runs, the pressure readings were found to gradually decrease in magnitude. One possible explanation for this occurrence is that during the negative pressure phase, the DC4 compound was gradually being sucked out due to depressurization and consequently being replaced by air. Grease being a thicker substance was used as an alternative to the DC4 compound and found to give better pressure readings. However, while running the experiment, grease conducted heat from the surroundings and eventually softened. Hence the same effect to that of the DC4 compound was finally observed. Then a commercial silicone rubber, bathroom sealant, was applied to the control volume. The rubber was allowed to cure and the excess silicone was carefully removed. The pressure measurements were in this case found to be very repeatable compared to the former compound. An additional advantage of using silicone rubber in the open cavity is that

the Poisson's ratio of $\nu = 0.5$ preserves the control volume and, therefore, allows the oil pressure to reach the sensor.

The silicone rubber proved to be very reliable as compared to the other compounds used before. However, it lasted only about a week. Upon inspection, after no pressure reading could be obtained, there was some trace of silicone on the sensor. A pressure check on the transducer revealed that the latter had seized to function. One possible explanation for the failure of the pressure sensor is that the bathroom sealant is corrosive to electronics. This type of silicone releases acetic acid while curing and this might have gradually attacked the diaphragm part of the transducer, thus leading to electronic failure.

A new pressure transducer has been purchased. It is a miniature silicon diaphragm transducer manufactured by Entran, model EPIH-412-20B. Table 3.2 compares the specification of the Entran sensor to the Kulite one. A special plug has been made to house the new sensor. Having experienced an expensive problem using the bathroom sealant on the previous pressure sensor, the use of a non corrosive silicon rubber is imperative. A silicone elastomer, Silastic 9161 RTV was selected, which was used on the Kulite sensor before to fill the control volume, since the latter is a neutral cure sealant, i.e. it does not release acid while curing. This is a two-part silicone rubber; a base and a catalyst. After mixing the parts with the right amount, a small blob was applied to the surface of the transducer. Then it was inserted inside the liner and any excess was wiped off. The silicone rubber was allowed to cure overnight to ensure it has been set properly.

	Entran EPIH-412-20B	Kulite XCQ-080-500
Rated pressure (bar)	20	35
Over range limit (bar)	40	52
Excitation (volt)	5.0	10.0
Reference	Sealed gauge	Absolute
Size (diameter mm)	2.03	2.0

Table 3.2: Specifications of Entran and Kulite pressure transducers

Pressure Transducer Calibration

An in-situ calibration for the new pressure transducer has been designed and was favoured over the dead weight method. The calibration device consists of a rig adapter which is clamped on the surface of the liner and connected to a Lucas hand pump.

Figure 3.22 shows the calibration setup of the sensor.

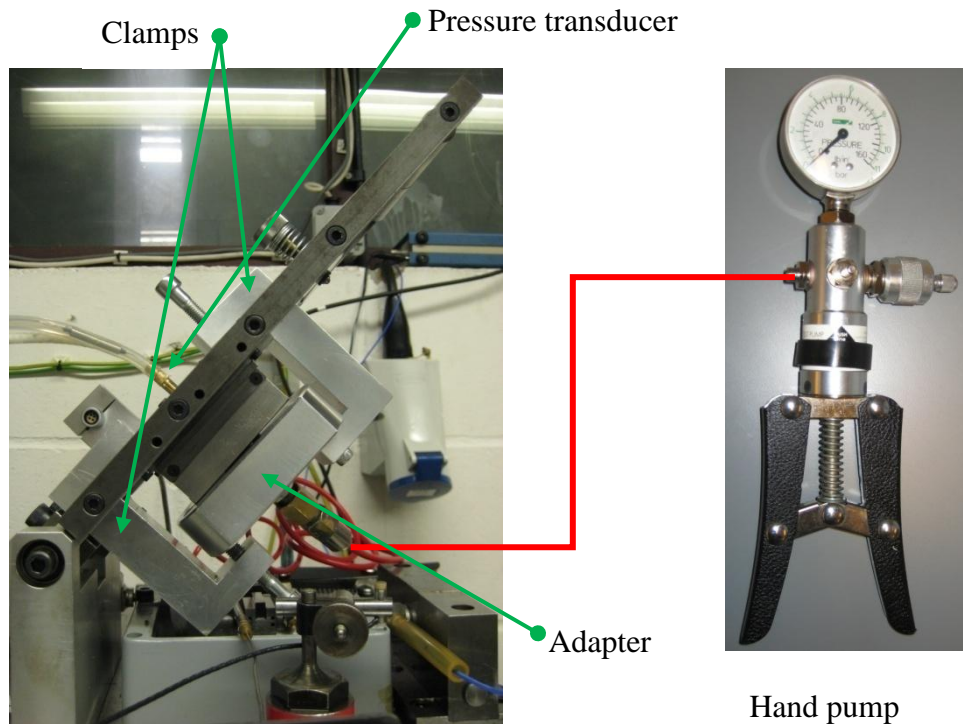
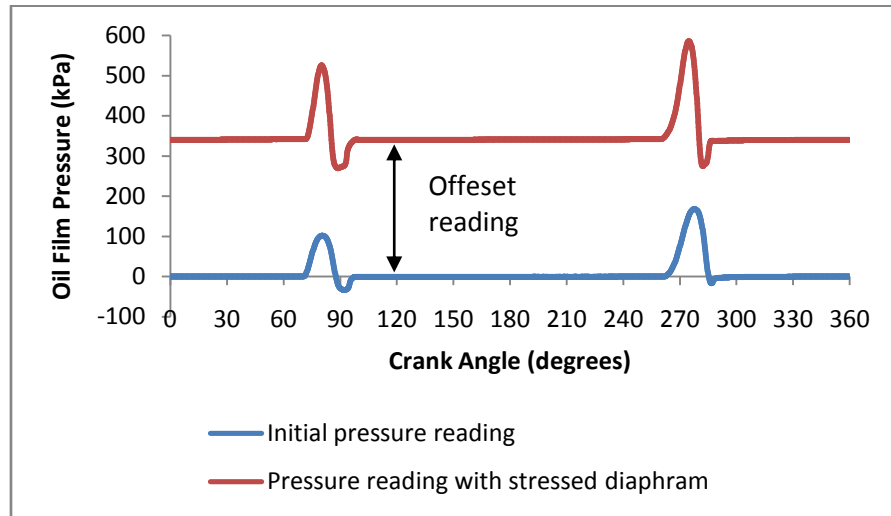


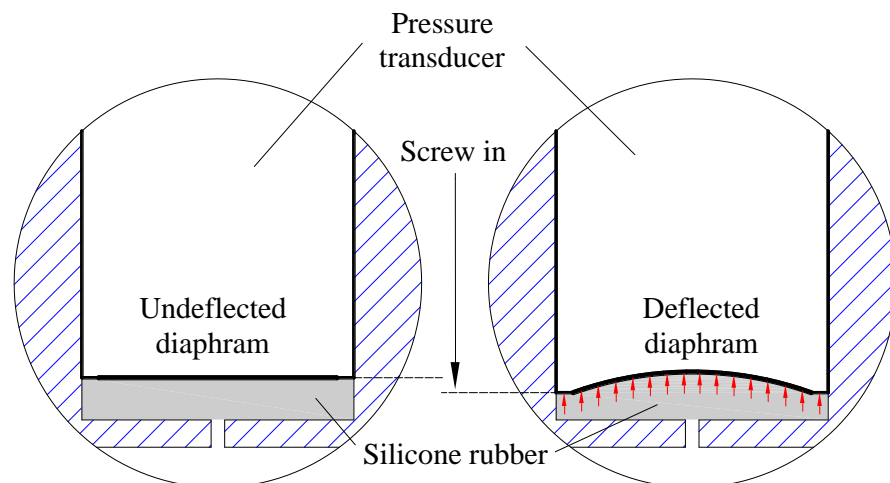
Figure 3.22: In situ pressure calibration setup

After the calibration of the pressure transducer, a sample pressure reading was acquired. A low magnitude of pressure was recorded and was not in agreement, for the same test conditions, with the one taken by the Kulite pressure sensor. Initially it was thought that the oil film pressure was not convecting properly to the sensor due to the latter being recessed from the surface of the liner; hence the latter had to be pushed in gently further towards the surface of the liner. However, this was not the case as Figure 3.23a reveals that the pressure transducer was not effectively recessed. By inserting the sensor further down, it had caused the silicon rubber to be in compression against the inner

wall, applying stress onto the diaphragm. This stress caused the diaphragm to deflect and thus to give an offset pressure reading (Figure 3.23b).



(a)



(b)

Figure 3.23: (a) pressure reading (b) schematic of diaphragm gauge

Therefore, it has been concluded that the silicone rubber used, Silastic 9161 RTV, is not elastic enough to cause the diaphragm of the Entran pressure sensor to deflect under a small pressure. One reason for this occurrence is that this silicone pack uses a catalyst to harden the silicone rubber and does not exhibit similar characteristics to a commercial silicone rubber. An alternative silicone rubber has been found, Silastic 3140 RTV, which is a one-part compound. Before applying this material on the transducer, advice from the manufacturer was sought. Coincidentally, the manufacturer does use 3140 RTV to seal the small gap between the diaphragm and the casing of the sensor to

prevent contamination. The 3140 RTV is non-corrosive and cures under humidity. It has a Poisson ratio of $\nu = 0.5$, it is flexible and does not cause any stress on the diaphragm. Thus it does not affect the pressure reading. The previous silicone rubber was thus carefully removed and the new silicone rubber was applied onto the sensor. The latter was mounted and the rubber was allowed to be cured. The pressure transducer was calibrated again using the in-situ method that was mentioned previously. Figure 3.24 shows the calibration curve for the Entran pressure transducer and a calibration coefficient of 201.74 kPa/volt has been found. A sample reading was taken and the sensor was found to be working properly.

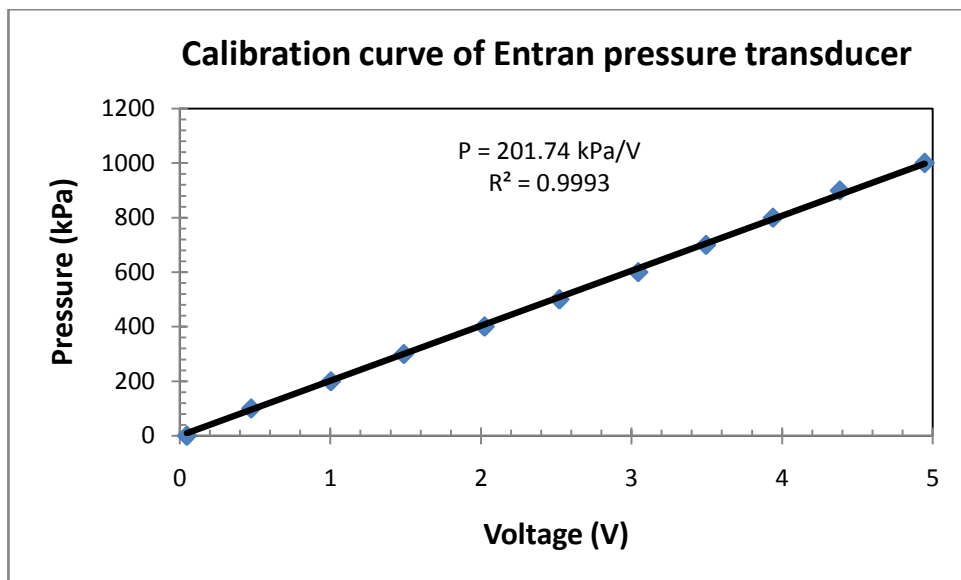


Figure 3.24: Calibration curve for Entran pressure transducer

3.3.5 DATA ACQUISITION SYSTEM FOR TEST RIG

A data acquisition system has been used to acquire signals from the measurement transducers during the experiment. It consists of a National Instruments 16-bit 6035E PCI data acquisition card and National Instruments SC-2345 signal conditioning unit. The 6035E device features 16 channels (eight differential) and a resolution of 16-bits. This card has a timing system of 50 ns resolution for time-related functions and is also capable of acquiring data at a sampling rate of 200 kS/s. The signal conditioning unit permits the acquisition of signals from the measurement transducers simultaneously during the experiment that are inputs to the unit itself and the Labview software with its graphical programming language is used for developing computer programs. The measurements from the transducers are a function of crank angle and are averaged over one revolution.

3.3.6 SHAFT ENCODER FOR TEST RIG

A shaft encoder is fitted to the base of the electric motor and such that 1000 and 1 signal per revolution can be read separately. The position of TDC corresponding to crank zero, is identified by one pulse emitted by the encoder per revolution which triggers the data acquisition system through a processor box to sample the data at a frequency of two thousand (2000) times a cycle (2 kHz). Hence data can be acquired every 0.18 degrees crank angle.

3.4 OIL FILM VISUALISATION

The reciprocating piston-ring assembly is one of the most loaded engine sub-systems, contributing to both frictional and mechanical losses. The former is due to insufficient lubrication in a number of contact zones, mainly between the ring and the liner, while the latter is due to significant out of balance inertial forces generated by the translational motion of its components. Inadequate lubricant film development between the ring and the liner which may result due mainly to the high relative motion between the piston and the cylinder liner replenishes the lubricant but also generates cavitation conditions at the outlet of the ring-liner conjunction. The onset as well as the development of cavities is heavily dependent on the relative velocity, with higher entrainment motion

leading to the cavities developing later in the ring/cylinder contact and lasting longer. The mechanism of oil film formation and pressure distribution in the ring-liner lubricated conjunction cannot be separated from cavitation development. Ideally such experiment should be performed in a combustion engine operating under firing conditions. However, the main disadvantage of such an approach is the difficulty of decoupling the individual contributions due to each physical phenomenon upon the development of cavitation. As a result the present work proposes an experimental approach for monitoring the formation of cavities in a simplified test rig which simulates the lubrication environment conditions in a piston-ring-cylinder assembly. The test rig described in section 3.2 has been modified by Dellis (2005) to allow the lubricant flow to be visualised. The onset and development of cavitation in the lubrication film present throughout the stroke between the specimen piston ring and the flat plate liner in the test rig was visualized initially by a charge-coupled device (CCD) camera and afterwards by a fast speed video camera.

3.4.1 GLASS LINER

The oil film visualisation experiments were made possible by an optically accessible liner. The metal liner was removed and replaced by a quartz glass window as shown in Figure 3.25. The quartz liner has a cross hat section with 27 mm \times 65 mm rectangular surface in contact with the piston-ring. The window is contained in an aluminium frame as shown in Figure 3.26 which is then fixed on the test rig.

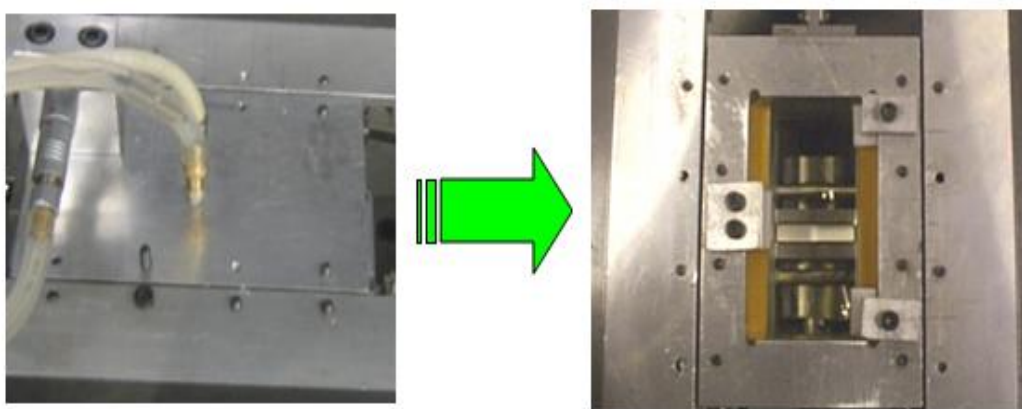


Figure 3.25: Metal to glass liner

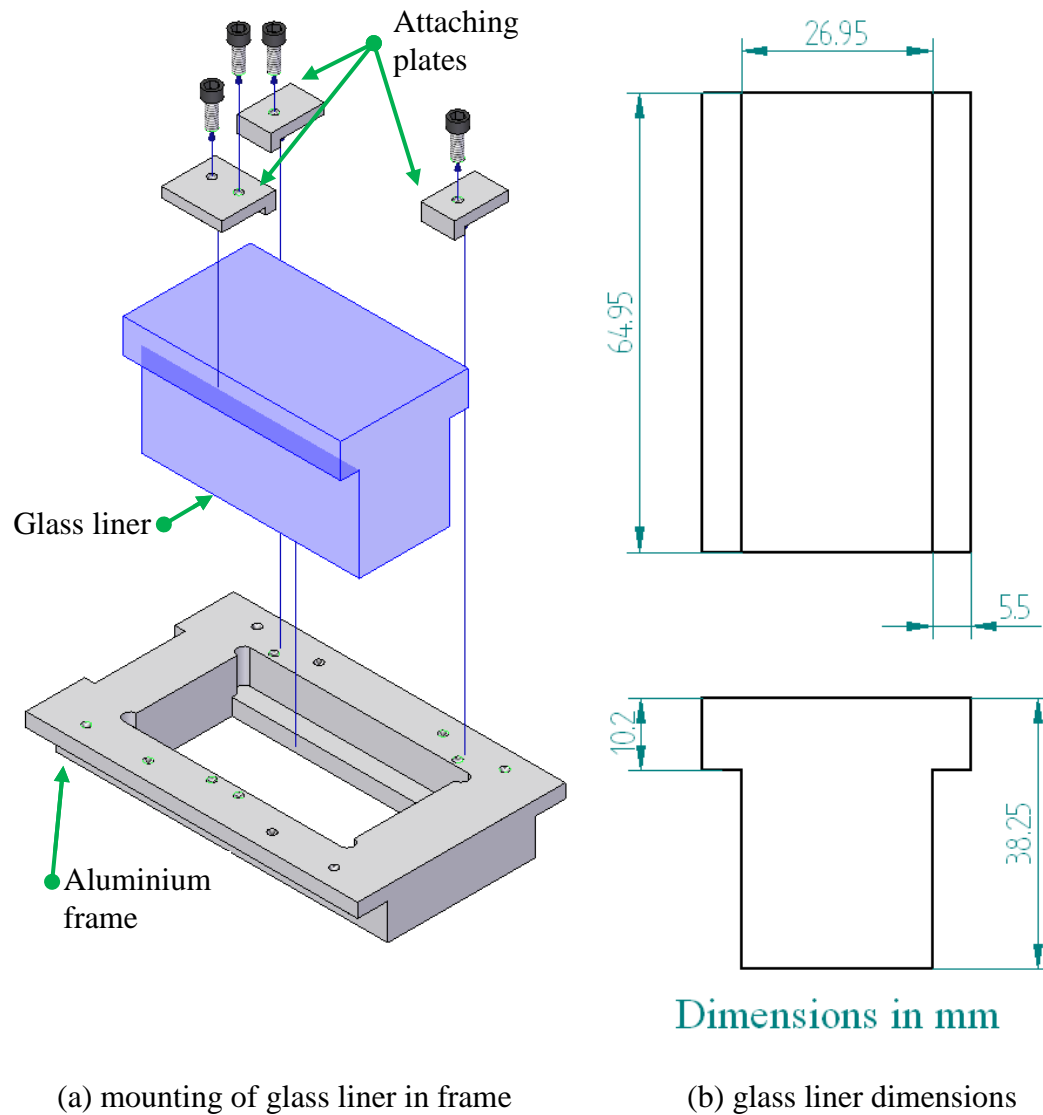


Figure 3.26: Schematic of glass liner

3.4.2 CCD IMAGING TECHNIQUE FOR TEST RIG

The still imaging was captured using a high speed CCD camera mounted on the top of the glass liner. Figure 3.27 shows the schematic view of the setup used for the still imaging of the cavitation structures between the glass liner and the specimen piston-ring. The CCD camera used was a 12bit fast-shutter Sensicam PCO with a resolution of 1280×1024 pixels and a minimum exposure time of 100 ns. To investigate the cavitation structures between the piston ring interfaces a K2 type long distance microscope (Infinity Photo-Optical Company) with CF-2 lens attachment was mounted

in front of the camera. This provided sufficient as well as efficient enlargement of the area of interest. The camera was connected to a PC via an image acquisition card. The triggering of the camera and flash lamp illumination was done by the acquisition system mentioned in section 3.3.5. All internal camera settings could be adjusted with the image acquisition software and the obtained pictures were downloaded. Images were taken every 2° crank angle. The shaft encoder signal was directly connected to the electric motor, which in turn provides a single signal for the TDC that was used to provide the trigger pulse for the CCD camera and the flash light lamp.

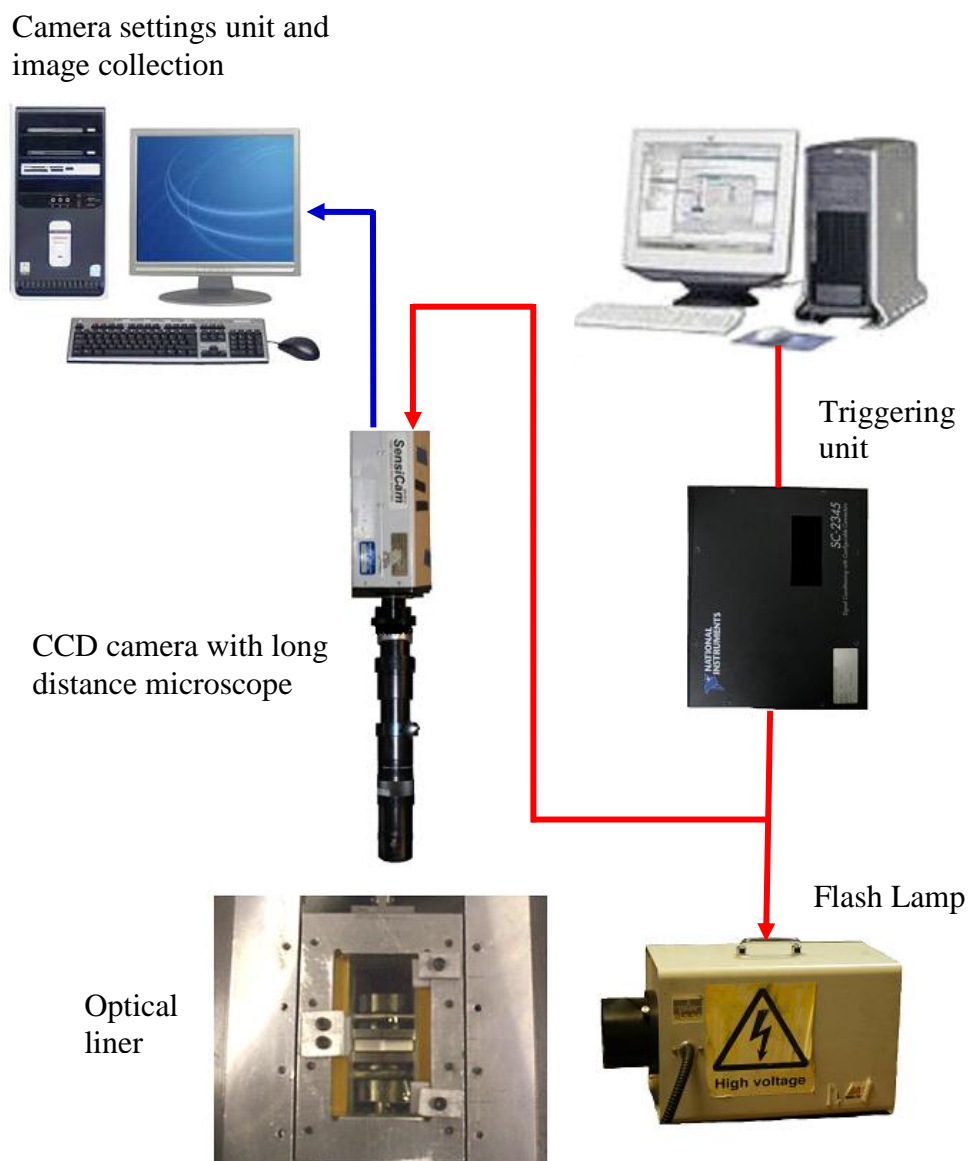


Figure 3.27: Schematic of CCD imaging experimental setup

3.4.3 HIGH SPEED DIGITAL VIDEO TECHNIQUE FOR TEST RIG

The oil flow features between the piston-ring and the glass liner have a highly transient behaviour. Therefore, to fully understand the complexity of the physical phenomena occurring during the formation of the cavity structure, a high speed digital video system (Fastcam-APX RS) was set up. This arrangement allows the capturing of the development of the cavitating oil flow in the piston-ring liner conjunction.

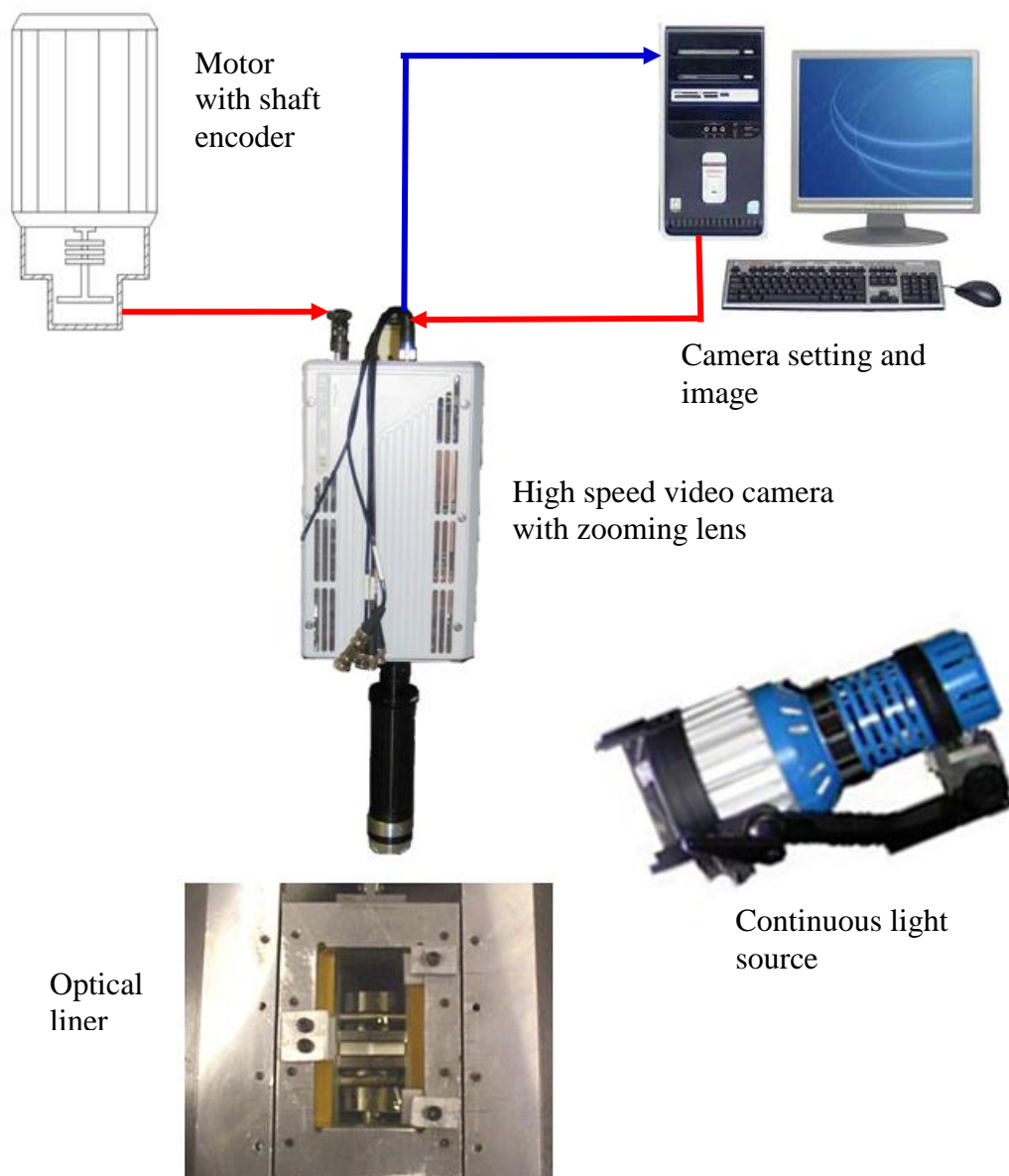


Figure 3.28: Schematic of high speed video camera experimental setup

Figure 3.28 displays a schematic of the 10 bit video system, which is capable of taking between 50 and 300 frames per second with a maximum resolution of 1024×1024 pixels. Higher frame rates of 5000 up to 250000 frames per second are possible but at progressively poorer resolution. For the single test rig experiment 10000 frames per second with a resolution of 512×512 pixels proved to be satisfactory for the imaging of the temporal development of the cavity structures. A zoom lens with a magnification factor of 3.1 times was used to view the interrogation area. The illumination of the test area was achieved with a strong halogen floodlight which proved adequate to provide enough light for the CCD video chip. The camera was triggered, synchronised with the TDC position pulse from the shaft encoder coupled to the motor, and controlled with the image processor unit via a computer. All single video frames of one imaging sequence were stored in the memory of the image processor. From this memory it was possible to instantly replay any sequence of images. Once stored on the PC's hard disk, it was possible to create movie files from single pictures of the same video sequence using the video camera software.

3.5 ENGINE EXPERIMENT

3.5.1 ENGINE CHARACTERISTICS

The engine used in the current study is a modified PHW1 Lister-Petter, one cylinder, direct injection, water cooled diesel engine. Initially the PHW1 engine was used within the lubrication group by Duszynski (1999) and Pyke (2000) where a Laser Induced Fluorescence (LIF) system had been developed to obtain measurements of the instantaneous lubricant film thickness in the piston-cylinder assembly under firing conditions. Subsequently, it had been altered to allow optical access into the liner by Dellis (2005) in an attempt to visualise the oil film between the piston-ring/liner interface. For the present study, this engine has been modified further and utilised to study the oil film characteristics between the piston-ring and cylinder liner as well as to measure its oil film pressure. The general characteristics of the Lister-Petter engine are shown in Table 3.3. The lubricating oil system for this engine remains unmodified. Oil is stored in the crankcase and supplied to the main gear bearings and valve rockers through a rotary pump which is mounted in the crankcase. The cylinder, small end bearings and camshaft are splash lubricated.

Engine Model	Lister-Petter PHW1
Cylinder bore	87.76 mm
Stroke	110 mm
Displacement	0.659 L
Compression ratio	16.5:1
Connecting rod length	231.9 mm
Conrod/Crank ratio	4.22:1
Oil capacity	2.8 L
Maximum speed	2000 rpm
Maximum engine torque	32.5 Nm @ 1700 rpm

Table 3.3: Lister-Petter engine characteristics

The engine is driven by a Plint dynamometer TE 46 and is shown in Figure 3.30. When used for motoring the power available is 0.85 times the absorption rating. Figure 3.30 depicts the power absorption envelope. An SSD computer control is used to operate the dynamometer. The computer control can also monitor the temperature of the inlet and outlet of the coolant, the air inlet, the exhaust gas and oil sump as well as its pressure.

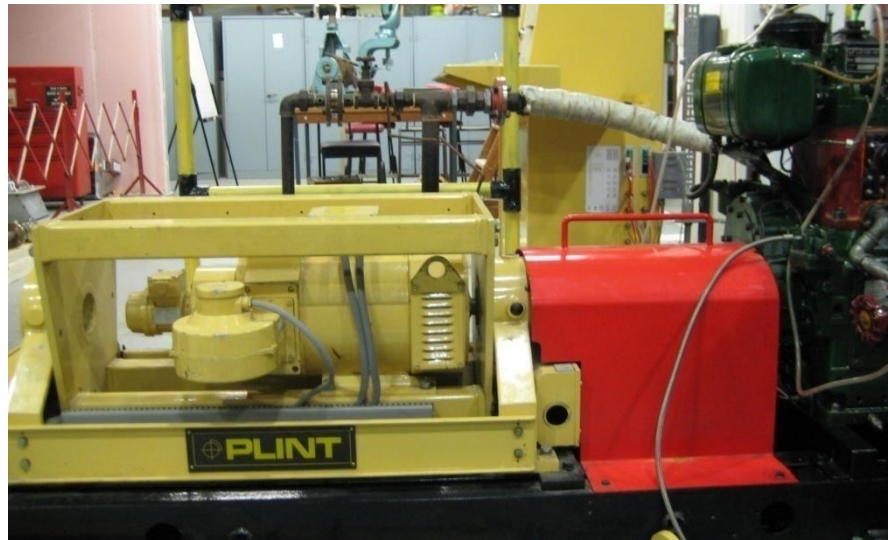


Figure 3.29: Plint dynamometer coupled to engine

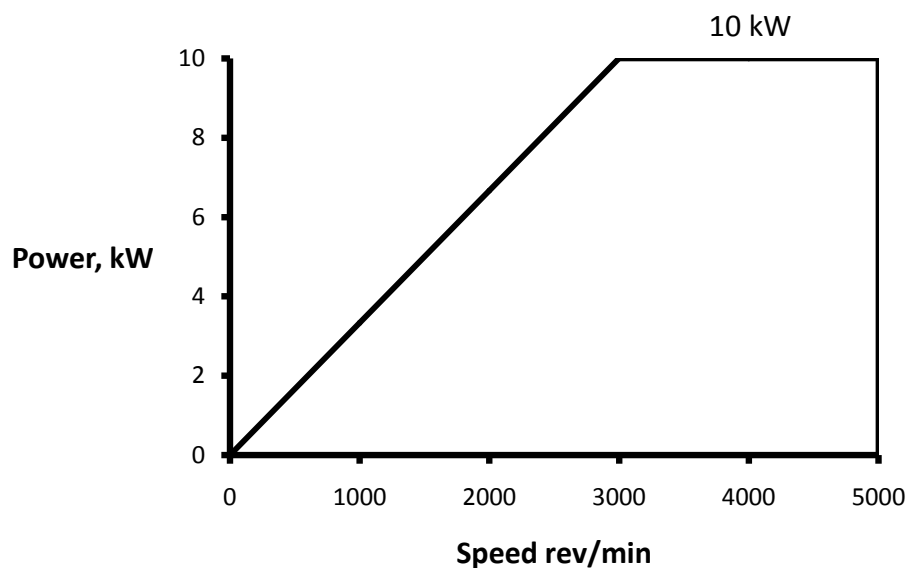


Figure 3.30: Power envelope for dynamometer, TE 46

3.5.2 ENGINE CYLINDER HEAD PRESSURE TRANSDUCER

The cylinder head is fitted with an AVL 144 (120P-250C) water cooled pressure transducer. The transducer was calibrated using a dead weight tester and connected to a type 5007 Kistler Charge Amplifier. The amplifier was set at 10 units sensitivity (10 mV/psi) and the gain was set at 80% when no pressure was applied at the dead weight tester. The calibration data were obtained with the amplifier set to “SHORT”, so that the voltage won't be decaying while taking the readings from the dead weight tester. Since the tests will be under motoring conditions, it was not considered necessary to calibrate the pressure transducer to the full scale limit. Secondly by doing so, the signal to noise ratio is improved. The obtained calibration curve shown in Figure 3.31.

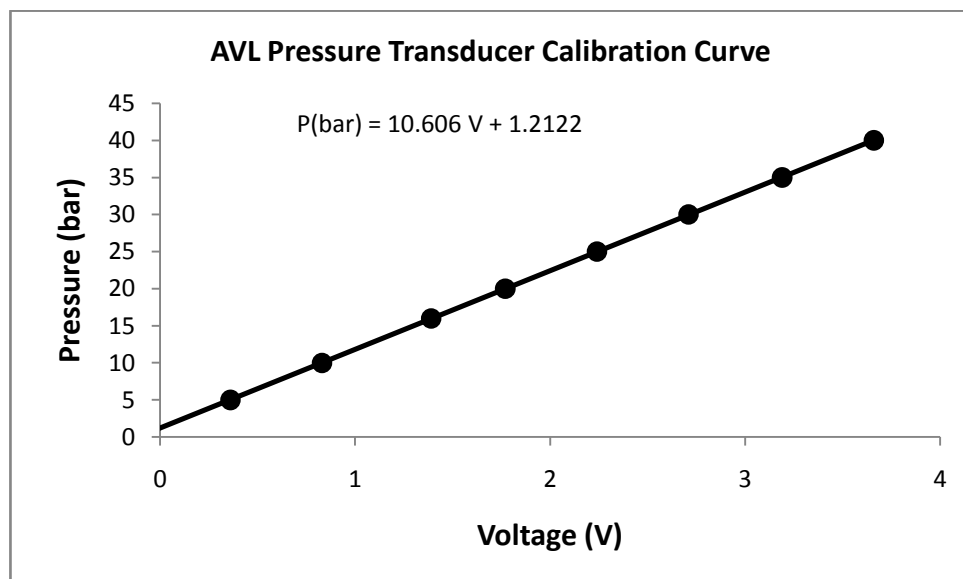


Figure 3.31: AVL pressure transducer calibration curve

3.5.3 DATA ACQUISITION SYSTEM AND SHAFT ENCODER

The data acquisition, described in section 3.3.5, used for the test rig was also utilised for the engine experiments. A shaft encoder, Muirhead Vactric Electric Model E25BC-4H-1000, is coupled directly to the engine's crankshaft and provided 3 pulse trains of output signal. One channel gives 1 ppr (pulse per revolution) and matches up to the TDC piston reversal point. The two other channels which are in quadrature give 1000 ppr. In order to further improve the measurement resolution of the encoder, the two 1000 ppr

channels were electronically gated (XOR) using a purpose built processor box. This configuration provides an option of having 1000 or 2000 ppr signals which corresponded to 0.36 or 0.18 degree of crank angle per pulse. Following some problems, the shaft encoder had to be decoupled in order to be fixed. Once repaired the shaft encoder had to be adjusted in such a way so that the 1ppr channel corresponded to the TDC piston reversal point. This was deemed useful so that accurate triggering could be setup for the experiments that required knowledge of the piston position at all times. The calibration was carried out by utilizing the cylinder pressure transducer as a reference pulse at TDC of the compression stroke. The shaft encoder was adjusted until the 1 ppr channel matched up with the peak cylinder pressure and Figure 3.32 shows the oscilloscope trace of the result.

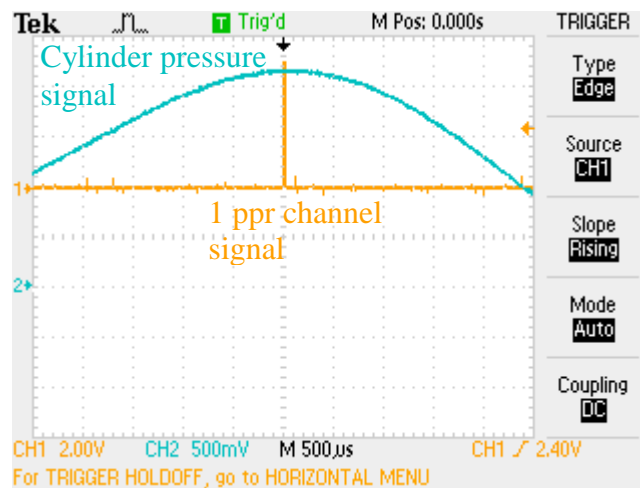


Figure 3.32: Oscilloscope trace for shaft encoder calibration

A proximity sensor was installed at the top of the valve rocker adjuster where the openings of the exhaust valve could be detected. This sensor acts as a marker by providing a reference pulse to the signal processor box to identify the strokes of the engine. The output signals allow a trigger output to be taken, 1 pulse per 4-stroke, at either TDC compression or TDC exhaust. Figure 3.33 illustrates the input and output signals of the signal processing box.

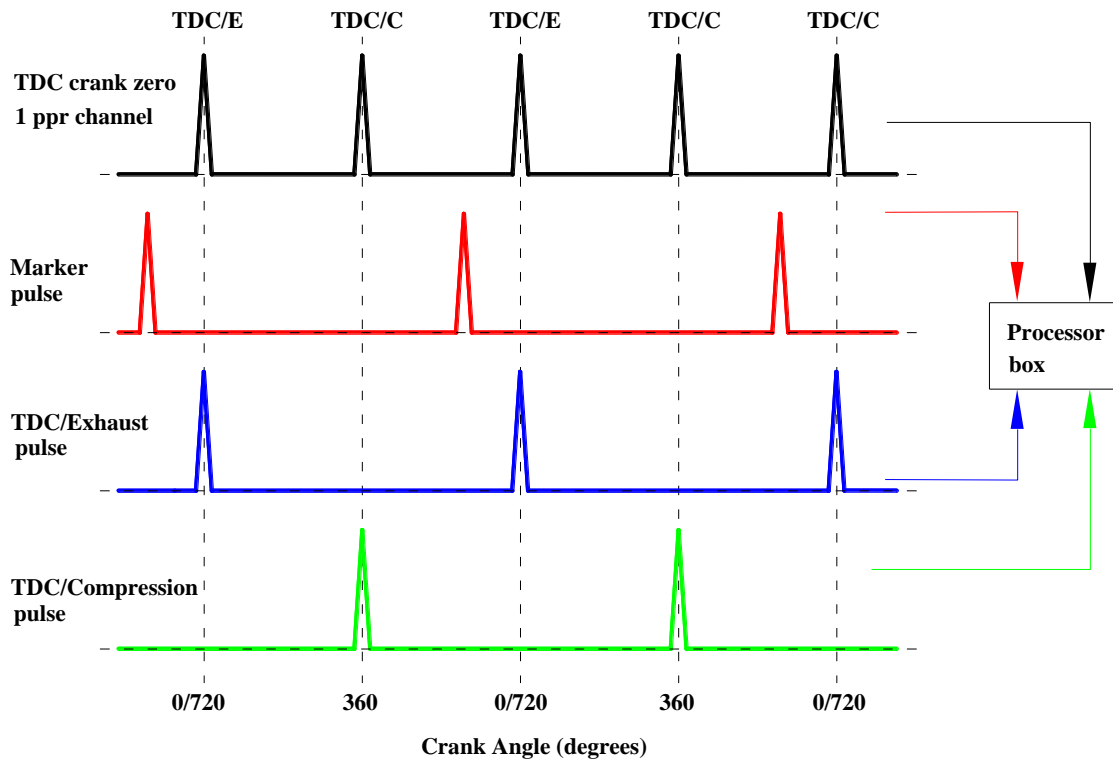


Figure 3.33: Signal processor box - input and output signals

3.5.4 MODIFIED ENGINE BLOCK AND OPTICAL ACCESS

The engine was prior modified by Dellis (2005) where slots had to be machined in the sides of the engine block so that to permit the imaging process through optical windows. The slots were spark eroded on two sides of the liner: thrust side and front side. The dimensions and positions are illustrated in

Figure 3.34. Quartz (synthetic fused silica) windows are inserted into the spark eroded slots of the liner of the engine. The windows are designed with a trapezoidal section in both vertical and horizontal direction to withstand better the compression pressure. The dimensions of the windows are shown in Figure 3.35. The inner surface of the quartz windows has the liner curvature and both inner and outer surfaces had been polished to offer good optical access. The windows were inserted from the inner side of the liner with high temperature epoxy glue (Loctite 9464A-B). The cooling jacket of the engine block had to be modified as well to allow optical access and it is shown in Figure 3.36.

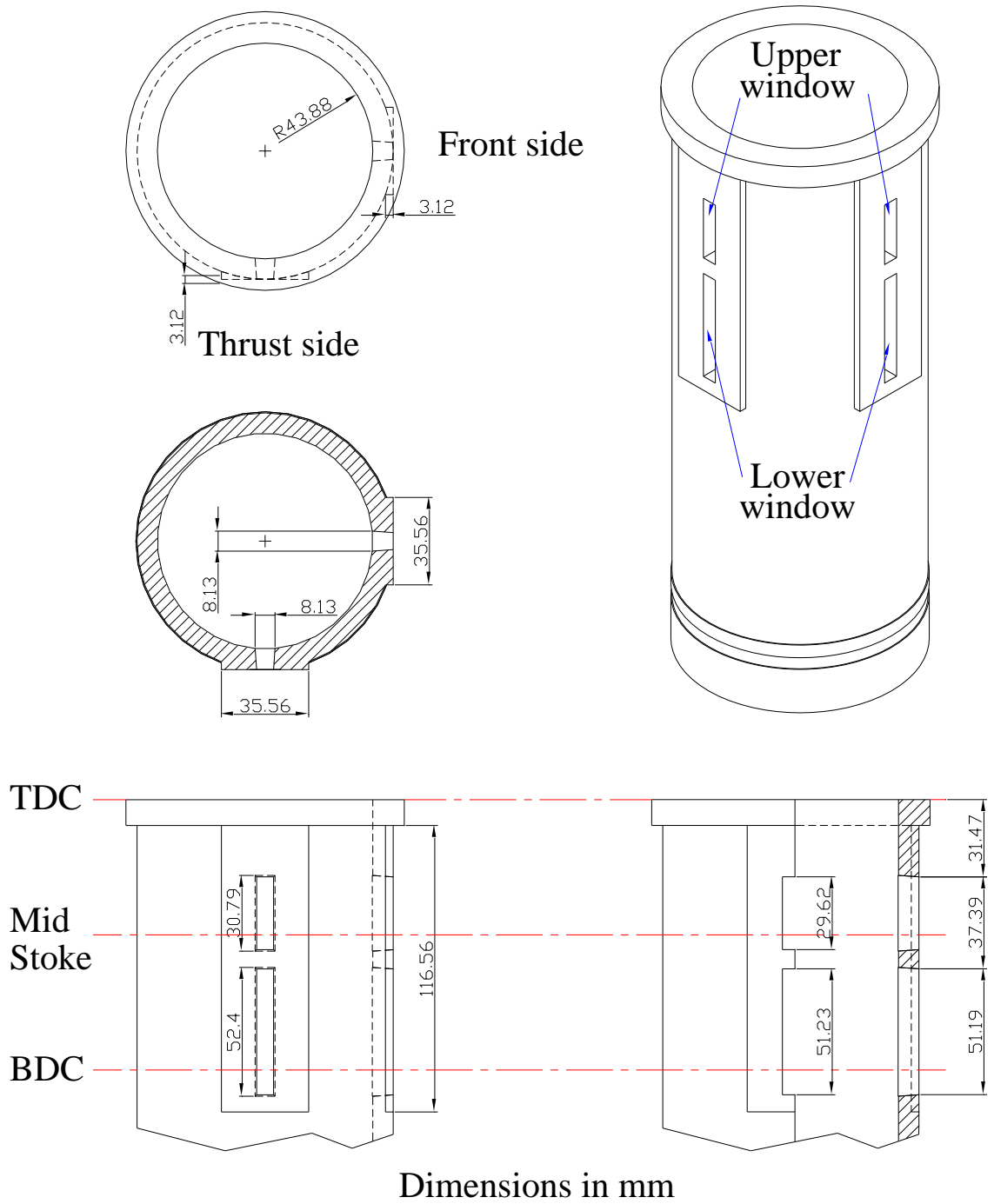


Figure 3.34: Dimensions and positions of the quartz window slots

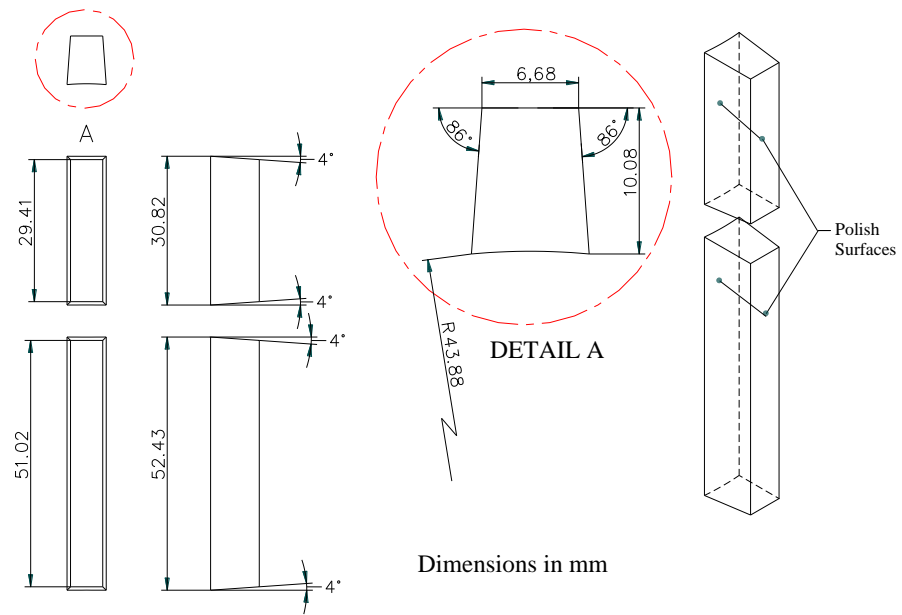


Figure 3.35: Quartz windows dimensions

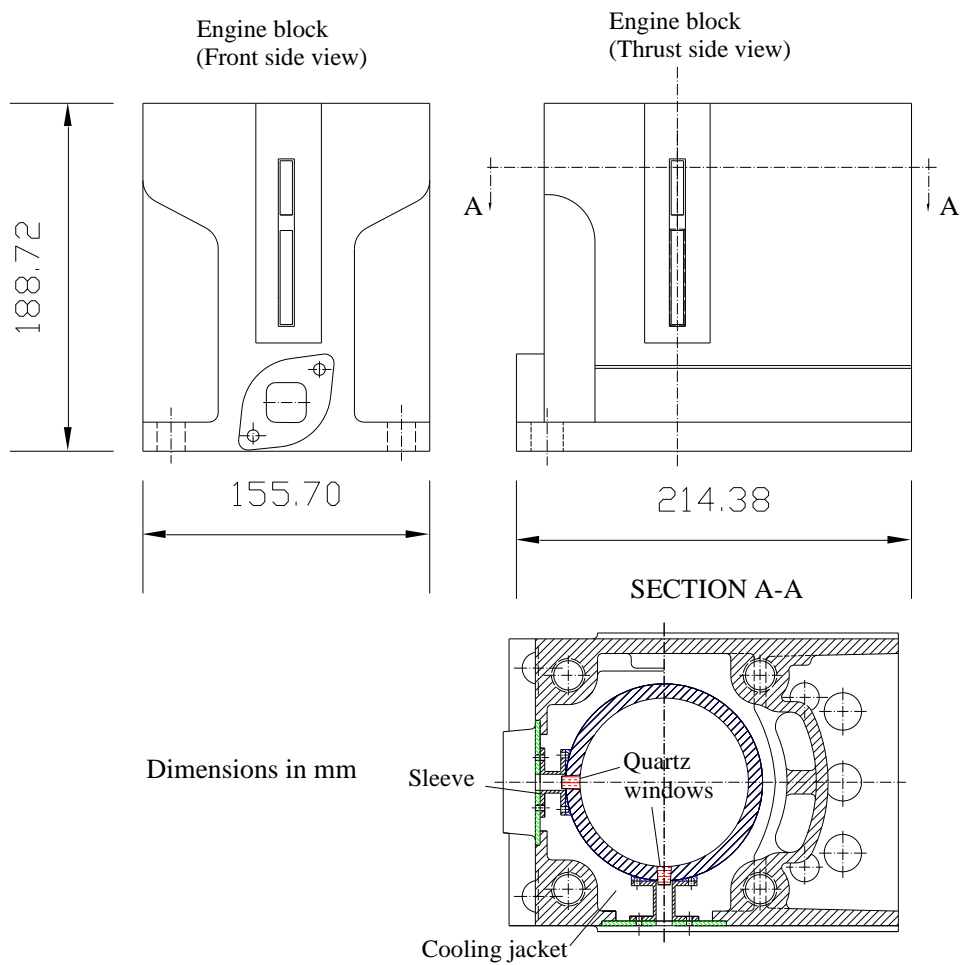


Figure 3.36: Engine block

3.5.5 MODIFIED ENGINE BLOCK FOR CURRENT WORK

During the previous engine experiments carried out by Dellis (2005), oil was found to leak through the quartz windows and as the liner temperature increased the leakage amplified; this was probably due to the quartz windows not sealed properly. Since cracks on some window surfaces have been identified. It is believed that the windows were too tight fitted into the spark eroded slots and tightening the bolts on the engine block might have added stresses to the corners of the windows leading to the observed cracks.

To rectify the leakage for the current work, it has been decided to replace all the windows. Synthetic fused silica was chosen again as it provides good optical quality as well as good mechanical properties, i.e. it is very scratch resistant (Thirouard, 2001). Since the experiments would be under motored conditions only, the thermal conductivity of the current material is not an issue. Although the upper and lower window slots were made to have identical dimensions on both sides of the liner, thrust side and front side, and despite the high manufacturing precision, they were found to differ slightly from each other. It is believed that this might have contributed to the oil leakage reported in Dellis (2005). To improve the seal, tailored made quartz windows for each individual spark eroded slot had been cut and sealed with high temperature epoxy glue (Loctite 9464A-B).

Dellis (2005) incorporated six stations on the liner: TDC, mid-stroke and BDC on both thrust and front sides of the liner, to record the oil film pressure. However, the re-boring of the liner had distorted and blocked some of the pressure measuring holes. For the current project the pressure holes in the liner were re-conditioned and the block holes have been spark eroded. Figure 3.37 shows the details of the pressure transducer fittings. The liner was test assessed for any leakages around the quartz windows. Two special plates were made to be mounted on top and bottom side of the liner as depicted in Figure 3.38. The liner was connected to a pressure line where it could be pressurized. Initially the liner was pressurized up to 1 bar and no apparent leakage could be noticed. However, when the pressure was increased to 5 bar some leakage by the windows became noticeable.

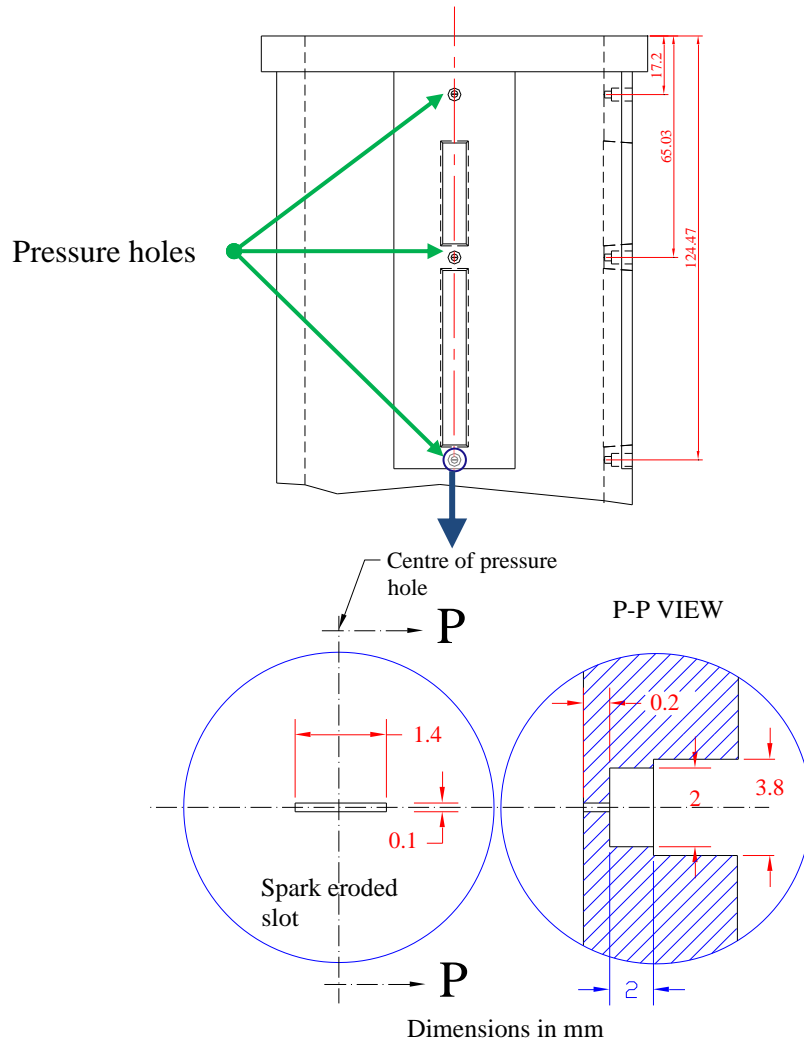


Figure 3.37: Details of pressure transducer holes

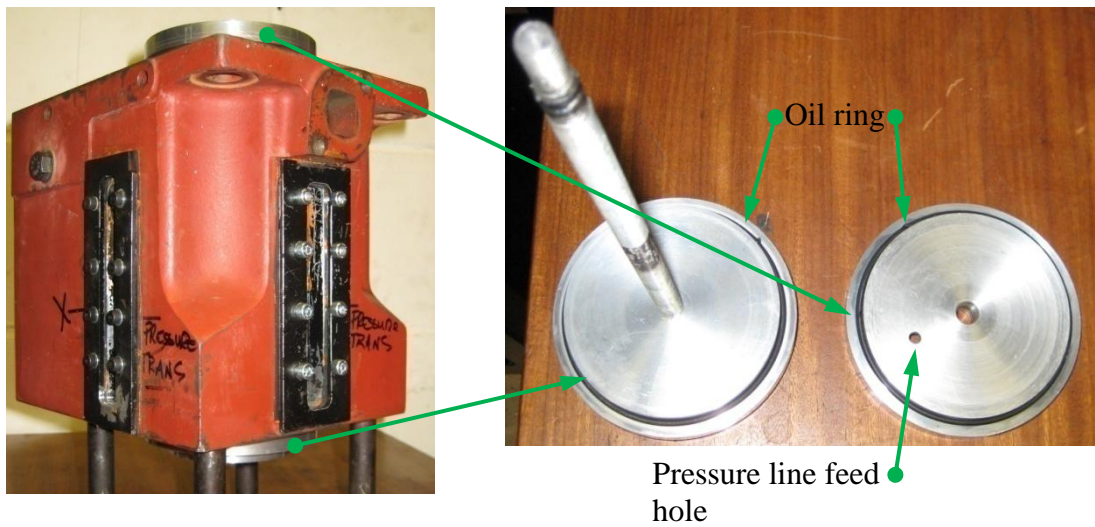


Figure 3.38: Seal plate for engine liner

Soapy water was used to identify the location of the leakage. On the thrust side of the liner, the leak came from the upper corner of the lower quartz window. However, on the front side leakage came from the middle pressure hole due to a mistake in the spark eroded hole made by the manufacturer. In order to correct this, the hole was drilled out completely and a plug made of same material of the liner (cast iron) was fitted into it. Then the spark eroded hole was redone on that plug. The improper sealing of that plug was thought to have allowed leaks to occur around that area. Following a thorough examination of the hole, a crack was identified and was clearly visible on the inside of the liner as depicted in Figure 3.39. To seal the leak on the thrust side and to repair the crack around the middle pressure hole, Loctite 9464A-B was applied on the outside of the liner. The liner was put under vacuum, around 0.5 bar, and left overnight to cure. In this way the compound could gradually fill the crevices and any excess collected inside the liner could be subsequently removed.

The liner was pressurized again to check for any leakage. On the thrust side no visible leak was found this time but on the front side the leak around the middle pressure hole persisted. Another attempt was made to repair the crack using the aforementioned method but with no avail. Due to the nature of the crack, this may grow further while the engine is in operation and thus may as well lead to structural weakness of the liner. For safety reasons, the front side of the liner was sealed completely.

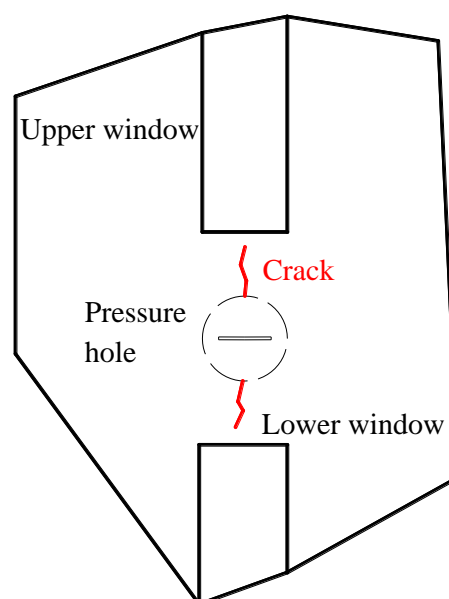


Figure 3.39: Crack around middle pressure hole

3.5.6 OIL FILM PRESSURE TRANSDUCER.

A miniature silicon diaphragm pressure transducer manufactured by Kulite, model XCQ-080-500, was used to measure the oil film pressure between the liner and piston ring of the engine. The pressure transducer has been connected to a Wheatstone bridge conditioner and its signal amplified by a FYLDE amplifier. To prevent the same problem occurring again in the test rig regarding the pressure measurements as described in section 3.3.4, a small amount of silicone rubber, 3140 RTV, was applied to the tip of the diaphragm of the sensor before inserting it in the pressure hole. Here as well an in situ calibration for the pressure transducer has been favoured over the dead weight method. The calibration device consisted of the seal plates, shown in Figure 3.38, previously used to seal the top and bottom of the liner for checking leakages around the window; one of them was connected to a nitrogen bottle. Figure 3.40 shows the calibration setup of the pressure sensor and the calibration curve.

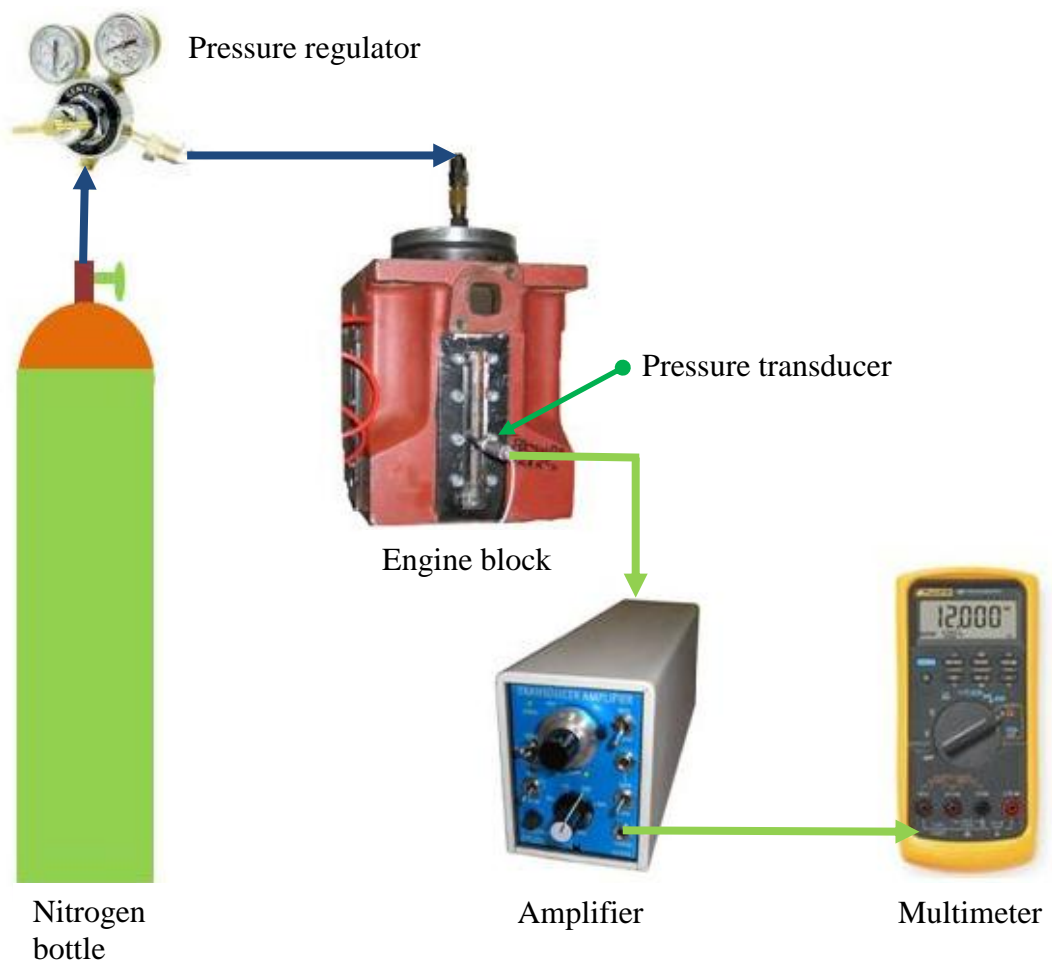


Figure 3.40: Oil film pressure calibration setup

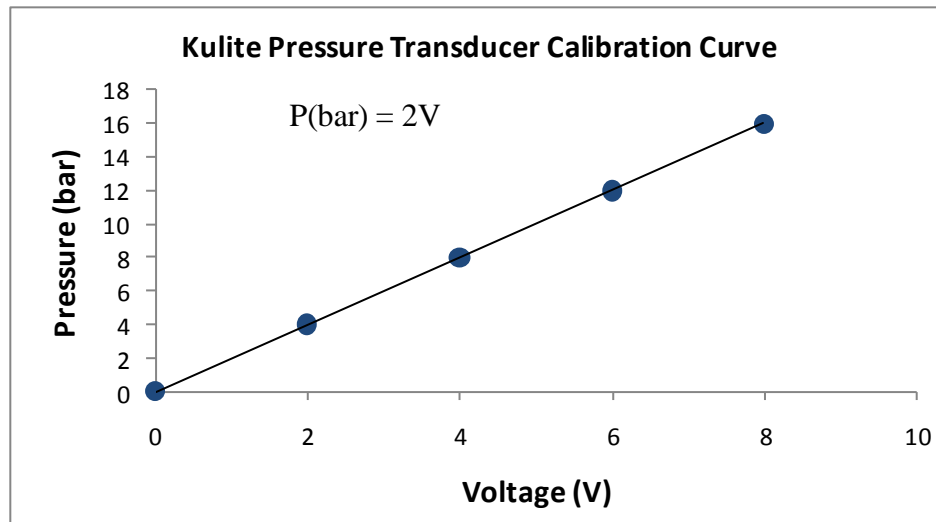


Figure 3.41: Kulite pressure transducer calibration curve

3.5.7 HIGH SPEED DIGITAL VIDEO TECHNIQUE FOR ENGINE

The high speed digital video system (Fastcam-APX RS), employed for the test rig imaging (section 3.4.3), was set up in conjunction with the modified engine. This arrangement allows the visualisation of the oil transport mechanism between the piston-ring and the cylinder liner. The camera was operated by its control unit which, in turn, was controlled by special software installed on the image collection computer. The software was responsible for programming critical operating parameters such as the desired frame rate, exposure time and triggering signals, to the camera's control unit. The shutter speed can be independently controlled regardless of the desired frame rate. The camera could be triggered at any crank angle position by coupling the pulse signal from the shaft encoder which is connected to the engine via the data acquisition box. All obtained images were stored at the image buffer, located in the camera's control unit, and downloaded onto a computer via a high-speed cable connection. A continuous light source, Solarc ELSV-60, provided high intensity white light for the CCD imaging chip. The light was transferred through a fibre optic cable to the interrogation zone. The lamp runs on a 60W without producing excessive heat. A reverse 50 mm lens was connected to the camera and the magnification of the viewing area could be adjusted by inserting ring spacers between the lens and the CCD chip. The schematic of the video system can be seen in Figure 3.42.

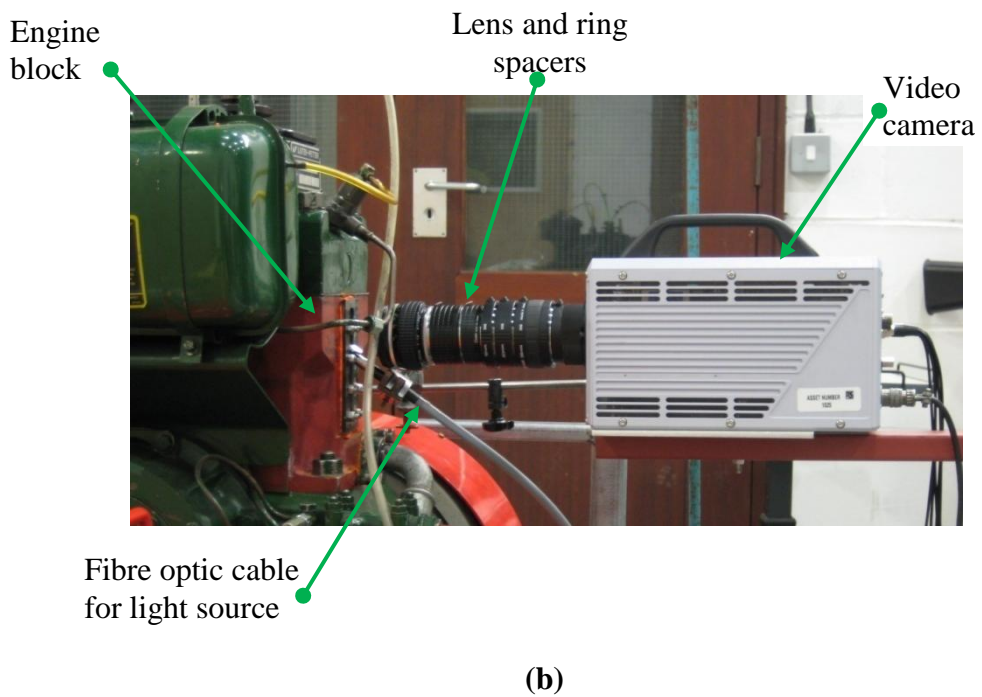
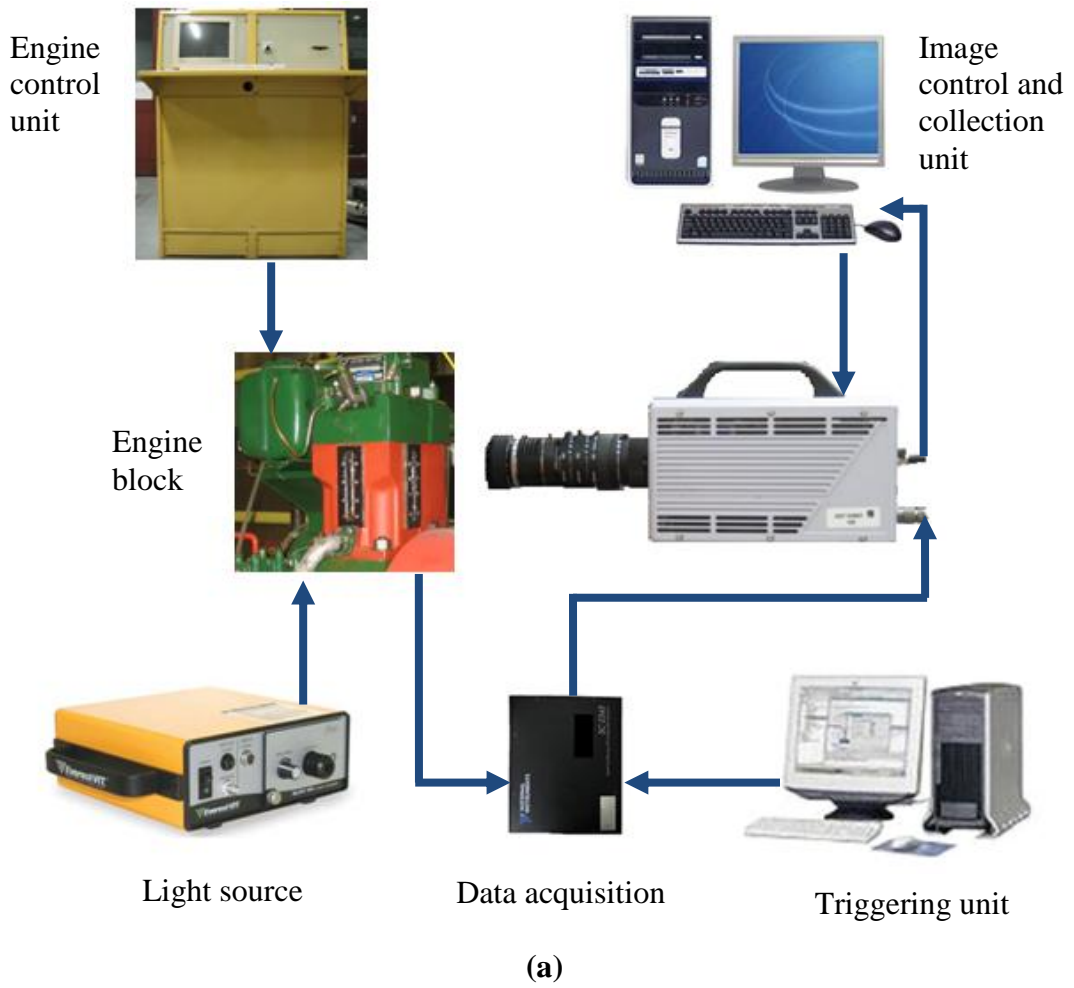


Figure 3.42: (a) Schematic of video imaging system (b) Engine visualisation set-up

3.5.8 PISTON RING PACK

The piston ring pack used in this current project is that most commonly used in today's diesel engines. It consists of two compression rings, a scraper ring and an oiler ring and is presented in more detail in Table 3.4.

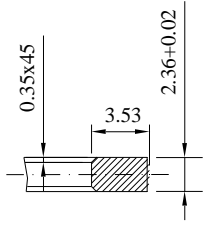
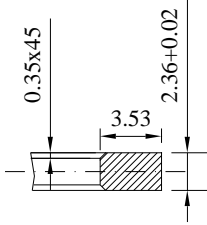
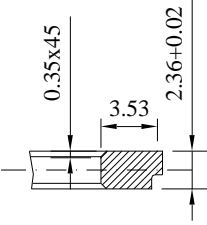
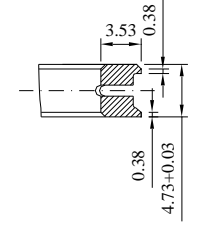
	Dimensions in mm	Tangential Ring Tension
First compression ring		14.36 – 19.21 N
Second compression ring		14.54 – 19.43 N
Scraper compression ring		13.16 – 17.57 N
Oil control ring		21.17 – 28.6 N

Table 3.4: Piston ring pack

3.6 SUMMARY OF EQUIPMENT AND TECHNIQUES

The investigations of the oil flow characteristics and cavitation incipience in the idealised test rig has involved numerous measurement techniques. This required improving and building the test rig so as to simulate better the lubrication action between the piston-ring and the liner. Various lubricants characteristics were successfully measured between the specimen ring and liner in terms of the oil film thickness by means of the capacitance method and friction by a force sensor. The implementation of an optical liner allowed the imaging of cavitation development through a still CCD camera and the integration of a high speed video system enabled the transient flow to be captured. Furthermore the measurement of oil film pressure with a miniature pressure transducer supported the cavitation findings. The application and the successful calibration of the LIF system provided further support to the the identification of cavitation incipience in the oil film between the ring/liner interface. The extensive investigation of the cavitating oil flow was further pursued in a motoring single cylinder engine by installing optical windows on the liner. The high speed video system was employed and the high frame rates proved to be very useful in capturing the highly transient flow. The transfer of knowledge acquired in measuring the oil film pressure in the test rig to that of the engine allowed the oil film pressure to be effectively measured. The hardware and software for both test rig and engine enhanced the quantitative and qualitative understanding of the cavitation development in the oil film.

Chapter 4

CHARACTERISATION OF OIL FILM IN THE IDEALISED TEST-RIG

The test rig, which represents the interaction of piston-ring/liner in a reciprocating engine, provides an opportunity to investigate a broad parametric study on lubricants under idealised conditions. The test rig allows quantitative measurements such as oil film thickness, friction between liner and specimen ring and oil film pressure to be obtained. Furthermore, the LIF technique has been used mainly to identify cavitation under the piston-ring. The rig also provides adequate optical access for qualitative visualisation of the oil flow in the regions of interest. These investigations provide information for improving the physical understanding of the dynamics of oil films, the cavitation initiation and development and its dependencies on various parameters such as for instance, viscosity and flow operating conditions. The results from these investigations are presented and discussed.

4.1 RESULTS: QUANTITATIVE MEASUREMENTS

A parametric study was carried out on a hydrocracked base oil. The tests for this oil, were carried out at four different speeds (300, 400, 500 and 600 rpm) and for four different loads (977 N/m, 1872 N/m, 2354 N/m and 2823 N/m). Capacitance, LIF, friction and pressure data are obtained. The stroke was set to 22 mm and the results are shown as averages over twenty cycles. The oil was maintained at 38°C approximately and their properties are shown in Table 4.1 while the surface characteristics of the ring and liner are given in Table 4.2. This parametric study on this particular oil is deemed important so as to give a better understanding of the visualisation experiments which are discussed in the next chapter. Figure 4.1 shows the movement of the liner in the down

and up stroke directions and the locations of the top (TDC) and bottom (BDC) dead centres. The profile of the specimen ring is shown in Figure 4.2.

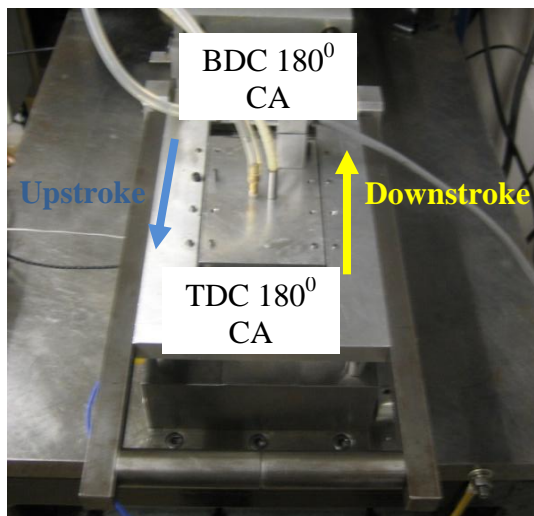


Figure 4.1: Liner movement

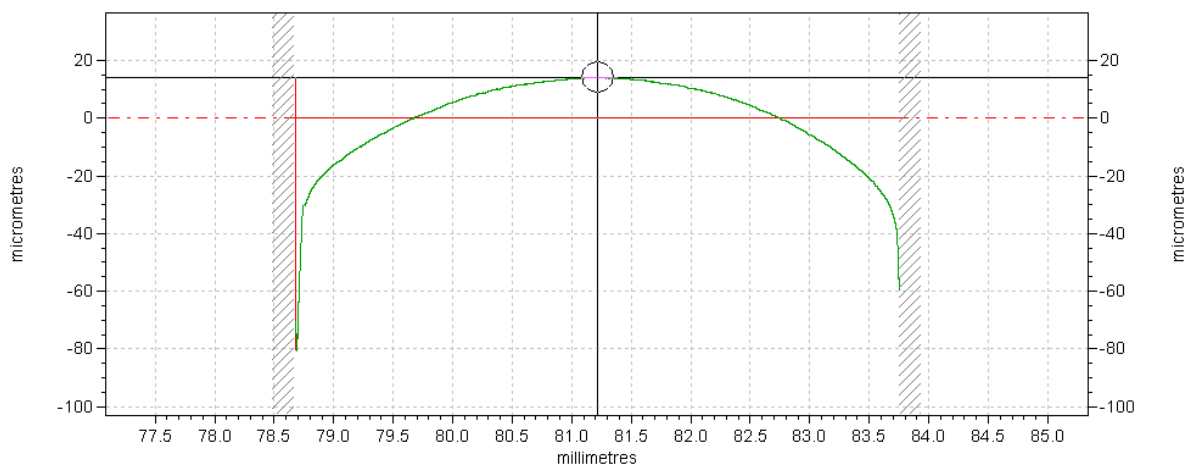


Figure 4.2: Specimen ring profile

Blend Code	002A
SAE Grade	5W-40
HTHS (mPa s)	4.05
V₁₀₀ (cSt)	14.97
V₄₀ (cSt)	97.8
VI	160

Table 4.1: Tested oil properties

	R_a (µm)	R_q (µm)
Piston - Ring	0.351	0.433
Liner	0.193	0.250

Table 4.2: Ring and liner surface characteristics

4.1.1 OIL FILM THICKNESS (CAPACITANCE METHOD) MEASUREMENTS

Figure 4.3 and Figure 4.4 present some samples of the measured oil film thickness which quantify the variation of the oil film thickness as a function crank angle (CA) at different speeds and loads. In general, at any operating condition, the capacitance results show two minima and two maxima values in the full cycle, with the first minimum value near TDC of the downstroke and then a second minimum value near BDC; similar trends can be seen in the upstroke cycle. The results clearly show that the oil film thickness decreases with increasing load at all speeds as can also be seen in Figure 4.4.

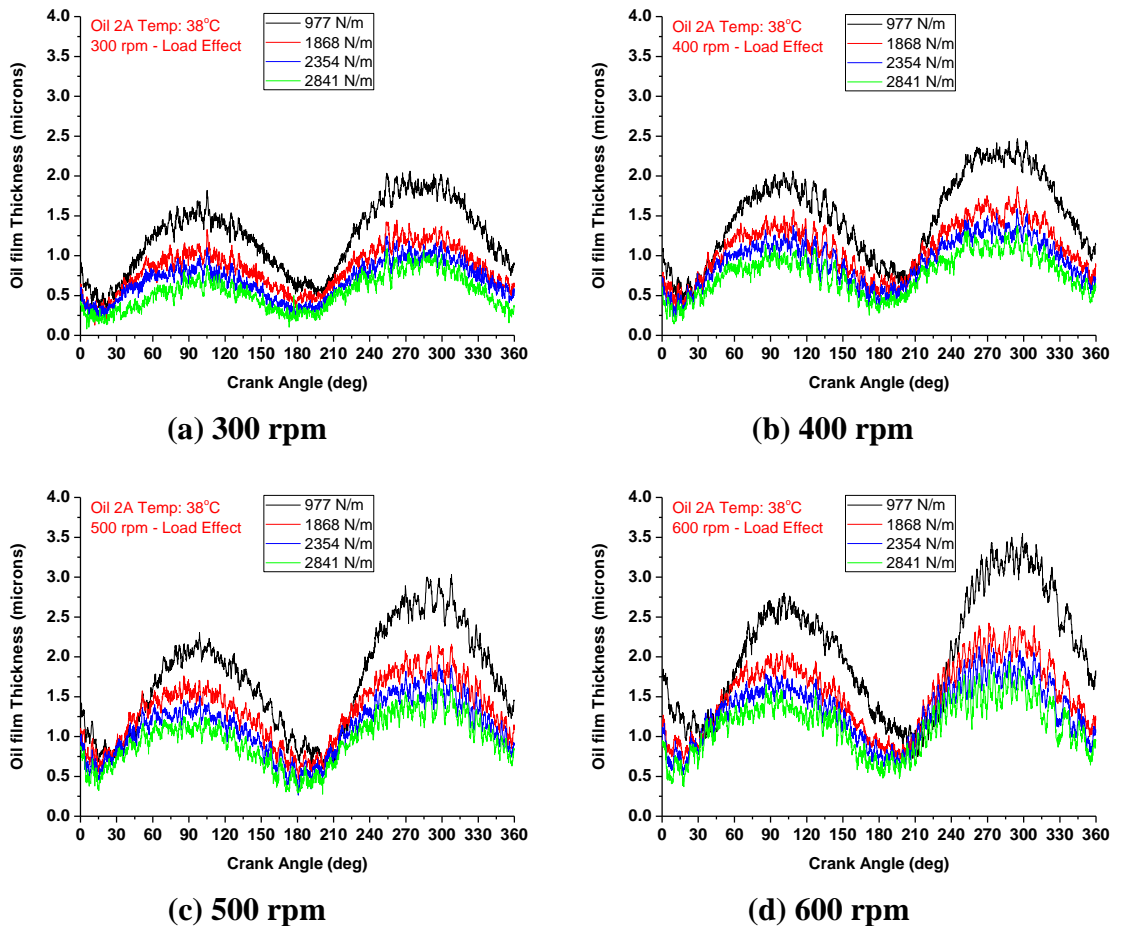


Figure 4.3: Variation of oil film thickness with CA at different loads for oil 2A

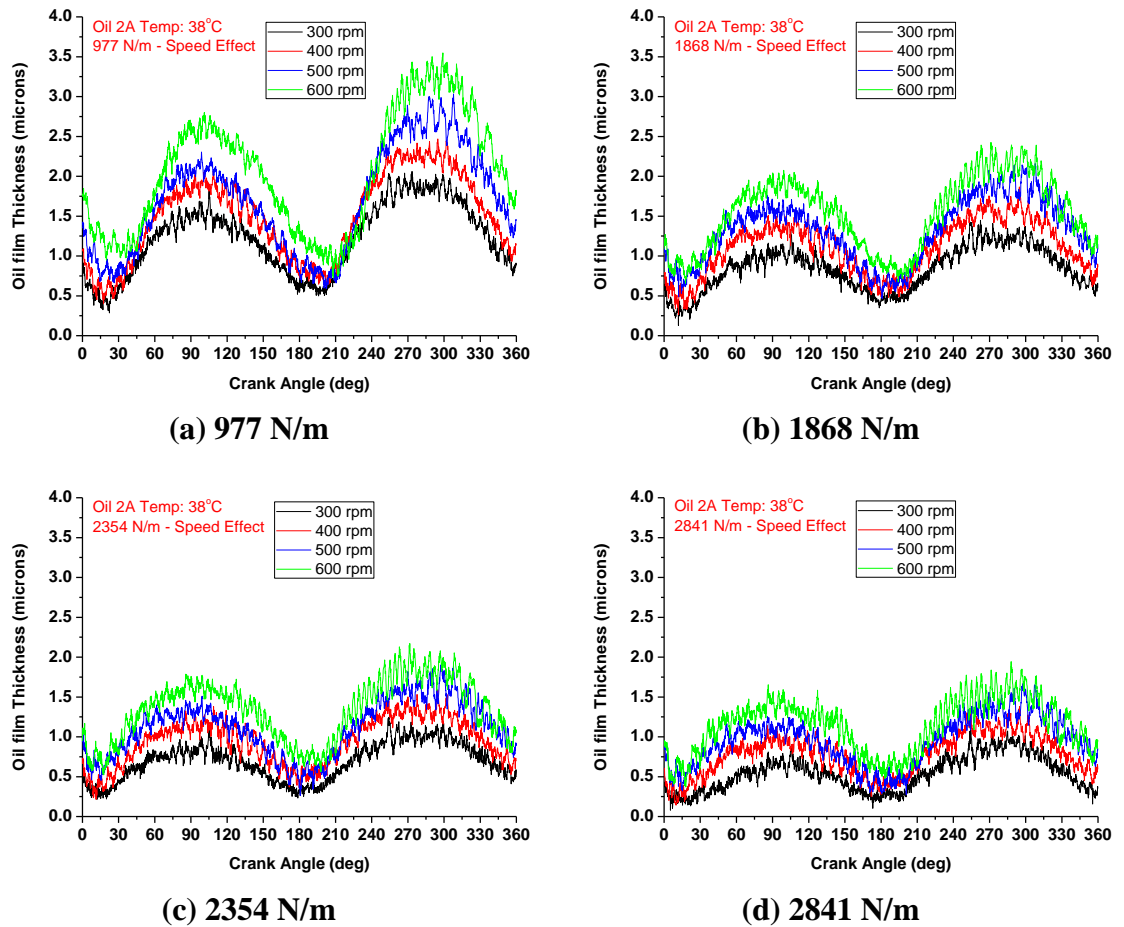


Figure 4.4: Variation of oil film thickness with CA at different speeds for oil 2A

The capacitance results for oil 2A also clearly show that the oil film thickness increases with speed (Figure 4.4) everywhere during the downstroke and upstroke, as would be expected, and this is more pronounced at the lowest measured load (Figure 4.3(a)) so that the maximum oil film thickness (OFT) is increased by 1.74 times in the upstroke for an increase of speed from 300 rpm to 600rpm. It is also clearly evident that higher OFTs were recorded in the upstroke measurements ($180^{\circ} - 360^{\circ}$) at all measured conditions than those of the downstroke ($0^{\circ} - 180^{\circ}$) mainly due to the asymmetrical profile of the ring, as illustrated in Figure 4.2. This was intentionally manufactured in order to investigate the effect of surface ring profile on the lubricant film. It should be noted that the relatively large minimum film thicknesses near the TDC (0° CA) and BDC (180° CA) is due to the fact that the flow reversal takes place later on in the stroke, lagging behind the mechanical movement of the liner forming a small film thickness. These cyclic variations of OFT can be correlated to the different regimes of lubrication that exist at different time in the full cycle and which are identified in the next section.

4.1.2 FRICTION MEASUREMENT

Friction results obtained from the friction measurements are presented next and are shown in Figure 4.7 and Figure 4.8; however, prior to discussing the results it may be useful to identify different regimes of lubrication during a full cycle of liner movement against the piston ring. Normally for a full rotation of the crank, the liner shifts through different regimes of lubrication. Figure 4.5 exemplifies the possible transitions over the downstroke movement of the liner. Just after the start of the stroke (after TDC), the ring is not separated by the lubricant, fluid effects are negligible and friction is mainly dominated by metal-to-metal contact between surface asperities (liner and ring). This part of the stroke is in the boundary lubrication region and is marked by the high spike in friction. Moreover, as the liner accelerates away from the TDC, a lubricant film separating the two contacting parts starts to form and here the acting load is supported partly by the asperity-to-asperity solid contact and partly by the lubricant present in the contact; this portion of the stroke is thus considered to be in the mixed lubrication regime. As the velocity increases, the load balance shifts further towards the lubricant because the surfaces separate and asperity interaction decreases.

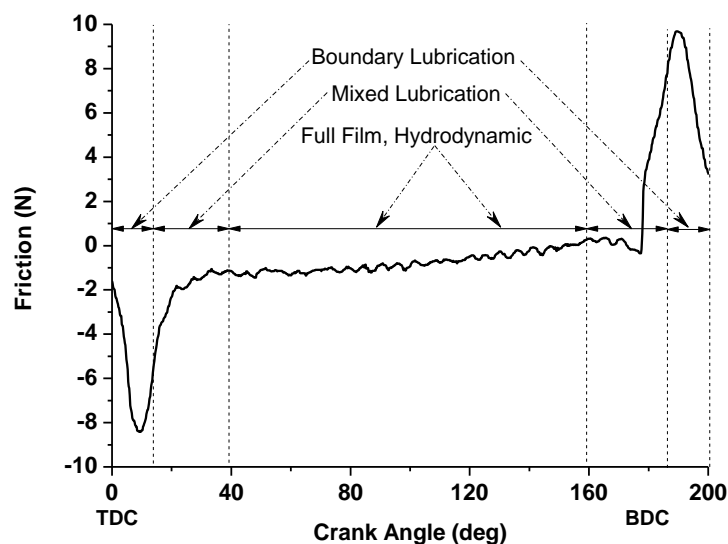


Figure 4.5: Possible lubricant regimes encountered during downstroke at 300 rpm with 1868 N/m

The frictional force at the ring/liner contact is due to asperity contact and viscous losses. However, the frictional force due to asperity contact (when it is present) is usually much higher than the viscous losses, resulting in a point of minimum friction as the ring

makes the transition from mixed lubrication to hydrodynamic lubrication. It can also be seen from Figure 4.6 that through the hydrodynamic lubrication regime, the lubricant film thickness reaches a maximum and, in this portion of the stroke, the lubricant film is thick enough to prevent any asperity interactions. Hence, it is expected that during the hydrodynamic lubrication regime, minimum friction should be achieved because there is no friction force due to asperity contact and the only friction component comes from the viscous drag. Indeed from Figure 4.5, it can be appreciated that the hydrodynamic lubrication regime is reached in this part of the stroke due to the presence of the viscous hump which provides evidence that the ring/liner has reached a state of hydrodynamic lubrication. It can also be observed that a local maximum in the friction curve occurs around mid-stroke since viscous shear is proportional to the relative speed of the liner. Furthermore, when the liner moves from mid-stroke to BDC, the opposite happens. The ring decelerates and this causes the hydrodynamic action of the ring to decrease and give rise to smaller film thickness. Smaller film thickness means the two surfaces are approaching each other and the possibility of asperity-to-asperity contact increases. Now the velocity continues to decrease and at a certain point it is no longer sufficient to build a film thick enough so as to keep the two surfaces separated completely from each other. Therefore, the ring returns back to a state of mixed lubrication and, as expected and seen from Figure 4.5, the asperity interactions and frictional losses continue to increase until finally the liner reaches boundary lubrication at the BDC, as shown in Figure 4.5. These effects can be realised more clearly through a simultaneous comparison between the friction and oil film thickness during a full cycle like that presented in Figure 4.6. From the results, it is evident that the maximum friction corresponds to minimum oil film thickness.

As it is customary to determine the combined R_a and R_q of the surfaces, the larger values are used here as an indication of the onset of asperity interactions:

$$R_{a_{contact}} = R_{a_{piston-ring}} + R_{a_{liner}} = 0.544 \mu m$$

$$R_{q_{contact}} = \sqrt{R_{q_{piston-ring}}^2 + R_{q_{liner}}^2} = 0.500 \mu m$$

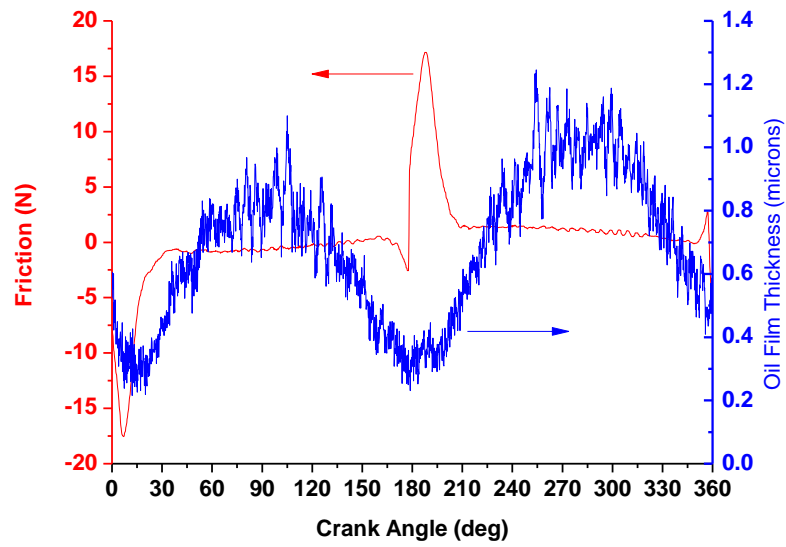


Figure 4.6: Relationship between oil film thickness and friction

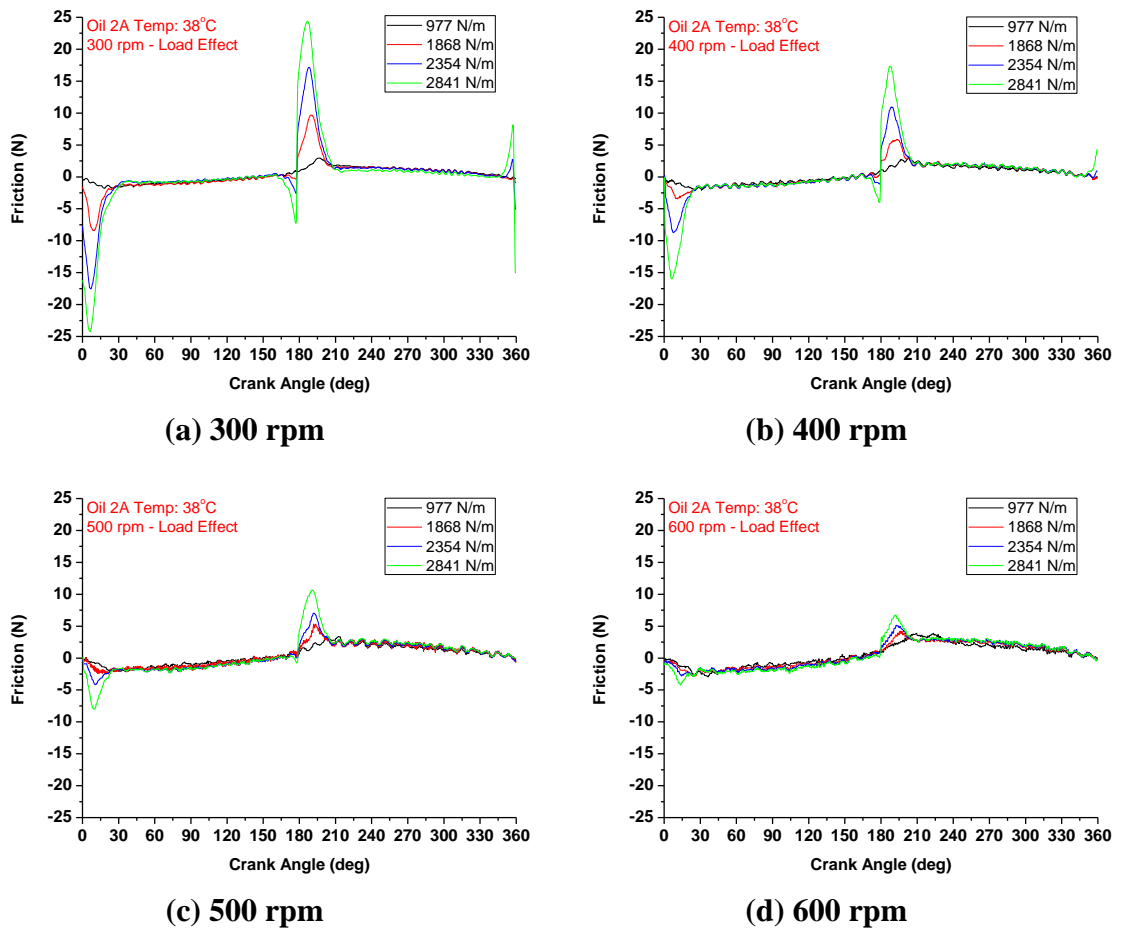


Figure 4.7: Variation of friction with CA at different loads for oil 2A

Figure 4.7 and Figure 4.8 show the variation of the frictional force with respect to the crank angle at different loads and speeds, respectively. From the figures it can be seen that through the complete cycle, the values of friction from TDC to BDC (during downstroke) are almost equal in magnitude but opposite in sign to values of friction from BDC back to TDC again (during upstroke). Therefore it can be deduced that the sign of friction dictates the direction of travel such that negative values of friction occur when the liner is moving from TDC to BDC and positive values of friction are present where the liner is moving from BDC to TDC.

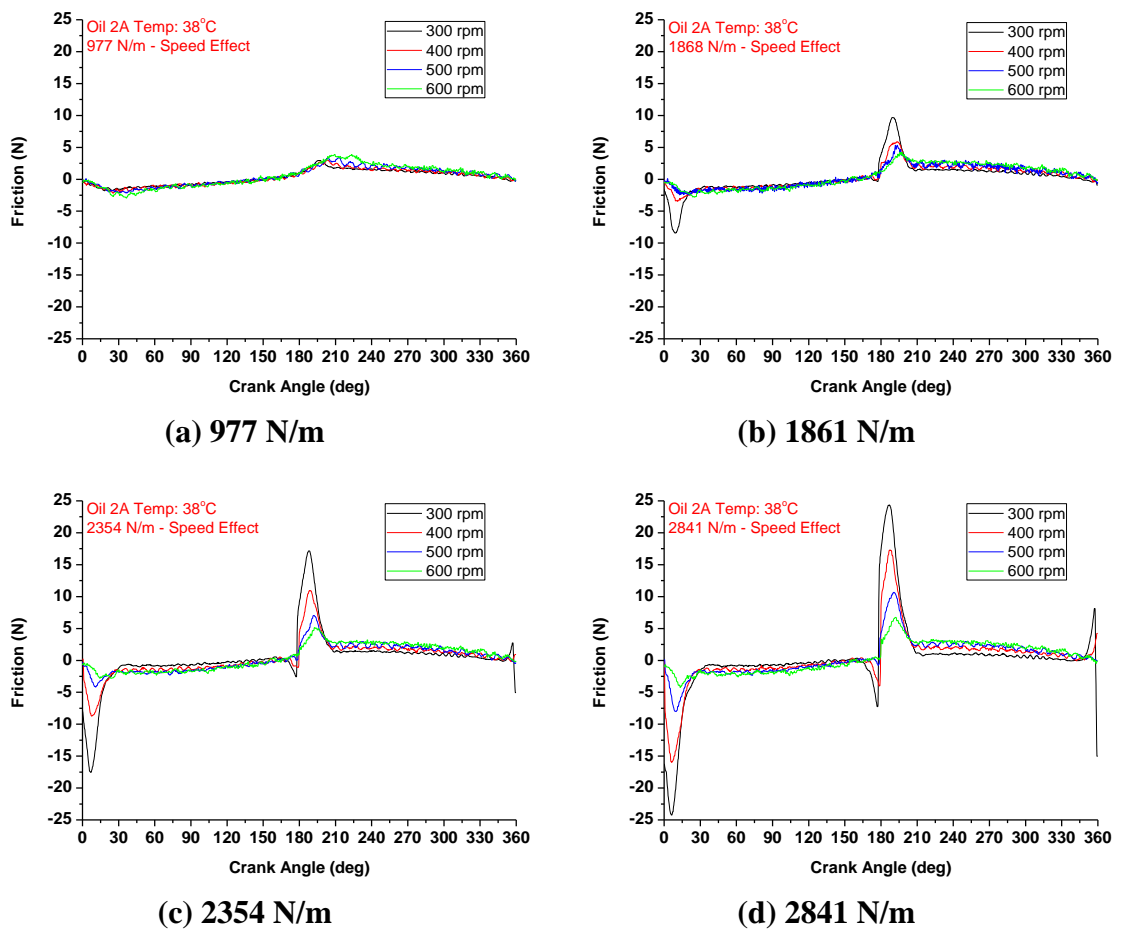


Figure 4.8: Variation of friction with CA at different speeds for oil 2A

Figure 4.7 illustrates the effect of load on friction at different speeds and demonstrates the very large values near TDC and BDC. As shown before in Figure 4.3, the lubricant film thicknesses were minima around TDC and BDC and decreased with increase in load. The latter in turn will increase the asperity interactions further around TDC and

BDC, where asperity interactions are already significant, which resulted in higher friction peak with load as is clearly evident from Figure 4.7 and Figure 4.8. This is justified due to the fact that the film thickness decreases with increasing load which causes the surfaces to approach each other even more, and favouring even more asperity-asperity contact at around the TDC and BDC.

Figure 4.8 depicts the effect of speed on friction where different loads are applied to the contacts. Hydrodynamic lubrication occurs in the converging section of the ring and this is responsible for generating the load-supporting pressure in the lubricant film. Increasing the sliding speed of the liner improves the wedging action of the converging ring profile which in turn, provides a better load capacity with a larger lubricant film thickness. This explains the increase in viscous friction as oil film thickness increases with speed, as shown in Figure 4.8. Another important feature of the graphs is the occurrence of peaks in the hydrodynamic friction region just after the dead centres. Since viscous shear is proportional to velocity, a more pronounced rise in viscous friction is seen with increasing speed. In this case, there will be no asperity-asperity contact and friction losses will be due just to viscous drag.

4.1.3 OIL FILM PRESSURE AND LIF MEASUREMENTS

To improve the current understanding of cavitation onset and evolution in the lubricant films, it is important to correlate the local lubricant pressure with the amount of oil present in the conjunction during the cavitation period. The results of pressure (Figure 4.9 and Figure 4.10) and LIF (Figure 4.13 and Figure 4.14) measurements are presented and discussed in this section and an attempt is made to correlate the two data sets, in particular during the cavitation process.

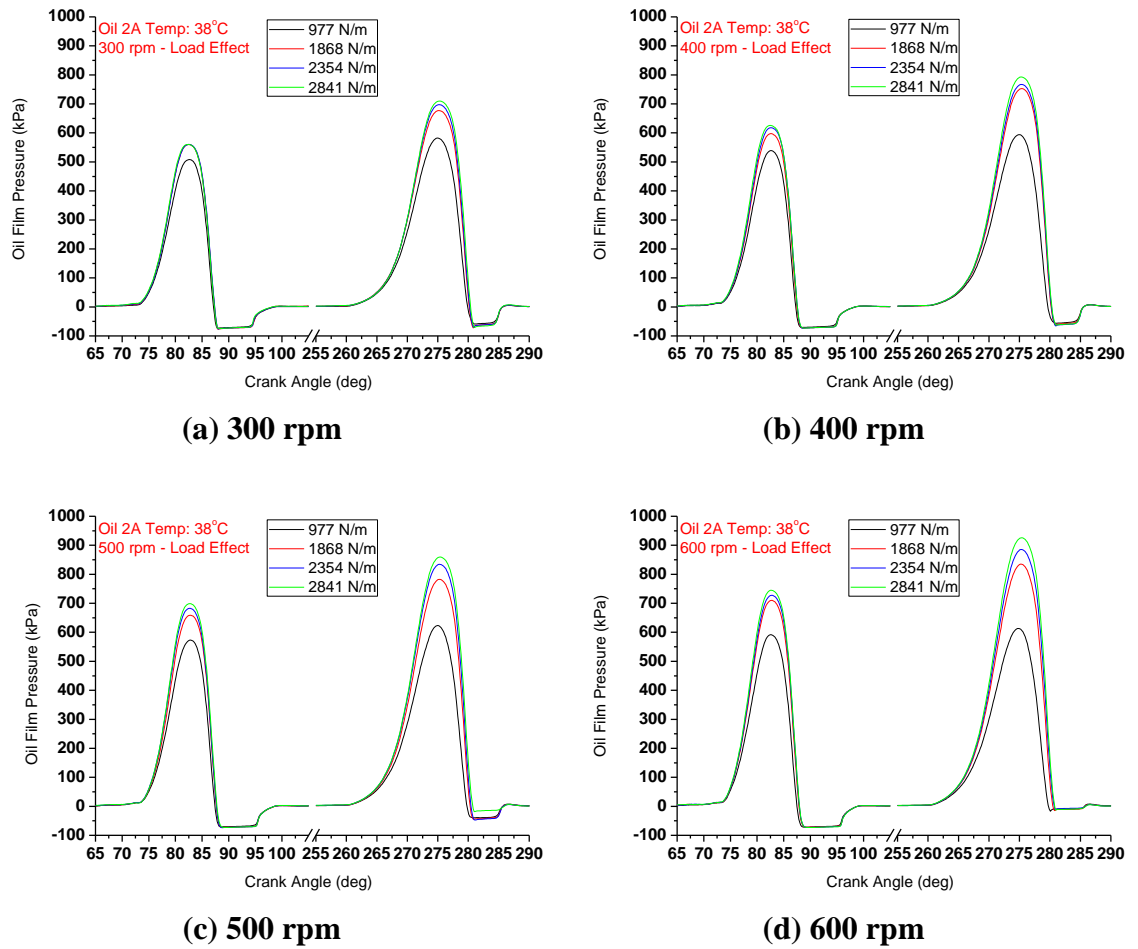
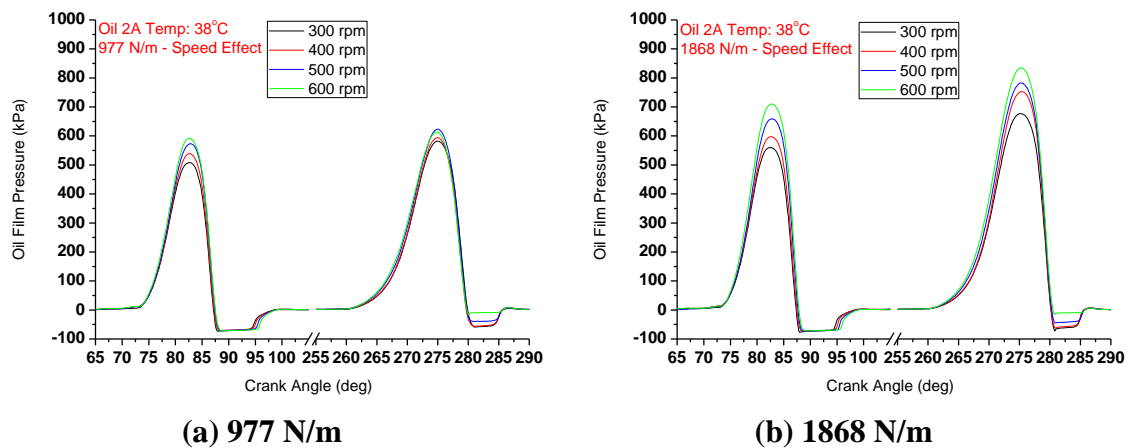


Figure 4.9: Variation of oil film pressure with CA at different loads for oil 2A



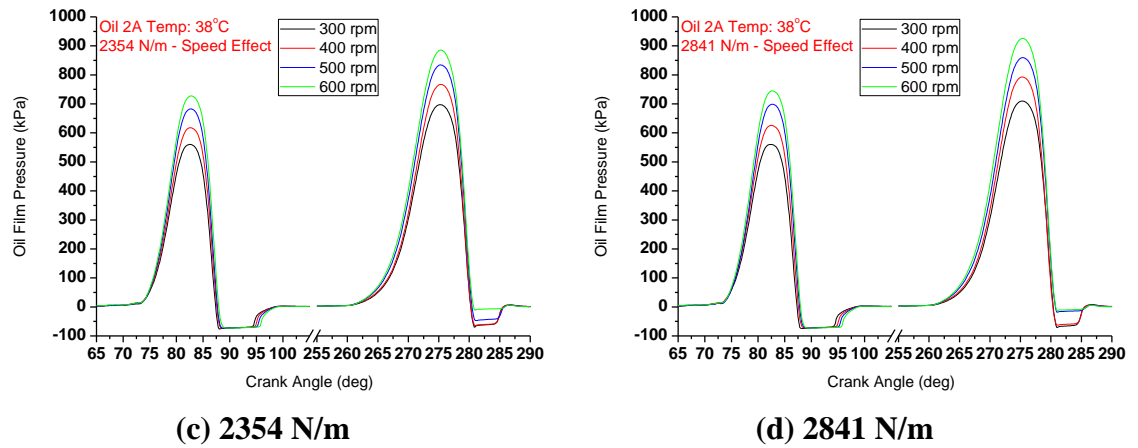


Figure 4.10: Variation of oil film pressure with CA at different speeds for oil 2A

Figure 4.9 and Figure 4.10 illustrate the oil film pressure variation with load and speed, respectively. As the speed and load increase, the hydrodynamic oil film pressure increases as well. Even if the maximum pressure changes substantially with applied load or speed, the extent of the cavitation region, sub-atmospheric pressure region, remains practically unchanged. However, it has been noted in the upstroke pressure measurements for the cases of speed 500 rpm at a load of 2841 N/m and speed 600 rpm at all loads that the sub-atmospheric pressure readings do vary. It is worth again mentioning that the pressure reading is an average over twenty consecutive measurements. The oil film pressures, for 500 rpm – 2841 N/m, for the 20 consecutive cycles are displayed in Figure 4.10 and Figure 4.12 which illustrate the averages with error bars between consecutive measurements from the acquired cycles; these cycles for the downstroke pressure measurements almost overlay each other, demonstrating very good repeatability, with minute variations and a standard deviation of 0.23, as depicted in Figure 4.12 (a). The same is true during the upstroke measurements, with the exception of the sub-atmospheric region. There the pressure varies randomly between a minimum of -5 kPa to a maximum of -65 kPa with most of them (> 70%) being closer to atmospheric pressure. Similar patterns have been noted for the 600 rpm case where the sub-atmospheric pressure lies closer to the ambient pressure. One possible reason for this occurrence is that the curvature of this part of the ring is shorter, compared to the downstroke measurements, and the speed is greater. In this case the cavities reach the trailing edge of the ring quicker where they are in contact with the atmosphere. Hence, their pressure becomes closer to atmospheric.

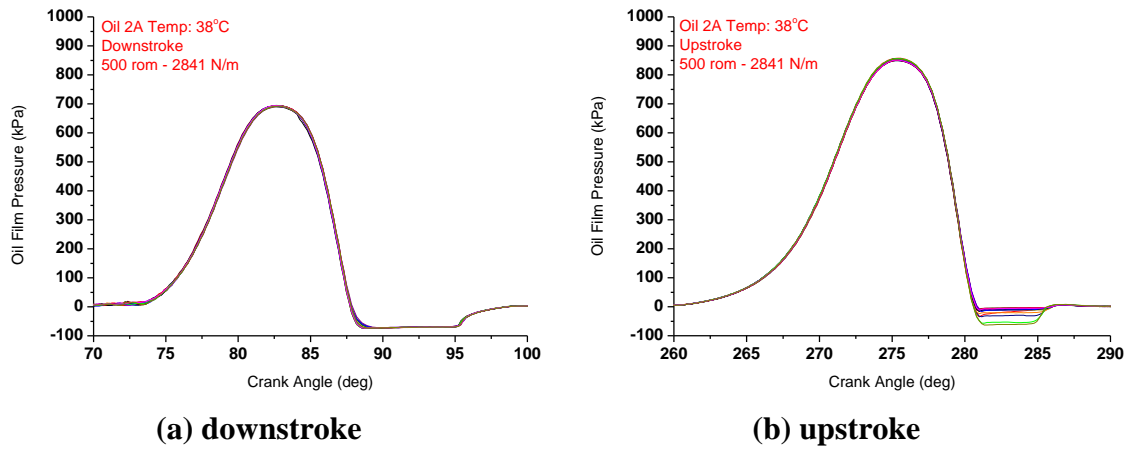


Figure 4.11: Pressure measurements over 20 consecutive cycles for 500 rpm - 2841 N/m

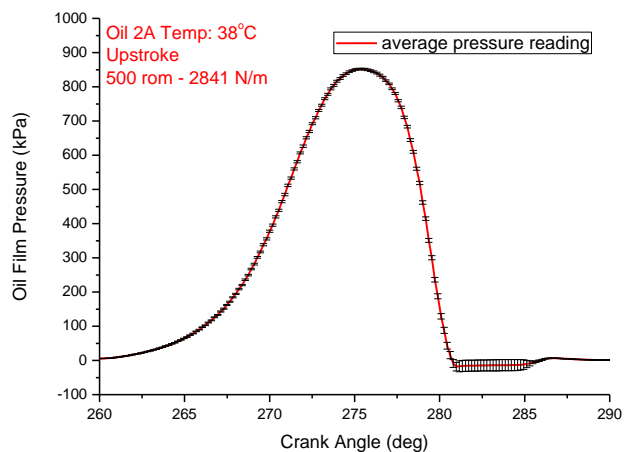
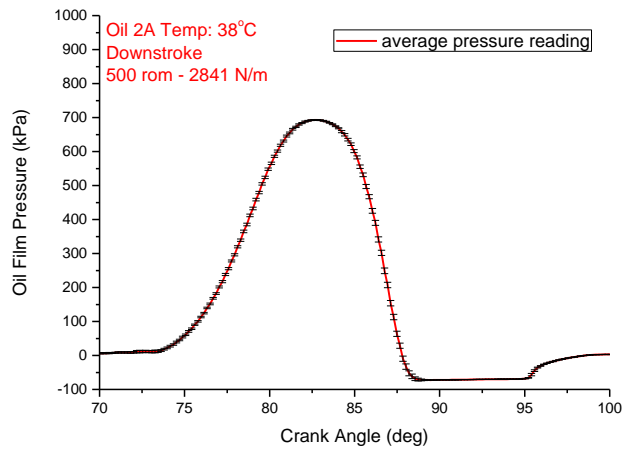


Figure 4.12: Average pressure reading and error bars based on 20 cycles

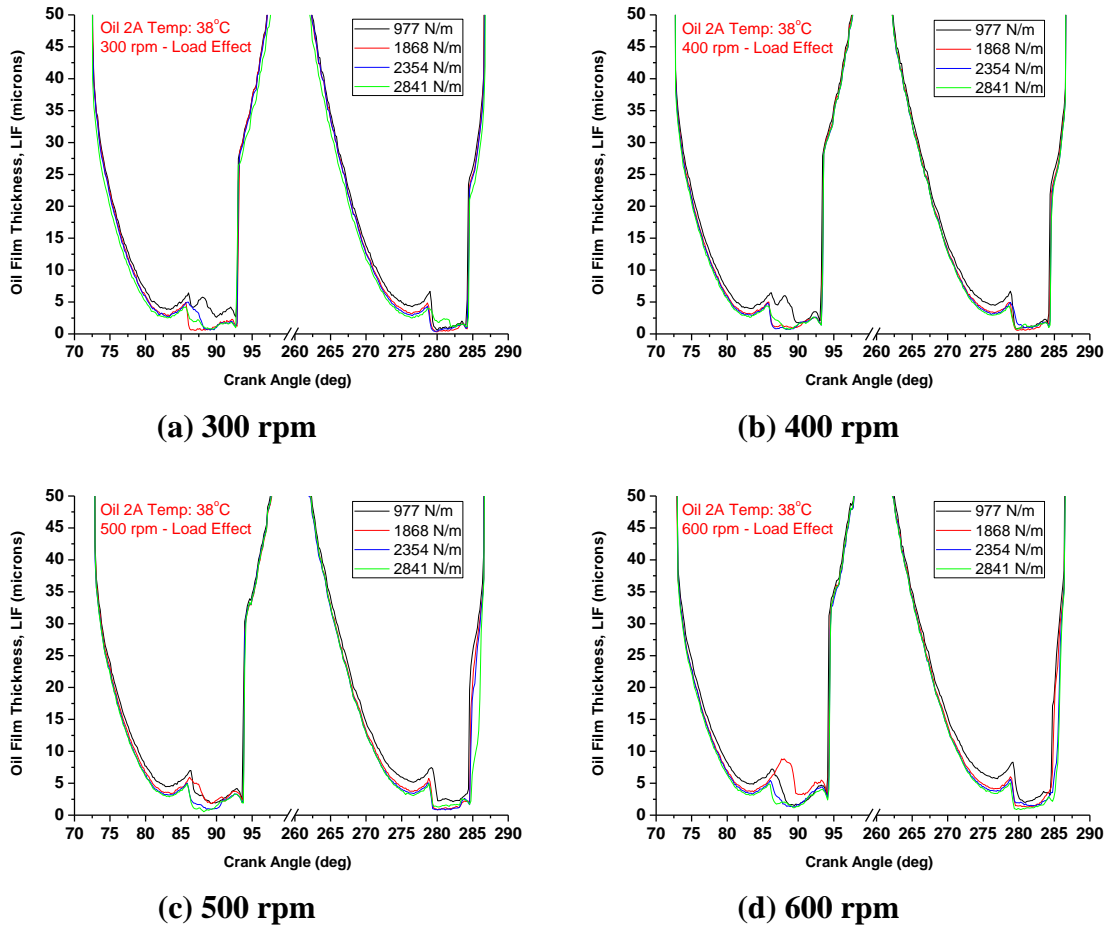
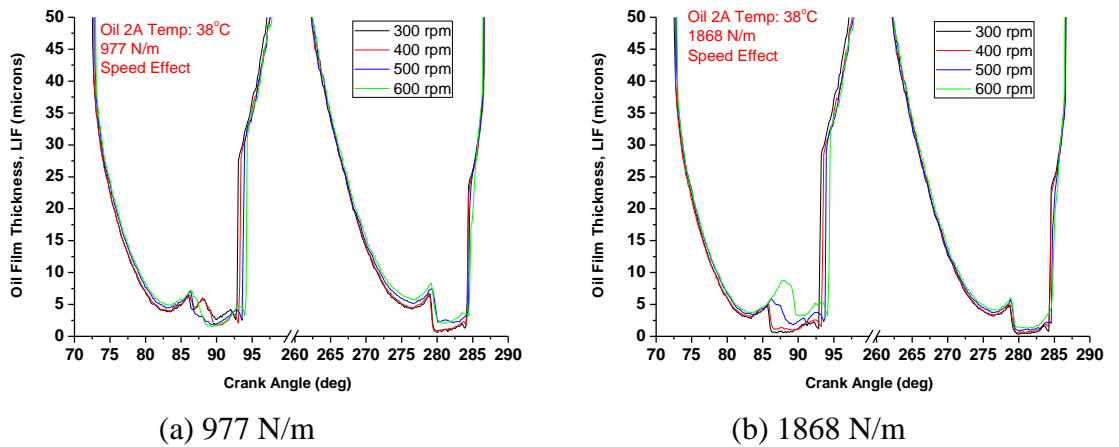


Figure 4.13: Variation of LIF measurements with CA at different loads for oil 2A



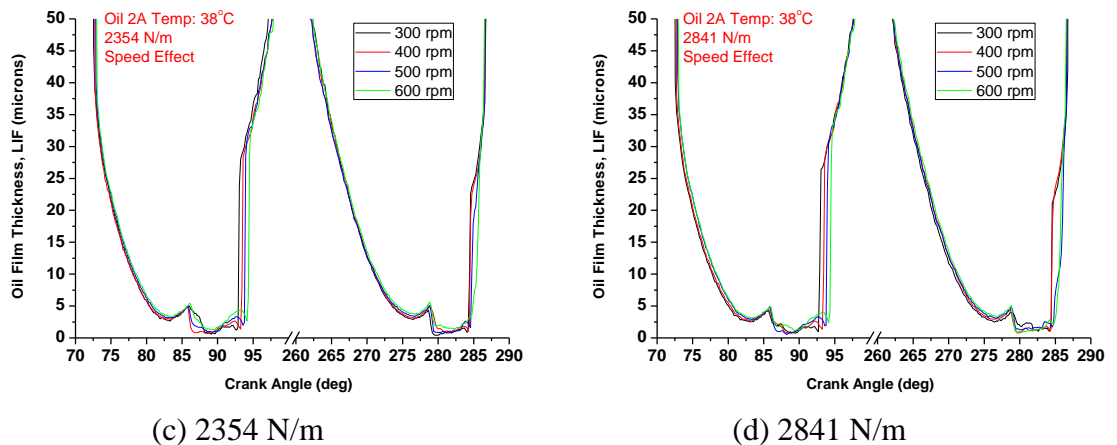


Figure 4.14: Variation of LIF measurements with CA at different speeds for oil 2A

The LIF technique (described in the previous chapter) measures the amount of oil present in a very narrow control volume. Using the calibration method previously described, this amount of oil can be further converted into a thickness of the oil film. The advantage of this approach is that the technique does not measure the distance between the two sides of the conjunction, but rather the amount of oil encountered by the laser beam. Therefore, considering that the liner is perfectly flat and neglecting the local deflections from either side of the conjunction, the LIF measurement should coincide with the ring profile in the regions where the film is continuous (before and after the cavitation region). If the oil film is partly depleted (because of cavitation), the method measures only the thickness of the oil film which adheres to either side of the conjunction; therefore, these areas can be easily identified as they deviate from the ring profile. The downstroke and upstroke LIF measurements have been superimposed on each other in Figure 4.15; it is clear that the LIF measurements match well the ring profile and the crank angle in the x-axis in all cases is in accordance to the width of the piston-ring.

In the downstroke the laser beam measures the oil film which adheres to the converging part of the ring, following the ring profile path. On reaching the diverging part of the ring a sudden drop of oil film is encountered but later in the stroke the oil film follows back the ring profile. In the upstroke measurement, the diverging part of the downstroke becomes the converging part of the ring. Here again the laser beam measures the oil film corresponding to the ring profile. Attaining the diverging part (converging part of

the downstroke measurement), depletion in oil film thickness is also noted before reforming again, when the liner reaches the trailing edge of the ring, in the later stage of the stroke. Figure 4.13 and Figure 4.14 show the downstroke and upstroke OFT measured with the LIF technique with load and speed respectively. Similar trend has been observed to that measured with the capacitance method. That is the OFT increases when the hanging load applied to the ring is reduced (Figure 4.13) and increases with increasing speed (Figure 4.14).

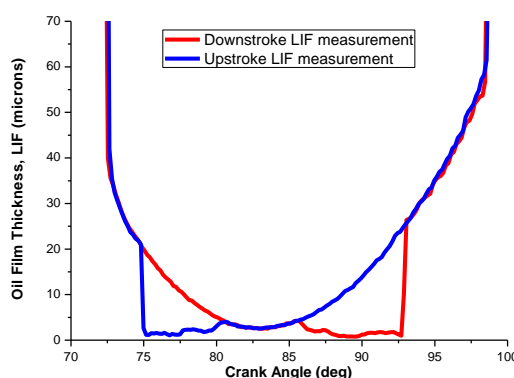
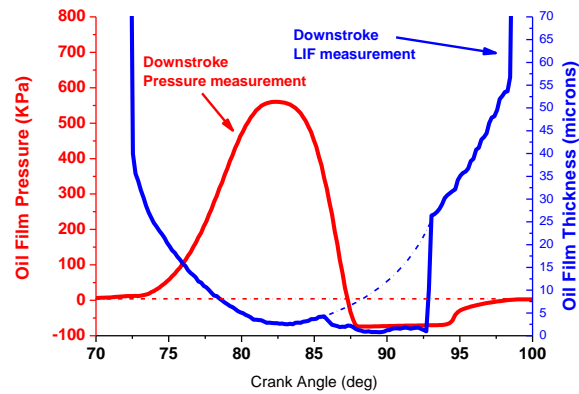
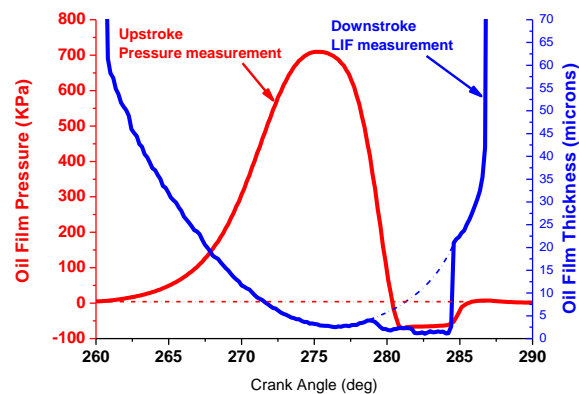


Figure 4.15: Downstroke and Upstroke LIF measurement

Figure 4.16 shows the oil film pressure and the film thickness as a function of the crank angle degree, for “downstroke” and “upstroke” movement of the liner at a corresponding motor speed of 300 rpm and a load of 2841 N/m. To understand these figures it should be taken into consideration that both sensors are rigidly mounted on the liner, which is rapidly sliding, moving the measuring point along the profile. It should also be noted that the ring profile is not symmetrical, having different radius of curvature on each side. This construction of the test rig can highlight the importance of correctly understanding the ring geometry. The blue line represents the ring profile and the red line the atmospheric pressure. As the oil travels through the diverging part of the ring, it creates a hydrodynamic oil film pressure. As the fluid film tries to occupy the clearance space of the increasing volume in the diverging region, the pressure in the piston-ring/liner drops below the atmospheric pressure. This drop below ambient conditions may cause the film to rupture or to cavitate. Furthermore, the LIF measurement (Figure 4.16 a and b) clearly shows that in the sub-atmospheric region there is a depletion of the oil film on the ring which provides further evidence that cavitation does occur in this region of the ring.



(a) downstroke measurements



(b) Upstroke measurements

Figure 4.16: Oil film pressure and corresponding oil film thickness

4.2 BASE FLUID RHEOLOGY CHARACTERISTICS OF MONOGRADE MARINE ENGINE OILS

The objective of this project is to assess the rheological behaviour of various base oils and their additive chemistry with a view to establishing the likely field performance in finished marine grades. A major oil company have successfully developed an experimental method that measures ring-liner oil film thickness in a marine 2-stroke diesel engine; this work programme which has been going on until recently, should provide a useful body of work for checking screening tests against known performance. Therefore, the test rig (described in chapter 3) could allow the required data as well as detailed information on the onset and development cavitation to be obtained that could prove to be lubricant specific. The project objectives are:

- To test whether the rig is able to discriminate between different viscosity lubricants and lubricants containing different chemistries in terms of the lubricant film thickness.
- To observe whether the rig provides data which is consistent with the ring-liner film thickness field trial results carried out by industry.
- To assess whether varying lubricant viscosity or chemistry has an effect on the onset and development of cavitation.

Six different oils are tested and their properties are shown in Table 4.3. Compared to oil 2A, these oils are monograde and each of them were made from highly refined base oils and consists of mainly dispersant and detergent additives (1-5 %). Film thickness, friction, pressure measurements are reported along with the test conditions of speed, load and temperature. All the oils are warmed up to approximately 40°C while testing. The stroke for these tests was set to 30 mm and the results are shown as averages over twenty cycles.

	Oil Code	Relative Viscosity	Viscosity Index	Flash Point (°C)	Density @ 20°C (kg/m³)
Reference	026A	1	101	204.5	930
Base Oil A	001C	1.04	112	204.5	930
Base Oil B	004B	1.08	112	204.5	930
Low Viscosity	AW004	0.91	100	203	930
High Viscosity	097A	1.13	95	>225	940
Reference Old chemistry	001A	1.06	106	204.5	930

Table 4.3: Properties of tested marine oils

Note: the viscosity of the oils are relative to the reference oil 026A

4.2.1 DISCUSSION OF LUBRICANT FILM THICKNESS STUDY RESULTS

Here the capacitance results for all the marine oils tested are shown which exhibit similar trends to that of oil 2A. That is the minimum OFT increases with speed (Figure 4.18, Figure 4.20, Figure 4.22, Figure 4.24, Figure 4.26 and Figure 4.28) and decreases when the load applied to the ring increases (Figure 4.17, Figure 4.19, Figure 4.21, Figure 4.23, Figure 4.25 and Figure 4.27). In all cases higher OFT was recorded in the upstroke measurements ($180^{\circ} - 360^{\circ}$) than in the downstroke ($0^{\circ} - 180^{\circ}$) due to the different profile of the ring, as stated previously, demonstrating once more the sensitivity of the employed technique.

Reference Oil: 026A

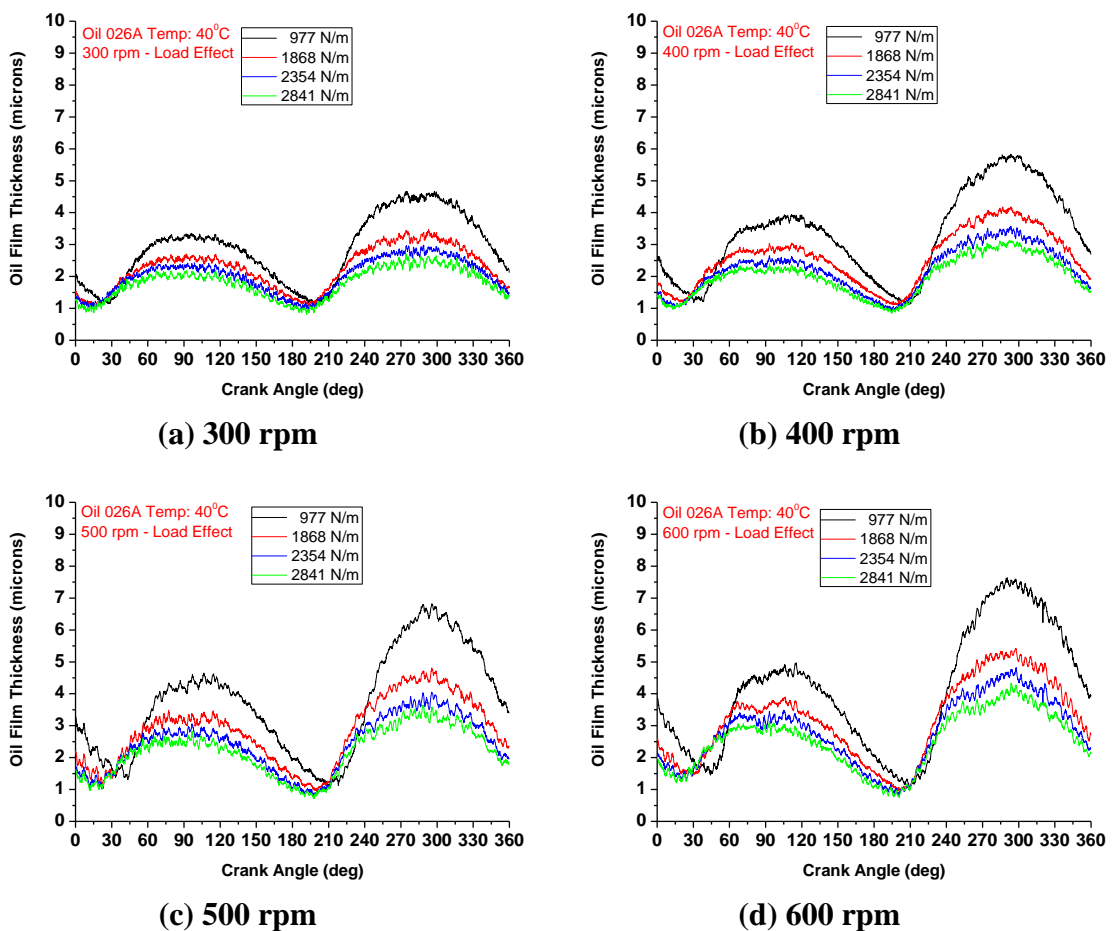
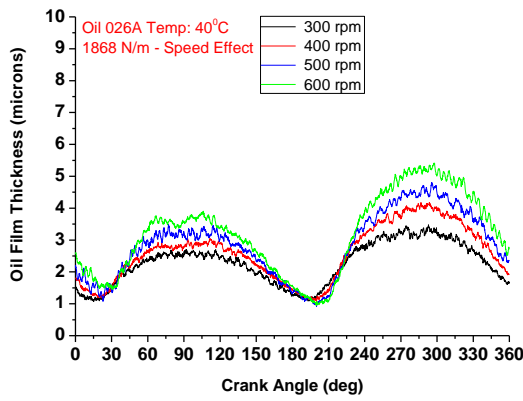
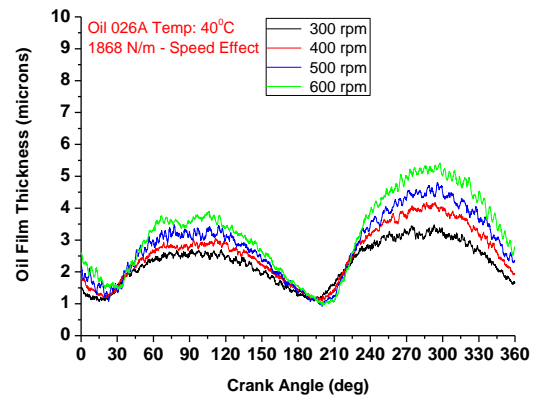


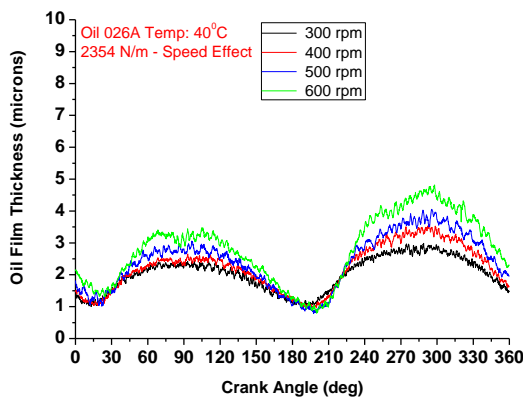
Figure 4.17: Variation of oil film thickness with CA at different loads for oil 026A



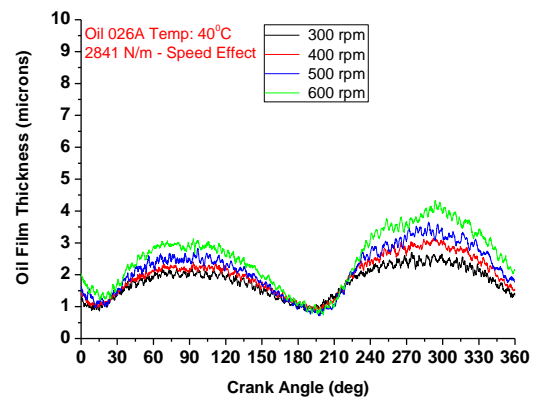
(a) 977 N/m



(b) 1868 N/m



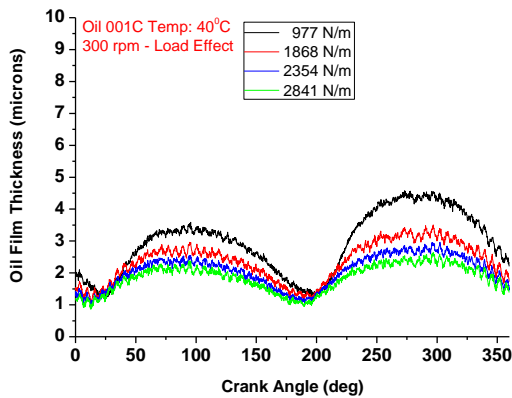
(c) 2354 N/m



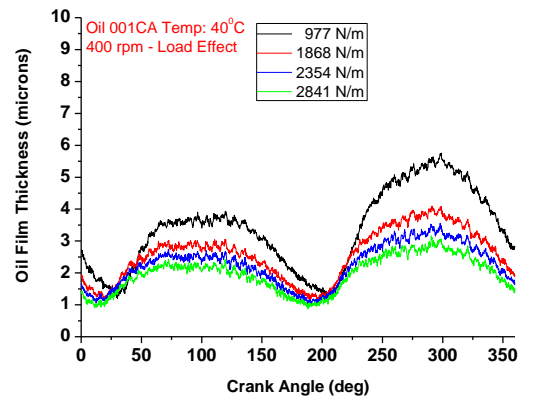
(d) 2841 N/m

Figure 4.18: Variation of oil film thickness with CA at different speeds for oil 026A

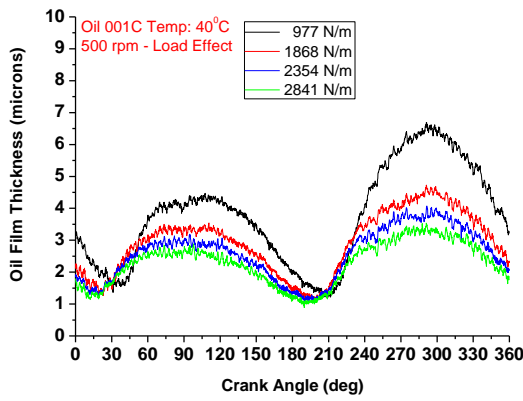
Base Oil A 001C



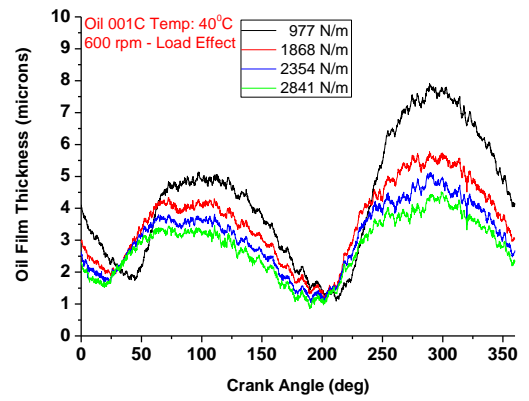
(a) 300 rpm



(b) 400 rpm

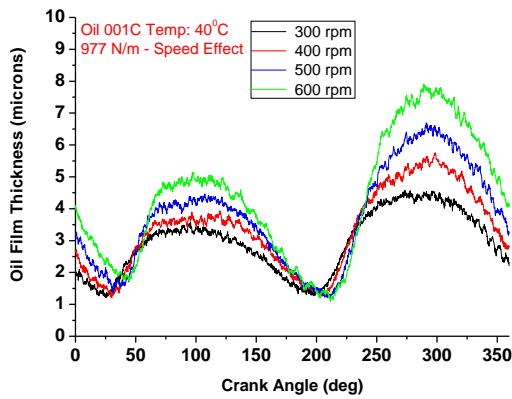


(c) 500 rpm

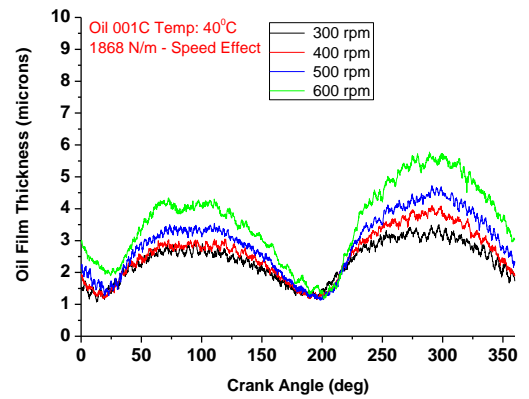


(d) 600rpm

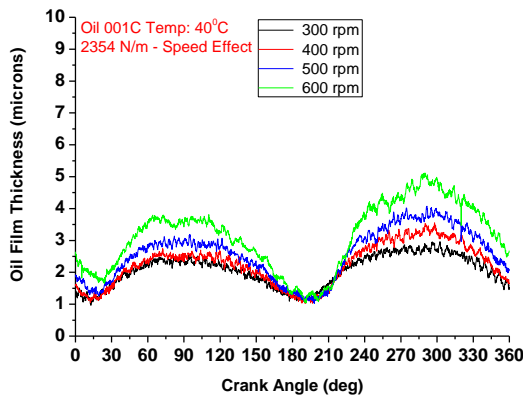
Figure 4.19: Variation of oil film thickness with CA at different loads for oil 001C



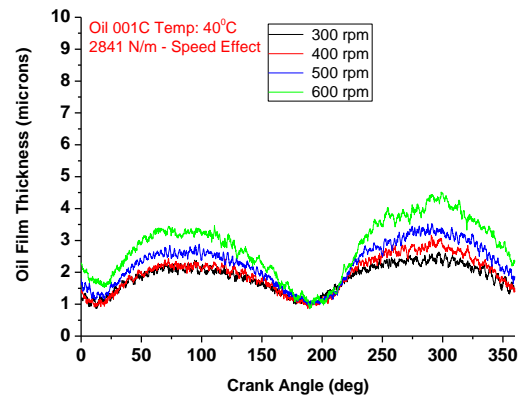
(a) 977 N/m



(b) 1868 N/m



(c) 2351 N/m



(d) 2841 N/m

Figure 4.20: Variation of oil film thickness with CA at different speeds for oil 001C

Base Oil B 004B

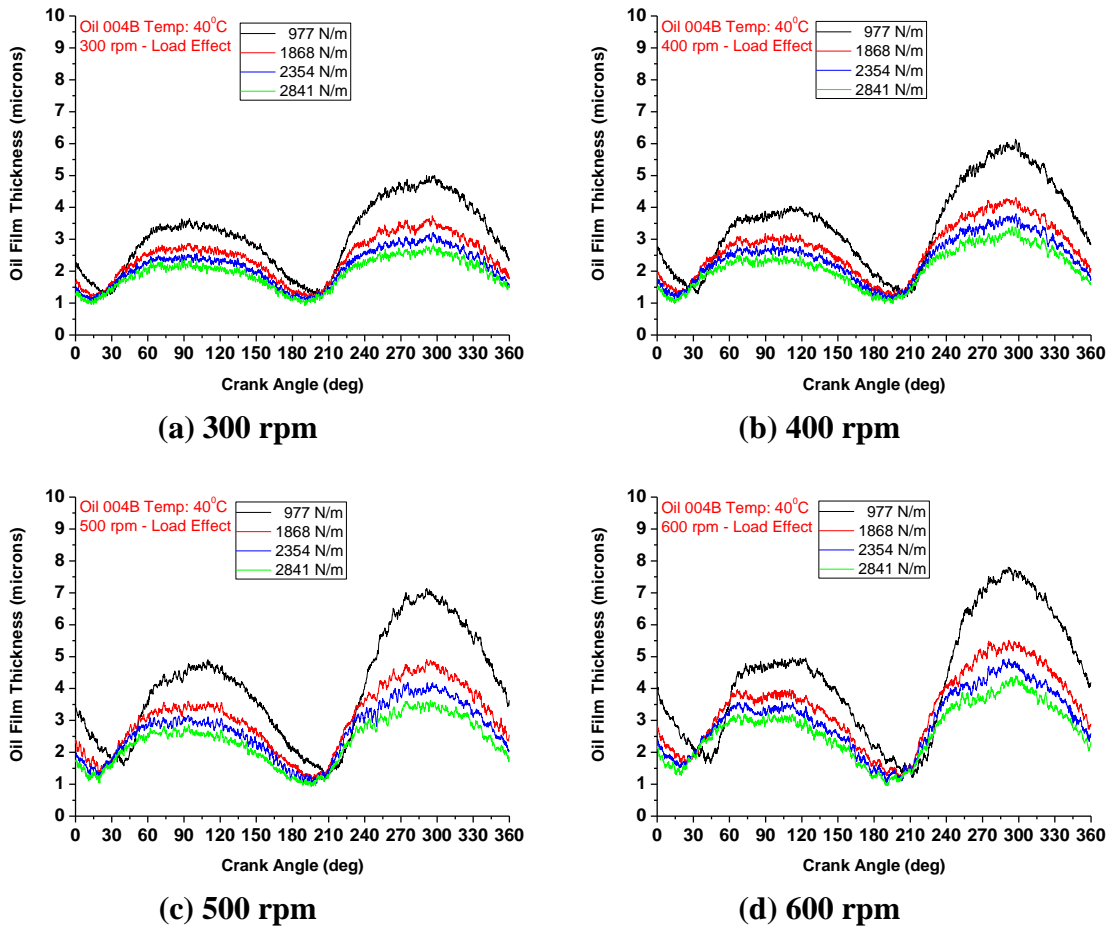
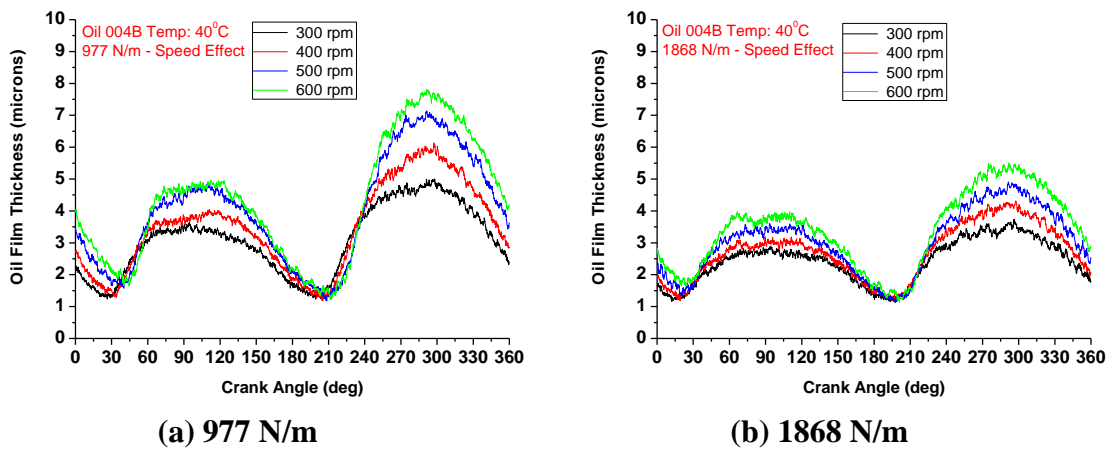
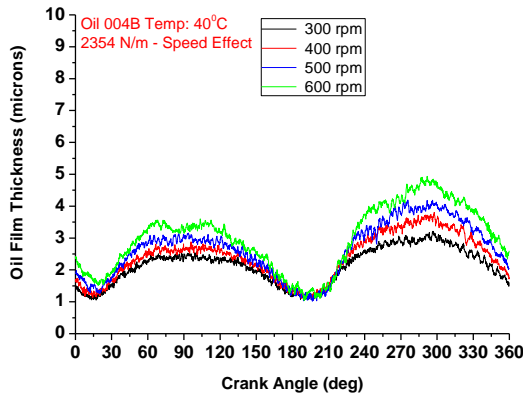
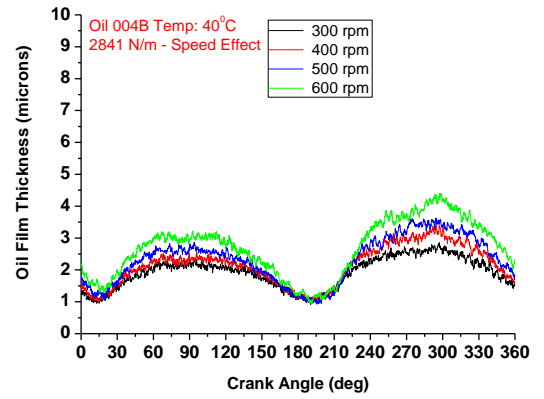


Figure 4.21: Variation of oil film thickness with CA at different loads for oil 004B





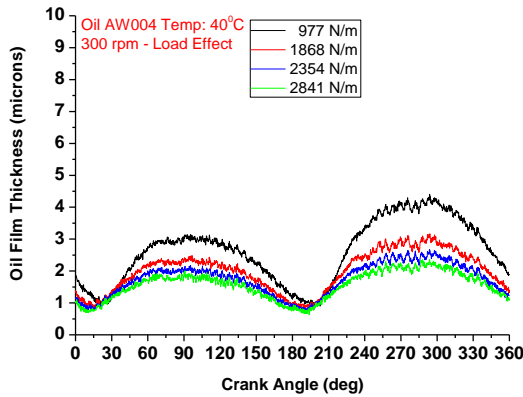
(c) 2354 N/m



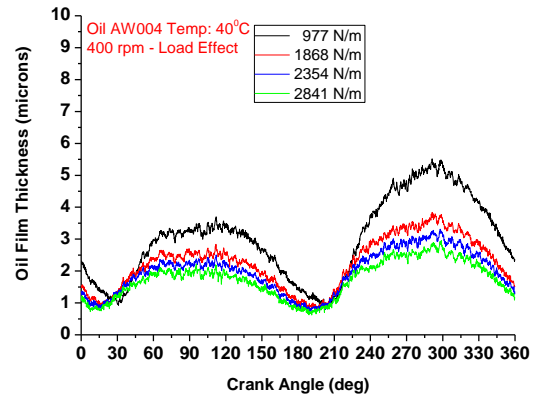
(d) 2841 N/m

Figure 4.22: Variation of oil film thickness with CA at different speeds for oil 004B

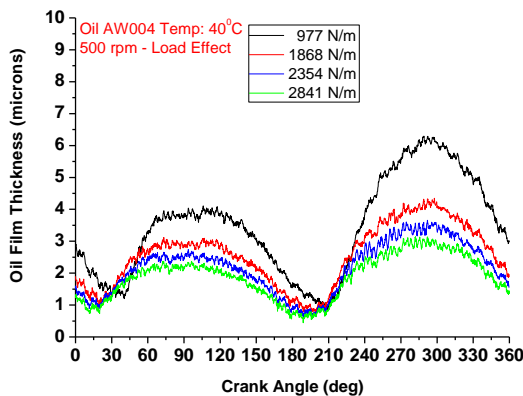
Low Viscosity Oil AW004



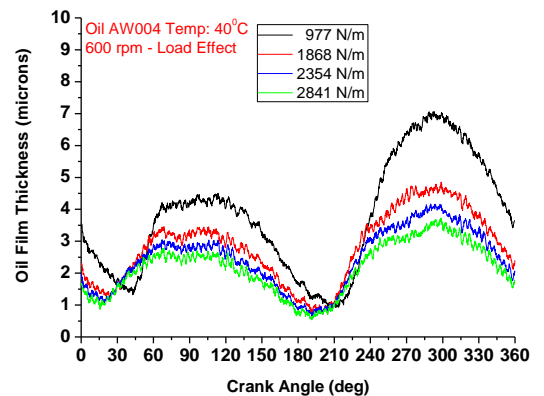
(a) 300 rpm



(b) 400 rpm



(c) 500 rpm



(d) 600 rpm

Figure 4.23: Variation of oil film thickness with CA at different loads for oil AW004

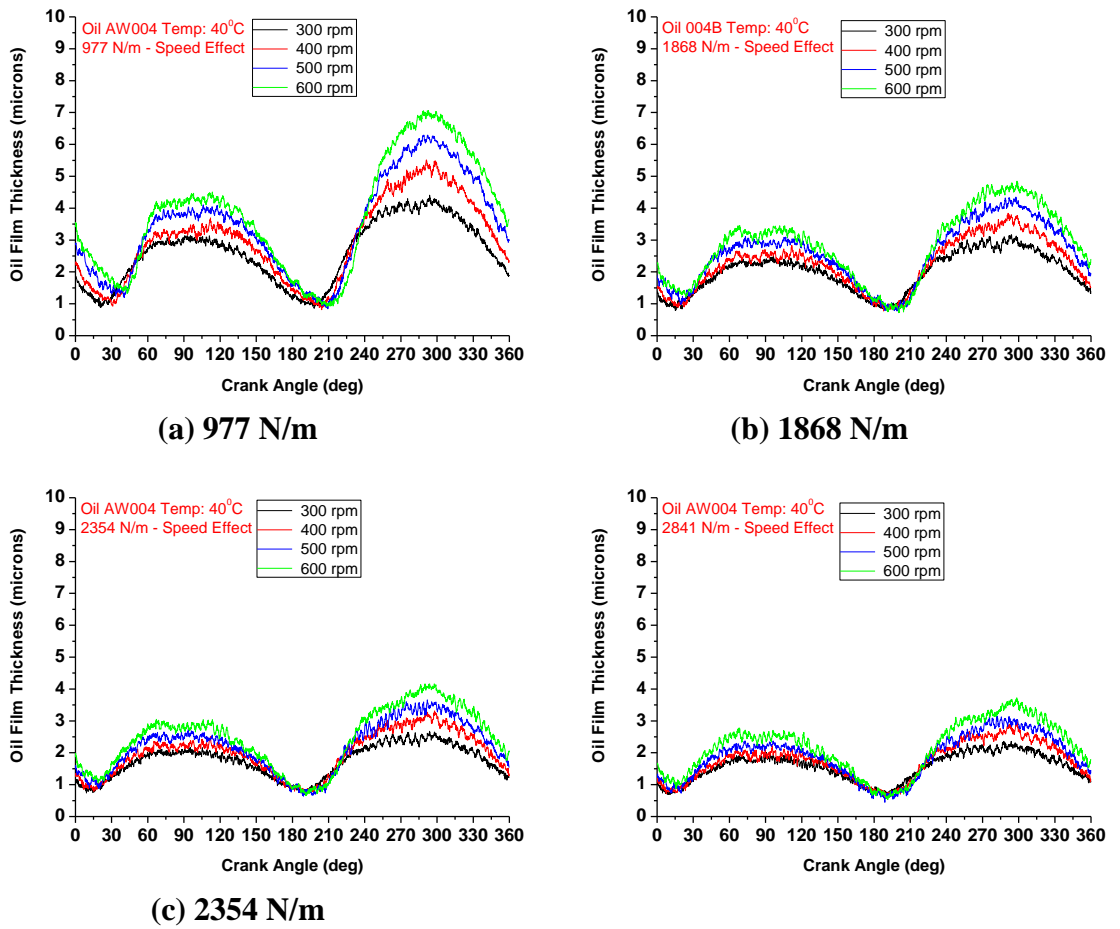
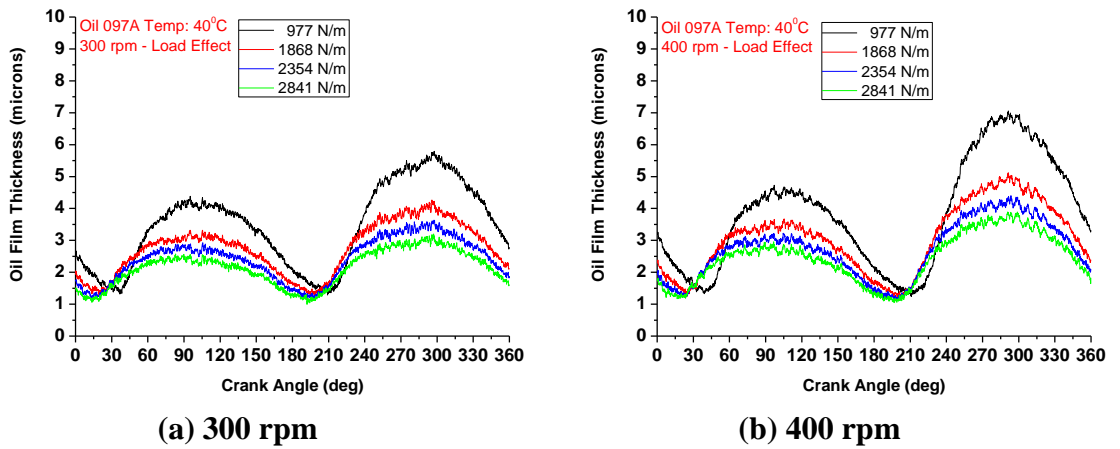
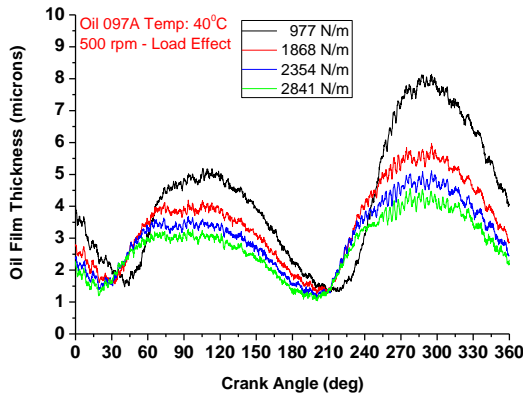


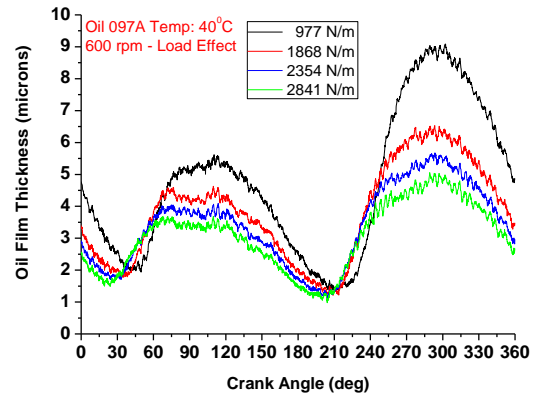
Figure 4.24: Variation of oil film thickness with CA at different speeds for oil AW004

High Viscosity Oil 097A



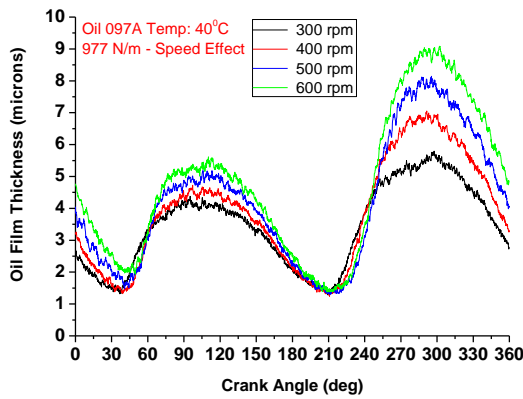


(c) 500 rpm

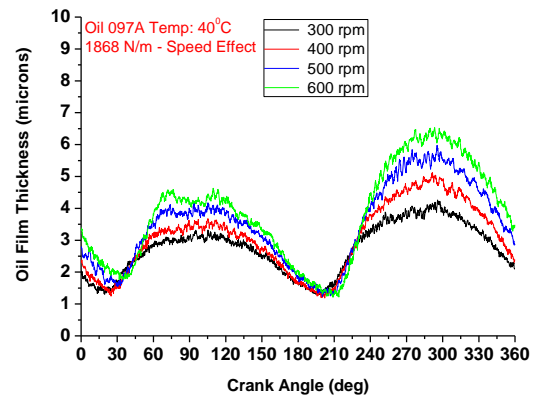


(d) 600 rpm

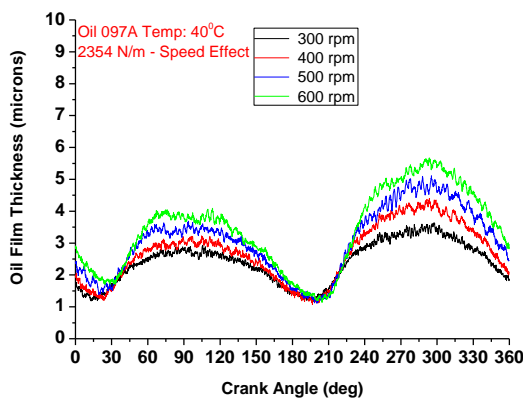
Figure 4.25: Variation of oil film thickness with CA at different loads for oil 097A



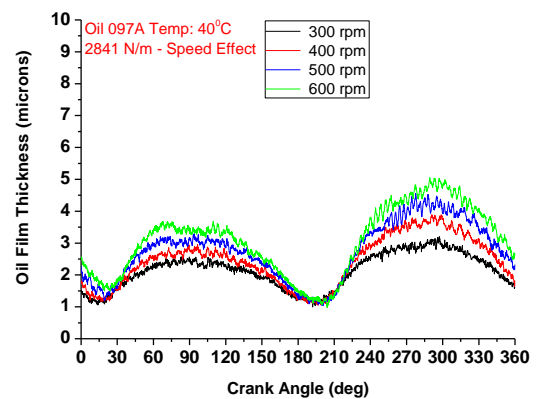
(a) 977 N/m



(b) 1868 N/m



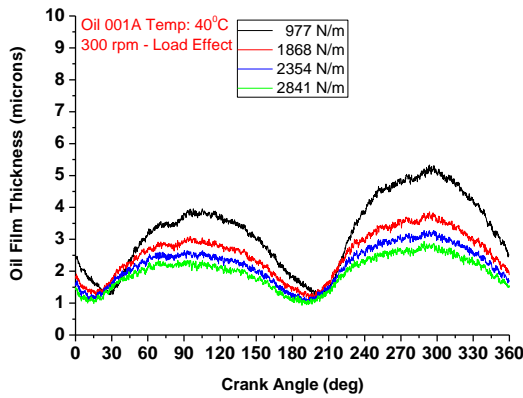
(c) 2354 N/m



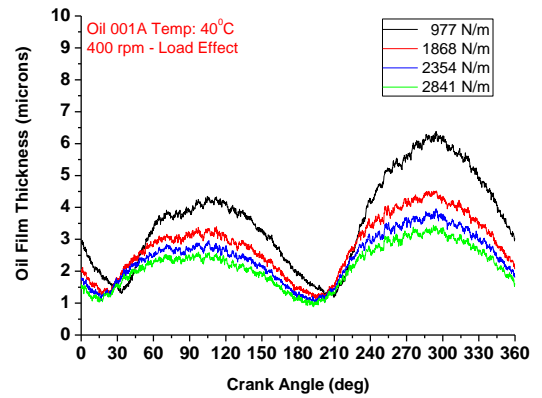
(d) 2841 N/m

Figure 4.26: Variation of oil film thickness with CA at different speeds for oil 097A

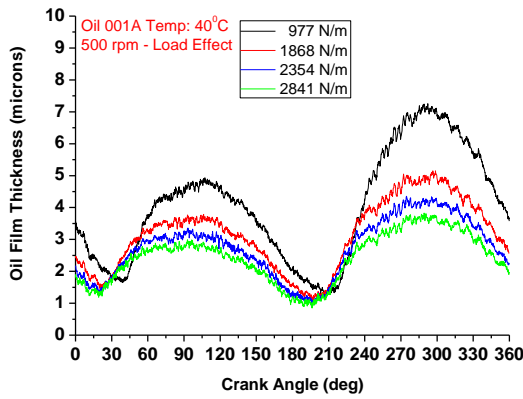
Reference Old Chemistry Oil 001A



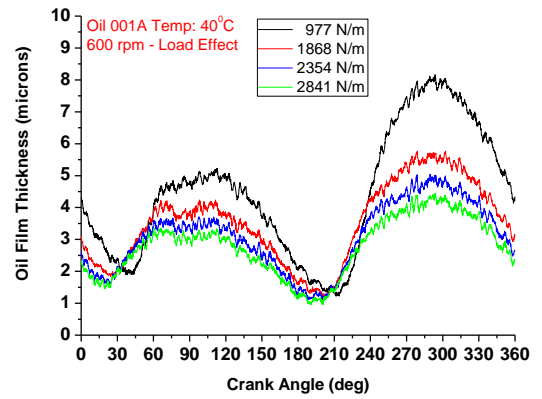
(a) 300 rpm



(b) 400 rpm

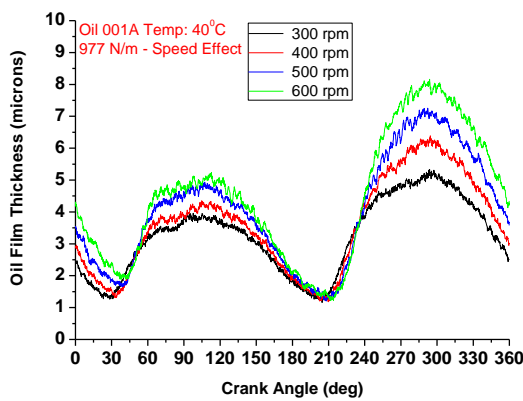


(c) 500 rpm

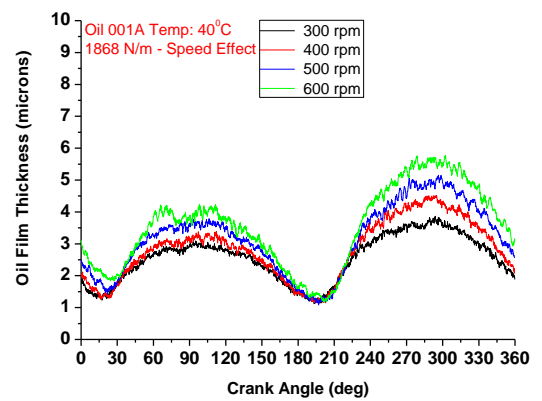


(d) 600 rpm

Figure 4.27: Variation of oil film thickness with CA at different loads for oil 001A



(a) 977 N/m



(b) 1868 N/m

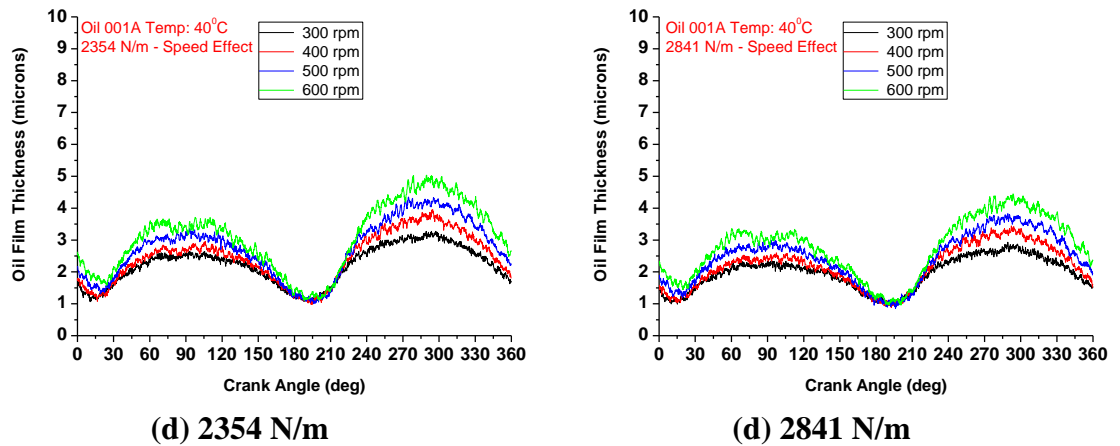
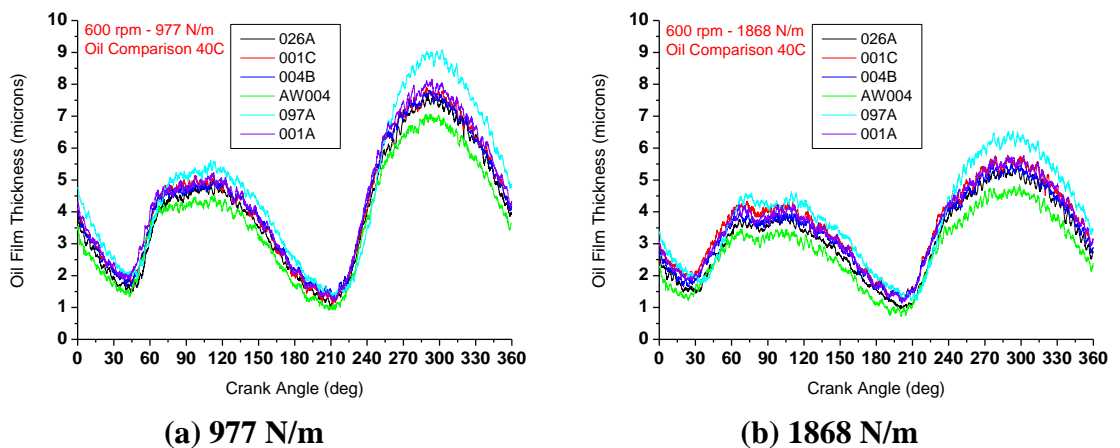
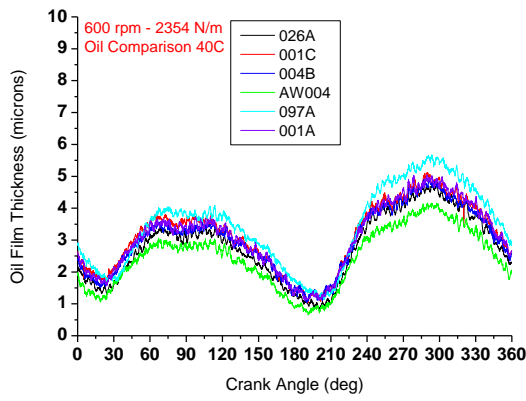


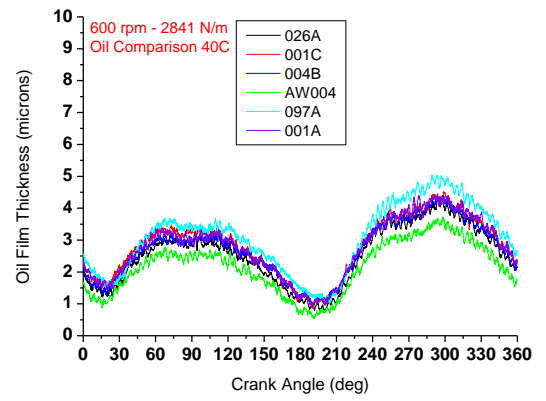
Figure 4.28: Variation of oil film thickness with CA at different speeds for oil 001A

The oils were compared with each other at different loads and speeds as depicted in Figure 4.29 and Figure 4.30. Oils 026A, 001C, 004B and 001A which have similar viscosity give similar OFT and oil AW004 which has the lowest viscosity of all oils shows a smaller OFT, as expected. On the other hand, oil 097A has the highest OFT as it has the highest viscosity. Figure 4.31 and Figure 4.32 show the OFT measurements as a function of temperature. From the temperature results the clear trend is that at higher temperatures the oil film thickness decreases and this happens with all the tested oils. Figure 4.33 demonstrates the relationship between temperature and relative viscosity where viscosity decreases with an increase in temperature.



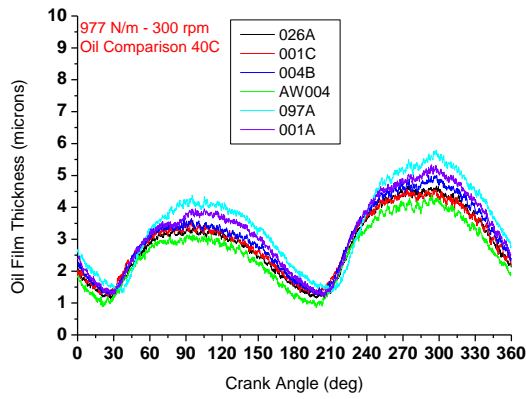


(c) 2354 N/m

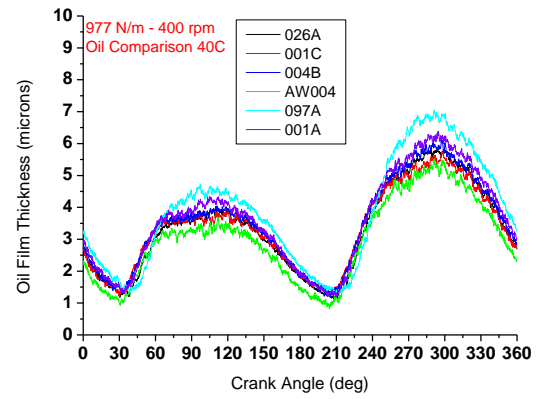


(d) 2841 N/m

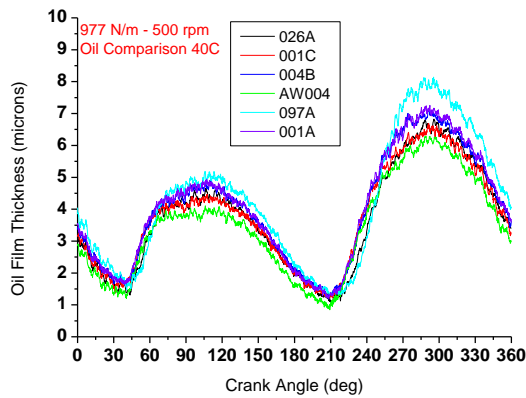
Figure 4.29: Oil Film Thickness- Oil Comparison, Speed 600rpm – Load effect



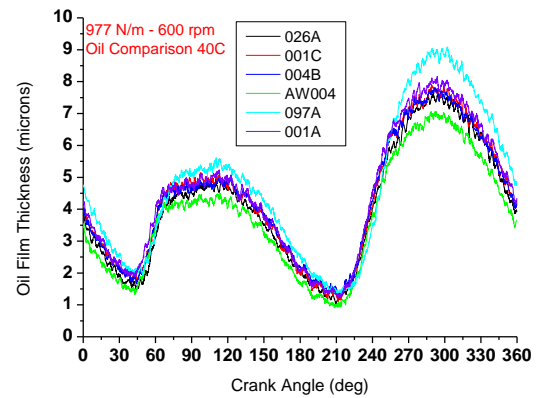
(a) 300 rpm



(b) 400 rpm

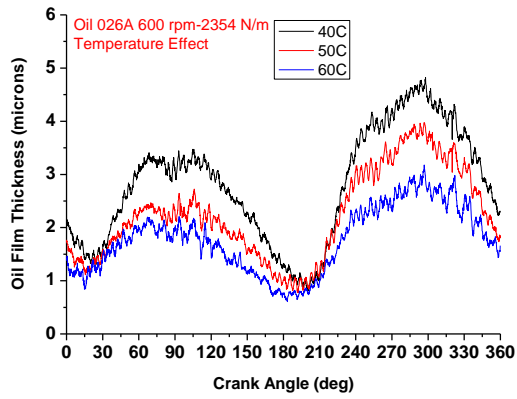


(c) 500 rpm

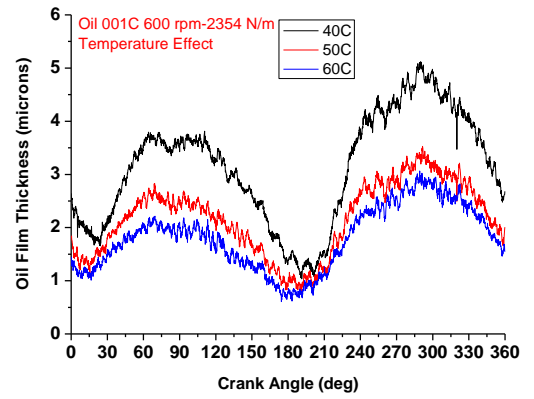


(d) 600 rpm

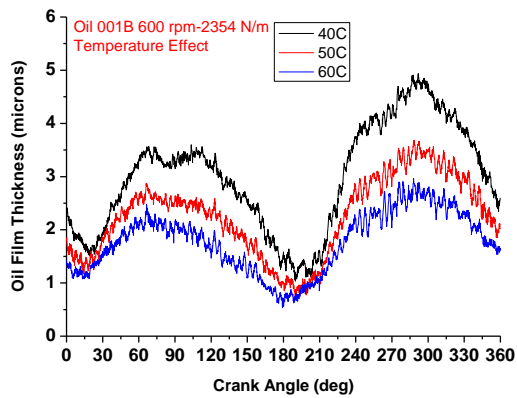
Figure 4.30: Oil Film Thickness- Oil Comparison, Load 977 N/m – Speed effect



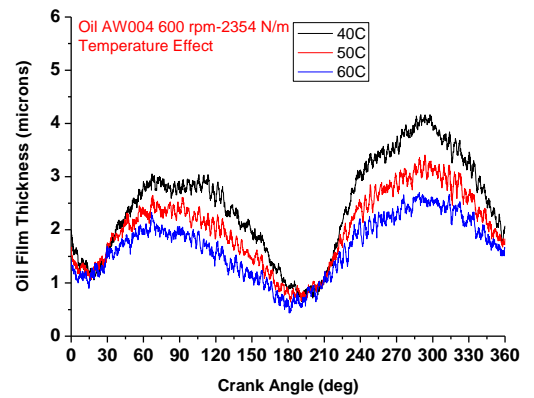
(a) oil 026A



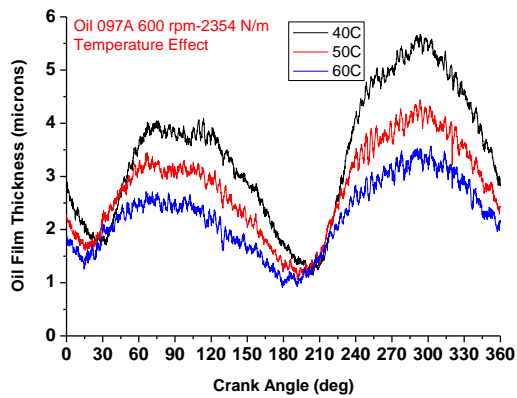
(b) oil 001C



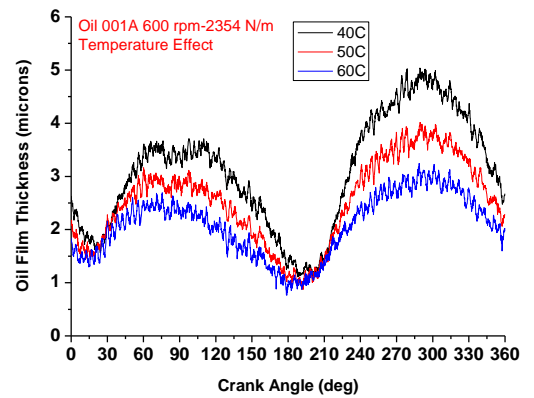
(c) oil 004B



(d) oil AW004



(e) oil 097A



(f) oil 001A

Figure 4.31: Oil film thickness- temperature effect, 600rpm - 2354 N/m

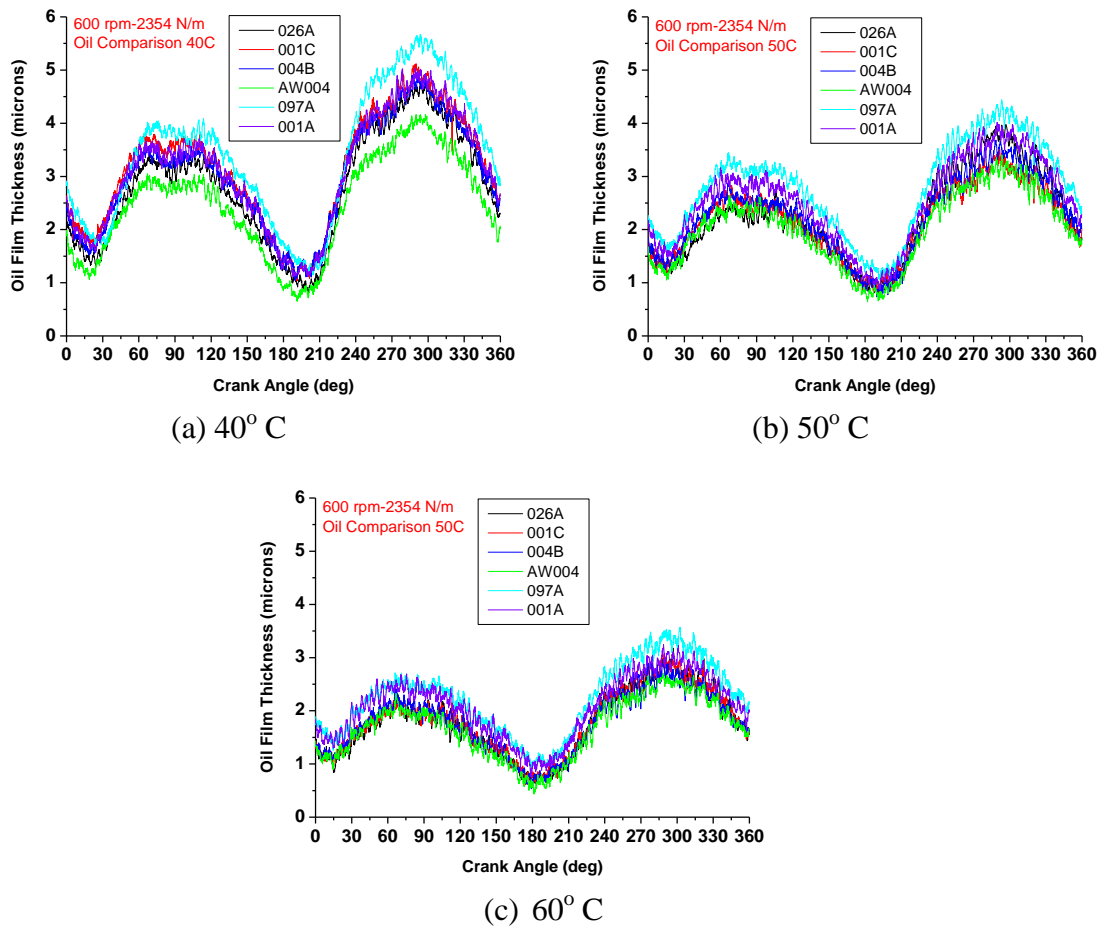


Figure 4.32: Oil film thickness (oil comparison) - temperature effect, 600 rpm – 2354 N

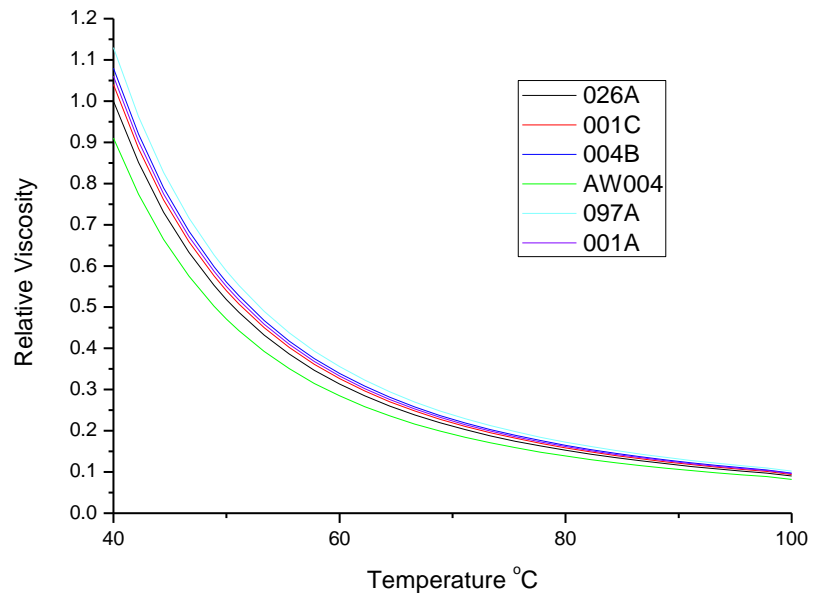
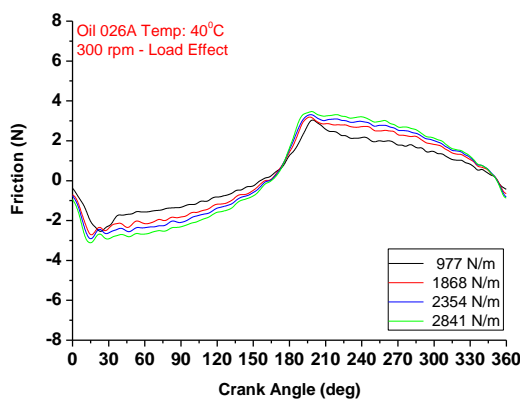


Figure 4.33: Relationship between temperature and viscosity

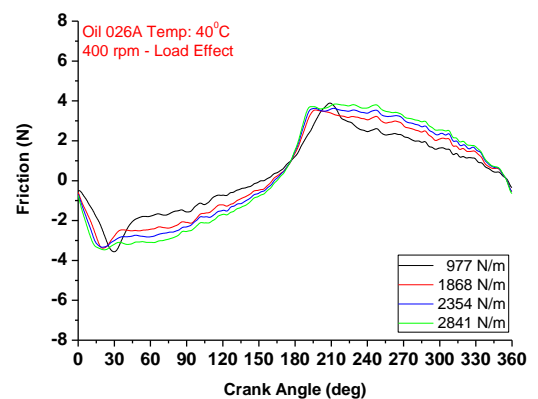
4.2.2 DISCUSSION OF FRICTION MEASUREMENT RESULTS

The hydrodynamic friction with respect to the crank angle, for all the marine oils, measured as a function of load and speed are depicted in Figures 4.34 - 4.45. From the film thickness measurements illustrated previously it is clear that the thinnest films occurring within the cycle exceed greatly the combined roughness of the surfaces. Thus no asperity interaction is expected for the conditions reported here and hence the reported friction measurements are mainly dominated by viscous drag. Based on Figure 4.35, Figure 4.37, Figure 4.39, Figure 4.41, Figure 4.43 and Figure 4.45, friction increases with liner speed, as the friction coefficient increases with film thickness (Hamrock *et al.*, 2004). Hydrodynamic friction also increases with load (Figure 4.34, Figure 4.36, Figure 4.38, Figure 4.40, Figure 4.42 and Figure 4.44), despite a reduction in the oil film thickness (friction coefficient). An important feature has been noted in the graphs where the occurrence of the peaks in the hydrodynamic friction takes place just after the dead-centres. At these locations, the oil film thickness measurements show that the ring and the liner are well separated and hence there is no contribution of friction due to asperity contact. One possible explanation for the occurrence of the peaks in the friction measurements is reversal points the viscous oil film opposes the motion of the liner. In the load experiments, it has been noted for speeds of the liner above 300 rpm for all the oils with the exception of the high viscosity oil 097A, the friction peaks decrease comparing to 977 N/m load case where it seems to be insensitive to further increase in load.

Reference Oil 026A



(a) 300 rpm



(b) 400 rpm

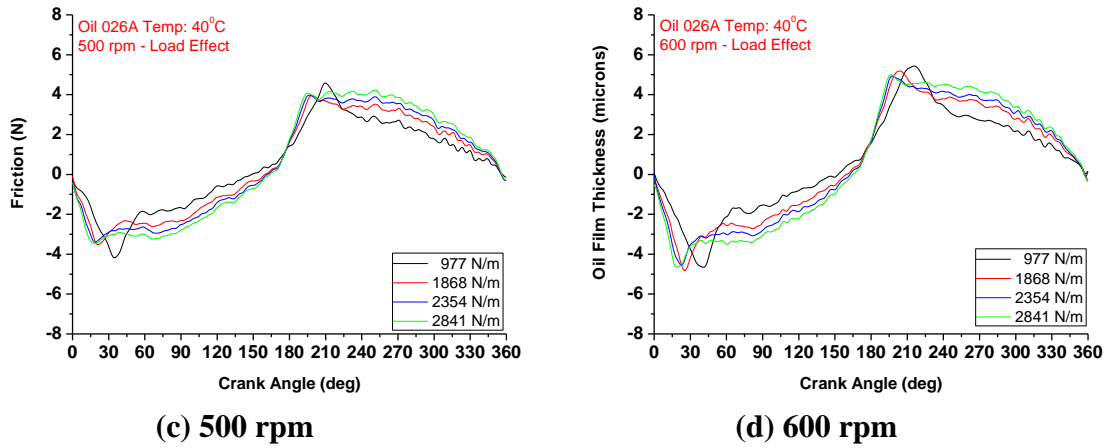


Figure 4.34: Variation of friction with CA at different loads for oil 026A

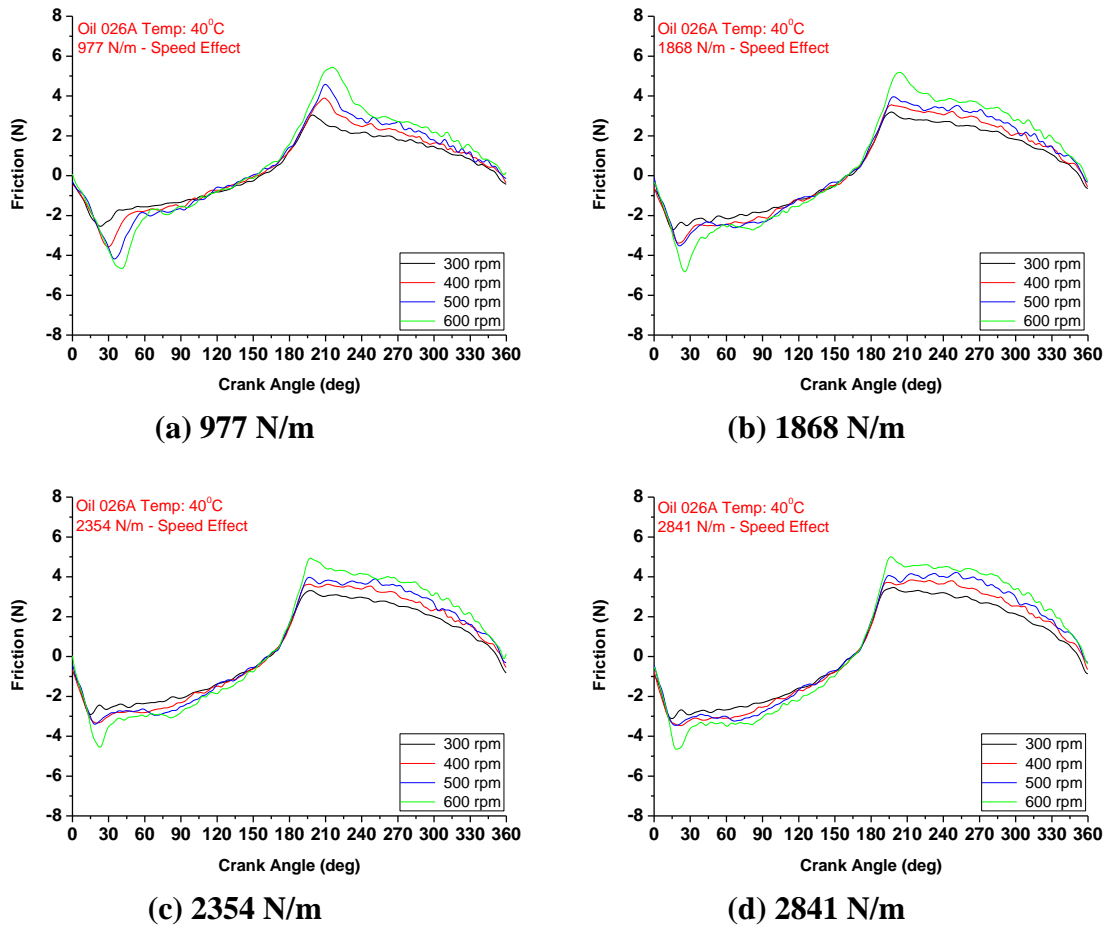
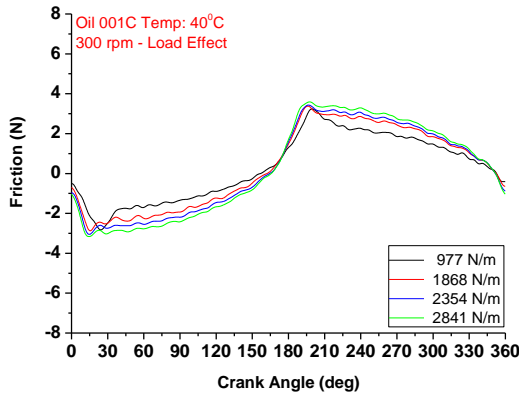
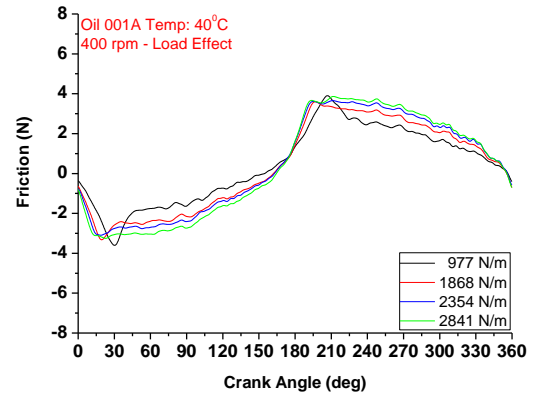


Figure 4.35: Variation of friction with CA at different speeds for oil 026A

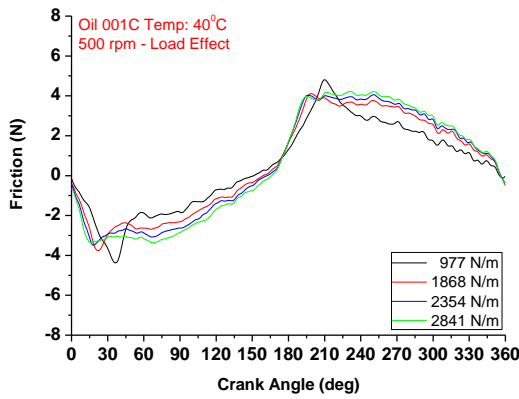
Base oil A 001C



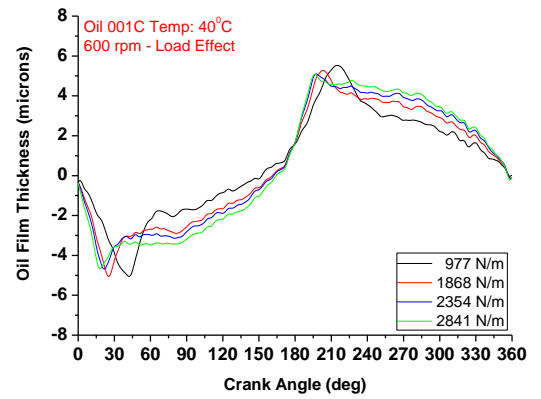
(a) 300 rpm



(b) 400 rpm

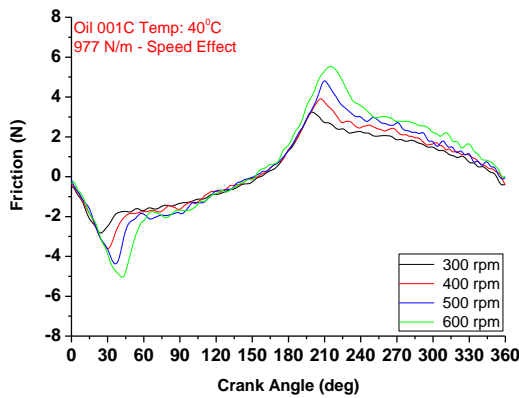


(c) 500 rpm

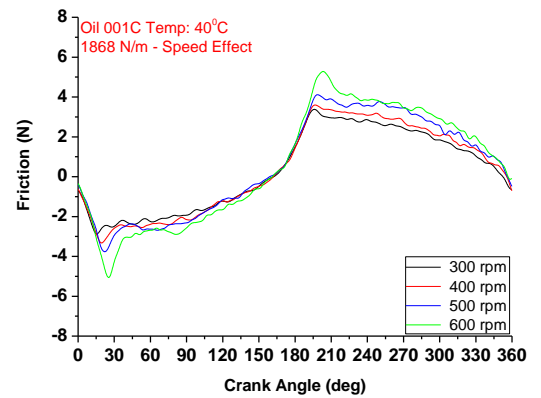


(d) 600 rpm

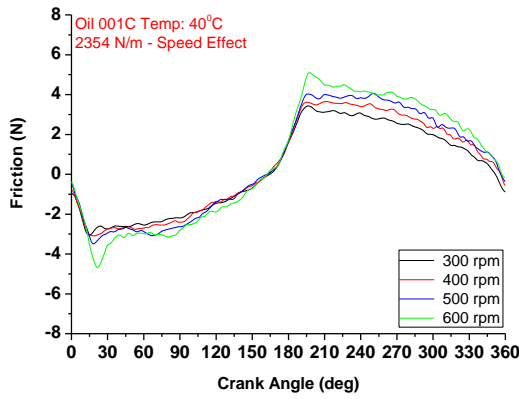
Figure 4.36: Variation of friction with CA at different loads for oil 001C



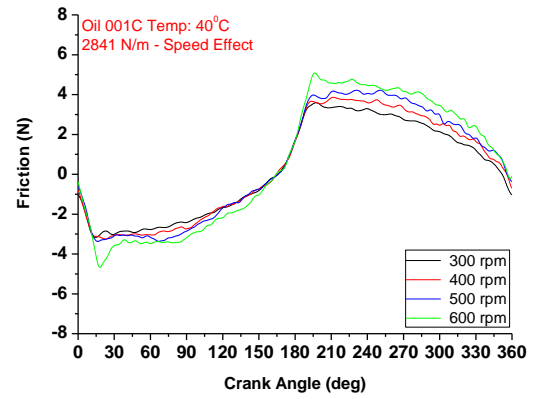
(a) 977 N/m



(b) 1868 N/m



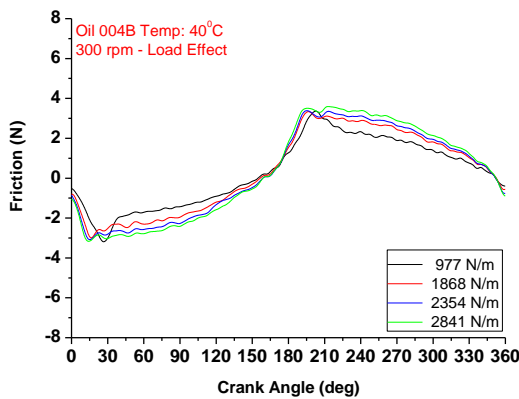
(c) 2354 N/m



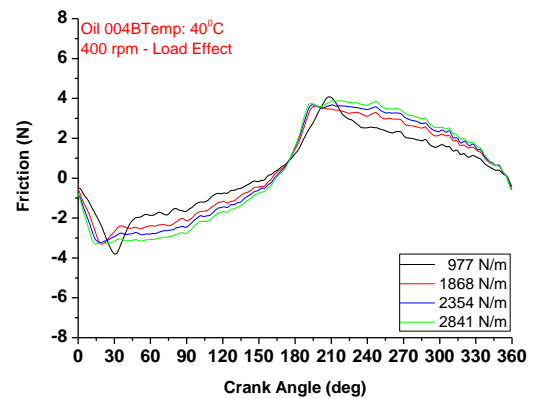
(d) 2841 N/m

Figure 4.37: Variation of friction with CA at different speeds for oil 001C

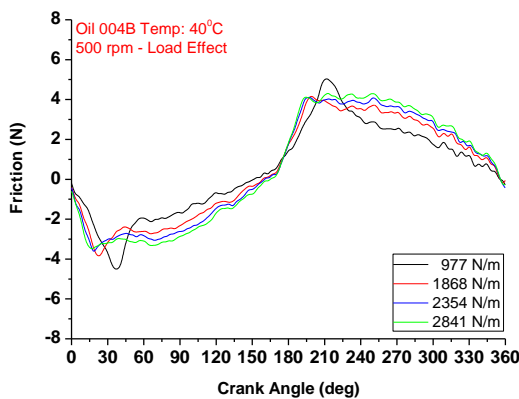
Base oil B 004B



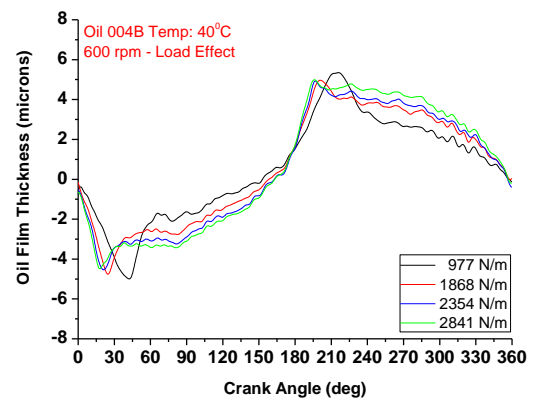
(a) 300 rpm



(b) 400 rpm

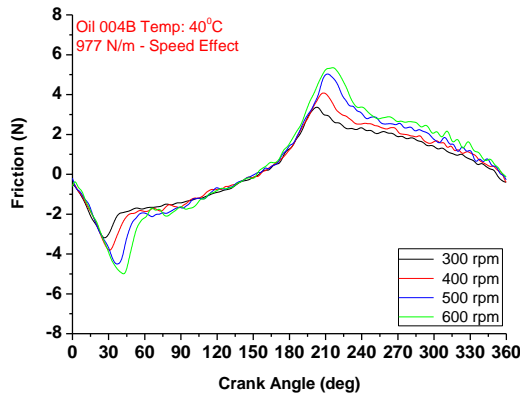


(c) 500 rpm

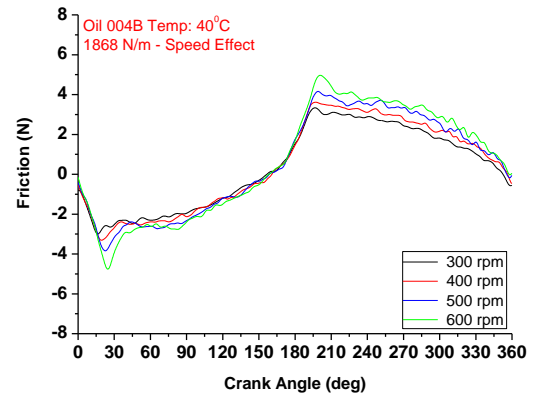


(d) 600 rpm

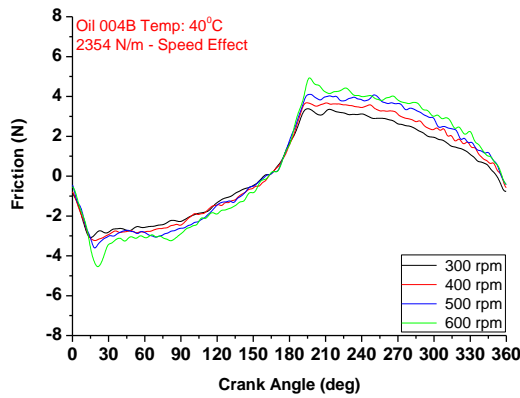
Figure 4.38: Variation of friction with CA at different loads for oil 004B



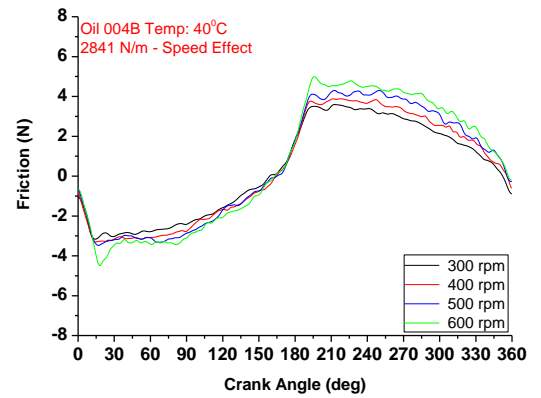
(a) 977 N/m



(b) 1868 N/m



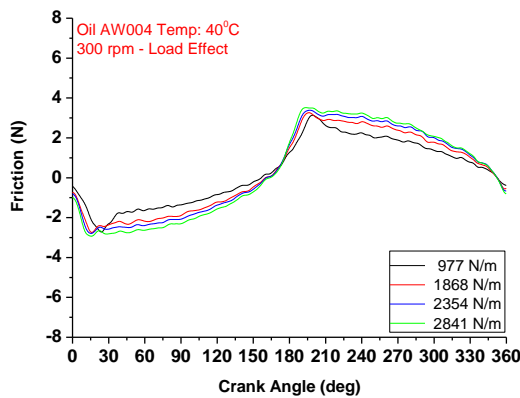
(c) 2354 N/m



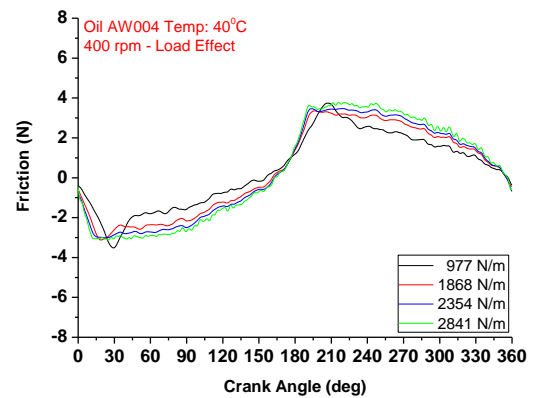
(d) 2841 N/m

Figure 4.39: Variation of friction as with CA at different speeds for oil 004B

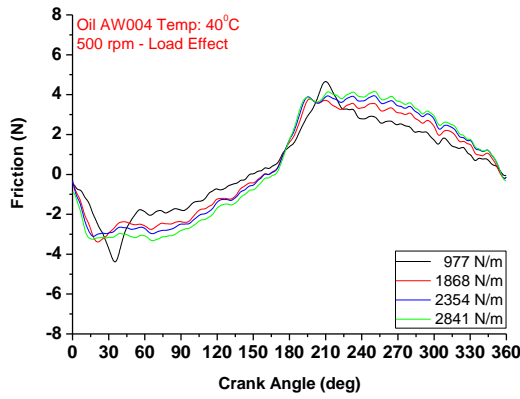
Low viscosity oil AW004



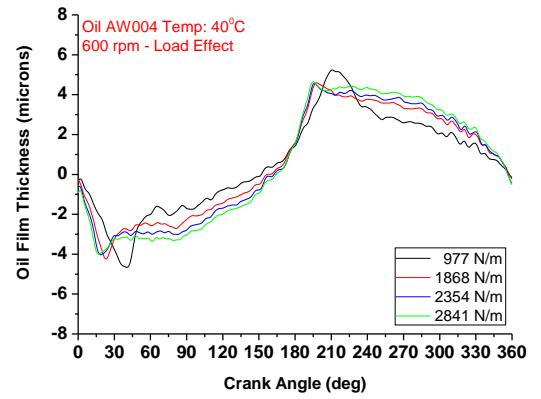
(a) 300 rpm



(b) 400 rpm

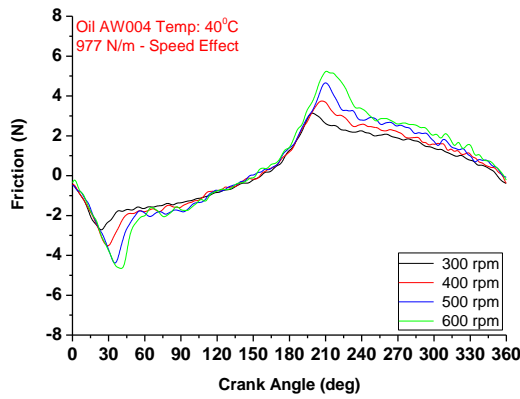


(c) 500 rpm

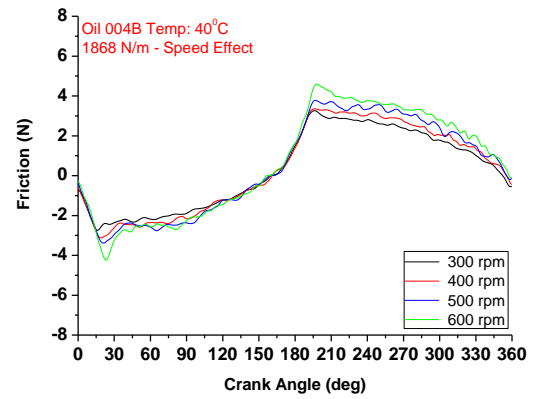


(d) 600 rpm

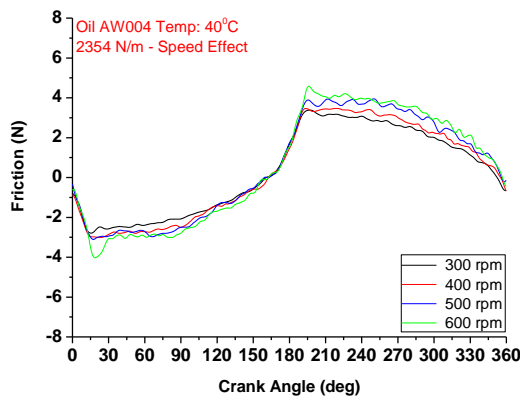
Figure 4.40: Variation of friction with CA at different loads for oil AW004



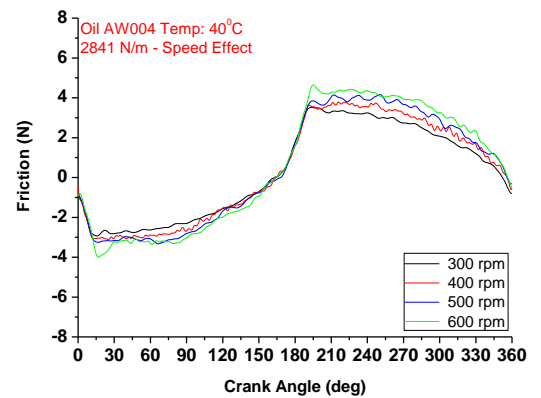
(a) 977 N/m



(b) 1868 N/m



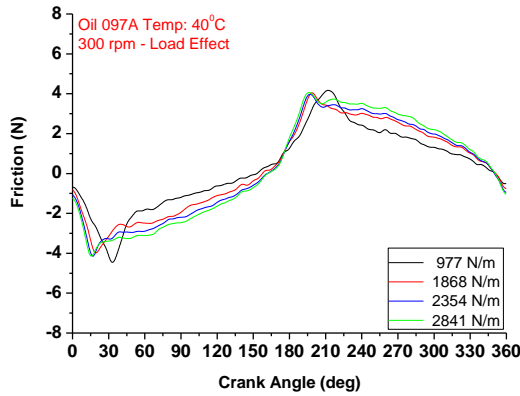
(c) 2354 N/m



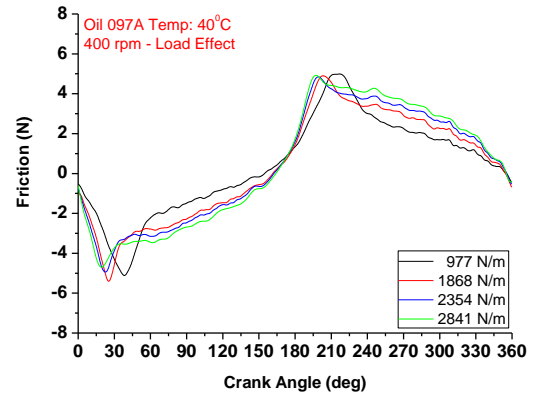
(d) 2841 N/m

Figure 4.41: Variation of friction with CA at different speeds for oil AW004

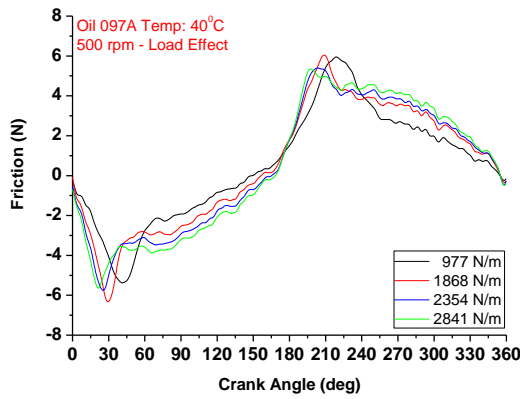
High viscosity oil 097A



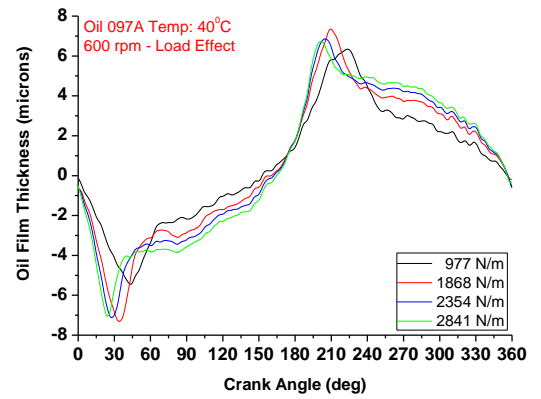
(a) 300 rpm



(b) 400 rpm

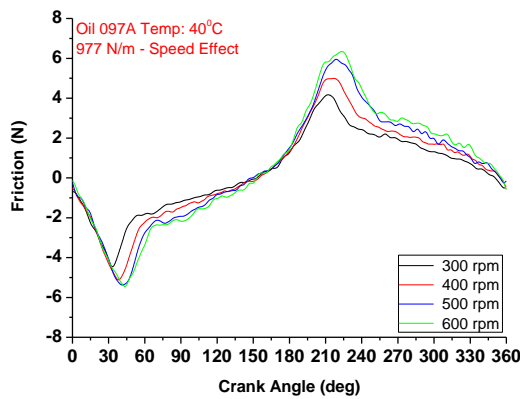


(c) 500 rpm

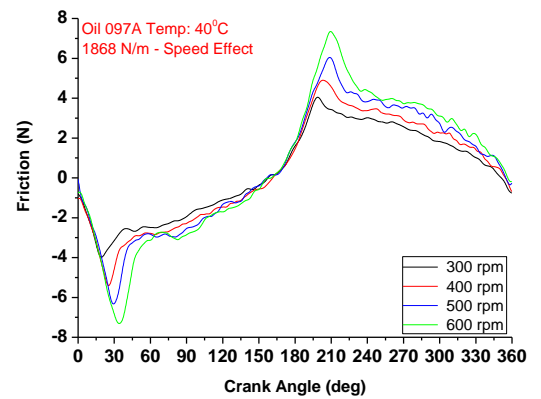


(d) 600 rpm

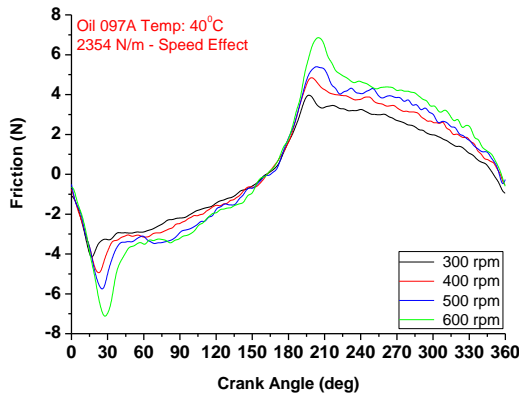
Figure 4.42: Variation of friction with CA at different loads for oil 097A



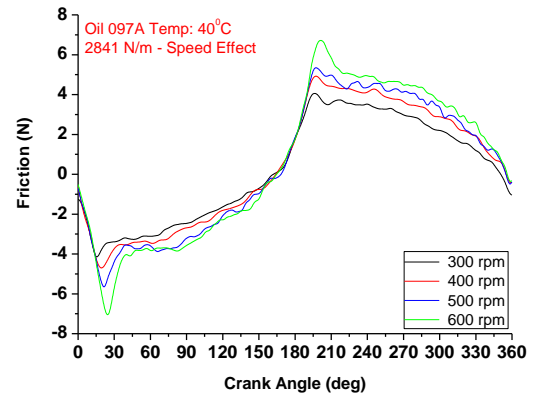
(a) 977 N/m



(b) 1868 N/m



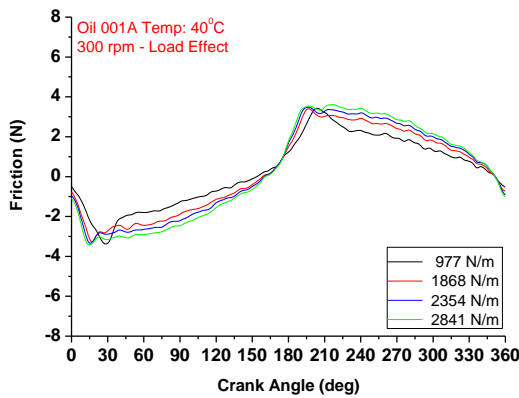
(c) 2354 N/m



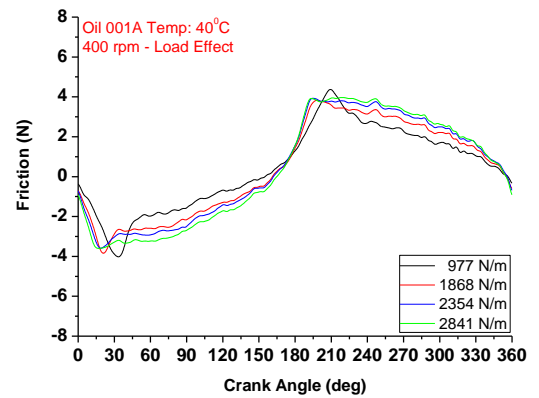
(d) 2841 N/m

Figure 4.43: Variation of friction with CA at different speeds for oil 097A

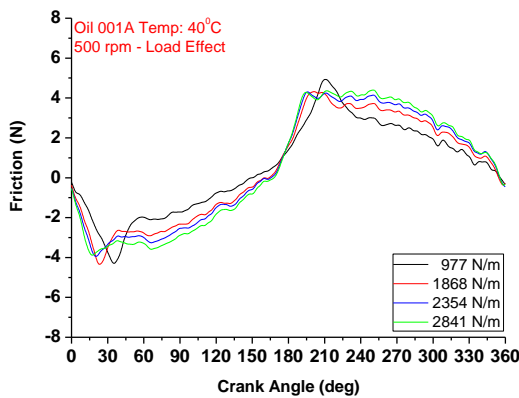
Reference old chemistry oil 001A



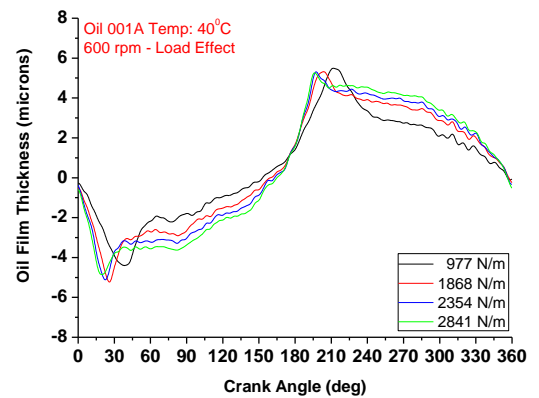
(a) 300 rpm



(b) 400 rpm



(c) 500 rpm



(d) 600 rpm

Figure 4.44: Variation of friction with CA at different loads for oil 001A

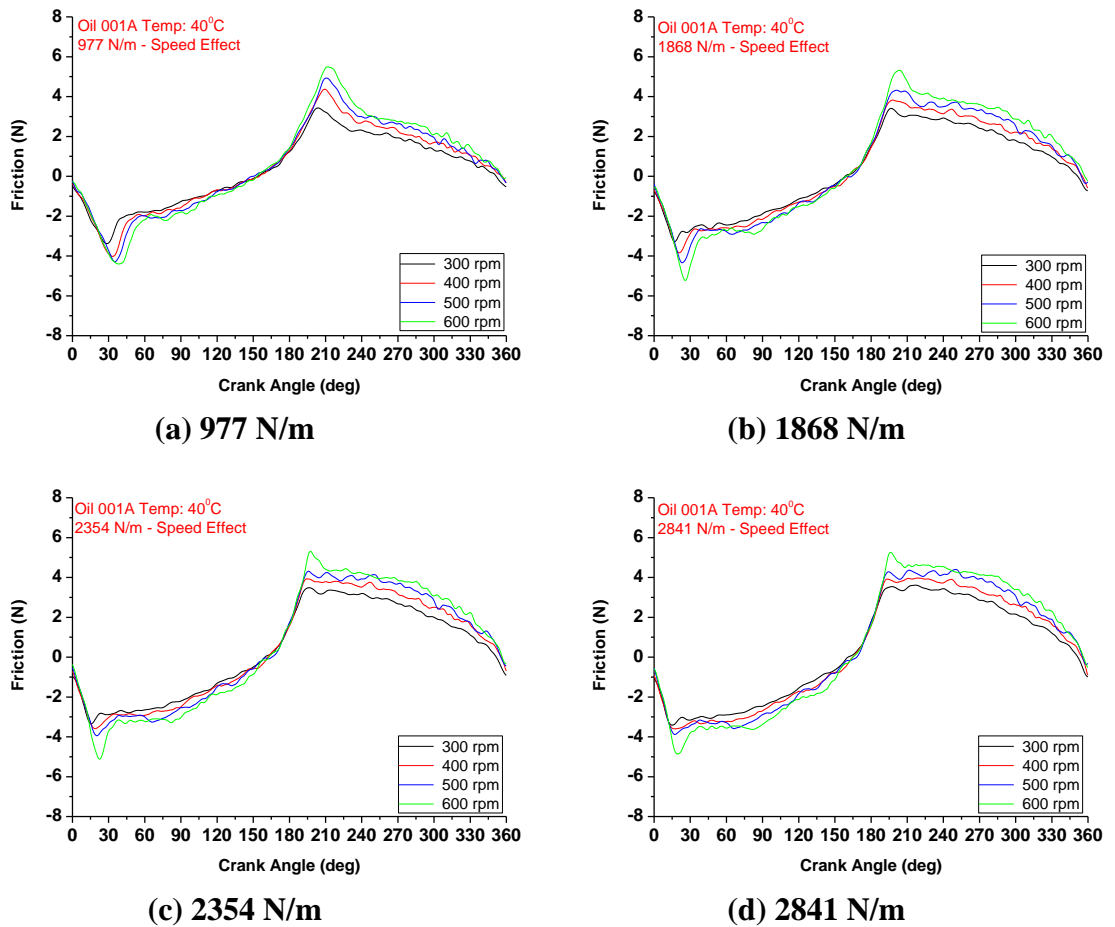


Figure 4.45: Variation of friction with CA at different speeds for oil 001A

Interestingly enough, oil AW004 which has the lowest viscosity did not show lower friction as anticipated but instead similar friction to the rest of the oils and it did not show much variation during the experiment over repeated cycles (Figures 4.46 and 4.47). Figure 4.48 and Figure 4.49 illustrate the effect of temperature on friction at a constant speed and load (600 rpm and 2354 N/m). Again based on the OFT measurements in most of the oils no asperity contact is apparent between the two surfaces (specimen ring and liner) and therefore no friction due to the roughness of the surfaces. It has been noted, as expected, that an increase in temperature decreases the overall friction of the oils in general since an increase in temperature reduces the OFT (viscosity) and hence less viscous drag is encountered. It has also been distinguished for oil 004B and AW004 at 60°C in the upstroke measurement just after BDC the friction spike increases. Their corresponding oil film thicknesses for this condition show that asperity contact may have been involved, thus explaining those peaks particularly

during the upstroke measurements. Figure 4.49 shows the oil comparison at different temperatures. Oils 026A, 001C, 004B and 001A which have similar viscosity give similar results and oil 097A has higher friction as it has higher viscosity. Oil AW004 which has lowest viscosity again did not show a lower friction as it would have been expected and instead it has similar friction with the rest of the oils.

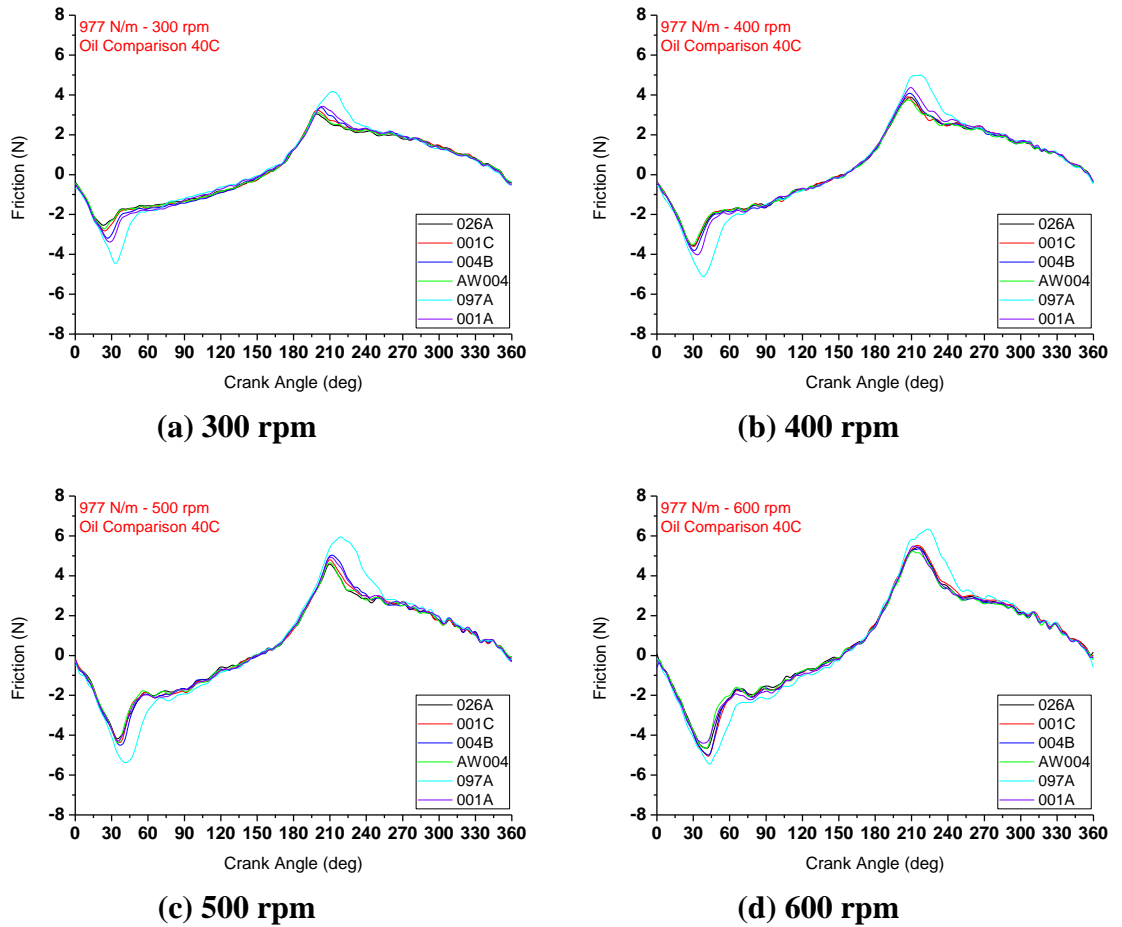
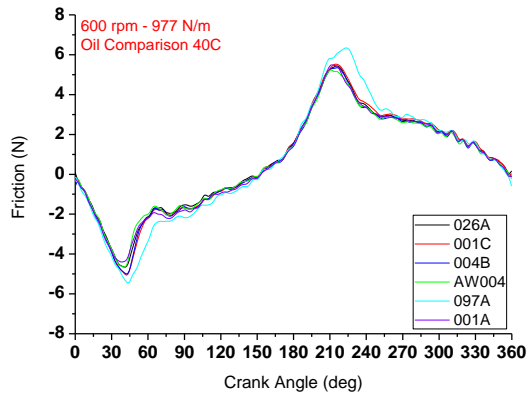
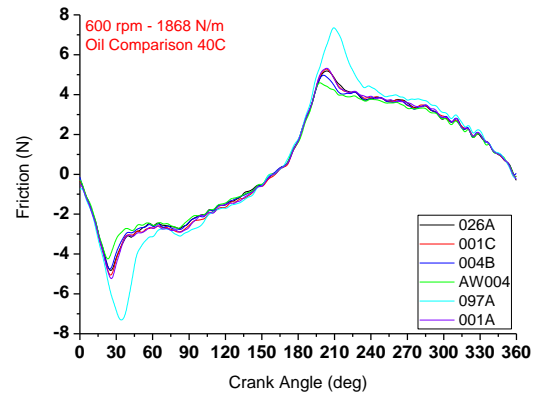


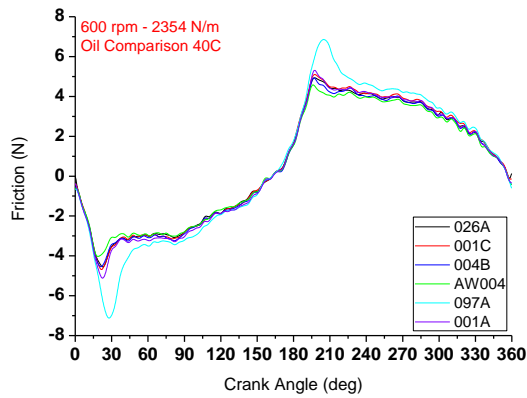
Figure 4.46: Friction measurement -oil comparison, 977 N/m - speed effect



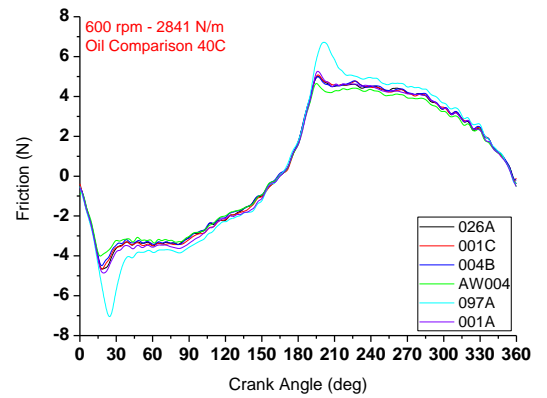
(a) 977 N/m



(b) 1868 N/m

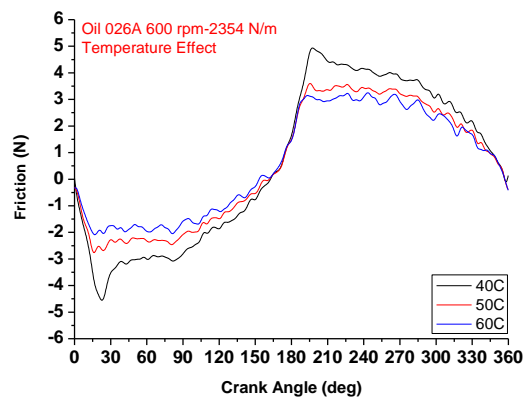


(c) 2354 N/m

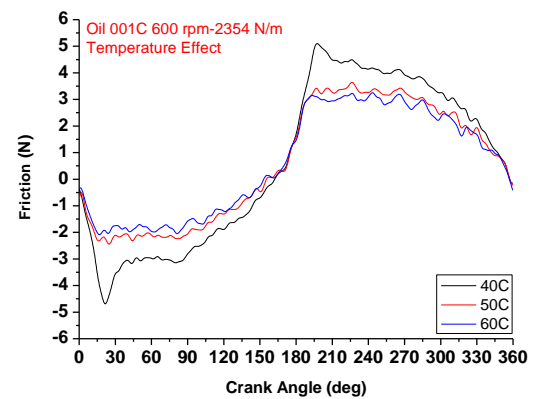


(d) 2841 N/m

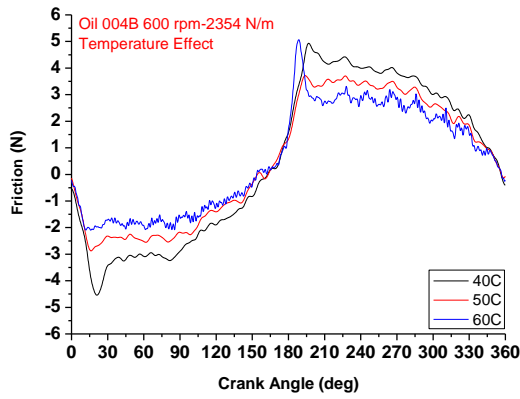
Figure 4.47: Friction measurement -oil comparison, 600 rpm – load effect



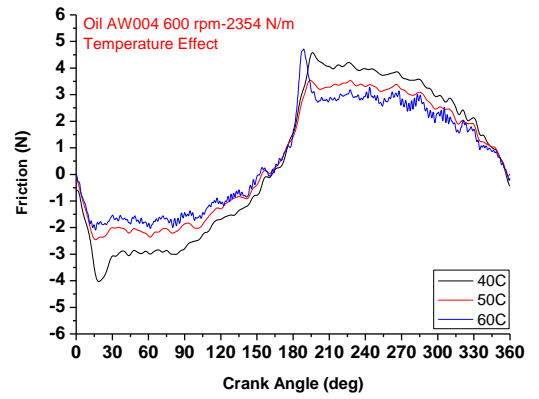
(a) oil 026A



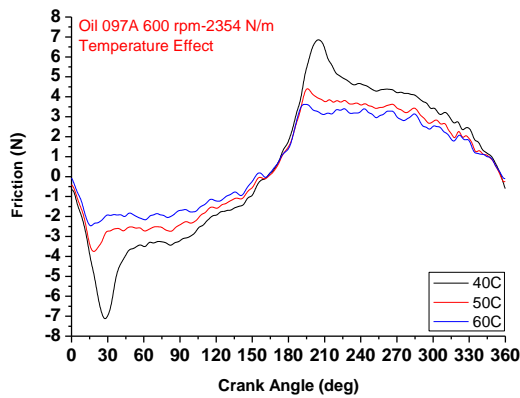
(b) oil 001C



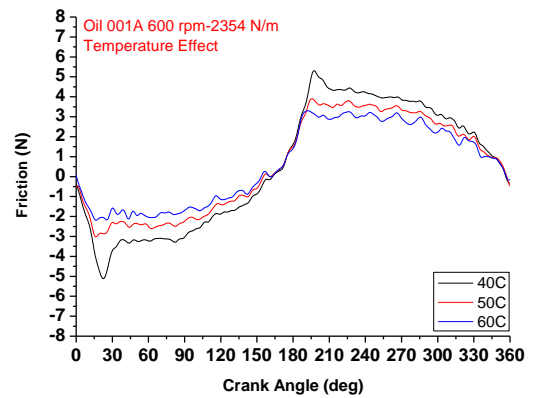
(c) oil 004B



(d) oil AW004

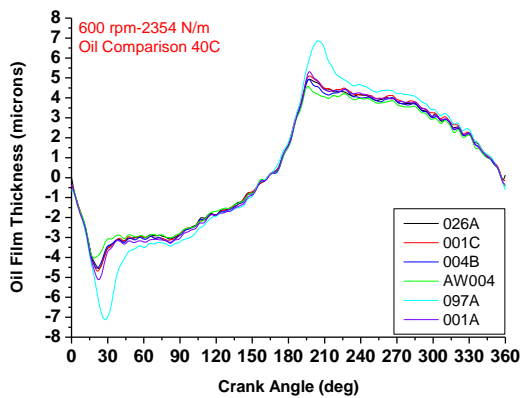


(e) oil 097A

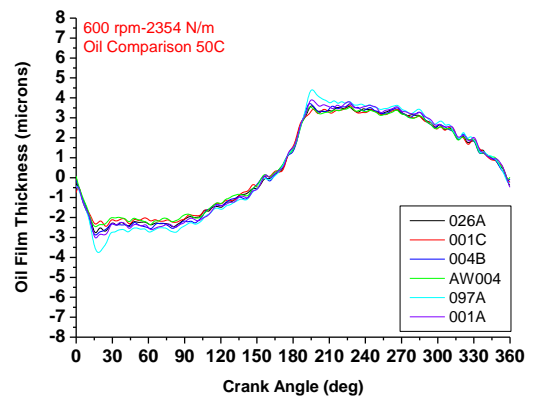


(f) oil 001A

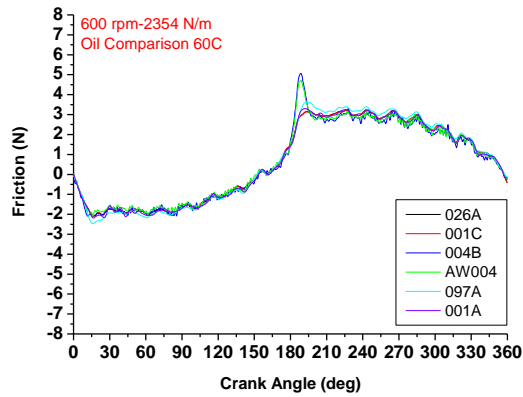
Figure 4.48: Friction measurements - temperature effect, 600rpm - 2354 N/m



(a) 40° C



(b) 50° C



(c) 60° C

Figure 4.49: Friction measurement (oil comparison) - temperature effect, 600 rpm – 2354 N

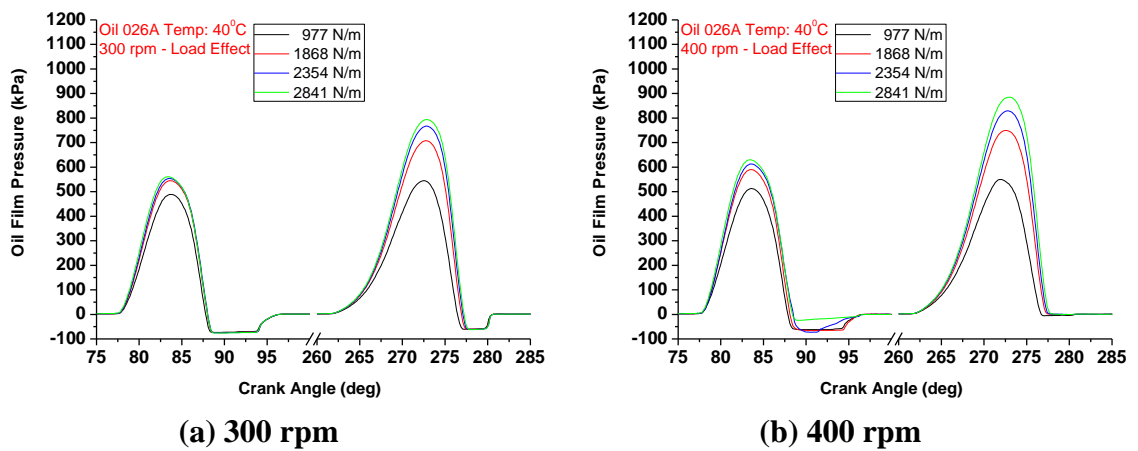
4.2.3 DISCUSSION OF OIL FILM PRESSURE STUDY RESULTS

Figures 4.50-4.61 show the oil film pressure variations with respect to speed and load for all the six marine oils tested. The common trend observed for all the oils during the tests is that oil film pressure increases with increasing load and increasing speed; the reasons are similar to those described previously in section 4.1.3. Negative or sub-atmospheric pressure is found to occur in the downstroke and seems to be virtually unchanged with speed and load. However, nowhere in the upstroke measurements there are any obvious negative or significant sub-atmospheric pressures. This happened only in the case of the slowest speed, 300 rpm, for oil 026A, 001C and AW004. Here again higher oil film pressure is observed in the upstroke measurements than in the downstroke due to the asymmetric ring profile. However, an odd behaviour has been observed for all the tested oils at the load 977 N/m case. It can be noted that at the liner speed of 500 rpm and 600 rpm the upstroke peak pressure reading becomes less than the downstroke one. For oils 097A and 001A this is found to occur earlier at the liner speed of 400 rpm.

Referring to the pressure measurements that are shown in Figure 4.50, Figure 4.52, Figure 4.54, Figure 4.56, Figure 4.58, Figure 4.60 where the film pressure is presented for varying loads, the pressure peaks do not appear at the same crank angle. The “effective” piston-ring width (the surface of the ring soaked in oil), which is the

corresponding piston-ring width for the pressure curve obtained, is different for each measurement. As discussed previously in section 2.4 (Chapter 2) only part of the ring surface is soaked with oil. Figure 2.2 has provided an insight into the effective piston ring width and how it changes with varying speed and load. For the load variation tests (Figure 4.51, Figure 4.53, Figure 4.55, Figure 4.57, Figure 4.59 and Figure 4.61) the pressure peaks appear to be more uniform. The “effective” ring width is altered as it gets narrower by a small margin while speed increases (Figure 2.2), whereas the pressure peaks do not have a big variation for each testing condition: the curve peaks are slightly shifted between them. Temperature tests showed that at higher temperatures the oil film pressure decreases (Figure 4.64) and this is a direct consequence of the decreasing OFT. It is also noted that a decrease in viscosity enables the pressure transducer to record negative or sub-atmospheric pressures in the upstroke movement of the liner. This occurs due to the lower viscosity the higher the momentum of the flow thus encouraging cavitation. Figure 4.65 illustrates the oil comparison at different temperatures and shows that oil 097A has the highest oil film pressure and the highest viscosity, while the rest of the oils have similar oil film pressures with the exception of oil 026A whose oil film pressure decreases at higher temperatures.

Reference oil 026A



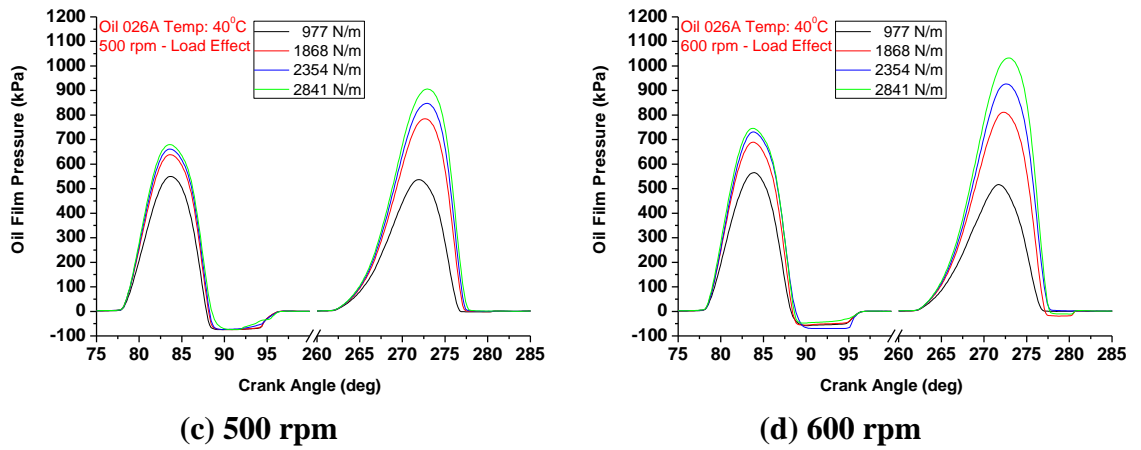


Figure 4.50: Variation of oil film pressure with CA at different loads for oil 026A

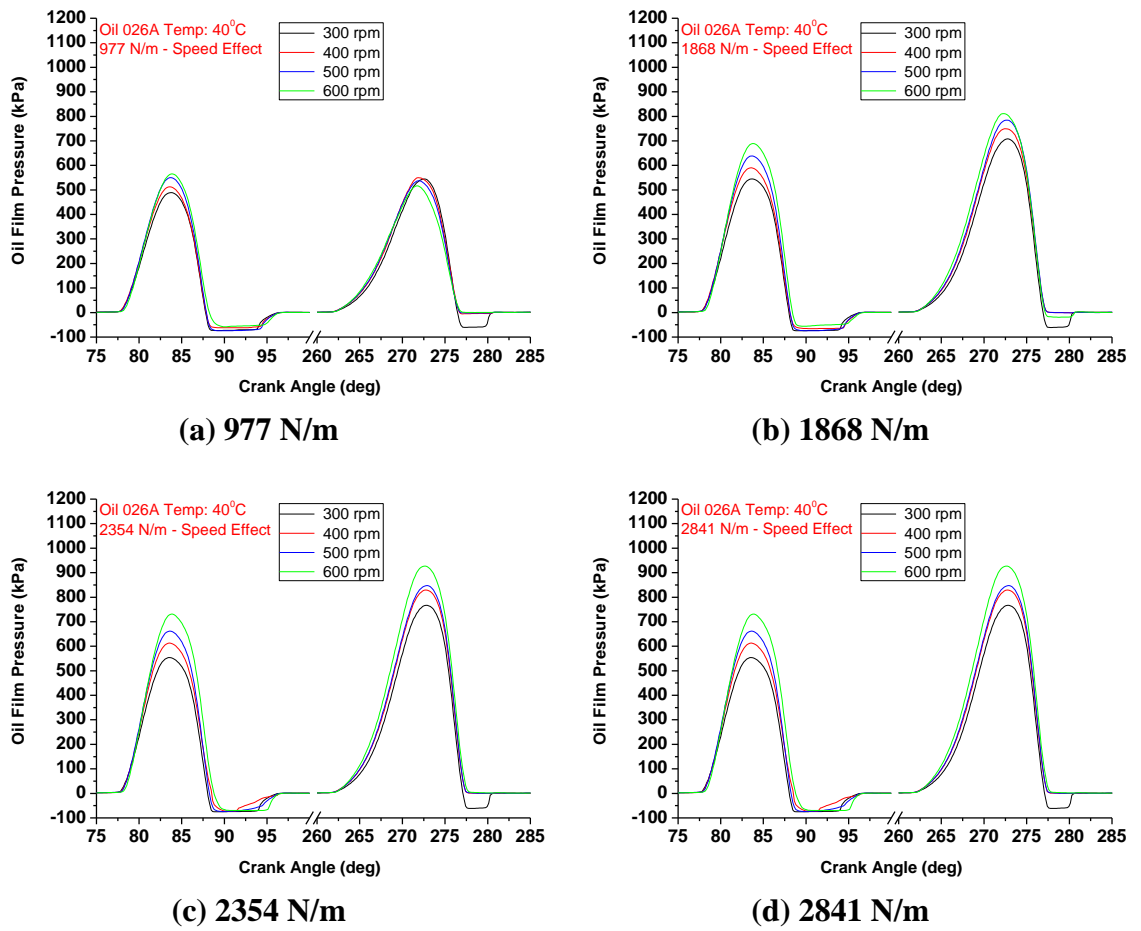


Figure 4.51: Variation of oil film pressure with CA at different speeds for oil 026A

Base oil A 001C

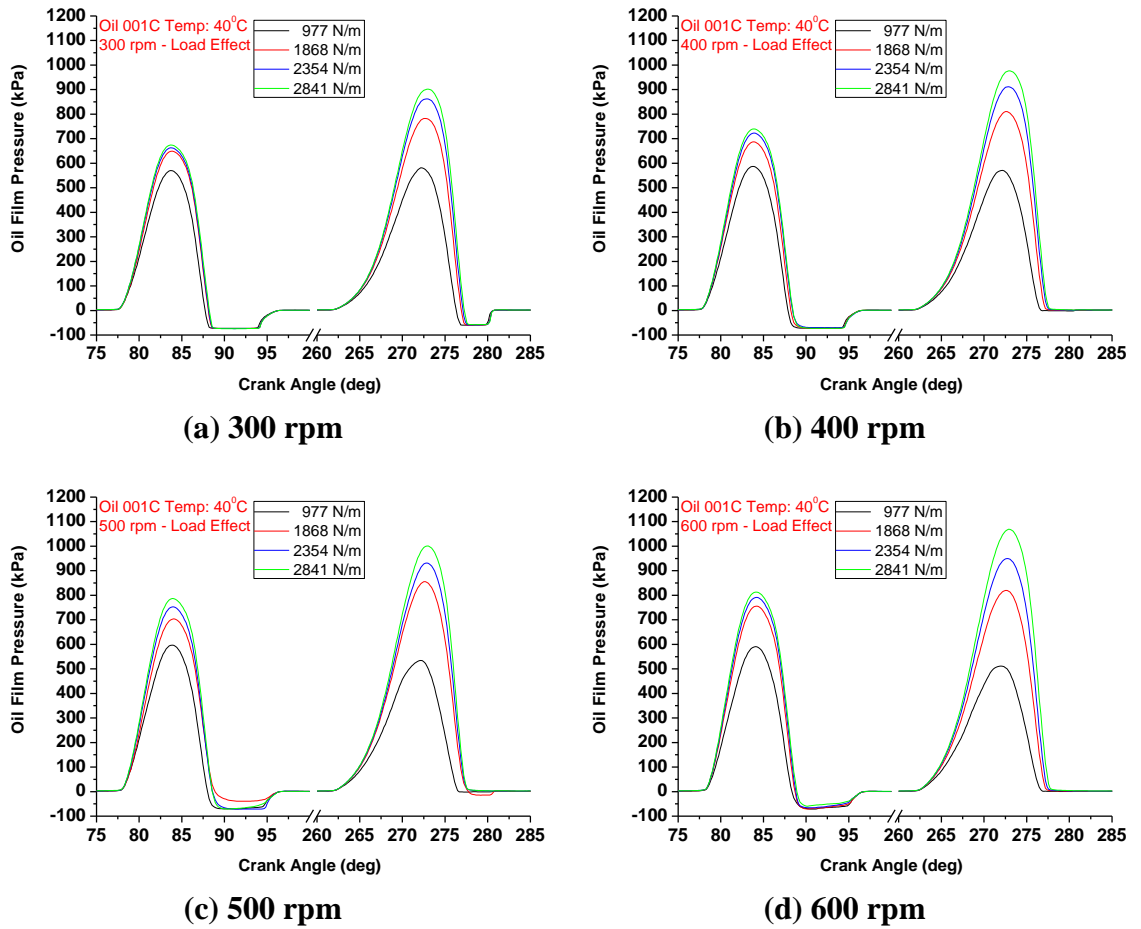
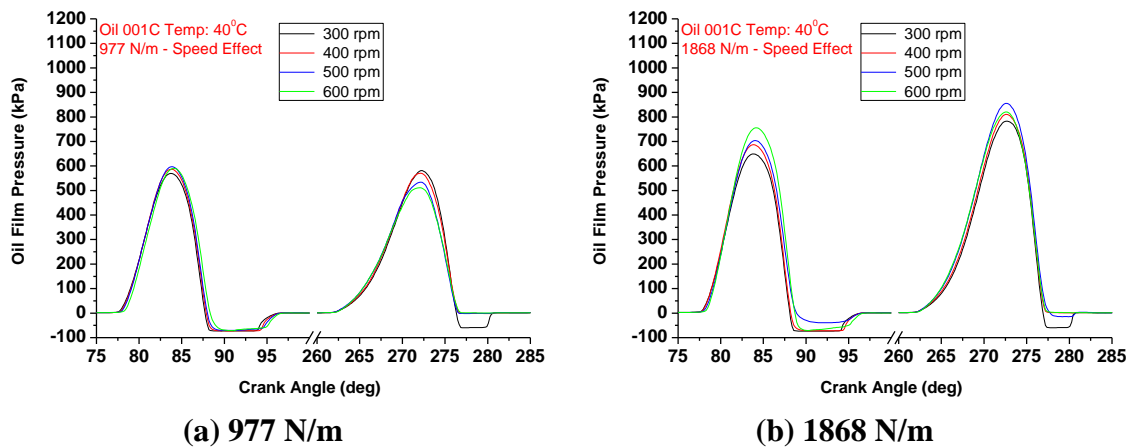


Figure 4.52: Variation of oil film pressure with CA at different loads for oil 001C



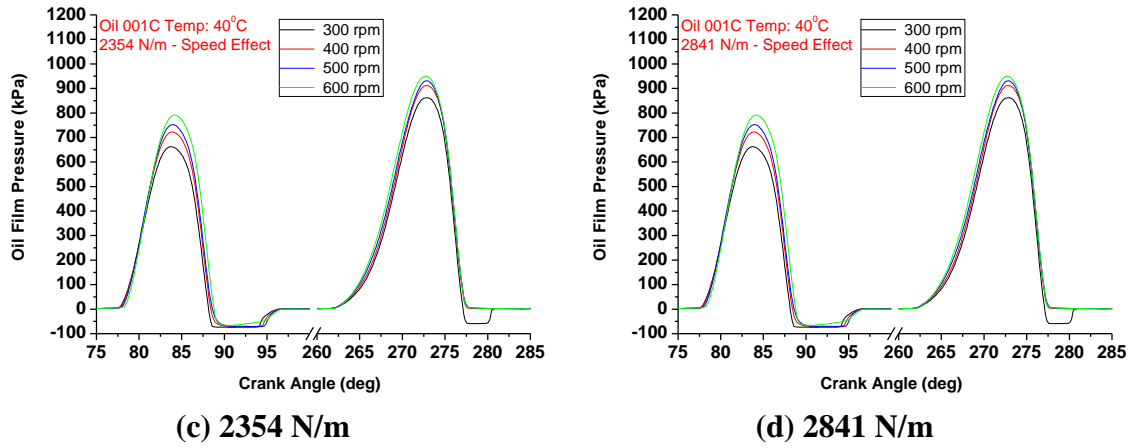


Figure 4.53: Variation of oil film pressure with CA at different speeds for oil 001C

Base oil B 004B

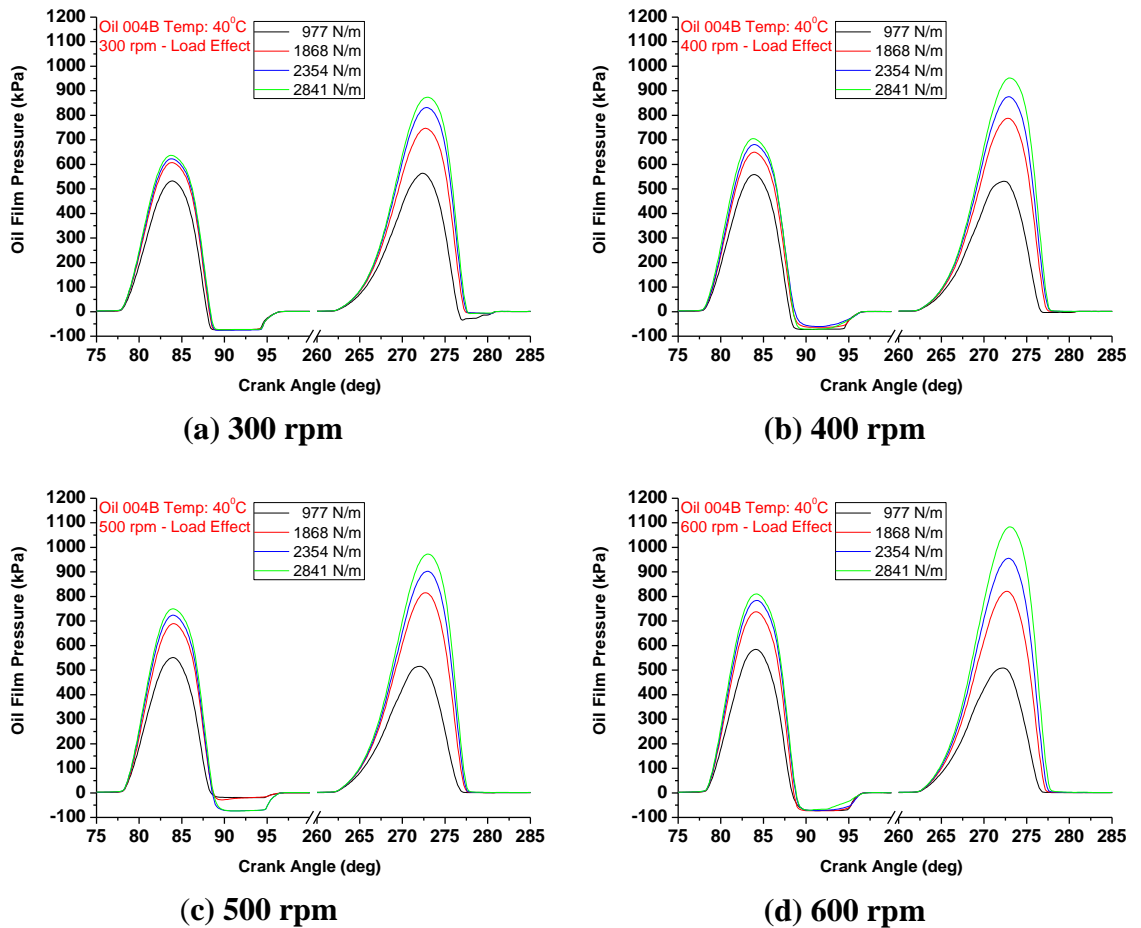


Figure 4.54: Variation of oil film pressure with CA at different loads for oil 004B

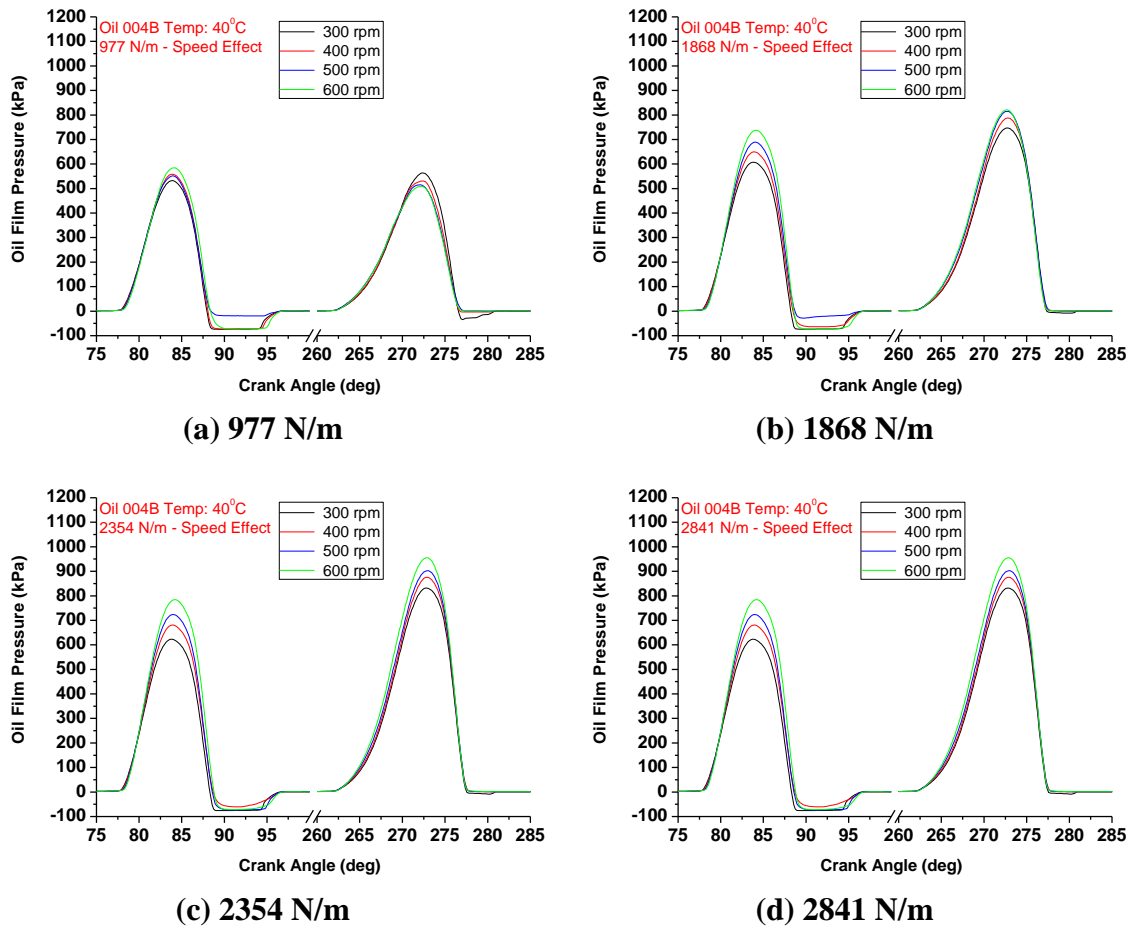
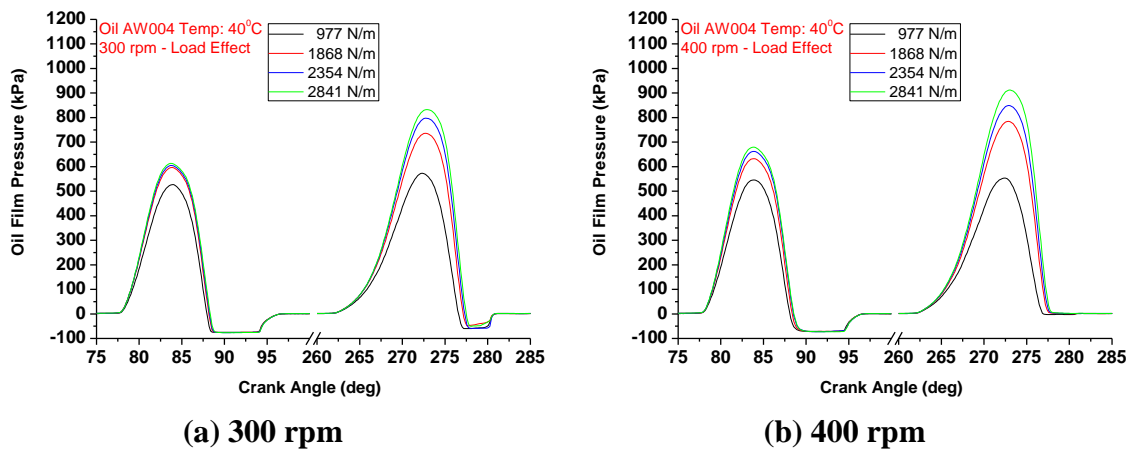


Figure 4.55: Variation of oil film pressure with CA at different speeds for oil 004B

Low viscosity oil AW004



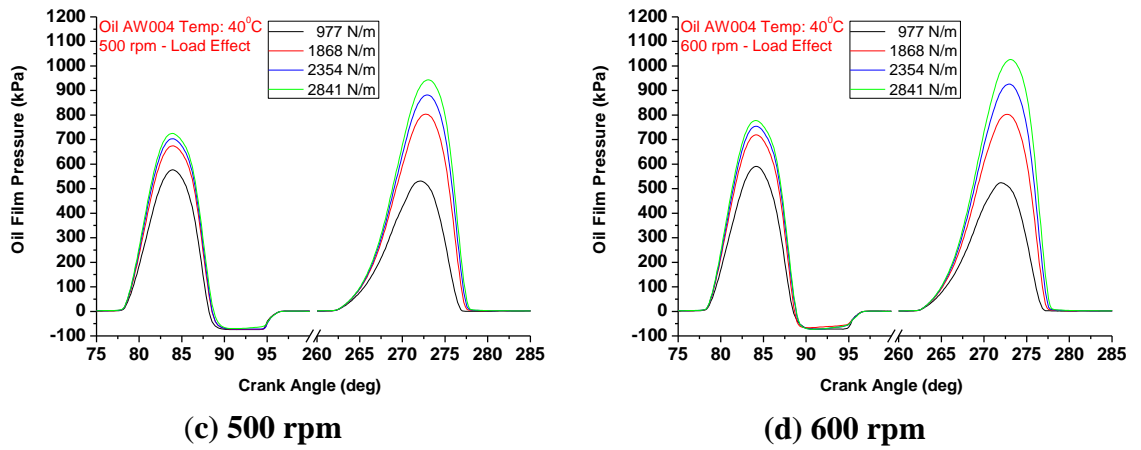


Figure 4.56: Variation of oil film pressure with CA at different loads for oil AW004

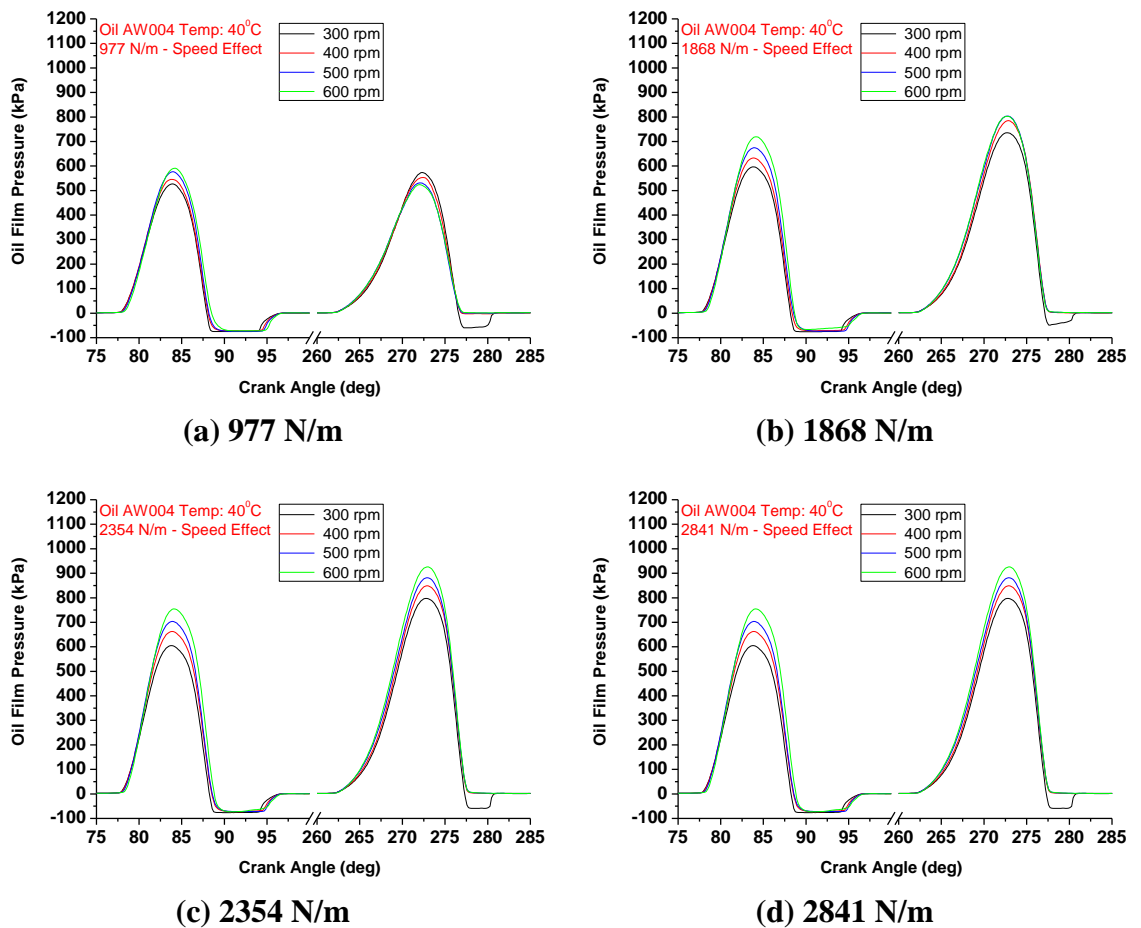


Figure 4.57: Variation of oil film pressure with CA at different speeds for oil AW004

High viscosity oil 097A

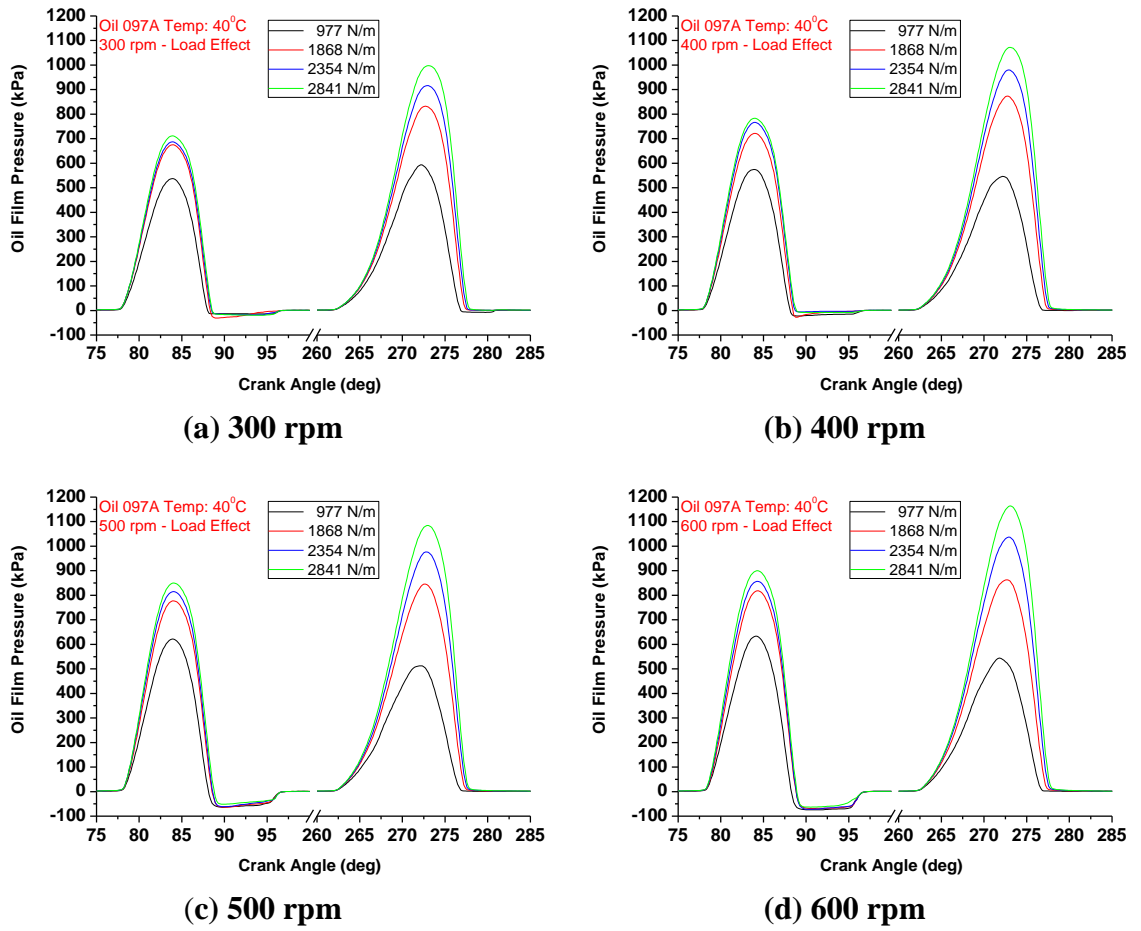
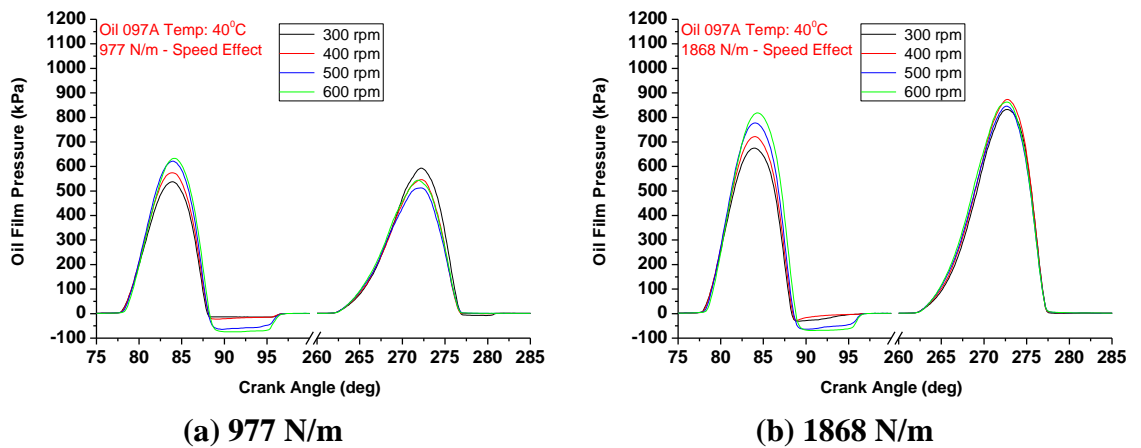
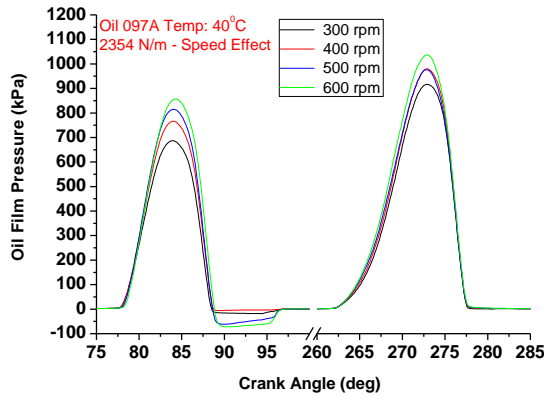
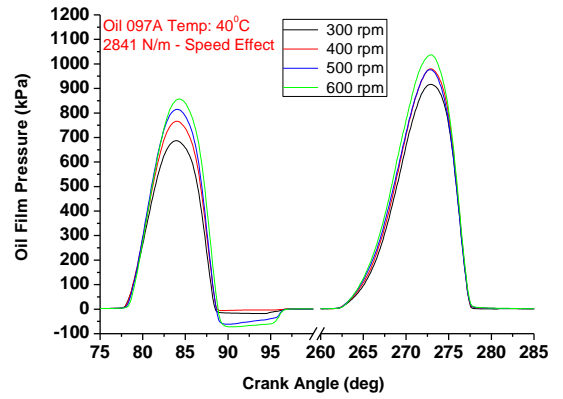


Figure 4.58: Variation of oil film pressure with CA at different loads for oil 097A





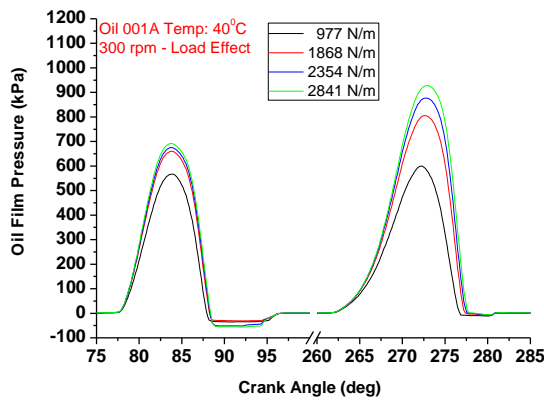
(c) 2354 N/m



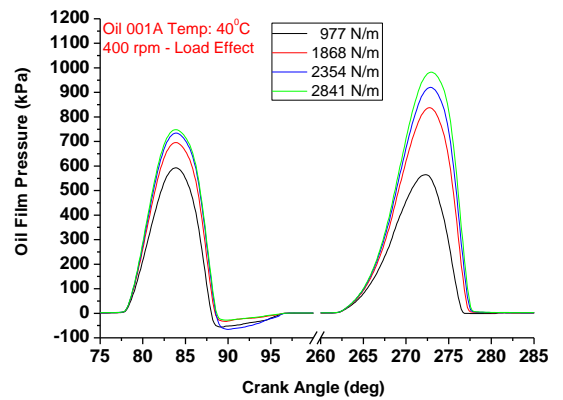
(d) 2841 N/m

Figure 4.59: Variation of oil film pressure with CA at different speeds for oil 097A

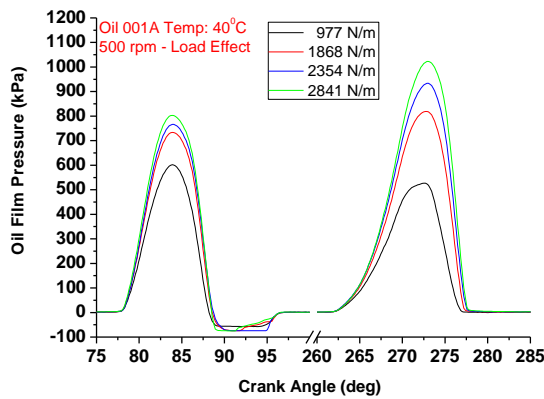
Reference old chemistry oil 001A



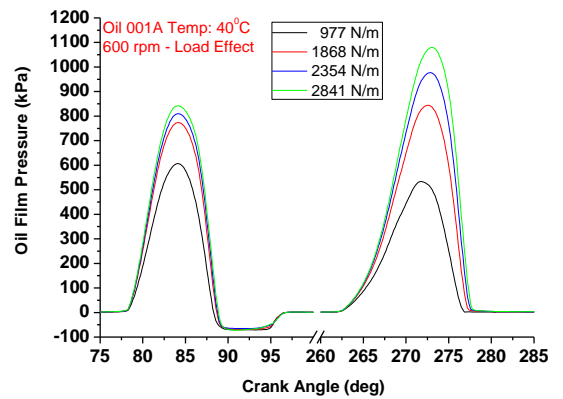
(a) 300 rpm



(b) 400 rpm



(c) 500 rpm



(d) 600 rpm

Figure 4.60: Variation of oil film pressure with CA at different loads for oil 001A

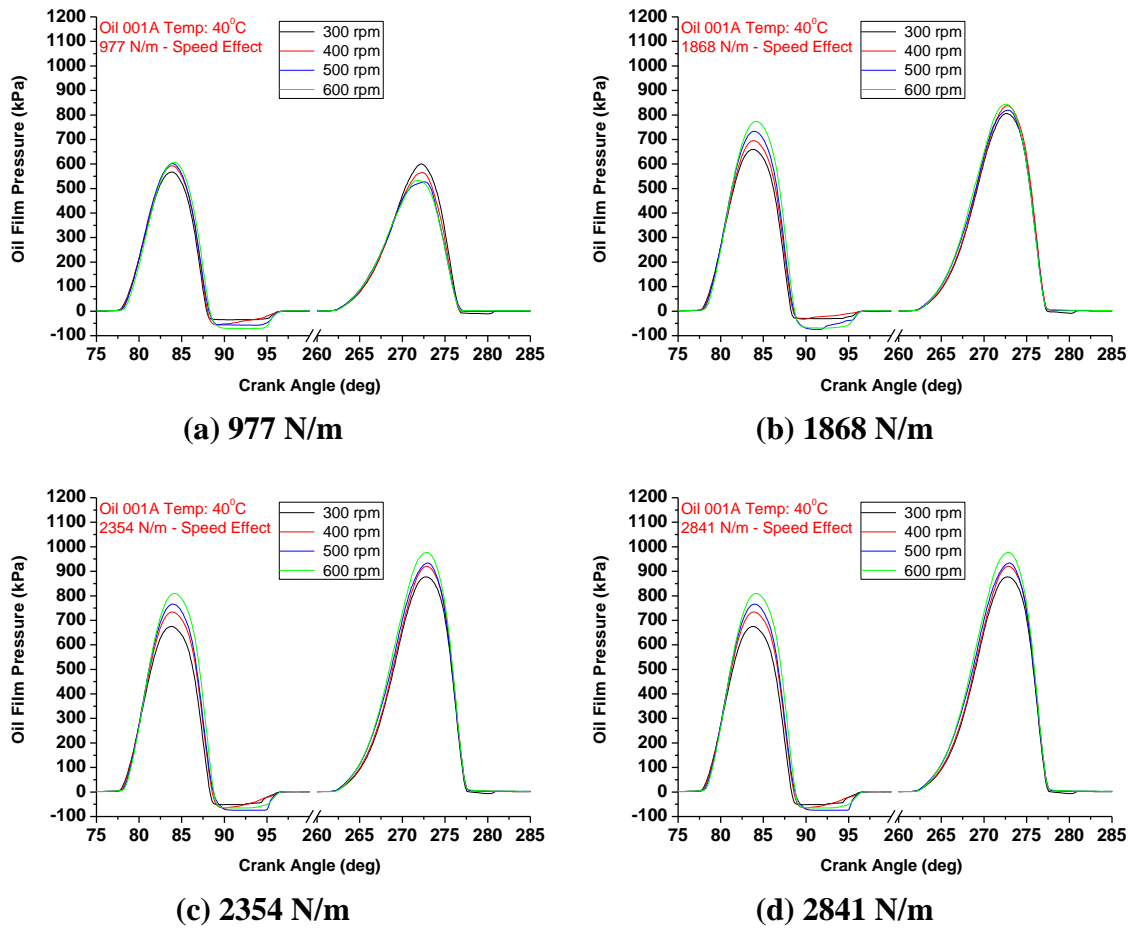
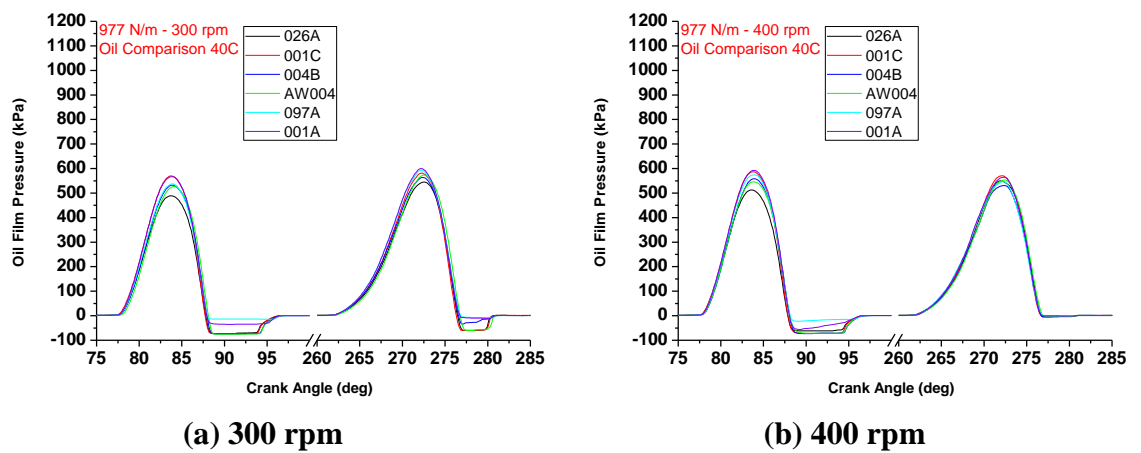


Figure 4.61: Variation of oil film pressure with CA at different speeds for oil 001A



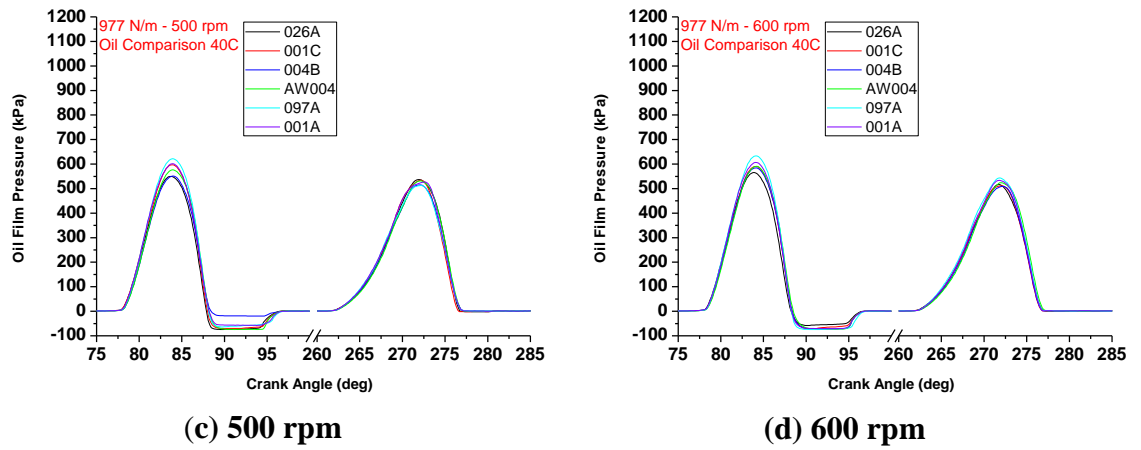


Figure 4.62: Oil film pressure - oil comparison, 977N/m - speed effect

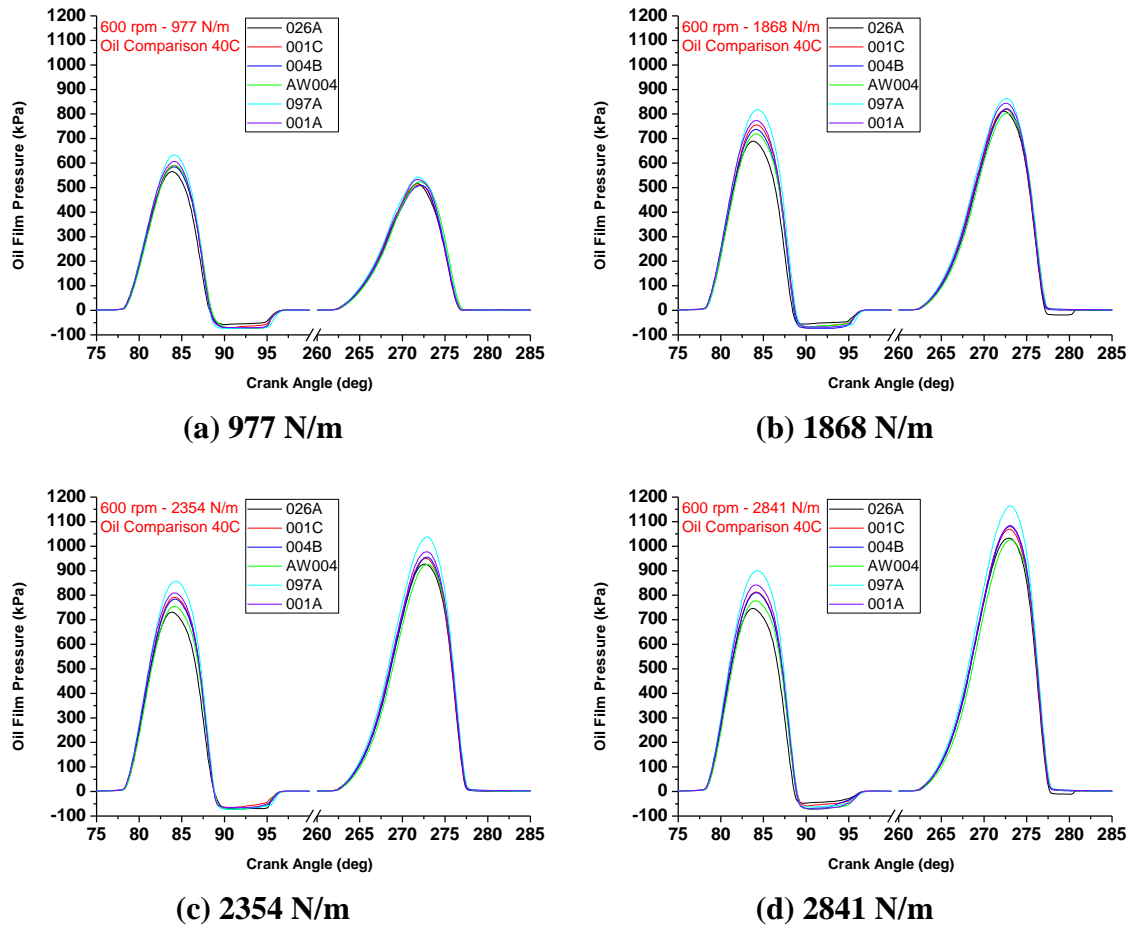
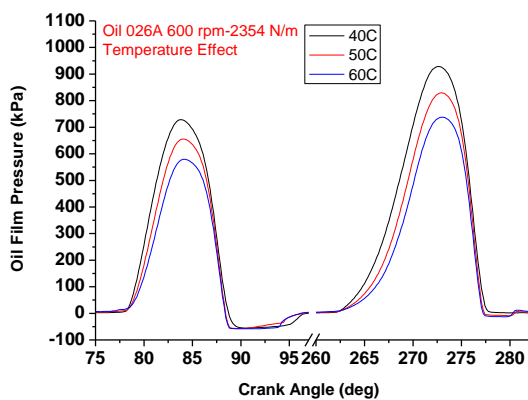
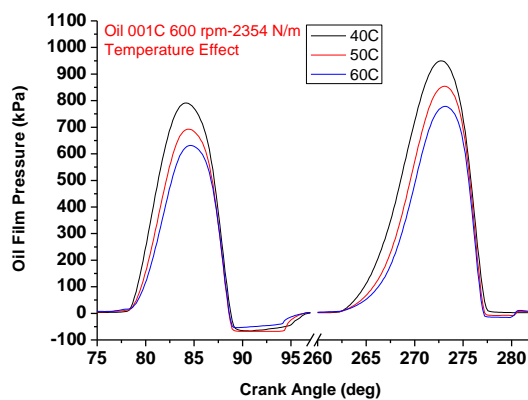


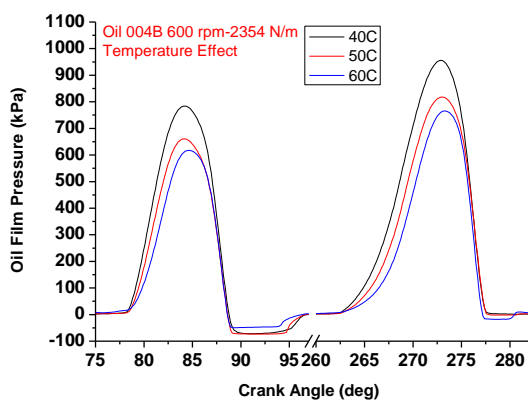
Figure 4.63: Oil film pressure - oil comparison, 600 rpm - load effect



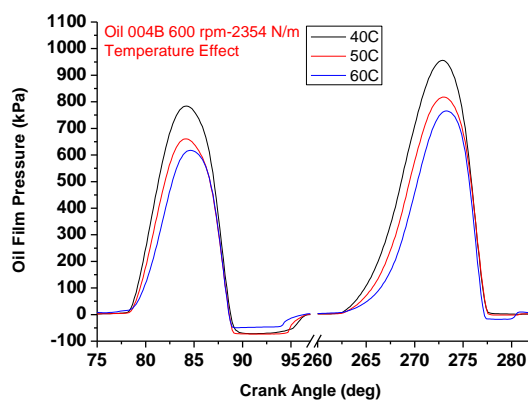
(a) oil 026A



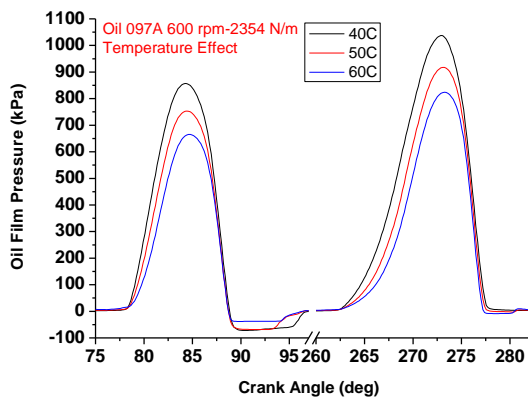
(b) oil 001C



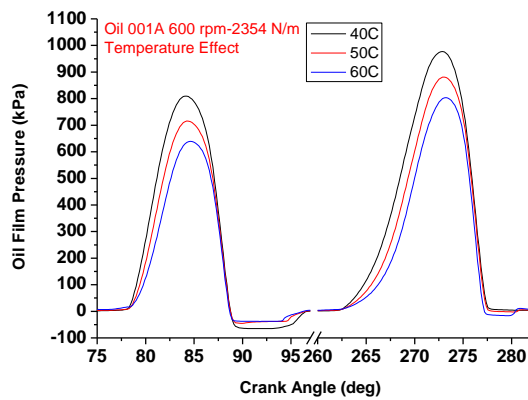
(c) oil 004B



(d) oil AW004



(e) oil 097A



(f) oil 001A

Figure 4.64: Oil film pressure - temperature effect, 600rpm - 2354 N/m

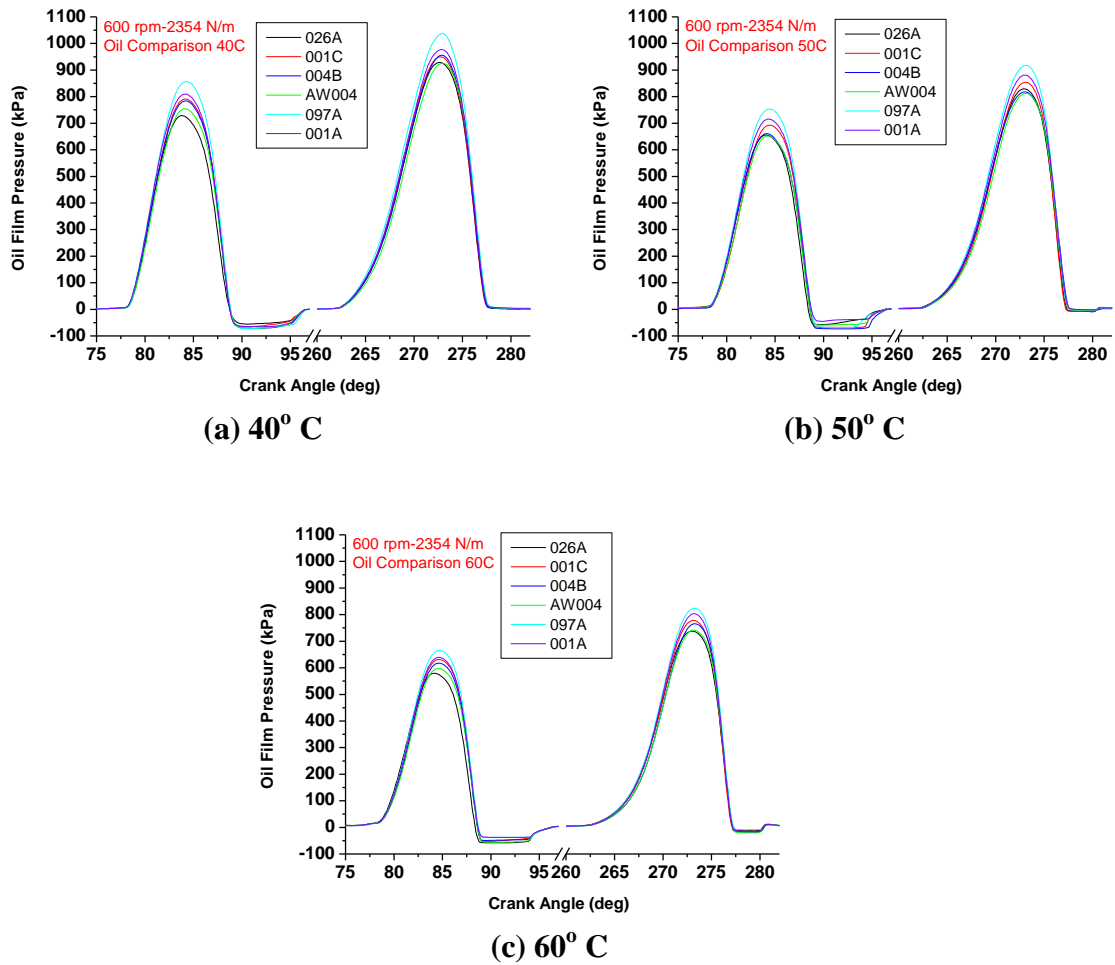


Figure 4.65: Oil film pressure (oil comparison) - temperature effect, at 600 rpm – 2354 N

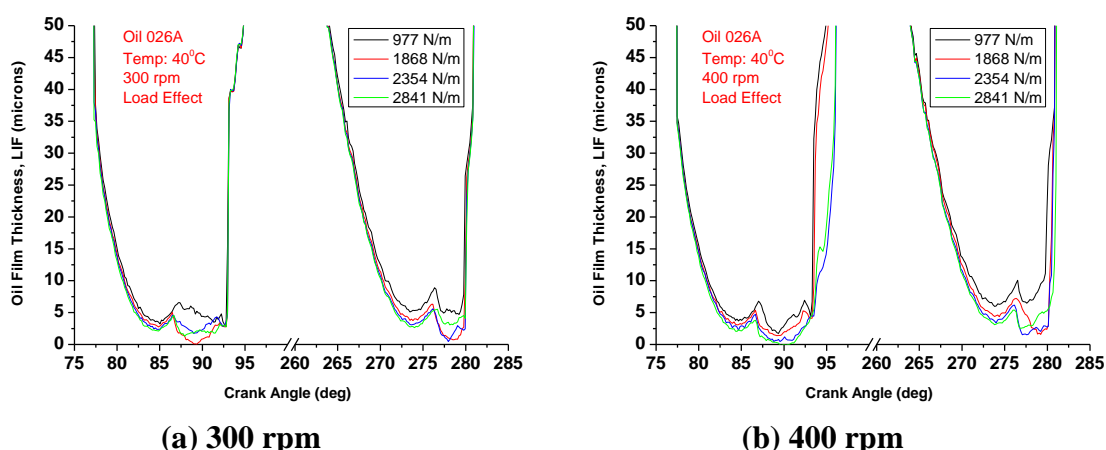
4.2.4 DISCUSSION OF LIF RESULTS

The LIF curves measured here have been calibrated using the method of matching the groove data against the LIF data, as described previously in Chapter 3. This technique measures the amount of oil encountered by the laser beam as opposed to the capacitance method which measure the gap between the sides of the ring and liner. Figures 4.66-4.77 show the downstroke and upstroke OFT measured with the LIF technique as a function of load and speed. It is noted once again (as in oil 2A) that the LIF measurements correspond with the ring profile where the film is continuous. That is, during the downstroke motion the laser beam measures the oil film which adheres to the converging part of the ring, following the ring profile path. On reaching the diverging part of the ring a sudden drop of oil film is encountered but later in the stroke the oil

film follows back the ring profile. The same is observed during the upstroke of the liner. The graphs (Figures 4.66-4.77) illustrate the downstroke that cavitation does occur in the diverging section of the ring at all the cases tested where as it was not evident in the pressure measurements. Despite all the six oils having different base oil (or constituents) to each other they exhibit similar cavitation behaviour. It is postulated (Brennen, 1995; Vijay and Arakeri, 1973) that viscosity has an influence on cavitation behaviour but in this section the LIF technique has not demonstrated otherwise. The effect of viscosity on cavitation has been investigated further in this work and it is discussed in the next chapter.

It has been noted that the OFT measured by LIF varies between 1 to 1.5 μm comparable to the values measured by the capacitance method. However, the LIF method used here is primarily focused on the qualitative measurements rather than in measuring the OFT accurately in absolute terms: it demonstrates the oil behaviour on the specimen ring and is useful for identifying cavitation. Although, there are some discrepancies between the two techniques of measuring OFT the LIF measurements demonstrate similarly findings to that of the capacitance method. That is; OFT increases with increasing speed and decreasing load everywhere during both downstroke and upstroke measurements. Figure 4.78 presents the temperature effect of the LIF measurements. It can be seen here that an increase in temperature reduces the OFT and, on the other hand, cavitation occurs in the diverging section of the ring. Therefore, once more demonstrating the sensitivity of the employed technique.

Reference oil 026A



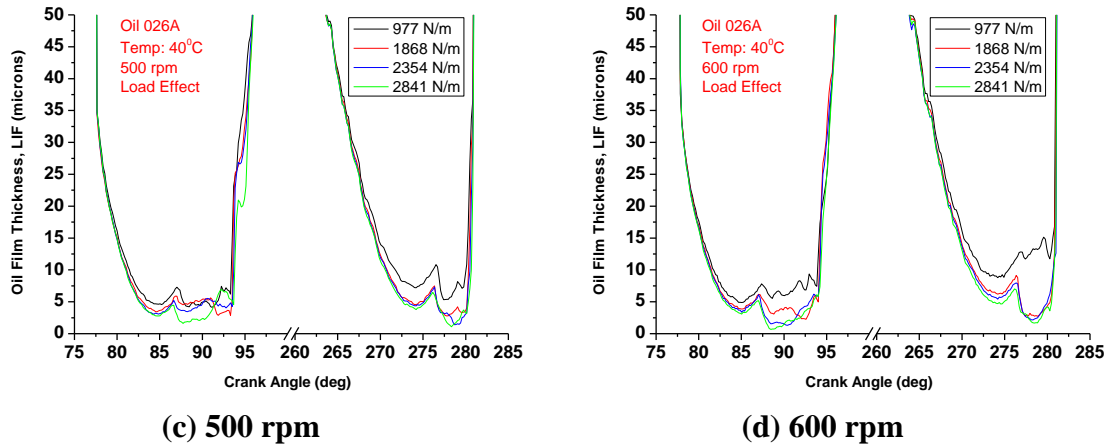


Figure 4.66: Variation of LIF measurement with CA at different loads for oil 026A

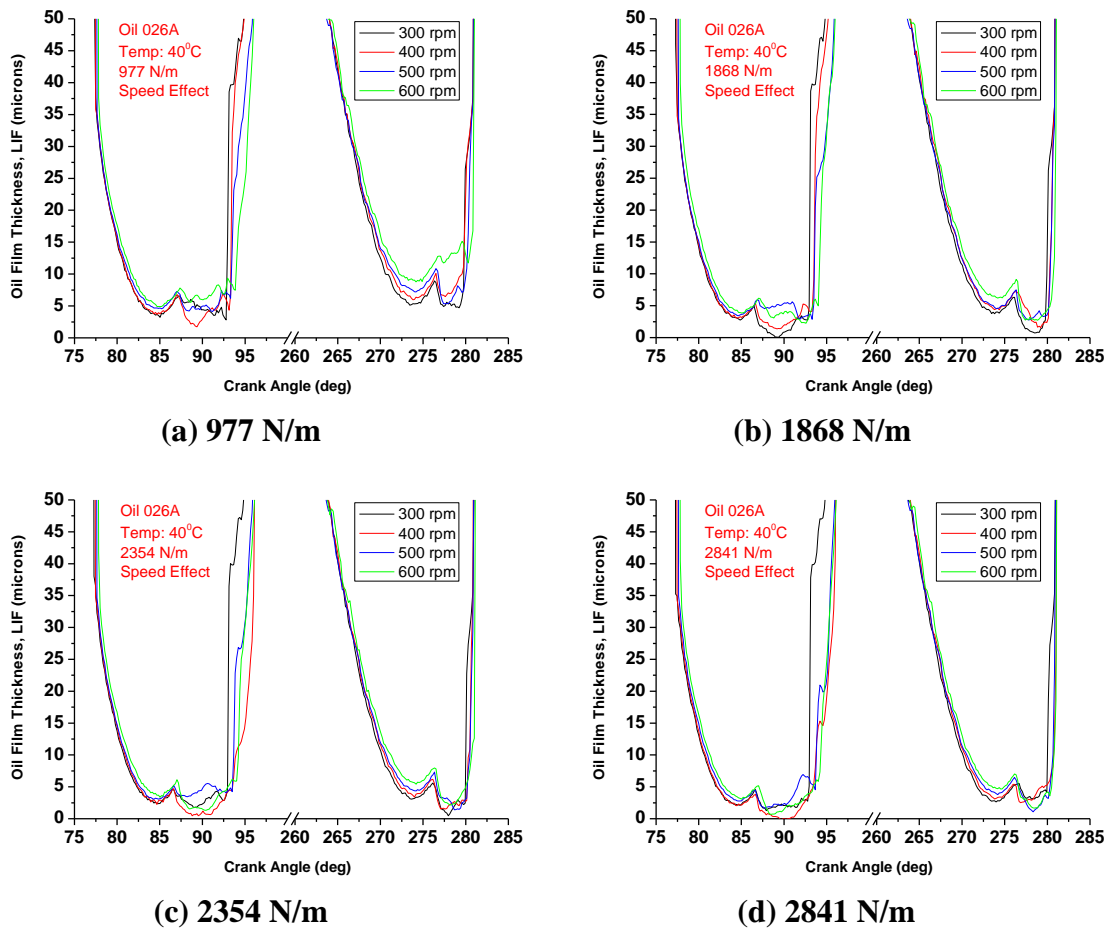


Figure 4.67: Variation of LIF measurement with CA at different speeds for oil 026A

Base oil A 001C

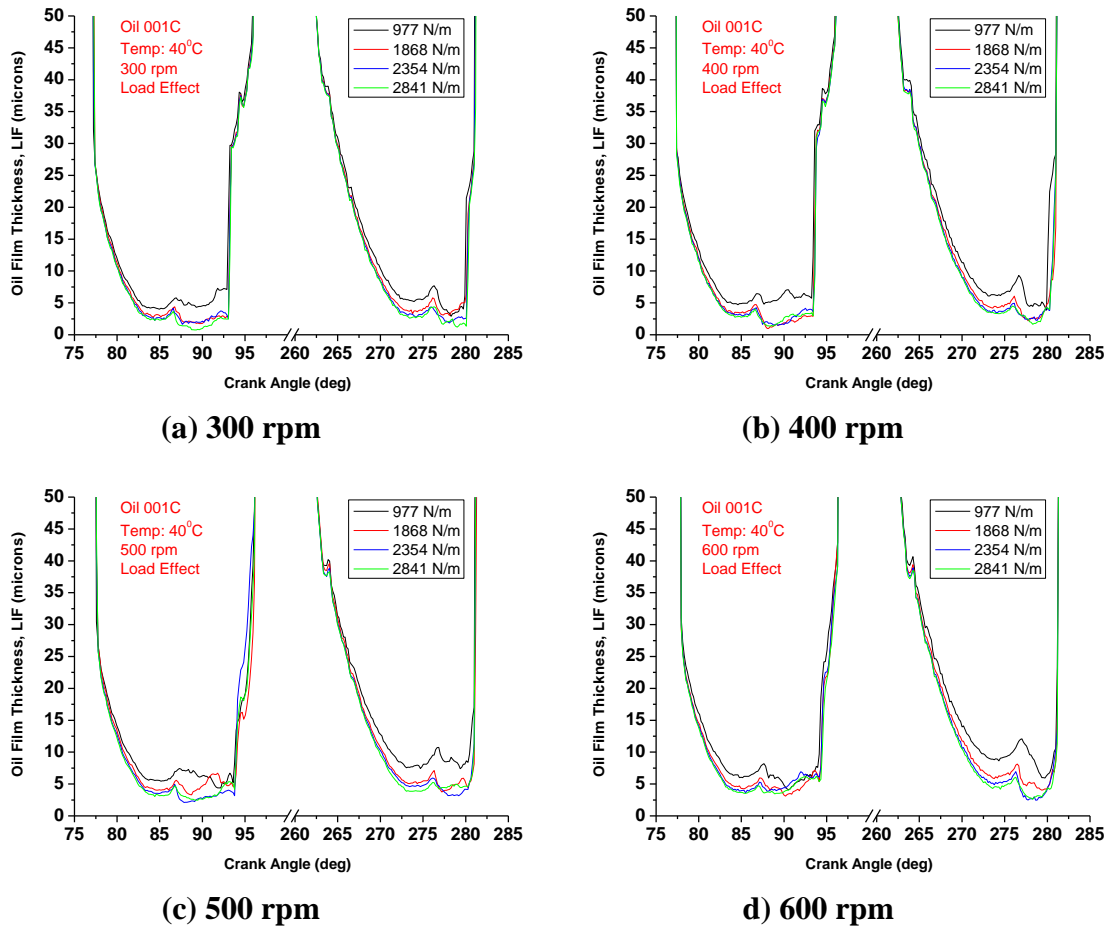
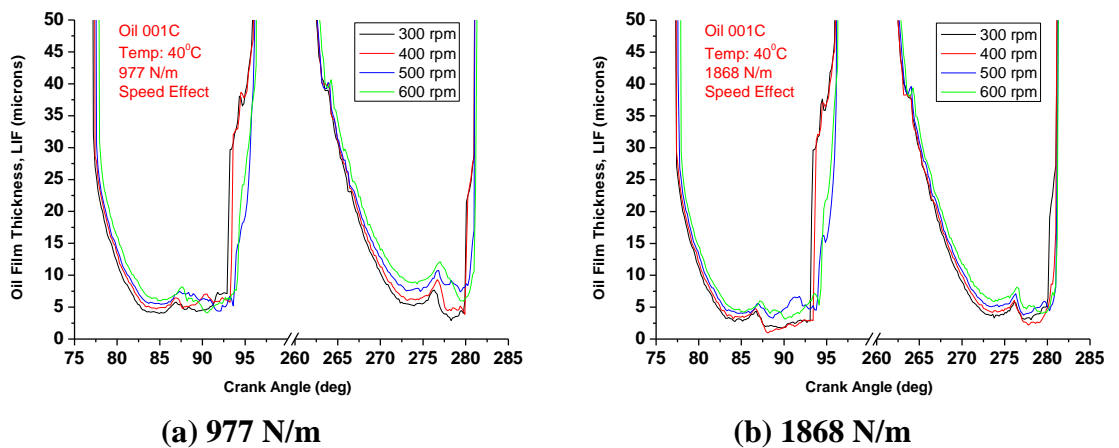
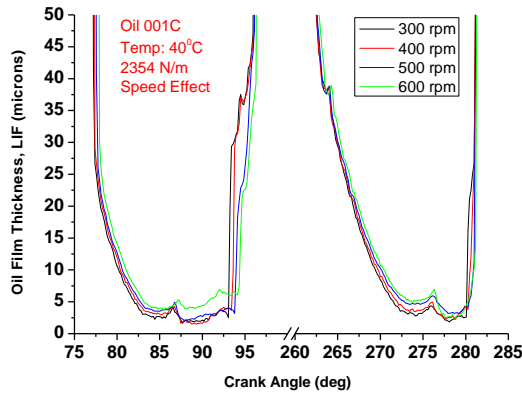
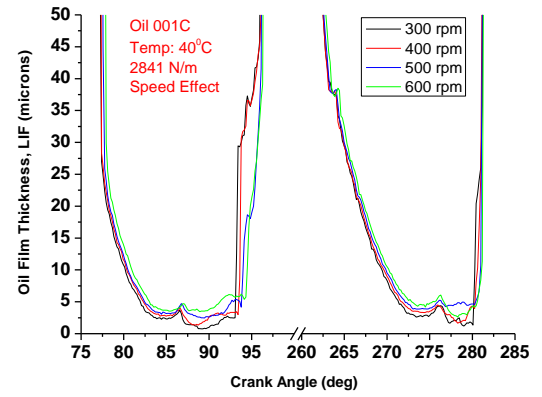


Figure 4.68: Variation of LIF measurement with CA at different loads for oil 001C





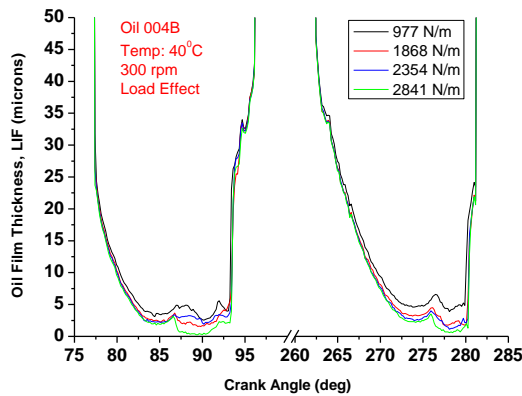
(c) 2354 N/m



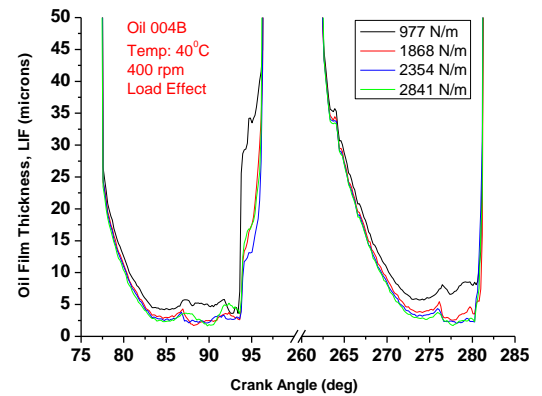
(d) 2841 N/m

Figure 4.69: Variation of LIF measurement with CA at different speeds for oil 001C

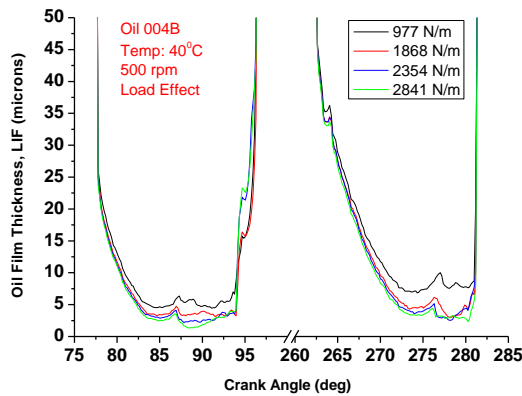
Base Oil B 004B



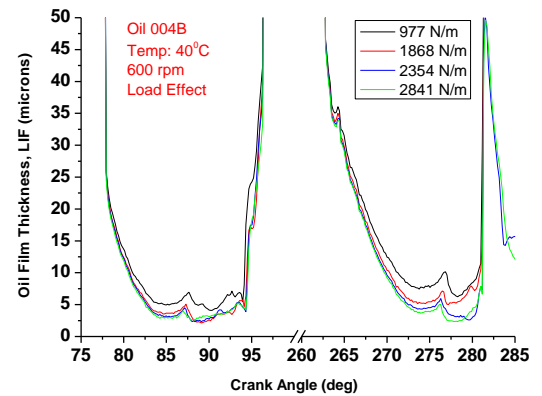
(a) 300 rpm



(b) 400 rpm

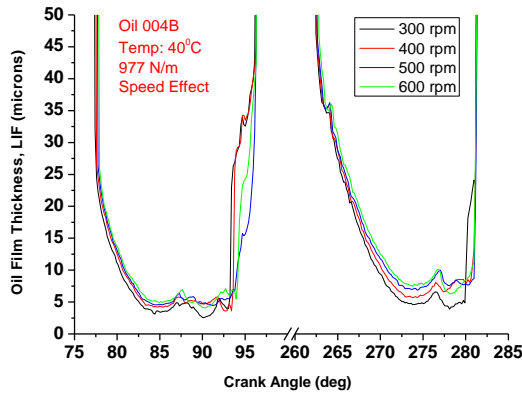


(c) 500 rpm

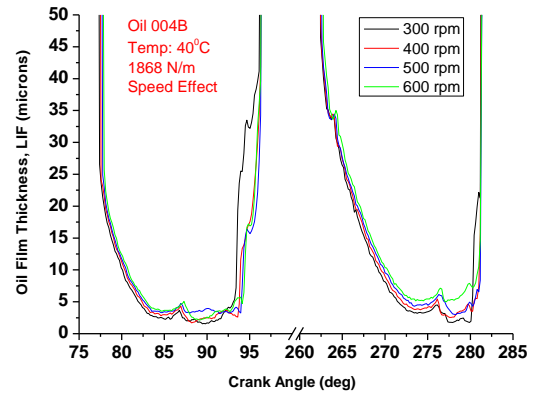


(d) 600 rpm

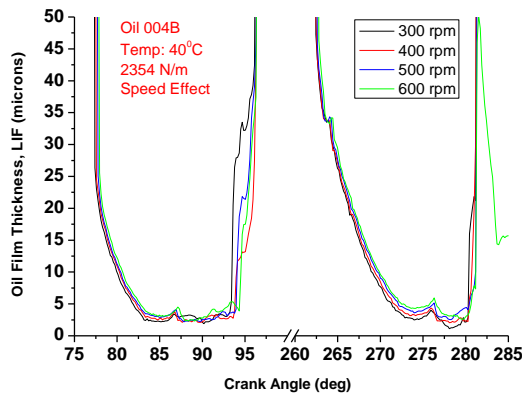
Figure 4.70: Variation of LIF measurement with CA at different loads for oil 004B



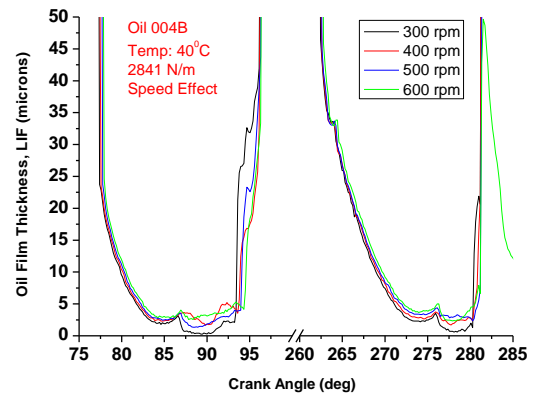
(a) 977 N/m



(b) 1868 N/m



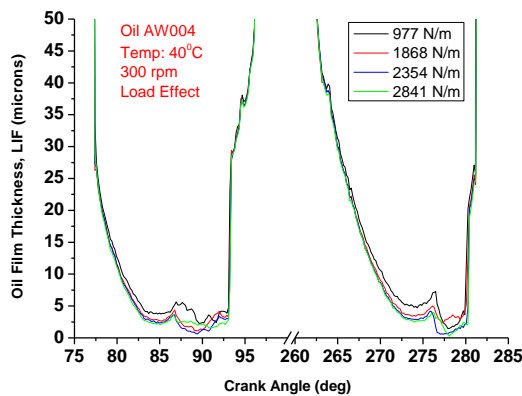
(c) 2354 N/m



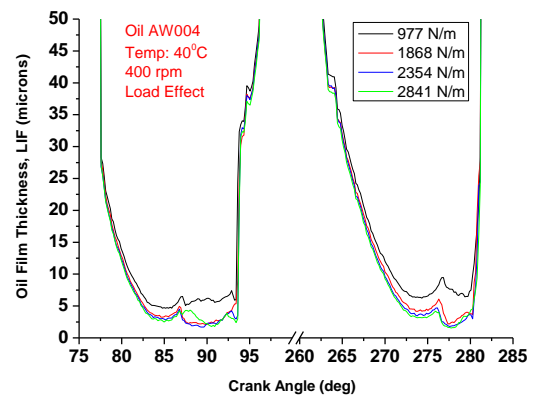
(d) 2841 N/m

Figure 4.71: Variation of LIF measurement with CA at different speeds for oil 004B

Low viscosity oil AW004



(a) 300 rpm



(b) 400 rpm

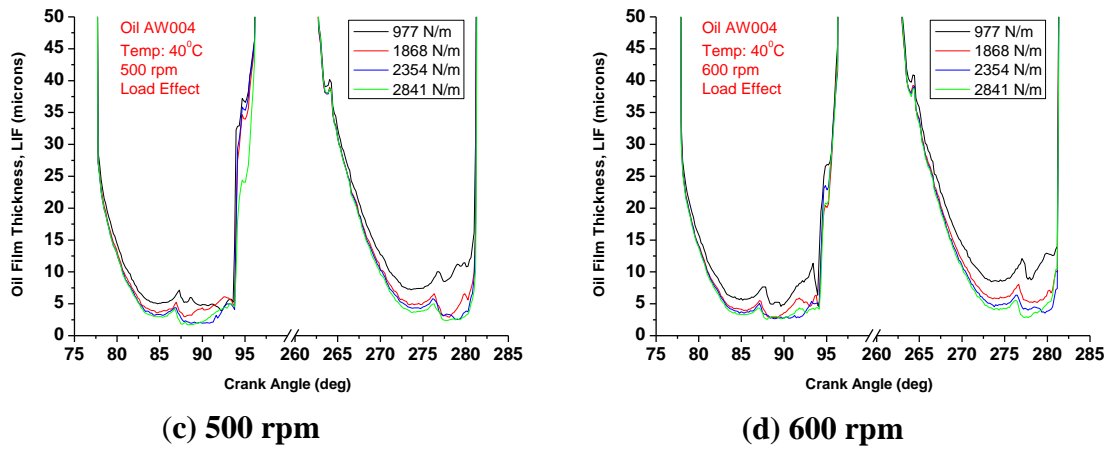


Figure 4.72: Variation of LIF measurement with CA at different loads for oil AW004

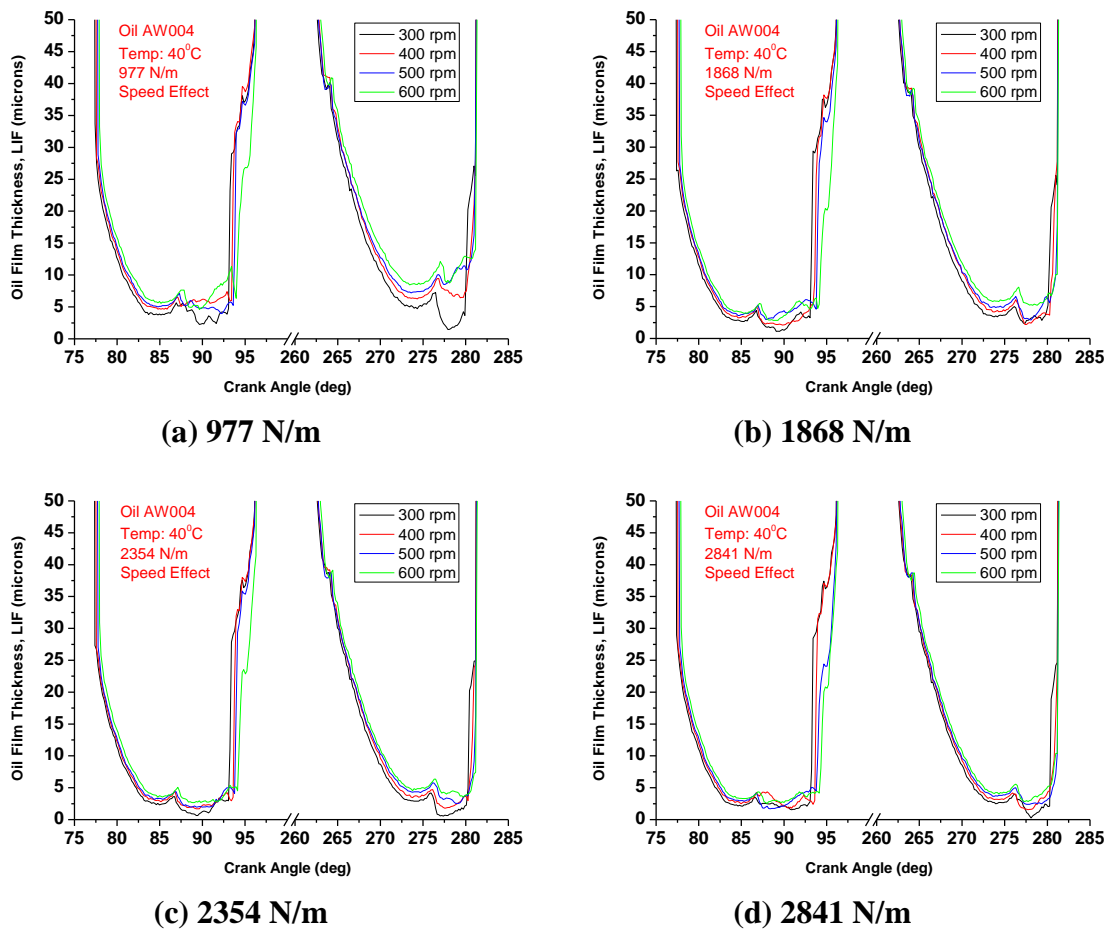


Figure 4.73: Variation of LIF measurement with CA at different speeds for oil AW004

High viscosity oil 097A

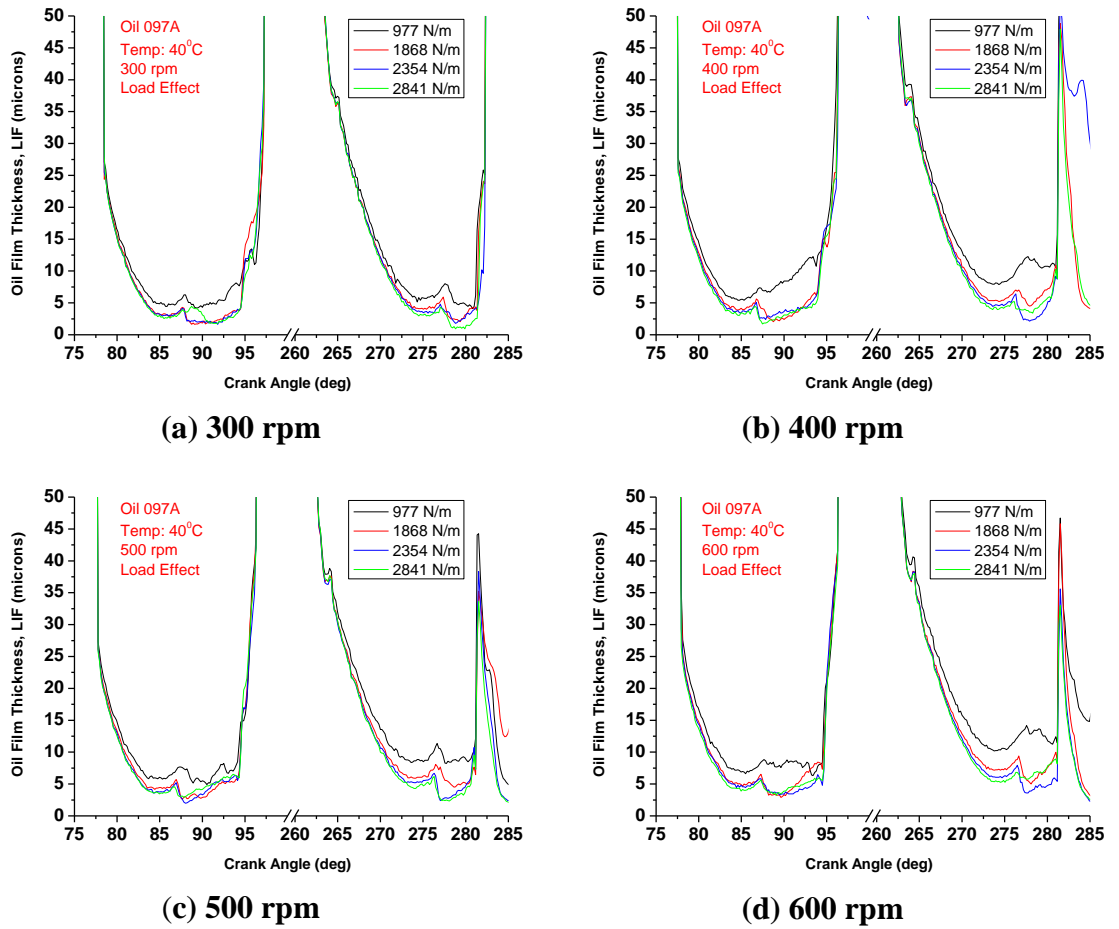
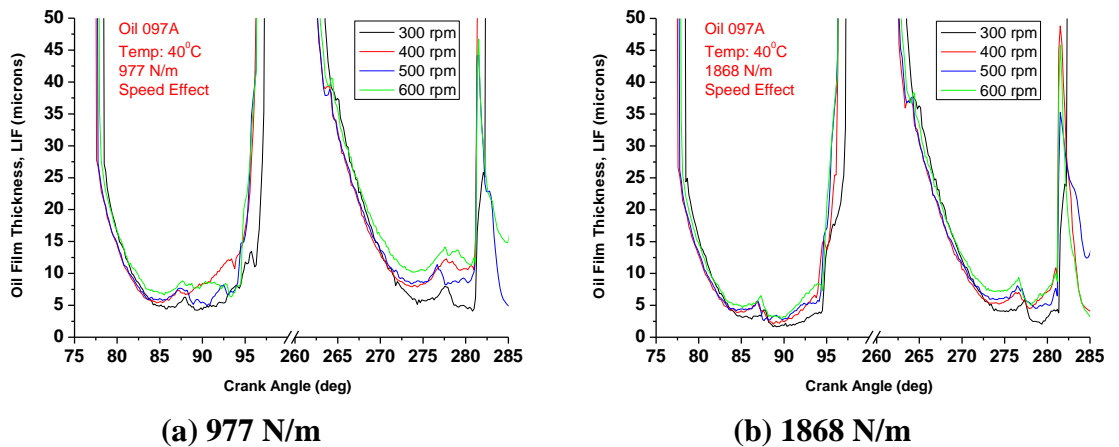


Figure 4.74: Variation of LIF measurement with CA at different loads for oil 097A



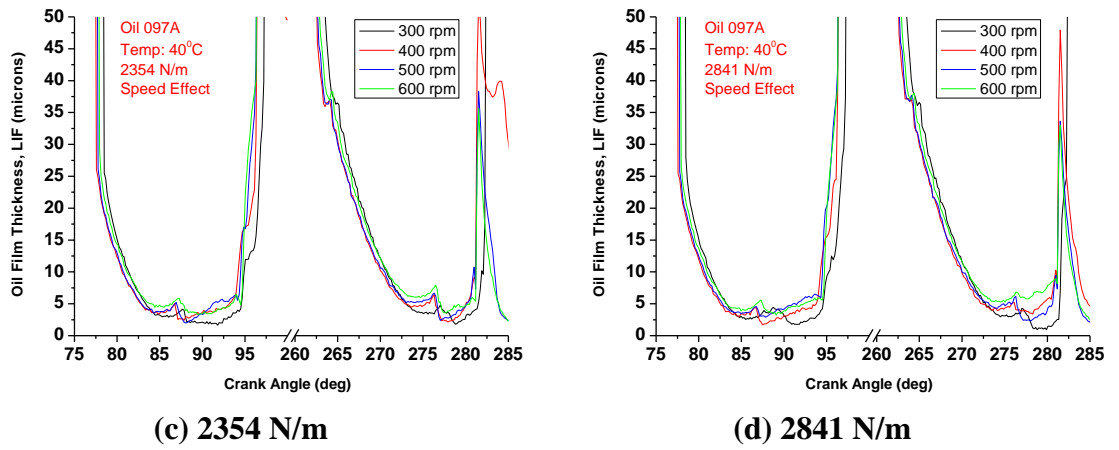


Figure 4.75: Variation of LIF measurement with CA at different speeds for oil 097A

Reference old chemistry oil 001A

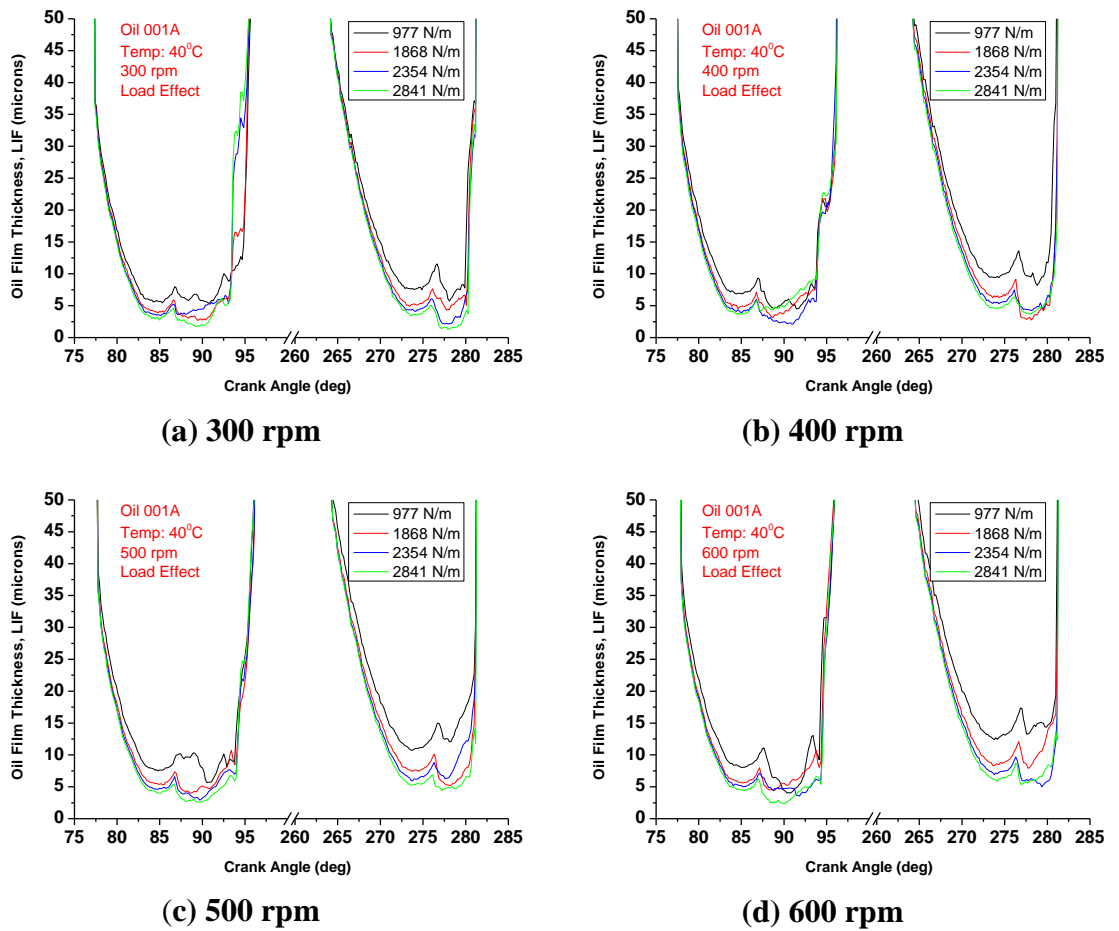
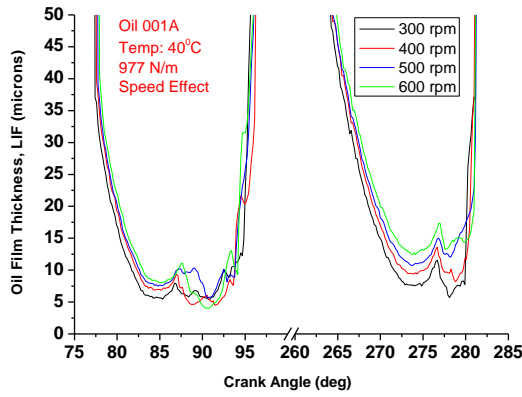
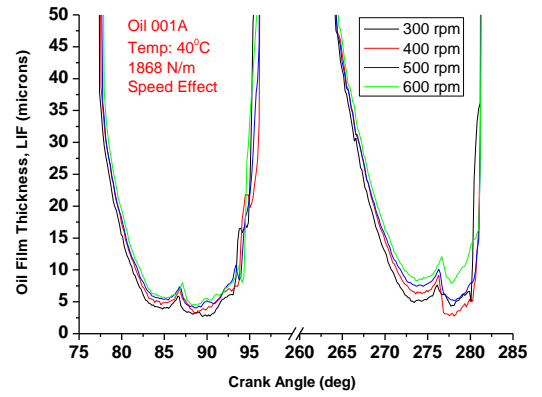


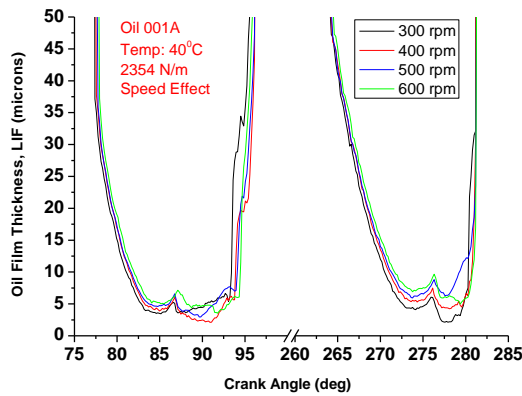
Figure 4.76: Variation of LIF measurement with CA at different loads for oil 001A



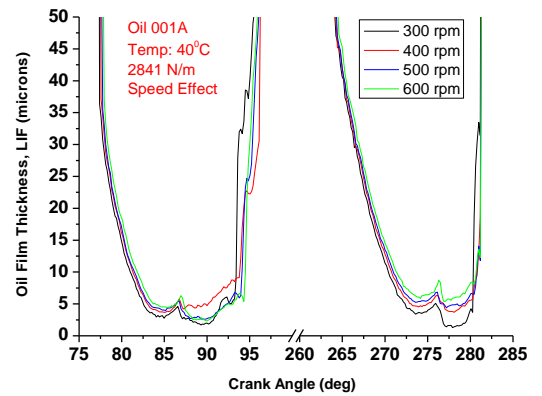
(a) 977 N/m



(b) 1868 N/m

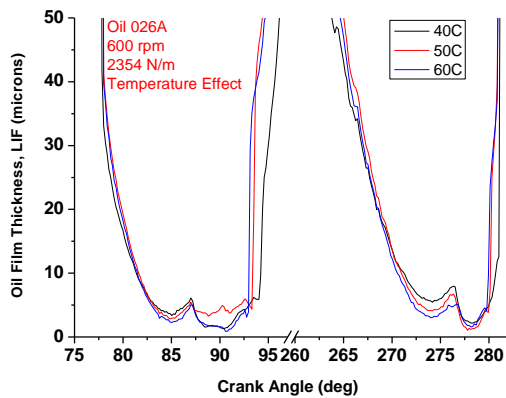


(c) 2354 N/m

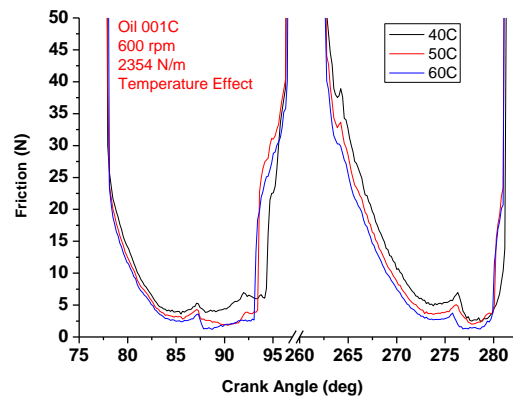


(d) 2841 N/m

Figure 4.77: Variation of LIF measurement with CA at different speeds for oil 001A



(a) oil 026A



(b) oil 001C

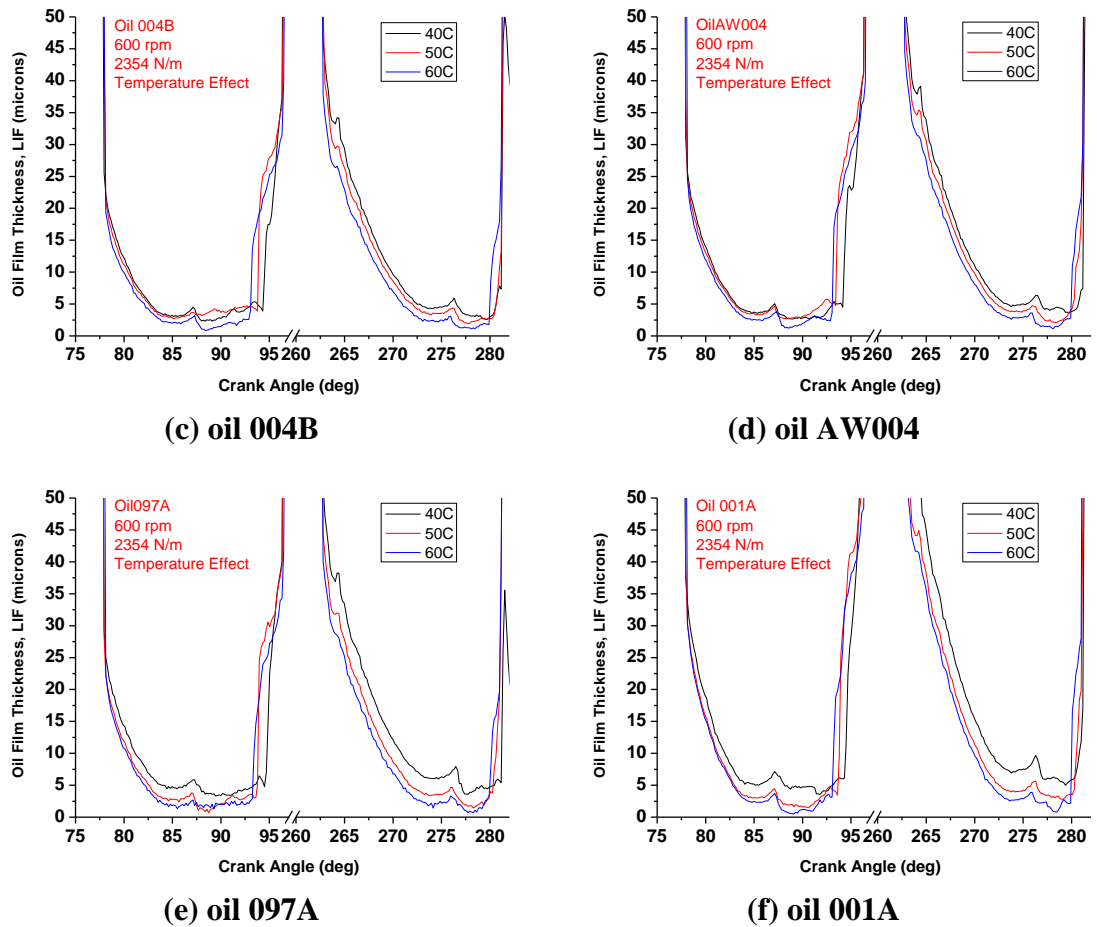


Figure 4.78: LIF measurements - temperature effect, 600rpm - 2354 N/m

4.3 SUMMARY

An idealised test rig has been employed to investigate the piston-ring-liner assembly lubrication conditions, the minimum oil film thickness and frictional force acting at the piston ring-cylinder liner interface, and the oil film pressure. The piston ring transitions through the entire range of lubrication regimes and the measured values for friction force and oil film thickness are used to investigate the lubrication condition throughout the stroke. The effect of piston speed, load and oil temperature has been quantified for a range of oils. Depending on the operating conditions, all three lubrication regimes can occur at different points in the stroke. As expected, friction is highest in the mixed lubrication and boundary lubrication regimes that occur near the TDC and BDC. The

effects of viscosity were evident during testing where the numerous figures show the trend noticed during the parametric study.

The cavitation regime between the ring and the liner occurs in the diverging section of the conjunction, when the pressure drops below the atmospheric level. This phenomenon is highly dependent on the localised kinetics within the contact region as well as the dynamics of the ring and piston. The current research is using a set of integrated experimental techniques to investigate cavitation onset and development. The oil film pressure and the film thickness obtained by the LIF technique are simultaneously measured, with the sub-atmospheric pressure regions corresponding to the depleted oil film thickness on the diverging part of the ring. This provides explanation to the occurrence of cavitation in that region. Unfortunately, the pressure transducer showed some deficiency in measuring negative pressures for some cases especially in the upstroke measurements. This is an area that should be further explored. However, LIF proved more reliable for detecting the cavitation region and confirmed that all oils cavitate in the diverging section at both strokes.

Chapter 5

VISUALISATION OF OIL FILM IN TEST-RIG AND DIESEL ENGINE

The oil transport and distribution in the piston-ring and liner interface is affected by various driving forces such as inertia, gas flow, ring motion and ring-liner lubrication. These factors, and the resulting oil transport and cavitation, vary significantly with engine load and speed. To advance the understanding of the complex cavitation phenomena occurring in the oil film between piston-ring-liner interfaces, the idealised test-rig modified to provide optical access has been employed to visualise the onset and development of cavitation under well defined conditions. Furthermore, the oil film visualisation investigation has been extended to a single cylinder diesel engine, which was modified by incorporating quartz windows in the liner for optical access, in order to explore whether cavitation is also present in an engine film under realistic operating conditions. Moreover, pressure measurements have been used to provide supporting evidence of cavitation to the visualisation results which are not always very clear and convincing.

5.1 TEST RIG VISUALISATION

5.1.1 HIGH SPEED VIDEO IMAGING

Previous investigations of Kim *et al.*(1995) and Dellis and Arcoumanis (2004) have used a still camera to visualise the onset and development of cavitation in a simulating rig where different pattern have been identified. However, due to the limitation of their photographic devices their presented results were not time resolved and hence was difficult to follow the dynamic and development of cavitation within the oil film. The next logical step was to use a device capable of time resolving the dynamic of the oil film cavitation. Therefore, a high speed video camera, previously described in section

3.4.3, has been employed in the oil film visualisation in the test rig and the results are presented in this chapter. Figure 5.2 depicts the flow development during the downstroke testing of baseline oil 2A (properties in Table 4.1) at 300 rpm with respect to crank angle. Initially the 300 rpm speed has been chosen so that to take full advantage of the high recording frame rate of the device. The following images were taken by the high speed digital video camera as previously described in section 3.4.3. The visualisation of the oil film was carried out around the middle part of the specimen ring (5.28mm x 5.28mm) and the covered area where the images were acquired is illustrated in Figure 5.1. The stroke for this experiment was set at 22 mm and an oil temperature around 38⁰ C was maintained. The following images shown below were acquired continuously in the same cycle. The test shows that the cavities start to appear in the diverging part of the surface, during the downstroke motion of the piston ring (can be first identified in Figure 5.2 (a) as circled). Later along the stroke they coalesce before forming in string cavities. The cavity shapes obtained were found to be very repeatable from cycle to cycle. The imaging results were compared to those taken at different speeds and loads.

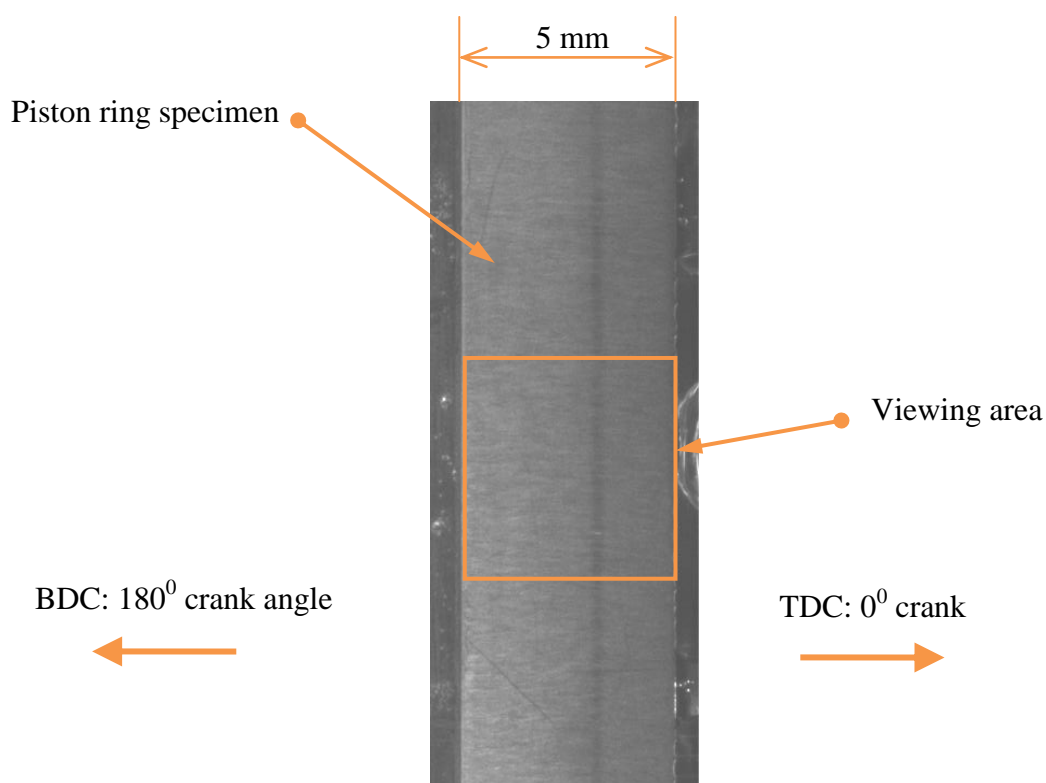
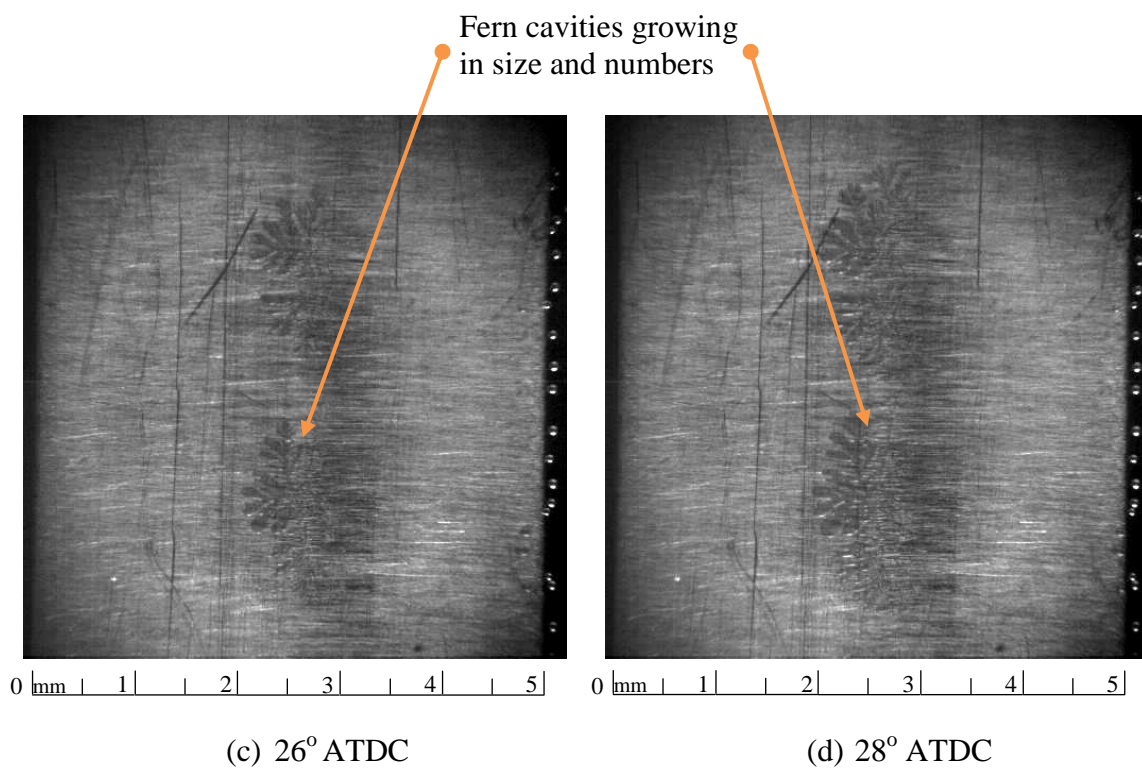
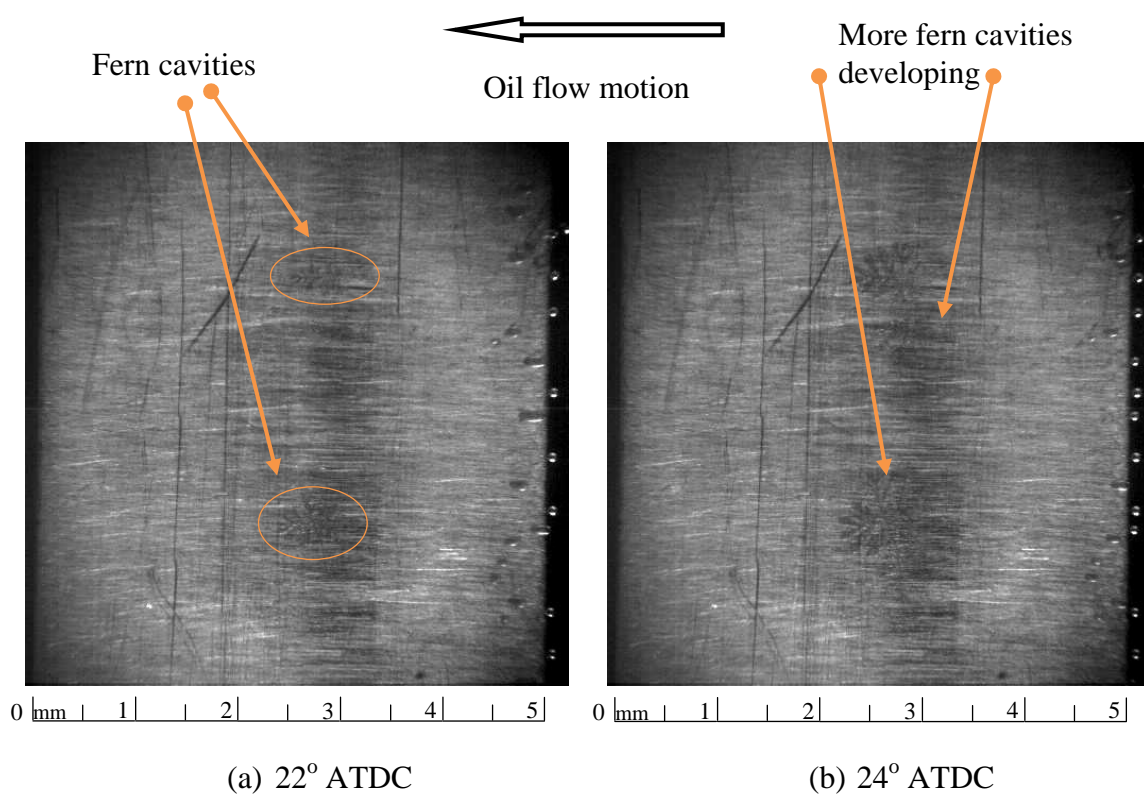
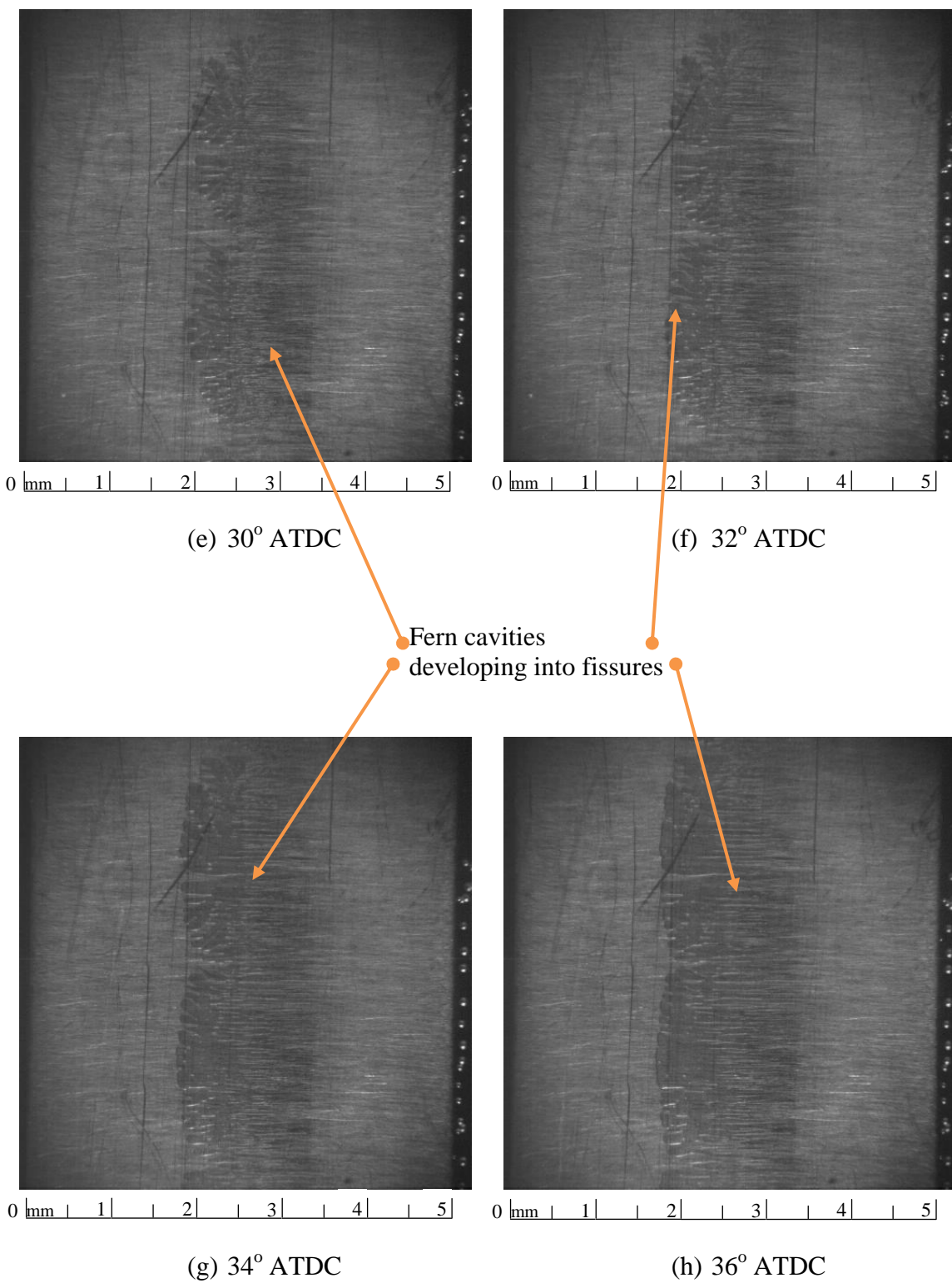


Figure 5.1: Viewing window for high speed video imaging in the idealised test rig



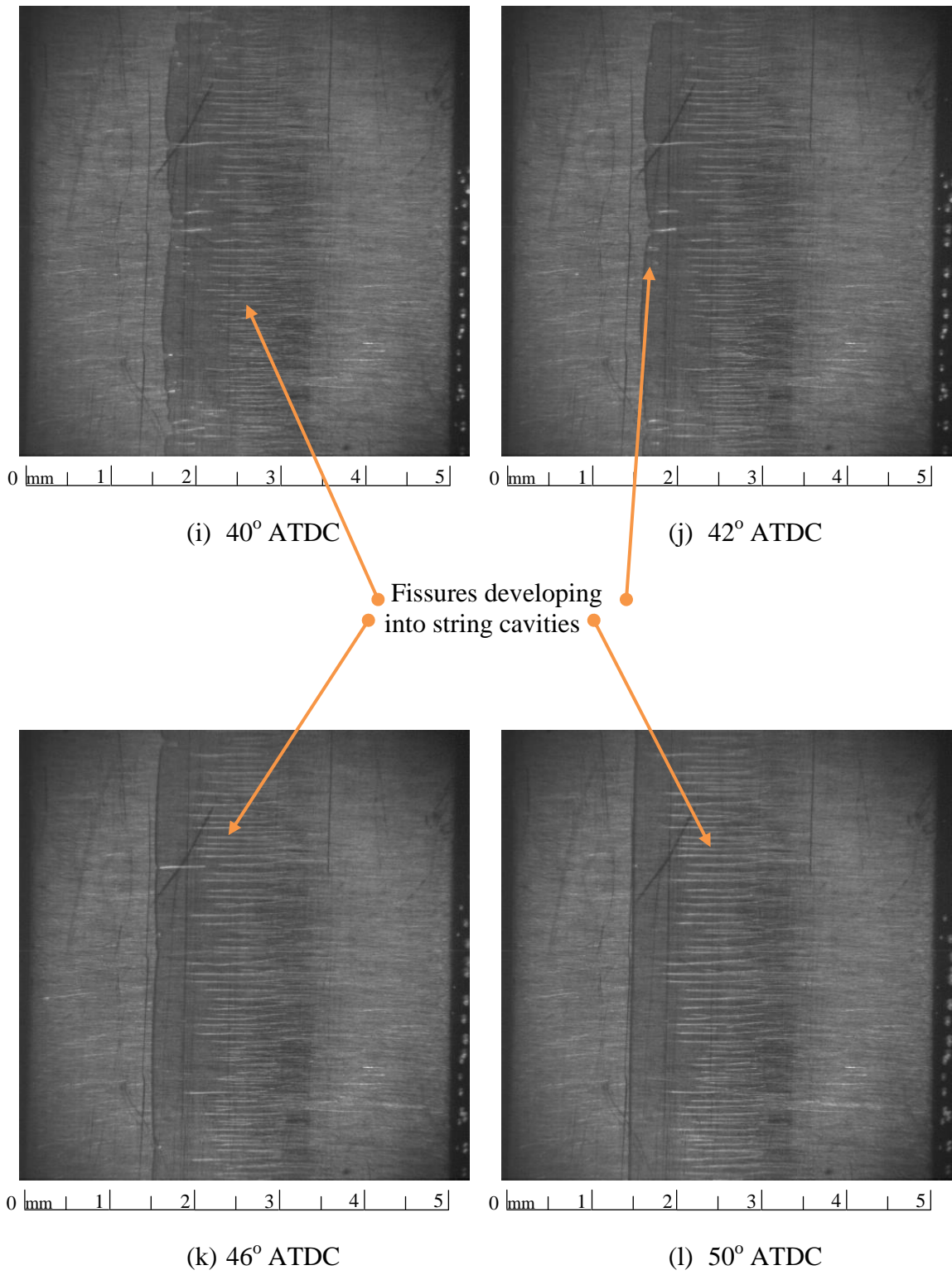


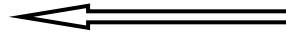
Oil flow motion



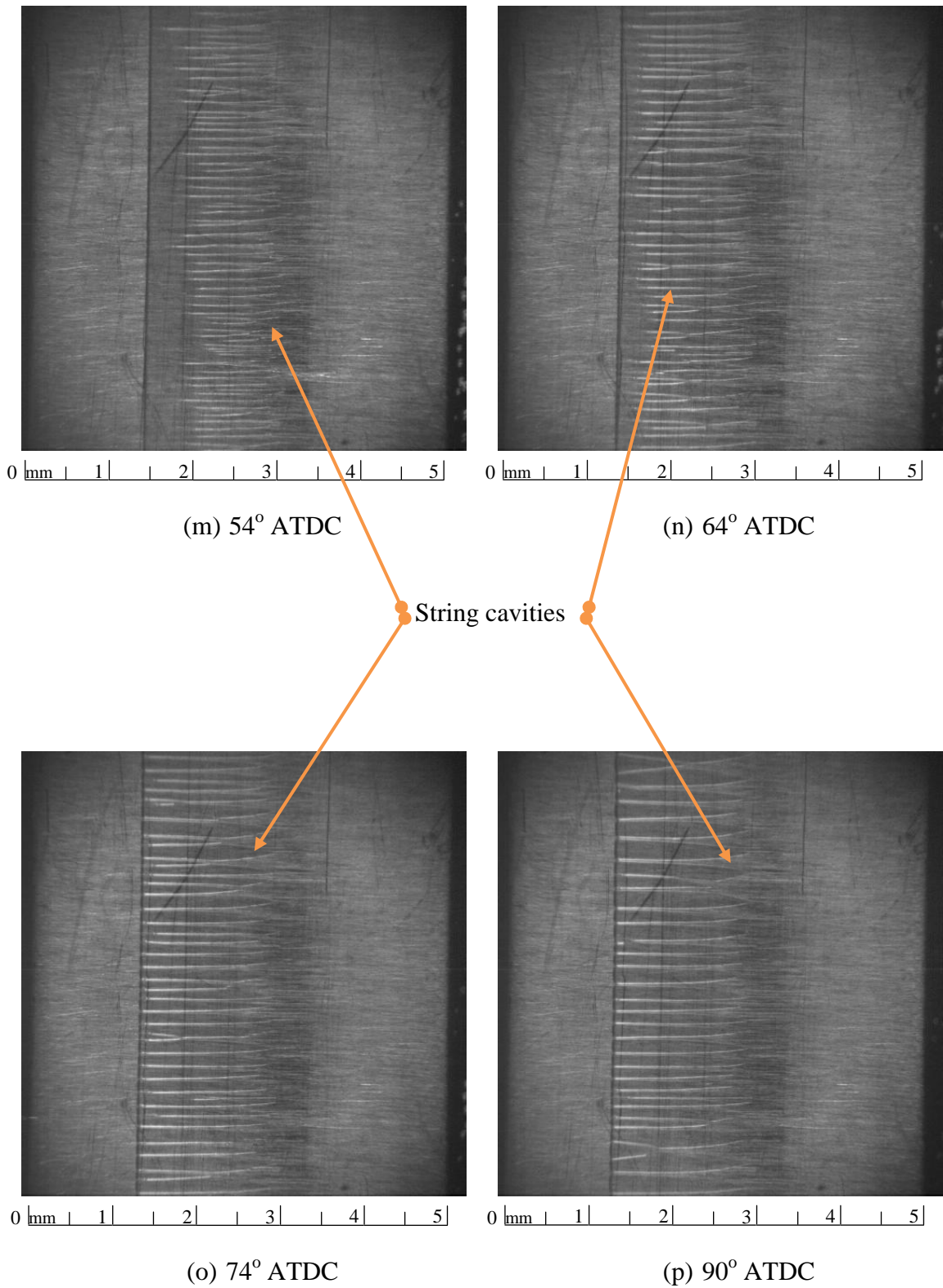


Oil flow motion



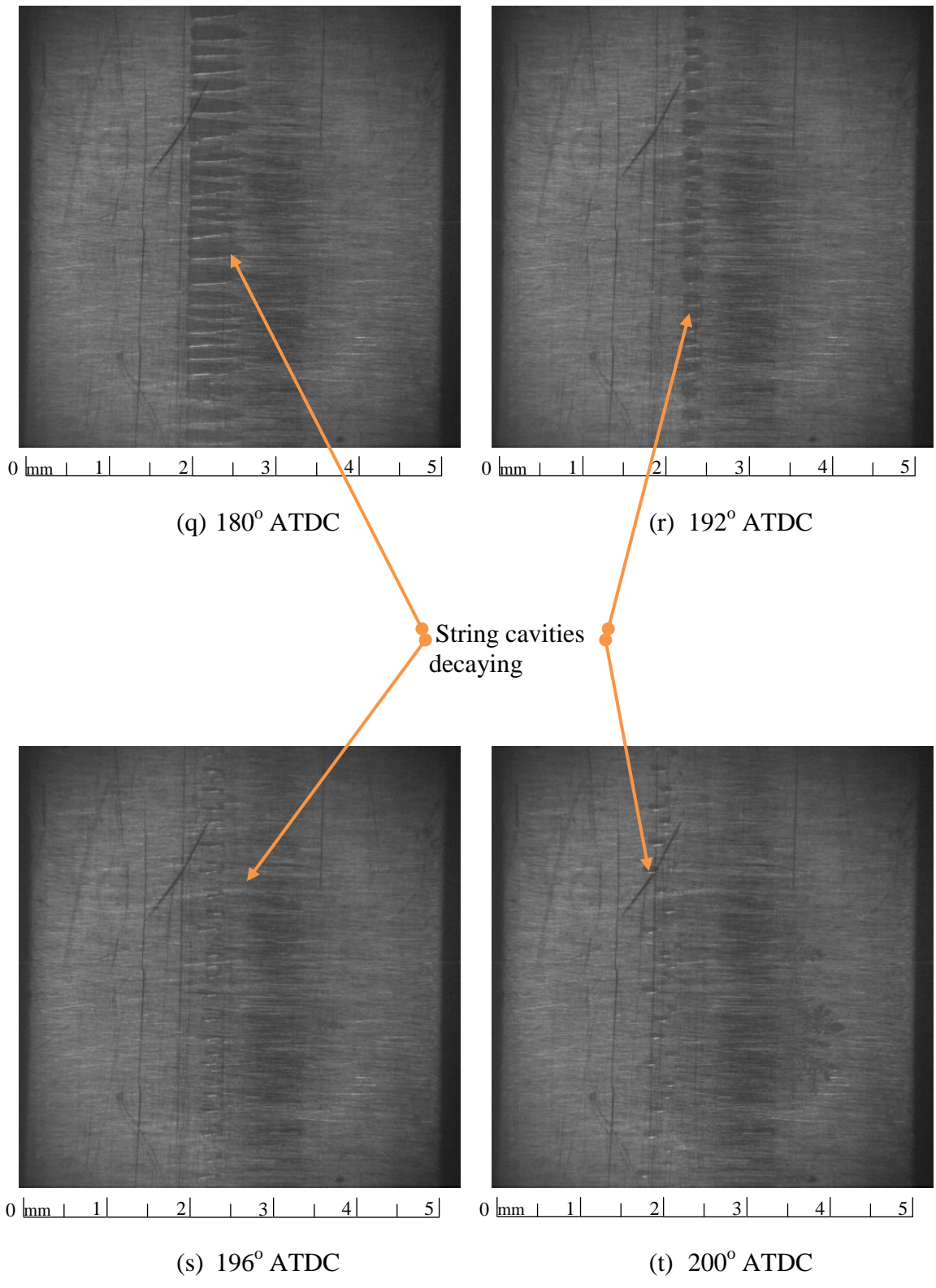


Oil flow motion





Oil flow motion



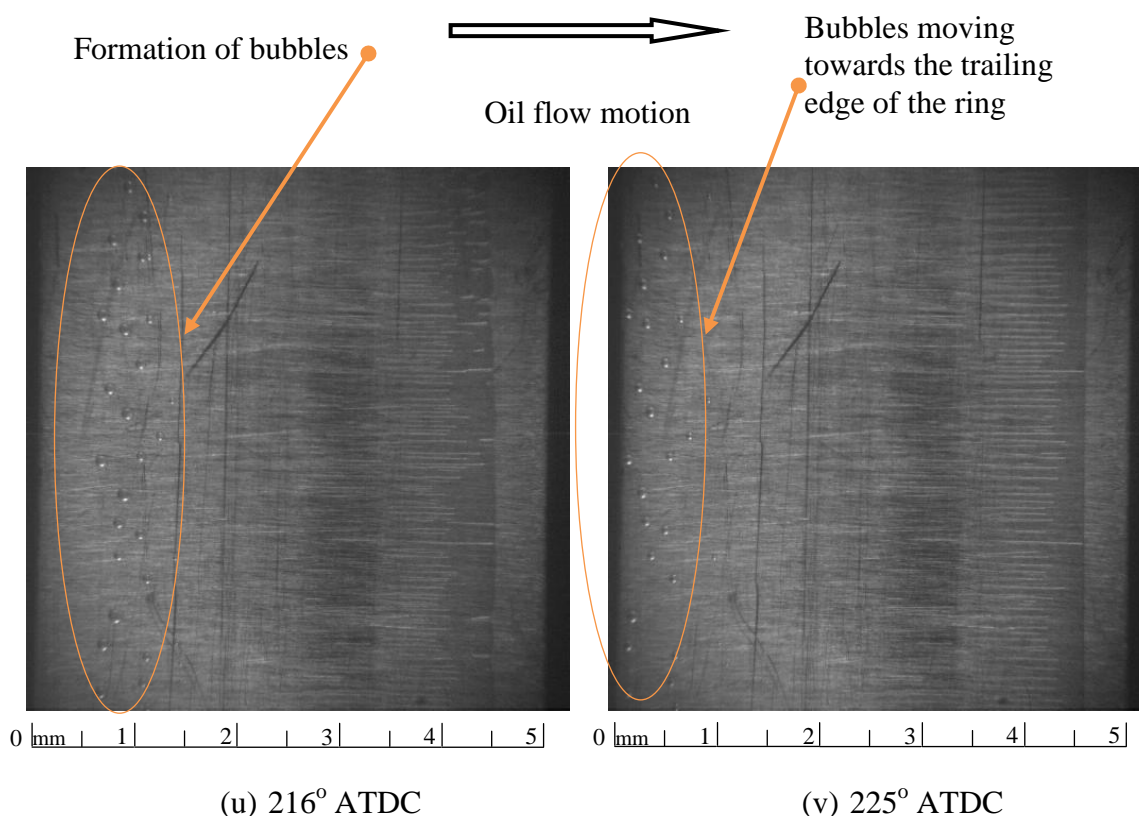


Figure 5.2: High speed video photographs of oil film ruptures at 300 rpm and 977 N/m

To study the influence of entrainment speed and load on cavitation formation, the fast speed camera was used to visualise the inception as well as the subsequent evolution of individual cavities. To explain some particularities of this process, the video film taken has been divided into several individual frames showing the different CA positions (a-v in Figure 5.2). Although it is expected that in each of the selected positions the pressure curve has a negative region in the divergent part of the conjunction (see Figure 5.4), it can be argued that cavitation does not start simultaneously in the entire area. It starts separately in several nucleation sites (Figure 5.2(a)) where it is believed that sub-micrometer scale features on either side of the conjunction lead to localised improved cavitation conditions. From these initial nucleation sites, the cavitation spreads rapidly in a fractal-like structure. Kim *et al.* (1995) and Dellis and Arcoumanis (2004) used a still frame camera to visualise the cavitation development between an optical liner and a ring specimen. They observed these structures and called them “fern cavities” and this term is used herein. The initial ferns extend rapidly and coalesce (22-32° CA in Figure

5.2) over the entire cavitation area, generating finger like structures known as “fissure cavities” (34-54° CA). The fissures are quickly replaced by the more stable structures known as “string cavities” (64-90° CA); later on these string cavities gradually decrease in length (90-180° CA) and are very similar with the ones encountered in journal bearing cavitation (Coyne and Elrod, 1970b; Dowson *et al.*, 1980; Hahn, 1957; Savage, 1977; Sawicki and Rao, 2004). The main difference is that in the current conditions, due to the highly transient reciprocal motion, these strings are short lived. Finally, as the flow reverses, the string cavities disintegrate and break down into bubbles which are released in the oil towards the trailing edge of the downstroke motion (200-225° CA). These bubbles could potentially become particularly hazardous for a combustion engine, as they tend to “foam” the oil and reduce the efficiency of the oil circulation. In engineering applications, to avoid this foam, oil is doped with specific anti-foam additives. It is hoped that a fundamental understanding of the mechanisms governing cavitation formation could ultimately contribute towards eliminating the need of such additives. It should be noted that similar cavitation patterns are observed in the upstroke motion of the liner.

The advantage of using a high speed camera technique is well demonstrated in Figure 5.2 (b)-(g) which reveals the transition between the initial “ferns” towards the later “fissures”. Figure 5.2 (a) shows that the initial nucleation sites were located in the lower side of the viewing window. Therefore, in this section of the contact the ferns developed earlier in the cycle. Consequently, the transition towards fissures also started earlier in this area. Meanwhile, the upper side of the viewing window was still dominated by the ferns cavitation. Considering that the cavitation area has an important role in the load carrying capacity of the contact, uneven development of cavitation generates uneven distribution of the load. This can slightly tilt the ring and induce an even greater difference in the cavitation development in different the zones of the contact.

Kim *et al.*(1995) and Dellis and Arcoumanis (2004) classified the cavities as they form in different periods/stages (described in section 2.3). Herein the above observations can be divided in to the stages following:

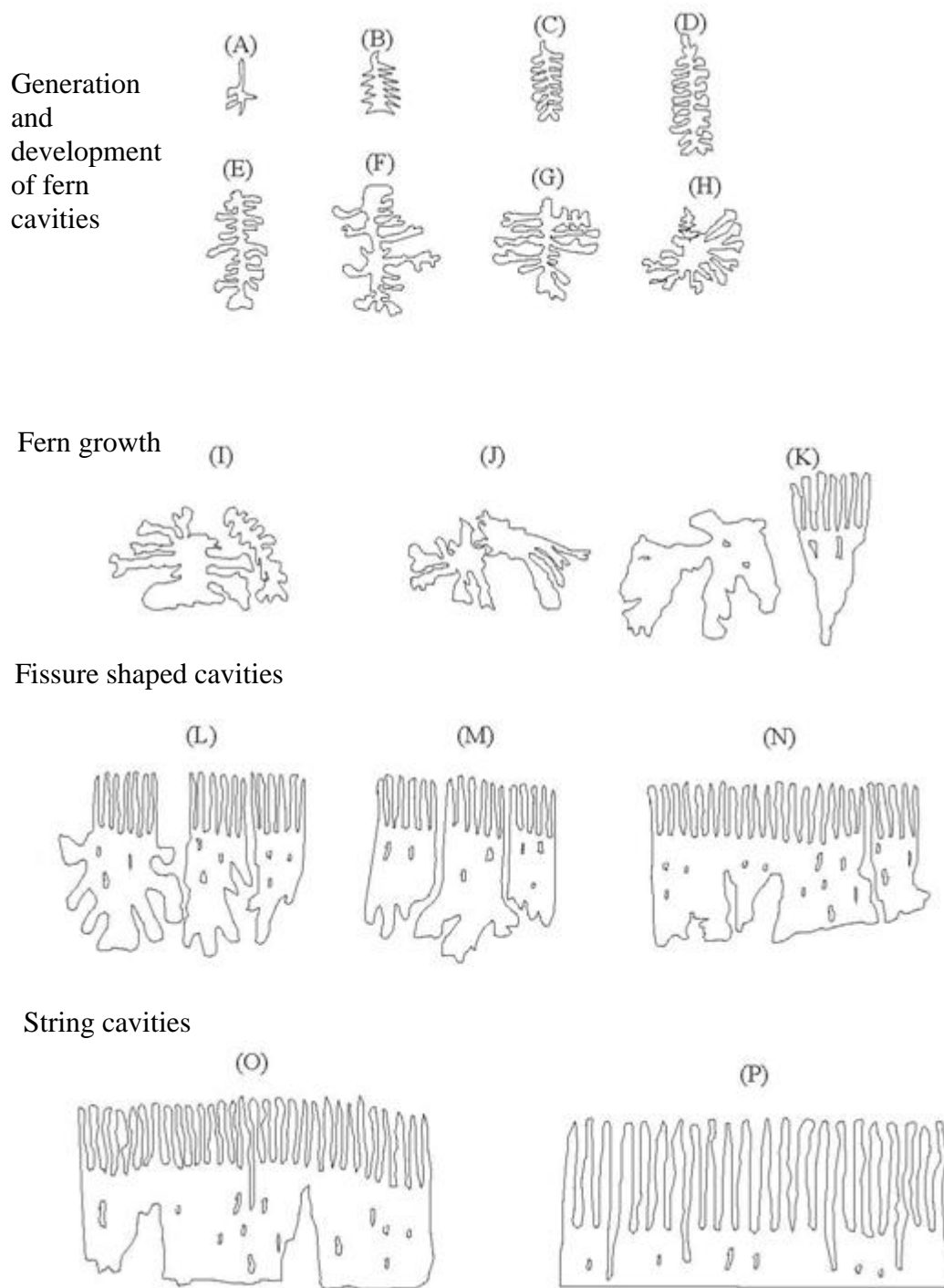


Figure 5.3: Development of cavities as they appear on the surface on the ring

Stage 1: generation and development. Small cavities, fern shape like, start to appear on the diverging surface of the specimen ring; their onset occurs at around 17°-30° CA depending on the operating conditions (Figure 5.3 (A) to (H)).

Stage 2: fern growth. The fern cavities grow in size, coalesce and eventually turn into fissure-shaped cavities (Figure 5.3 (I) to (K)).

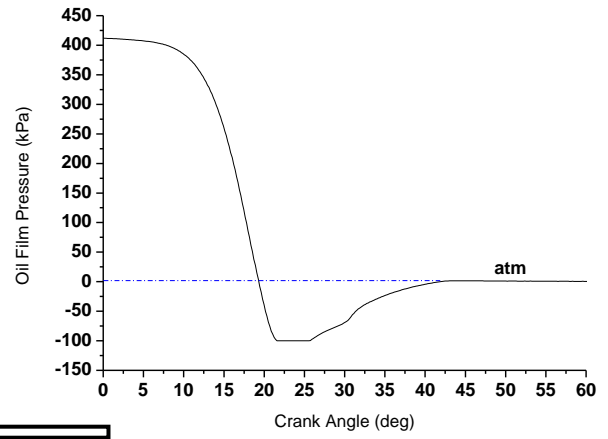
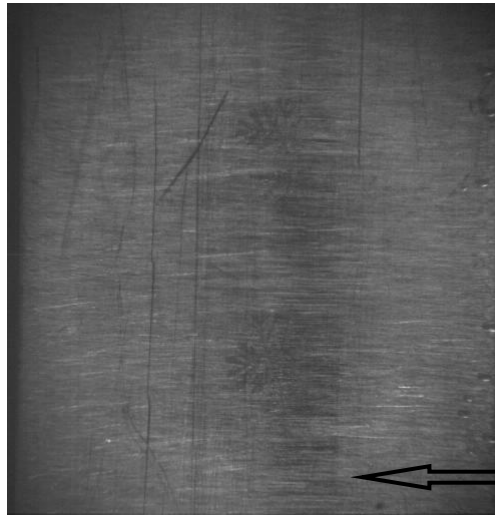
Stage 3: fissure shaped cavities. These structures spread over the diverging part of the ring and finally develop into string cavities (Figure 5.3 (L) to (M)).

Stage 4: string cavities. The string shaped cavities grow further towards the trailing edge of the ring until they reach a stable period (Figure 5.3 (O) and (P)).

Stage 5: decay and bubbles. As the liner reaches the dead centre and its velocity decreases, the string cavities decrease in length and decay towards the downstream side until they finally disintegrate into bubbles.

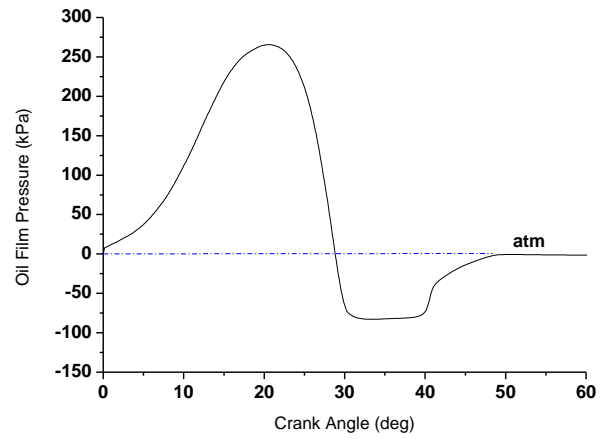
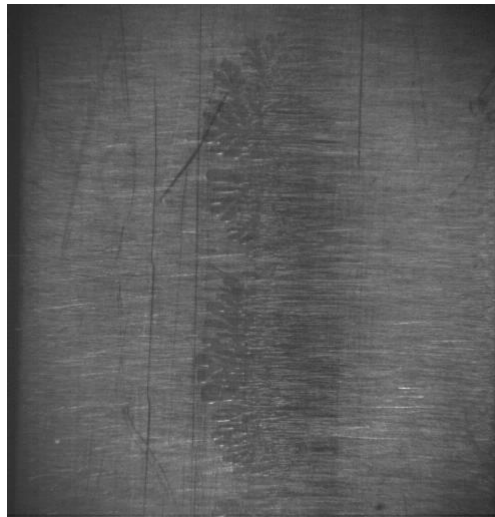
5.1.2 VISUALISATION OF CAVITIES AND OIL FILM PRESSURE DISTRIBUTION

Figure 5.4 depicts the oil film pressure distribution together with photographs of the oil film at the development stage of the cavities (the pressure readings are obtained separately at around the locations presented in Figure 5.4 where the data were acquired at the corresponding crank angle of the images by moving the liner sideways. This was achieved by moving the liner $\pm 0.5\text{mm}$ where the pressure trace was acquired for that space). The cavitation region is characterised by a significant drop in the lubricant pressures below the ambient atmospheric pressure and a consequent collapse of the intervening fluid film. In the contact between the glass and the ring specimen there is a region (in the diverging side of the contact) where the lower pressure encourages the formation of cavities. The decay stage occurs rapidly as the flow reaches the trailing edge of the ring (160°-180° CA) and is exposed to opening to atmospheric conditions as depicted in Figure 5.4(e).

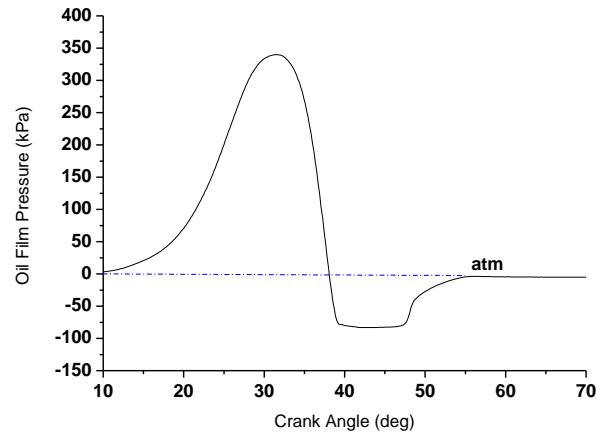
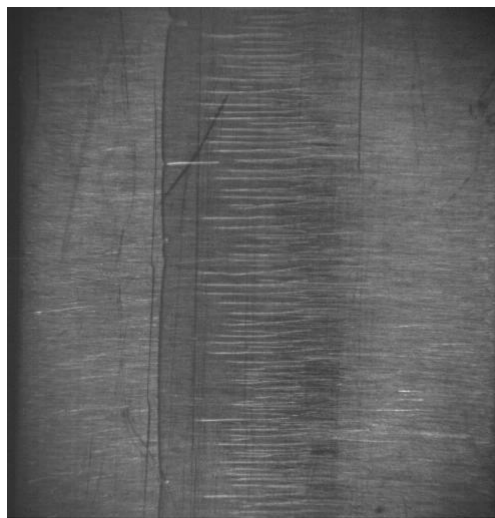


Flow entrainment

(a) 22⁰ CA



(b) 30⁰ CA



(c) 46⁰ CA

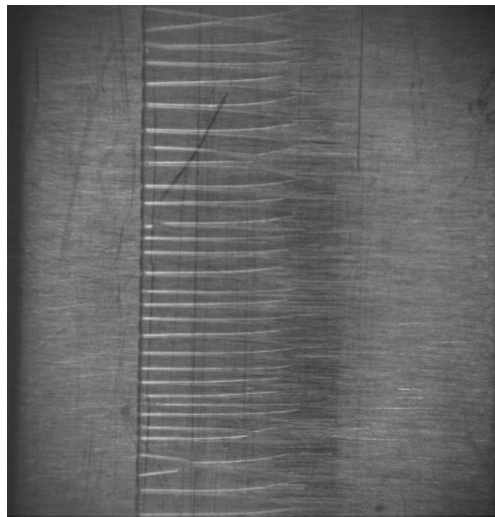
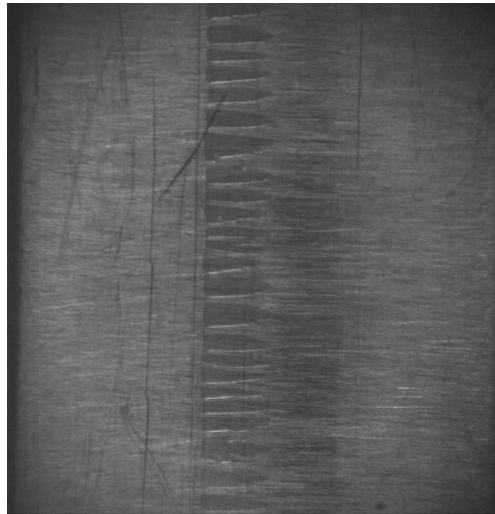
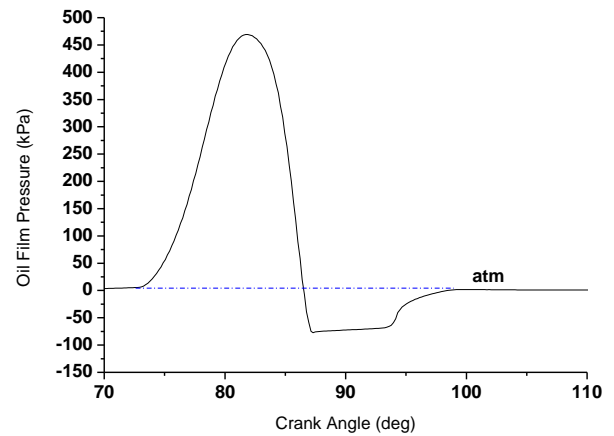
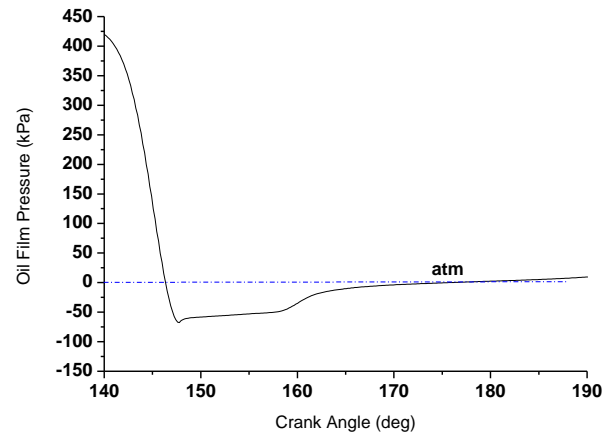
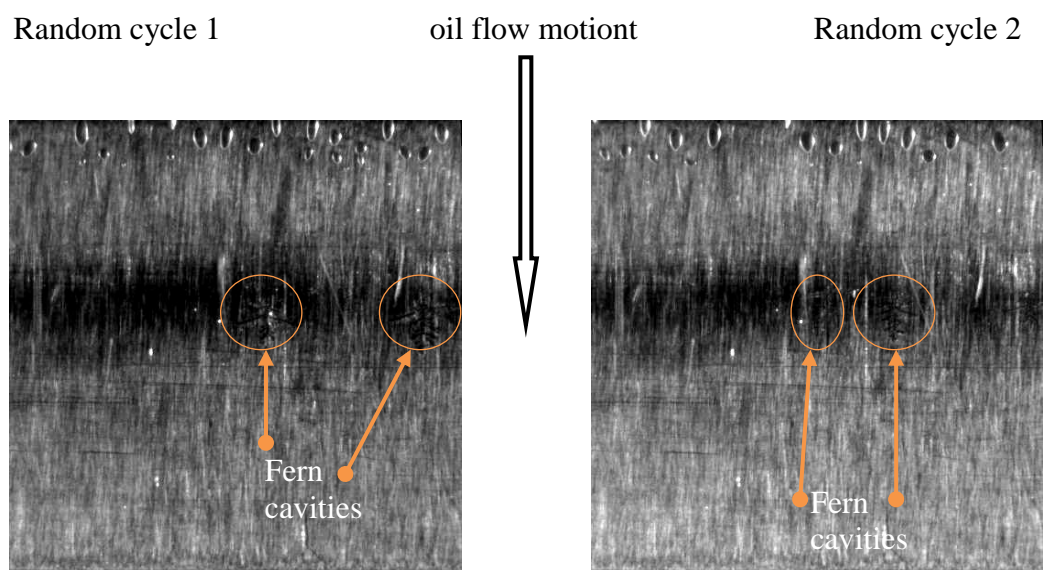
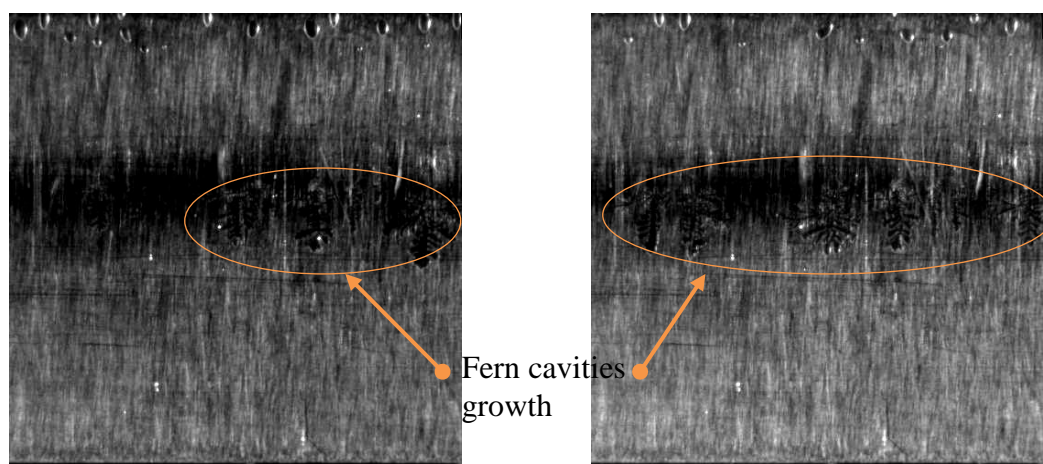
(d) 90⁰ CA(e) 180⁰ CA

Figure 5.4: Development of internal cavities and corresponding pressure measurements at 300 rpm

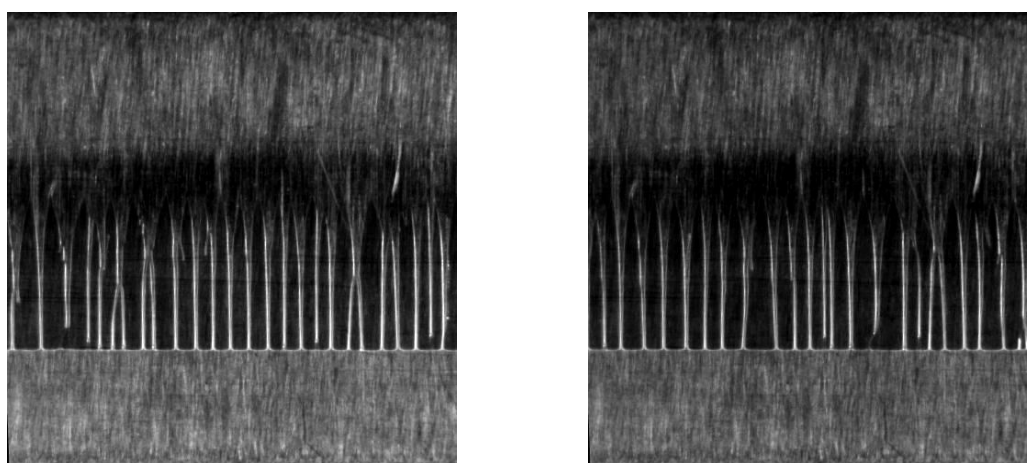
It was observed that the shape of the cavity strings is consistent over a large number of cycles; however, their exact location along the ring profile cannot be accurately predicted. Figure 5.5 shows images taken with the still CCD camera where shots were taken at a particular fixed CA in random cycles. It can be seen in the following images from two random cycles, for example in Figure 5.5 (a), that the generation of cavities occurs at different location within the diverging section of the ring. The same can be seen in subsequent frames (Figure 5.5 b-c) although, the cavitation structures look similar.



(a) 22° CA – fern cavities initiating at different locations



(b) 26° CA



(c) 88° CA

Figure 5.5: Still imaging at random cycles

Therefore, it is reasonable to expect that in successive tests, the laser beam for the LIF tests measures the film thickness either within one of the empty areas of the cavity or in the thicker string between two cavities (see schematic in Figure 5.7). As depicted by the LIF trace in Figure 5.6 possibilities are:

- (i) In the space between the string cavities most of the time
- (ii) Mixed: oil film and cavities
- (iii) In the cavities from the beginning

The LIF measurements can predict the location of the cavities to some extent and also provide further evidence that these structures do not occur at the same position from cycle to cycle variation.

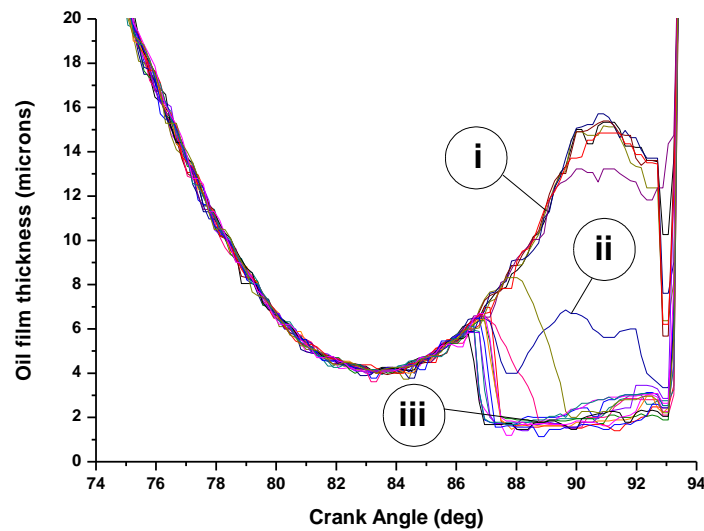
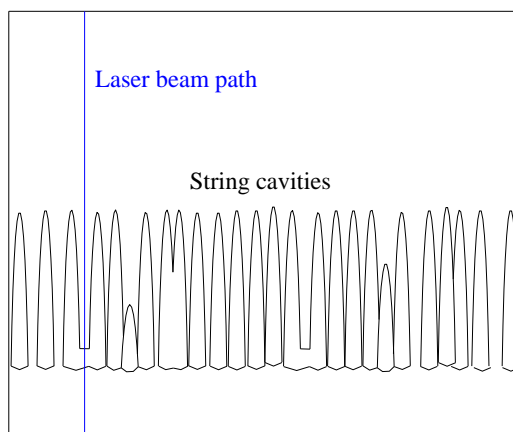
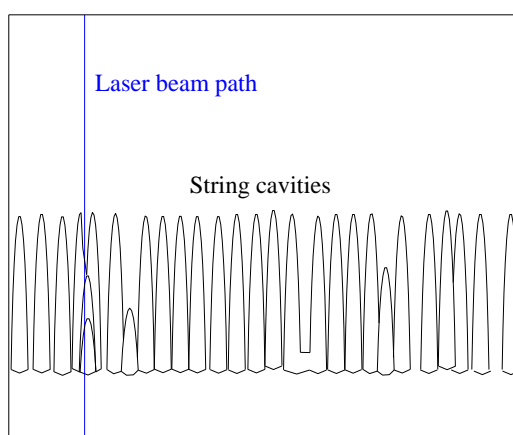


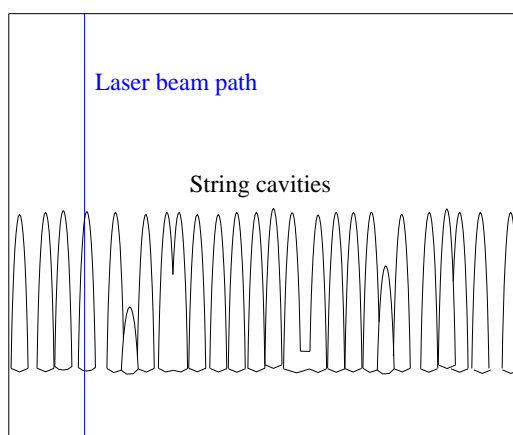
Figure 5.6: LIF measurements over 20 cycles at 300 rpm



(i) In the space between the string cavities most of the time



(ii) Mixed: oil film and cavities



(iii) In the cavities from the beginning

Figure 5.7: Laser beam path with respect to string cavities at random cycles

5.1.3 LOAD AND SPEED TESTS

Different speeds and loads were employed during the visualisation experiments to investigate whether they have any effect on the cavitation structures and patterns. It has been observed that the higher the load is, the sooner in the stroke the fern cavities appear and the smaller their size is. One possible explanation for this behaviour is linked to the squeezing action of the film which increases with load and, hence, influences the oil surface tension (Floberg, 1973). On the contrary, the higher the speed is, the later in the stroke the cavities appear and the bigger their size is. These current findings seem to be in agreement with the works carried out by Coyne and Elrod (1970b), Kim *et al.* (1995) and Dellis and Arcoumanis (2004). Figure 5.8 illustrates the timing (CA) of the initiation of fern cavities in the downstroke direction with load and speed. These are an average readings based on eight observations.

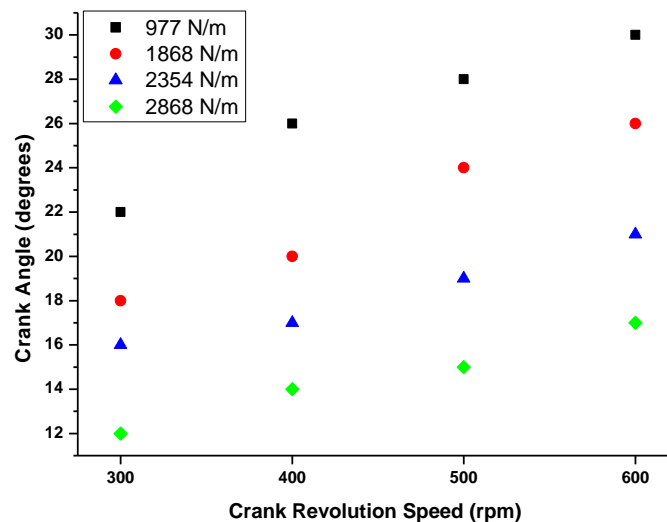


Figure 5.8: Initiation of fern cavities for different loads and speeds

Figure 5.9 presents an estimate of the number of string cavities per mm encountered at mid-stroke, where they are in a stable condition, plotted against the reciprocating speed. It indicates that the load and speed do influence the number of string cavities quite considerably. At higher loads the number of string cavities increases and the width of the string decreases. On the other hand, at higher speeds the number of string cavities decreases and the width of the string increases. In an investigation carried out by Hamilton *et al.* (1966a) in a liquid-lubricated face seals, the authors found that the

number of striations or streamers (string cavities) increases when the applied load increases. Other studies published by Coyne and Elrod (1970b), Floberg (1973), Pitts and Greiller (1961) and Taylor (1963) have also concluded that both load and speed have an influence on the number of string cavities. Floberg (1965) developed a cavitation theory relating tensile strength of a liquid lubricant to the number of streamers (string cavities) which was later verified by experiments. During the film visualisation it has been observed that the flow entrainment lags behind the mechanical movement of the sliding liner and was more evident during the load effect. This also explains the shift in the oil film thickness measurements in Chapter 4 where the maximum OFT occurred after mid-stroke.

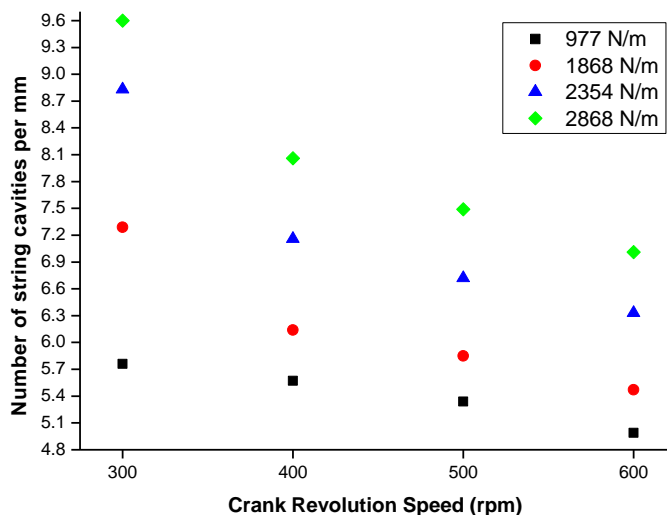
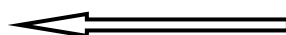


Figure 5.9: The number of string cavities per mm at mid-stroke

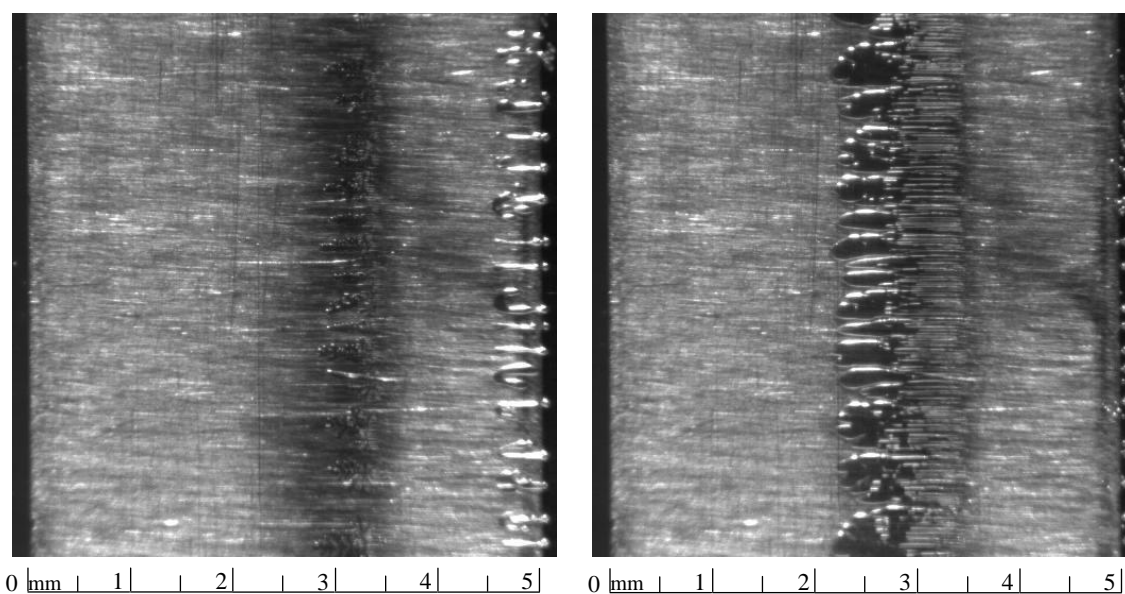
5.1.4 CAVITATION IN MONOGRADE MARINE ENGINE OILS

A parametric study on oil film visualisation in monograde marine lubricants was carried out in order to distinguish whether these oils have a different cavitating pattern compare to the baseline oil 2A. Moreover, testing different types of base oil would allow identifying whether the cavitation structures described earlier are lubricant specific. Three marine oils were employed, oil 001A, oil AW004 and oil 097A, with oil AW004 and oil 097A having the lowest and highest viscosity, respectively (properties in Table 4.3). Compared to baseline oil 2A previously used, the marine oils viscosity is around

two times higher. The stroke for this experiment was set at 22 mm and a temperature around 38-40⁰ C was maintained. Images of cavitation incipience were taken using the high speed video camera as in the previous experiments (Section 5.1.1). Similar cavitation development and patterns to those found previously in oil 2A were again discovered in these three oils as shown in Figure 5.10 despite having different blends. The only differences that have been observed in the marine oils, for the same operating conditions their cavitation fern structures are smaller, they occur much earlier in the stroke and are greater in numbers than those found in oil 2A (see Figure 5.10(a)). The development of cavities for oil 001A, oil AW004 and oil 097A can also be classified into five stages as described above in section 5.1.1. However, the decay period occurs differently. Just after the stable stage, the flow suddenly detaches towards the trailing edge of the specimen ring (Figure 5.10(e)), where about three to five string cavities merge together (Figure 5.10(f)) forming a lump type structure before gradually disintegrating into ligaments and then break down into droplets/ bubbles (Figure 5.10(g – j)).

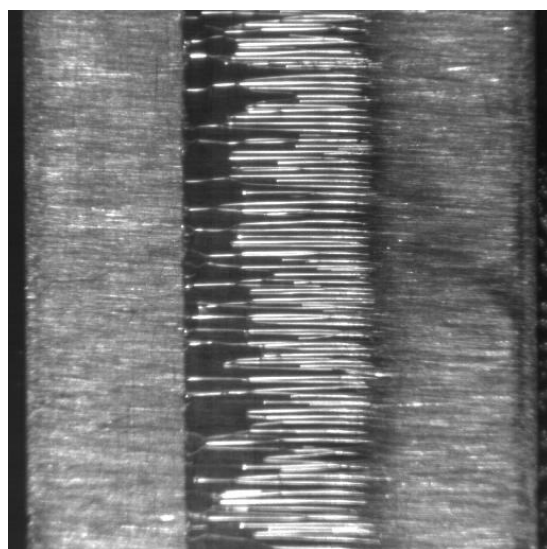


Oil flow motion

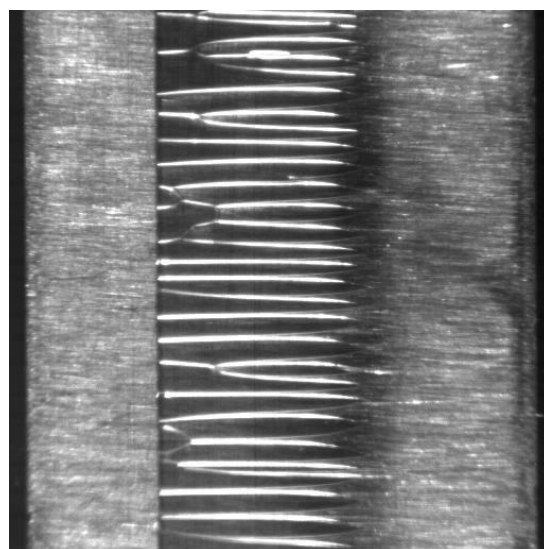


(a) 12° ATDC

(b) 22° ATDC



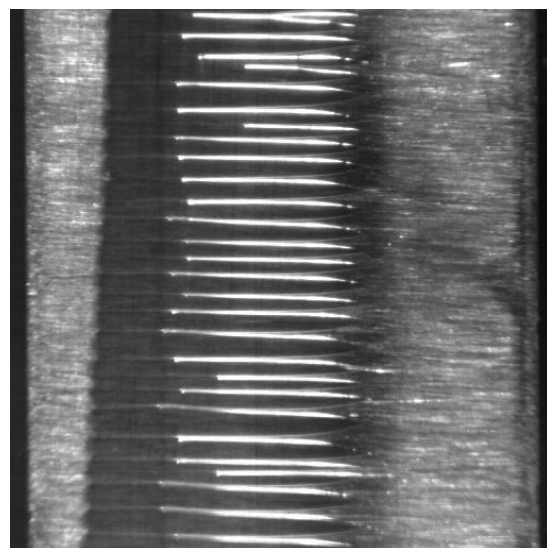
(c) 42° ATDC



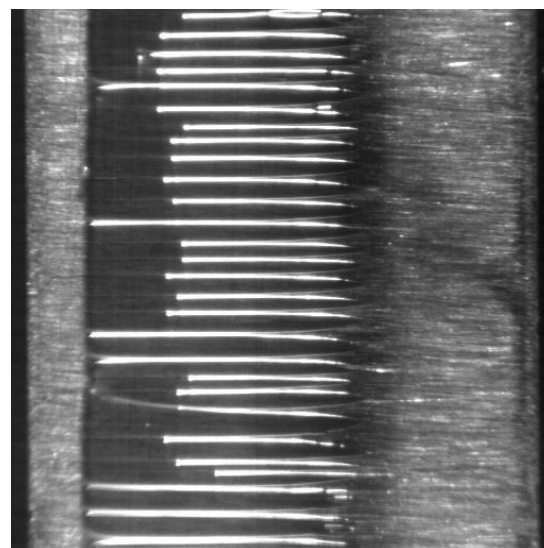
(d) 118° ATDC



Oil flow motion



(e) 126° ATDC



(f) 150° ATDC

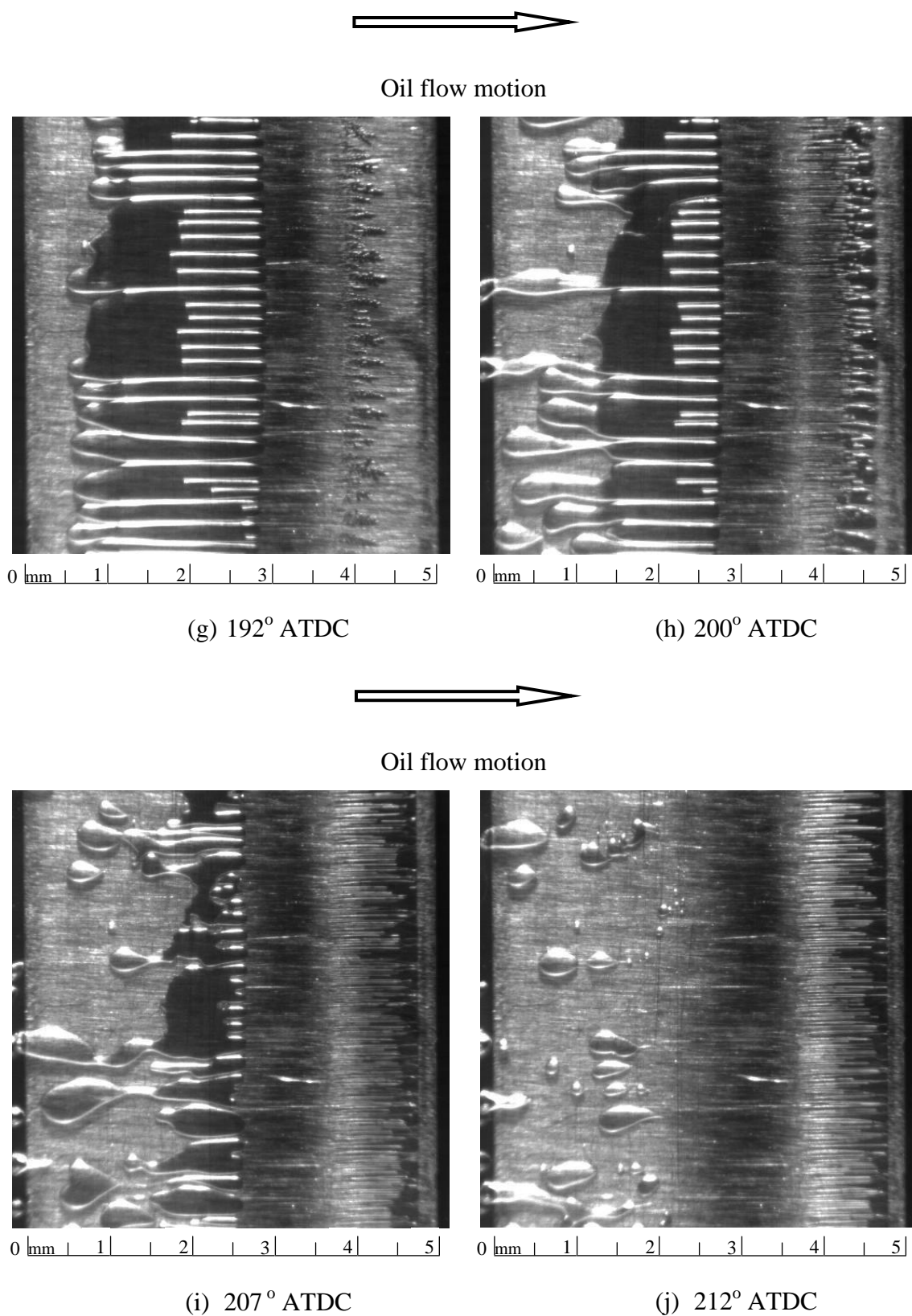


Figure 5.10: High speed video images of film rupture for oil 001A

The marine oils are compared with each other in terms of cavitation development and formed cavity string numbers and sizes. The fern shapes in oil 001A and oil AW004 were found to originate around the same crank angle in the stroke but the number of fern shapes was less in oil AW004. On the other hand, in the case of oil 097A the ferns were found to develop later in the stroke, to be larger in size and less in numbers compared to oil AW004.

Figure 5.11 depicts their differences in fern shape numbers and sizes. Figure 5.12 shows the development of cavitation strings along the stroke for the three marine oils. Their number and size of the strings were obtained by an image processing tool developed in MatLab; the results are based on an average of eight cycles. Oil AW004 with the lowest viscosity has fewer string cavities of wider size. It can be seen in the more viscous oil that the number of string cavities increases and their width decreases. It should be noted here that the three marine oils have different blend themselves. Although it is well known that viscosity plays an important role in the way a fluid cavitates (Brennen, 1995; Coyne and Elrod, 1970a; Taylor, 1963), it is believed here that the differences in string numbers and sizes of the oils are mainly attributed to the way they have been formulated.

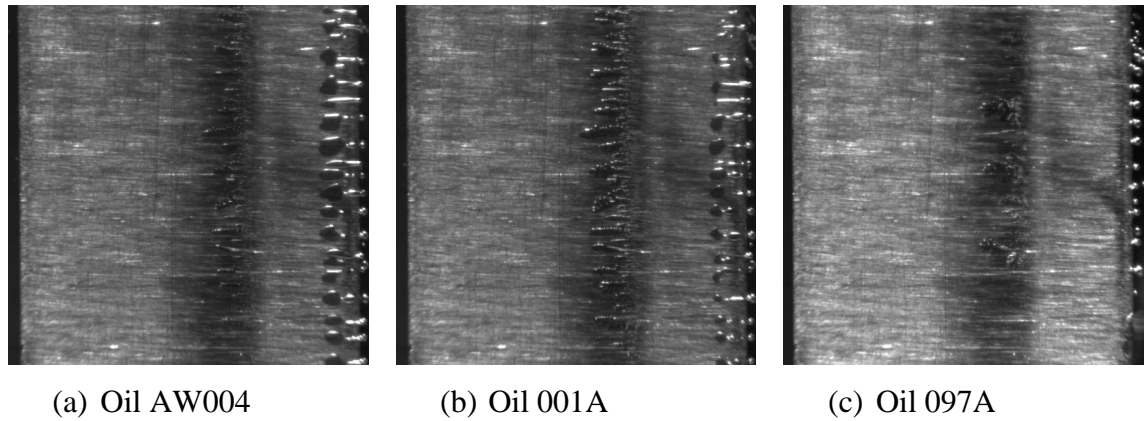


Figure 5.11: Fern shape number and size for marine oils at 600rpm

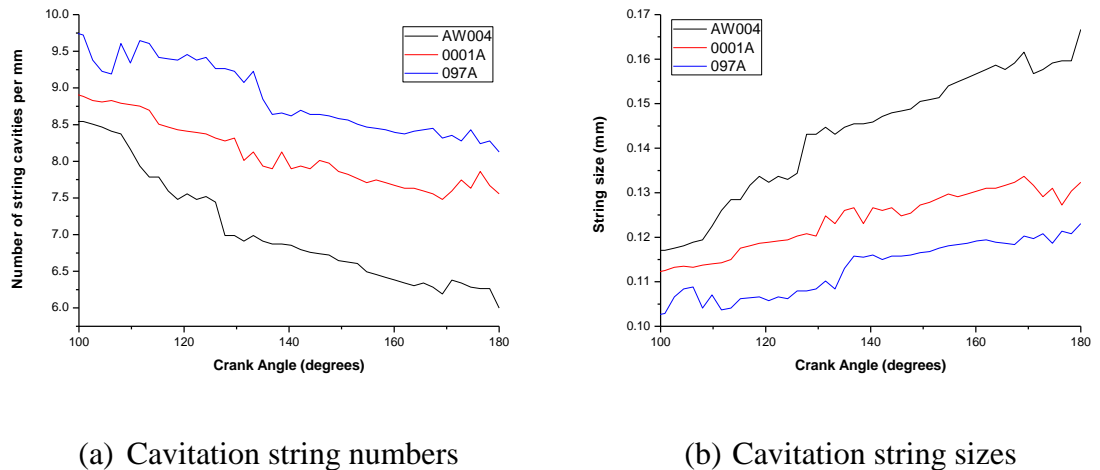
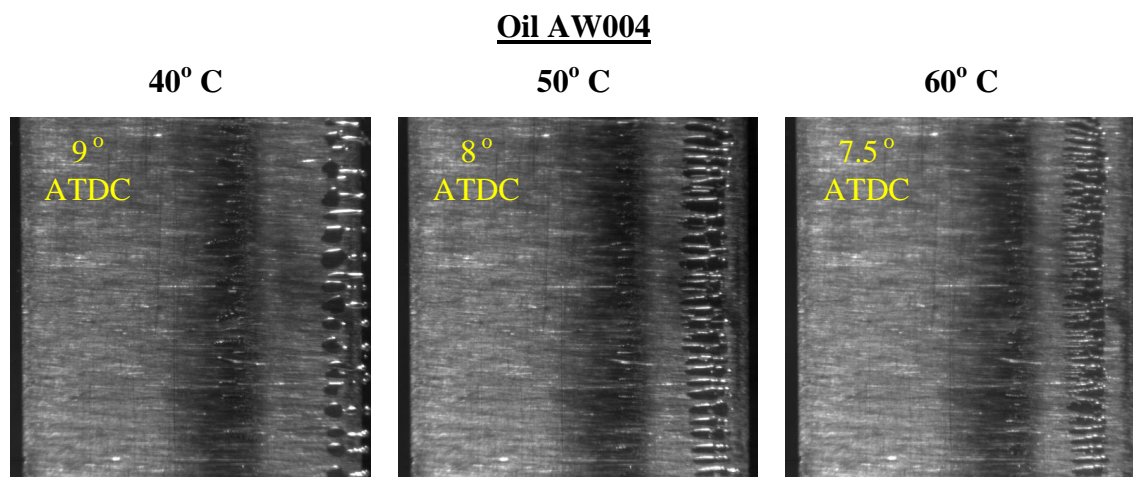
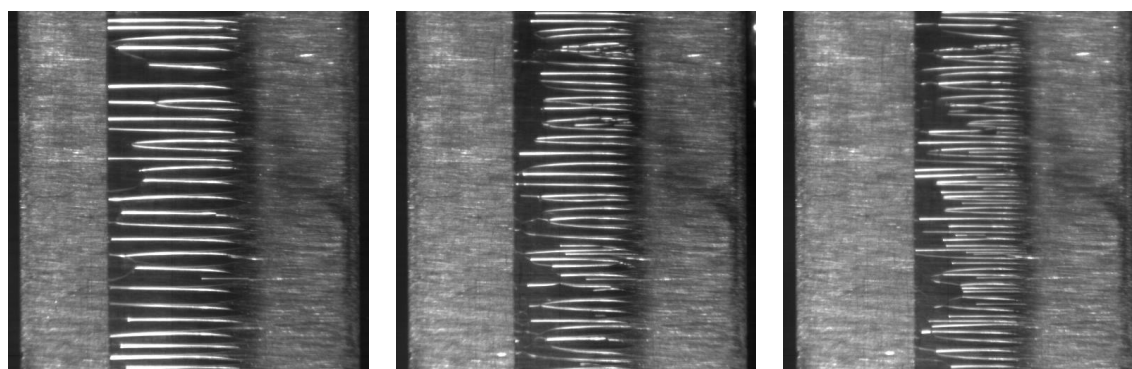


Figure 5.12: Development of cavitation strings along the stroke at 600 rpm

Further investigations on the effect of temperature in these oils have been carried out. It has been noted in all of the lubricants that, as the temperature increases, the cavitation initiates earlier in the stroke. Moreover, as it can be seen in Figure 5.13, Figure 5.14 and Figure 5.15, the number of string cavities increases and their corresponding width decreases with a rise in oil temperature. Figure 5.16 presents a variation of cavitation string numbers versus oil temperature for the three marine lubricants.



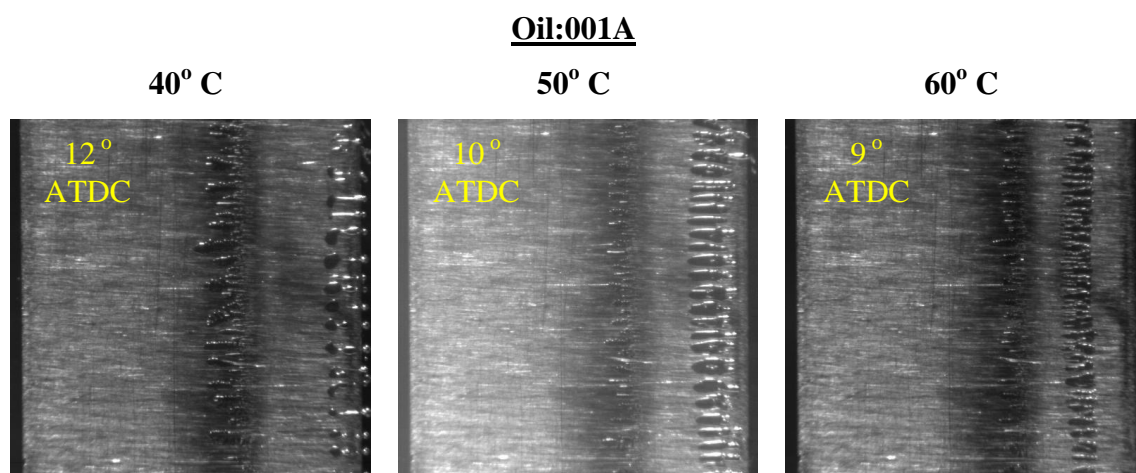
(a) Initiation of fern cavities



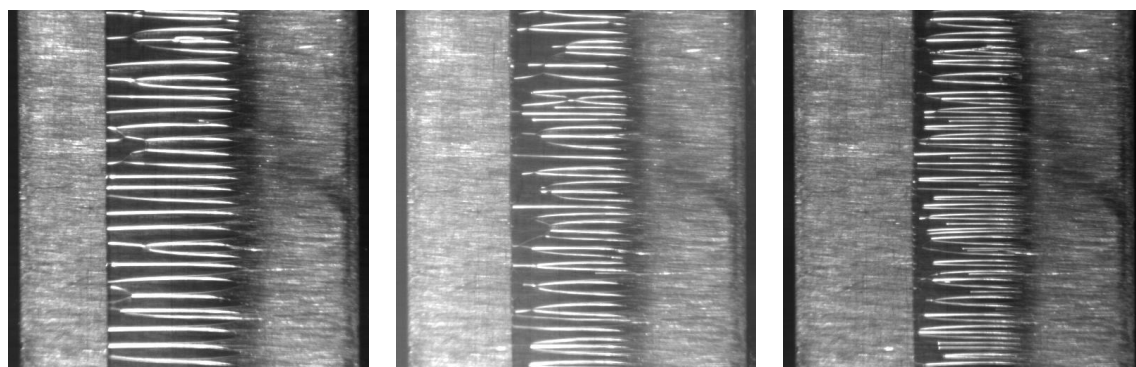
⇨
String cavities increase in numbers and decrease in width

(b) String cavities

Figure 5.13: Temperature effect on oil AW004



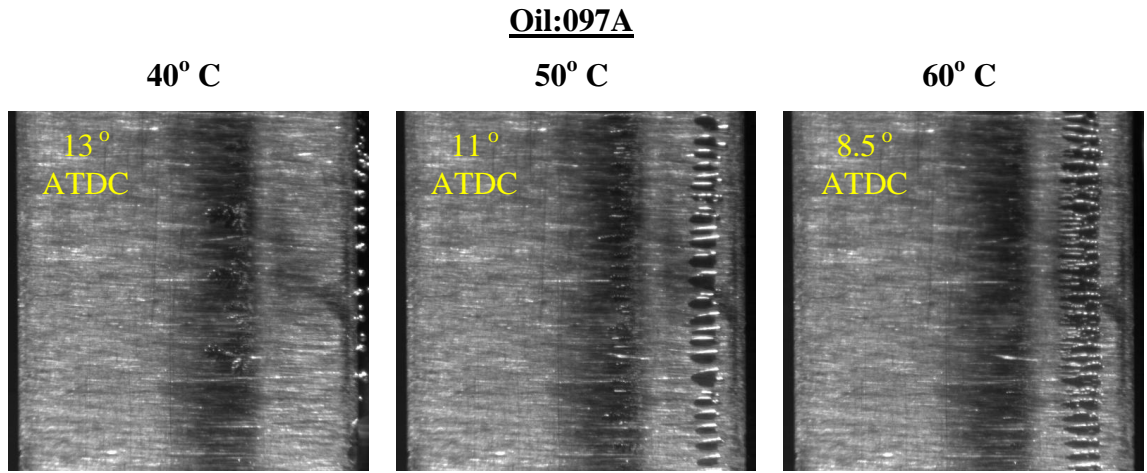
(a) Initiation of fern cavities



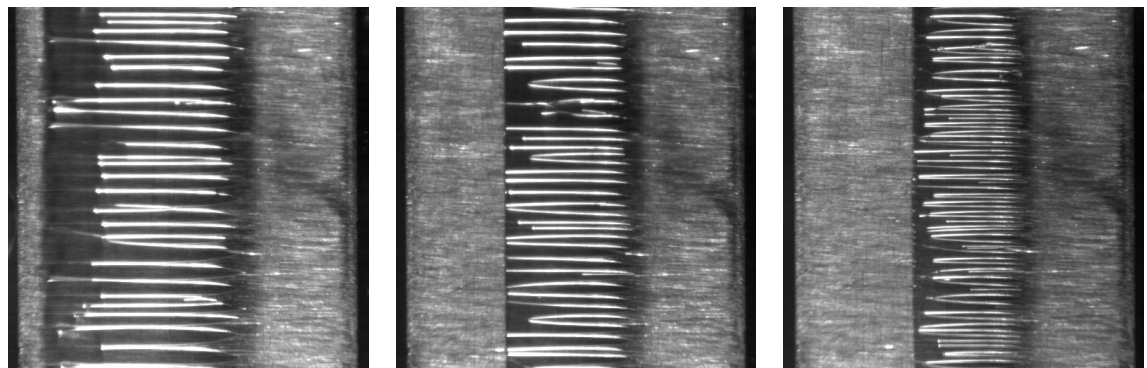
String cavities increase in numbers and decrease in width

(b) String cavities

Figure 5.14: Temperature effect on oil 001A



(c) Initiation of fern cavities




 String cavities increase in numbers and decrease in width

(d) String cavities

Figure 5.15: Temperature effect on oil 097A

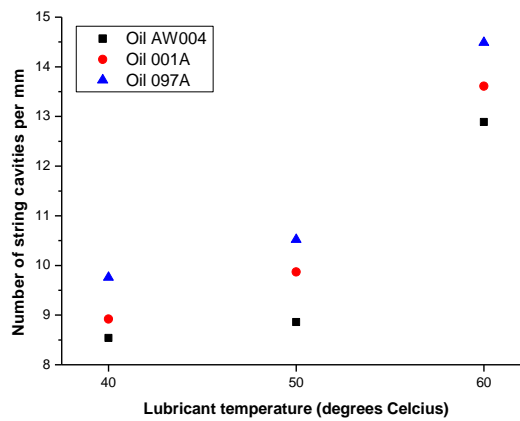


Figure 5.16: Number of string cavities per mm at mid-stroke for marine oils

5.2 DIESEL ENGINE VISUALISATION

Following the visualisation experiments in the idealised test rig, a diesel engine (Lister Petter) has been modified to accommodate similar investigations. These modifications included fitting of quartz windows to provide visual access to the lubrication film characteristics between the piston-rings and cylinder liner and, furthermore, introduce measurement stations at top dead centre, mid-stroke and bottom dead centre for obtaining oil film pressure measurements. The extension of the visualisation investigations to the diesel engine was necessary in order to determine if similar cavitation structures or patterns to those found in the test rig could be identified. An insight into the oil transport mechanisms in piston-rings contributing to oil consumption and some previous works on oil film visualisation are discussed first in order to provide support to the interpretation of the visualisation results in the diesel engine.

5.2.1 OIL CONSUMPTION SOURCES AND OIL TRANSPORT MECHANISMS IN PISTON-RINGS ASSEMBLIES

Oil consumption from the piston-ring assembly system drastically contributes to the total engine oil consumption which is widely recognised to be a major contributor to pollutant emissions in automobile engines. Much of the pertinent information has been examined in section 1.7 during the review of engine on lubricants and emissions. Investigations of engine oil consumption in internal combustion engines have been performed by engine manufacturers and other researchers in relation to with the stringent emissions standards. Some possible oil consumption sources have been suggested to contribute to the total oil consumption of engines (Herbst and Priebisch, 2000; Tian and Wong, 2000; Yilmaz *et al.*, 2004). In particular, Yilmaz and co-workers have classified the oil consumption into the five sources depicted in Figure 5.17.

It has been found experimentally that oil consumption has been associated to the mechanical transport of liquid oil in the combustion chamber due to inertia forces caused by acceleration and deceleration of the piston (Inagaki *et al.*, 1995; Thirouard *et al.*, 1998). Depending on the amount of oil accumulated on the piston's top land, this may be thrown off (Figure 5.17a) directly into the combustion chamber due to these inertia forces.

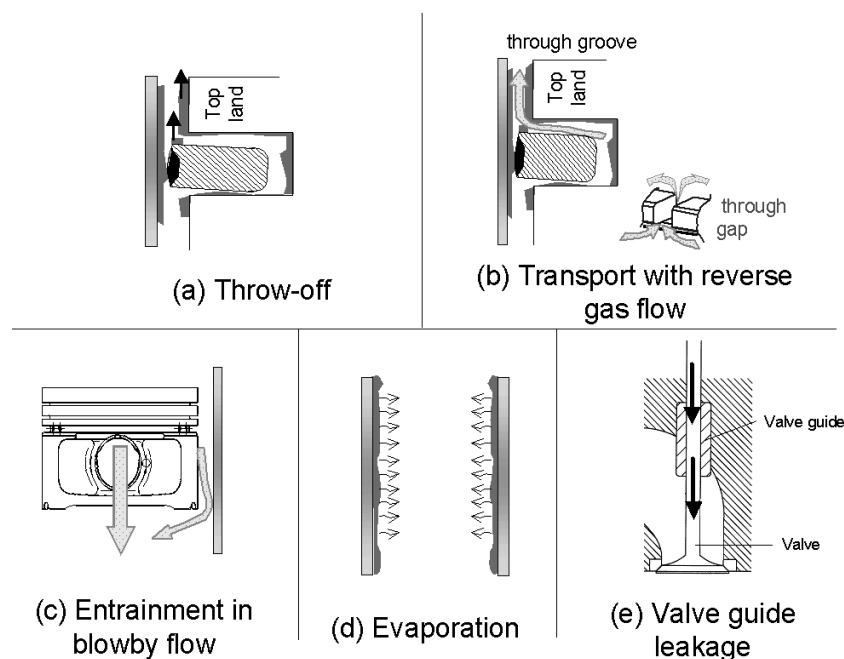


Figure 5.17: Schematic of oil consumption sources (Yilmaz *et al.*, 2004)

Nakashima *et al.* (1995) have observed that direct oil transport into the combustion chamber relies on gas flow in the piston-ring-liner assembly. Gas pressures in the second land clearance, the volume between the top ring and second ring, can become greater than the combustion chamber pressure during some periods of the engine cycle. This pressure gradient may cause a reverse gas flow into the combustion chamber through the top ring gap and around the top ring groove if the top ring is not tightly fixed into the groove. The reverse gas flow may transport oil in both liquid and mist form into the combustion chamber as illustrated in Figure 5.17b, which can then burn, contributing to the engine-out emissions.

Blowby is the leakage of combustion gases to the engine crankcase through the piston-ring's gaps and crevices or even due to poor sealing caused by worn rings. It normally consists of combustion gases, unburned mixture and lubricating oil in the form of liquid particles and mist (Figure 5.17c). To prevent the emission of pollutants in the blowby gases into the atmosphere, the gases are recycled and fed into the intake manifold system. Studies have confirmed the presence of oil mist in the combustion chamber and this source of oil consumption is observed in specific engines only (Yilmaz *et al.*, 2004).

Several experimental projects (Casey, 1998; Didot *et al.*, 1987; Furuhashi, 1985) have pointed out that oil evaporation from the piston and liner (Figure 5.17d) can make a subsequent contribution to oil consumption especially during harsh operating conditions when the thermal loading of the engine components is high. Oil transport, usually in older spark ignition engines, from the cylinder head through the valve guide into the intake port has contributed significantly to oil consumption during part load conditions, when the intake manifold pressure is sub-atmospheric (Figure 5.17e). However, this source of oil consumption is not considered to be a major contributor to the total oil consumption in today's advanced engines.

Oil transport mechanisms have been studied by a two-dimensional laser-induced fluorescence technique and by a CCD camera in a diesel engine which has been modified to include a quartz window (Thirouard *et al.*, 1998). The system has enabled studies on the oil distribution on piston surfaces and between the rings and the liner. Oil accumulation on the crown land has been investigated by authors from the MIT Lubrication Research Group and observed that the accumulation of oil was most probably caused by the top-ring up-scraping. Two oil flow mechanisms were observed on the second land:

- (a) oil flow by inertia in the axial direction and
- (b) oil being dragged by the gas flow in the circumferential direction.

The top ring up-scraping of oil was observed at engine speeds above 1600 r/min. Owing to increased gas pressure, the piston was found to tilt towards the thrust side. The tilting piston and the ring twist caused the ring upper corner to start scraping oil from the liner wall, as there was no hydrodynamic pressure supporting the radial forces; the up-scraped oil was transported to the crown land. A second mechanism of oil transport to the crown land was also observed where oil flows to the crown land whenever there is oil present on the second land (Thirouard *et al.*, 1998).

Thirouard and co-workers further observed that there were three possible mechanisms of oil transport to the second land:

- (1) Oil can be scraped to the second land in the top ring down-scraping (downstroke) or second ring up-scraping (up-stroke); with a tapered profile on the second ring, the up-scraping becomes impossible.

- (2) Oil can flow through the two upper ring grooves; oil flows into the ring groove and is pumped out of it as a result of the radial ring movement in the groove.
- (3) Oil can be carried through the gaps in the ring pack by gases, which flow either towards or from the combustion chamber (Thirouard et al., 1998).

In a more elaborated work, within the same research group, (Thirouard, 2001) a comprehensive oil support scheme showing the main path and mechanisms of the oil transport within the piston ring pack was proposed. It highlighted that the rate at which oil is lost to the combustion chamber results from the competition between the inertia-driven oil transport, which carries oil across the land and through the ring grooves towards the top of the piston, and the gas-driven oil removal, which returns oil to the crankcase. Eventually, a region by region analysis of the piston ring pack indicated that there are three main locations where the rate of oil transport to the combustion chamber can be controlled.

- (1) The oil control ring which determines the oil supply to the third land and the part of the liner located between the scraper ring and the OCR.
- (2) The second ring and its groove where the rate of oil transport from the third to second land can be controlled by detailed geometrical features and/or second ring flutter.
- (3) The second land where the balance between the oil supply and the gas driven oil removal determines the total amount of oil accumulated on the second land and thus, the rate of oil supply to the top ring groove.

Inagaki et al. (1995) used a single-cylinder spark ignition engine to investigate the behaviour and the thickness distribution of a lubricant film between a piston, piston-ring and liner. Clear images of the oil film thickness distribution on the piston skirt, piston land and piston rings were obtained under both firing and motoring conditions. Their results show that the oil spouts from the first ring gap and the oil splashes into the combustion chamber increase with a decrease in the intake manifold pressure. By firing, they are decreased as the stronger blowby gas, which flows through the first ring gap, blow off the lubricants on the second region at the expansion stroke. For speeds greater than 3000 rpm, the oil spouts occur when the piston is in the exhaust stroke.

5.2.2 HIGH SPEED VIDEO IMAGING IN DIESEL ENGINE

The high speed digital video camera, used previously in the idealised test rig, has been employed to visualise the oil film between the piston-rings and the liner in the diesel engine under motoring condition. Oil 2A considered as the baseline in this project was used in the engine throughout the experiments. Figure 5.18 shows the camera viewing window relative to the engine TDC position and its magnified view of the piston ring. A set of visualisation images, depicted in Figure 5.19, show the oil entrainment between the piston and liner during a cycle at an engine speed of 600 rpm. The images are taken at 45 mm from TDC, are magnified 3 times and are at a recording rate of 15000 fps (frames per seconds). At this current viewing position the piston crown land, first compression ring, second compression ring, scraper ring and the third land can be visualised. Figure 5.19 shows the oil displacement that was found at different strokes. The evolution of the oil distribution on the third land of the diesel engine to the scrapper ring are shown in Figure 5.19a and b. Oil accumulated on the second land (Figure 5.19c) is found to be travelling axially, but in the opposite direction of the piston, away from the scrapper ring, and later is entering the converging edge of the second compression ring (Figure 5.19d). During the intake stroke (Figure 5.19e) oil is observed to enter the first compression ring forming a film on the converging part of the ring.

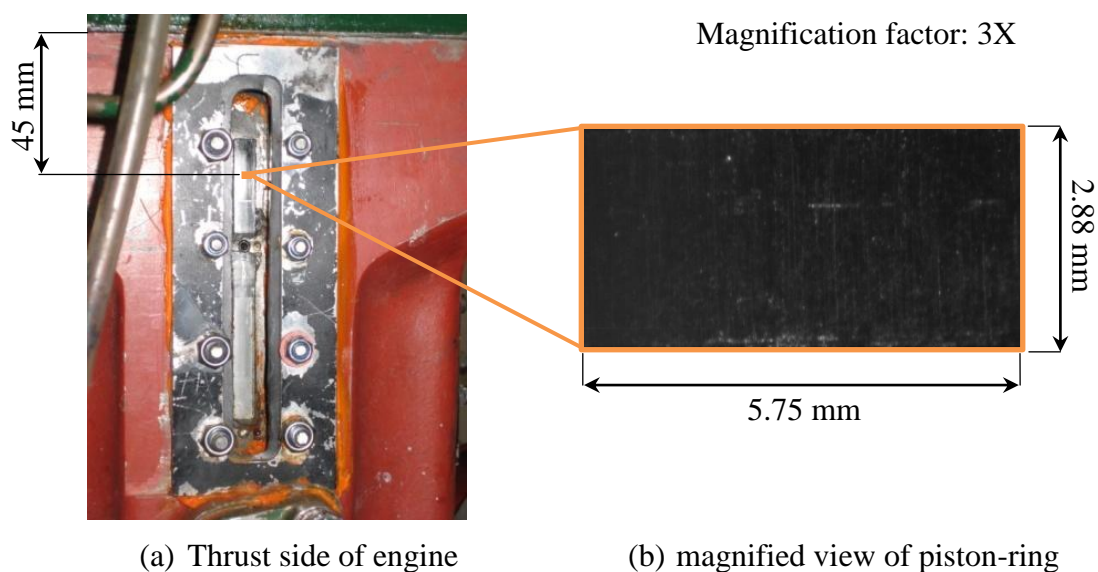
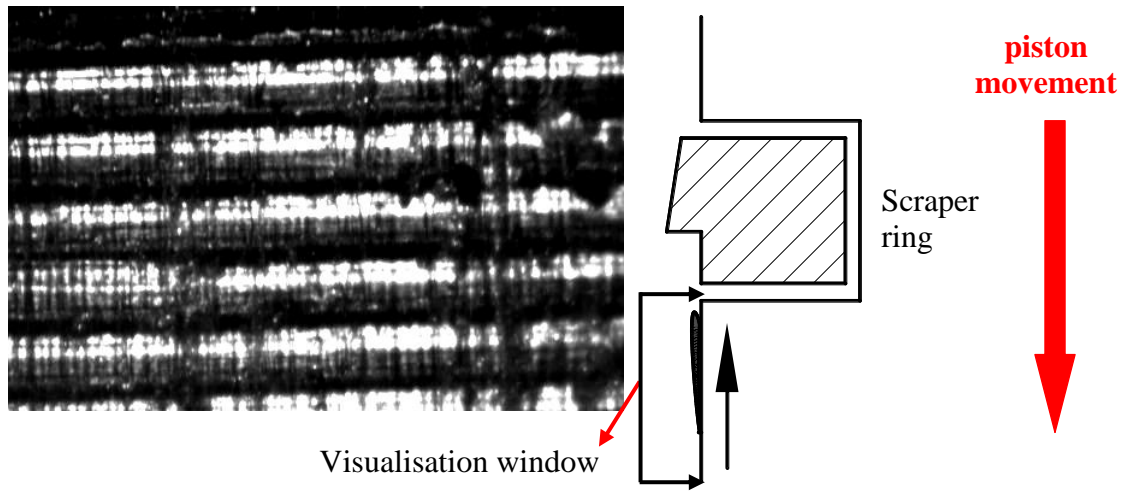
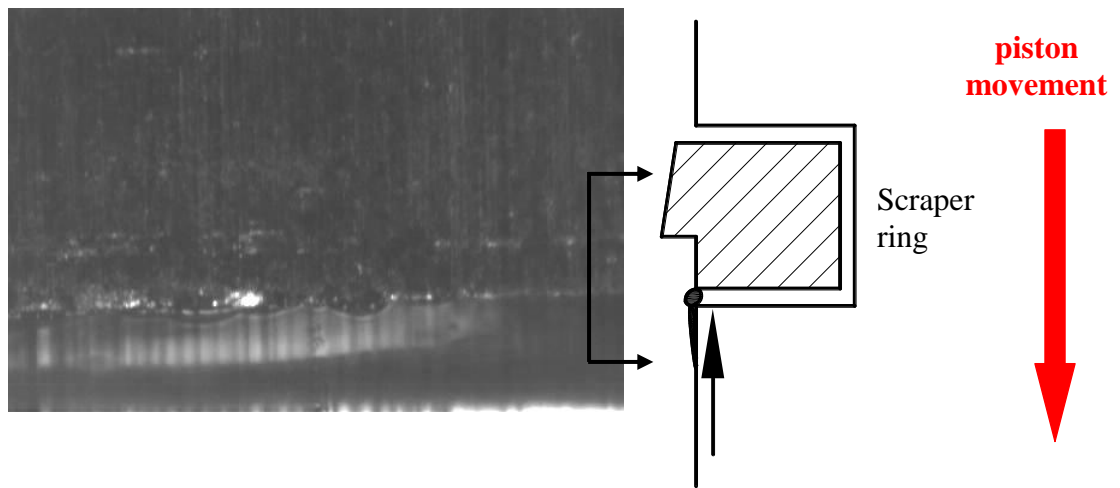


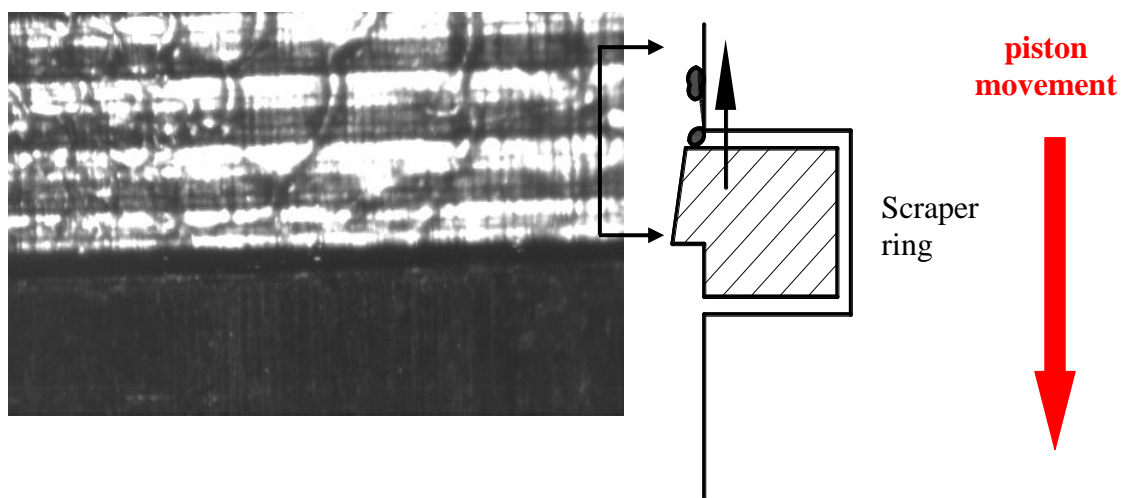
Figure 5.18: High speed video imaging window for diesel engine



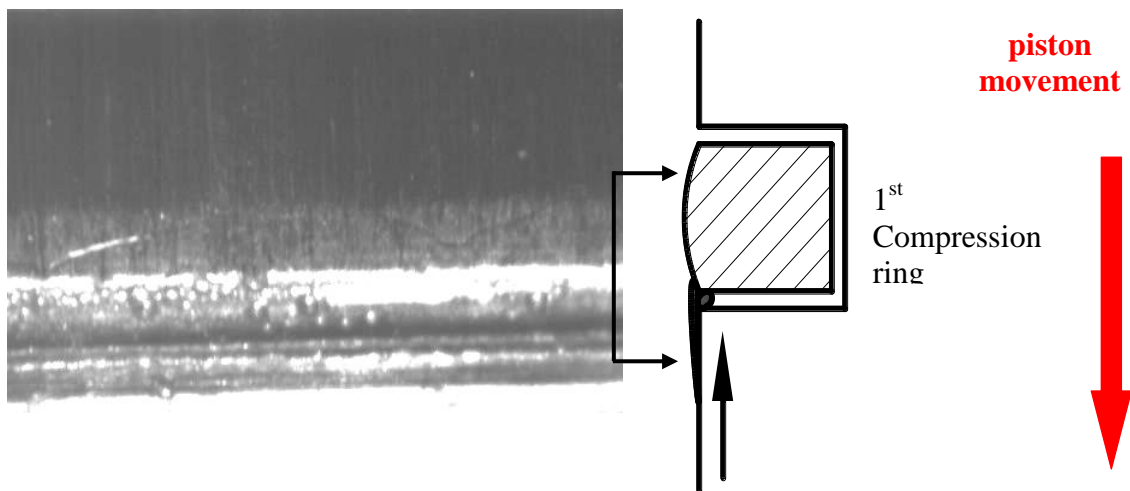
(a) 34° ATDC (intake stroke)



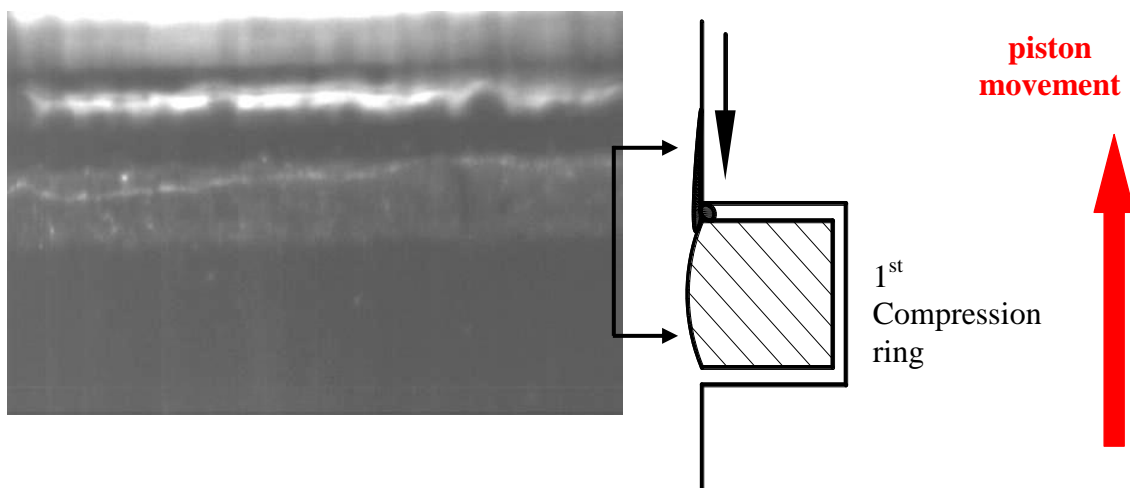
(b) 36° ATDC (intake stroke)



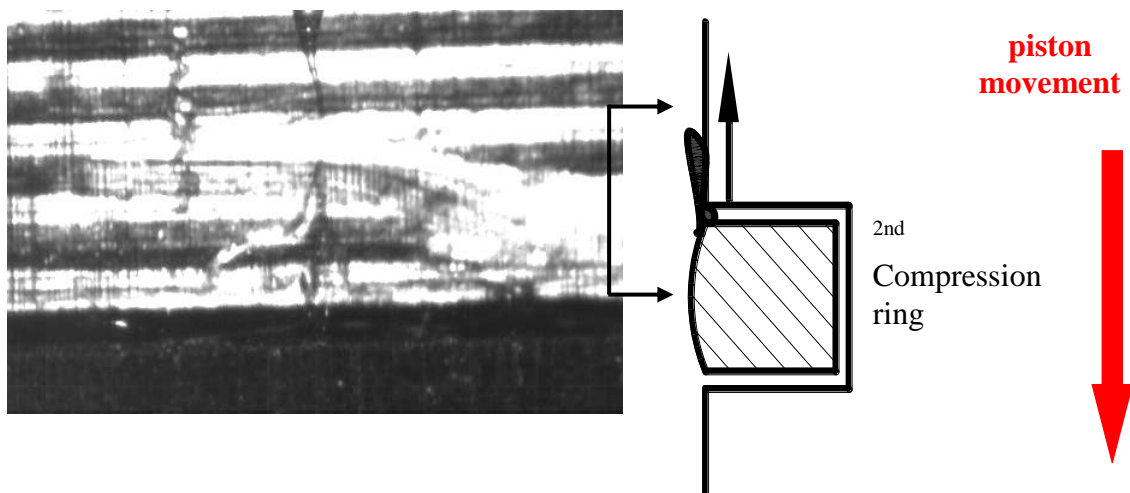
(c) 38° ATDC (intake stroke)



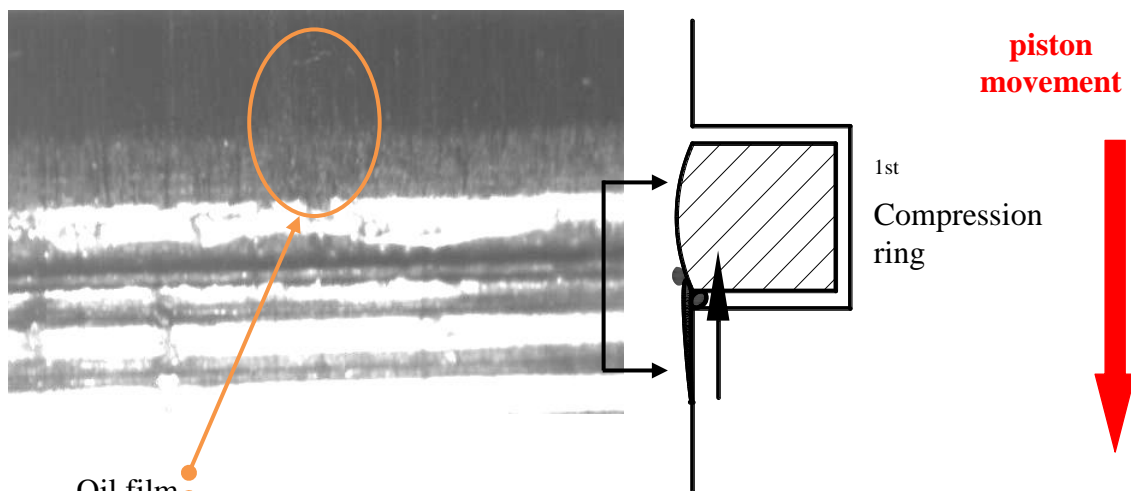
(d) 42° ATDC (intake stroke)



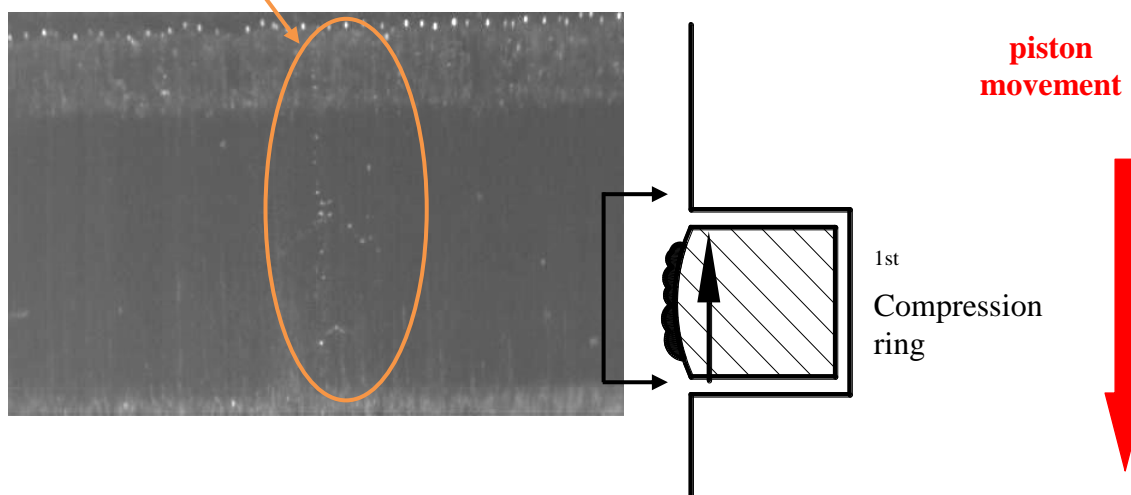
(e) 318° ATDC (compression stroke)



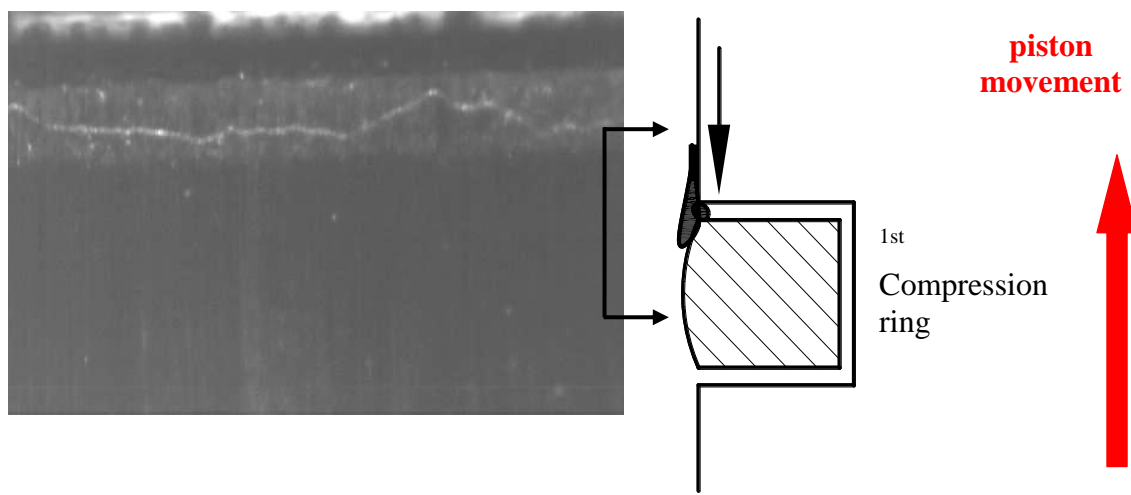
(f) 576° ATDC (expansion stroke)



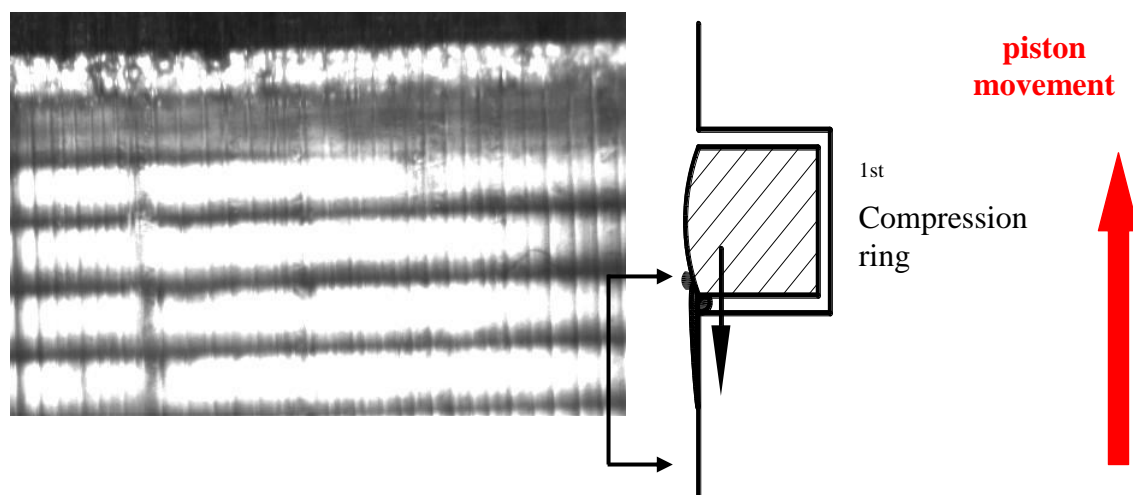
(g) 579° ATDC (expansion stroke)



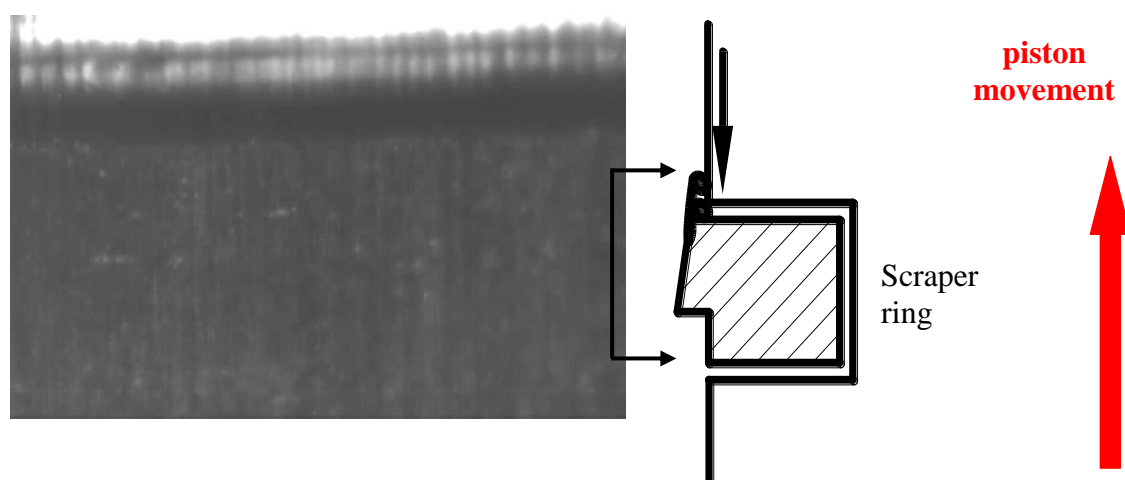
(h) 582° ATDC (expansion stroke)



(i) 678° ATDC (exhaust stroke)



(j) 682° ATDC (exhaust stroke)



(k) 689° ATDC (exhaust stroke)

Figure 5.19: Cycle oil distribution around piston-rings and land at 600 rpm

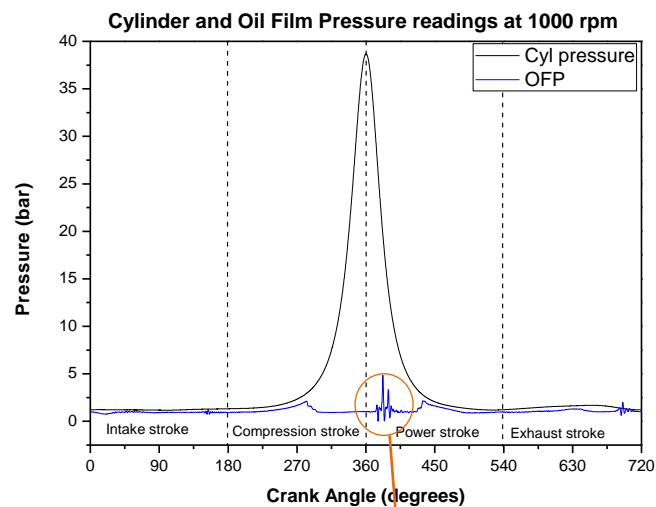
Figure 5.19f (expansion stroke) shows oil and bubbles/oil droplets leaving the second compression ring forming a ligament shaped like that on the first land and travelling towards the first compression ring. Oil is observed to enter and to form a film on the surface of the ring (Figure 5.19g and h). During the exhaust stroke the oil film is also observed to be flowing axially but in the opposite direction to that of the piston. The evolution of the oil film pattern presented in Figure 5.19 is found to be driven by inertia forces resulting from the piston reciprocating motion. Similar behaviour has been observed in the work of Inagaki *et al.* (1995) and Thirourd *et al.* (1998). It should be added that the pattern also depends on the volume of oil available on the piston land.

5.2.3 OIL FILM PRESSURE MEASUREMENTS IN DIESEL ENGINE

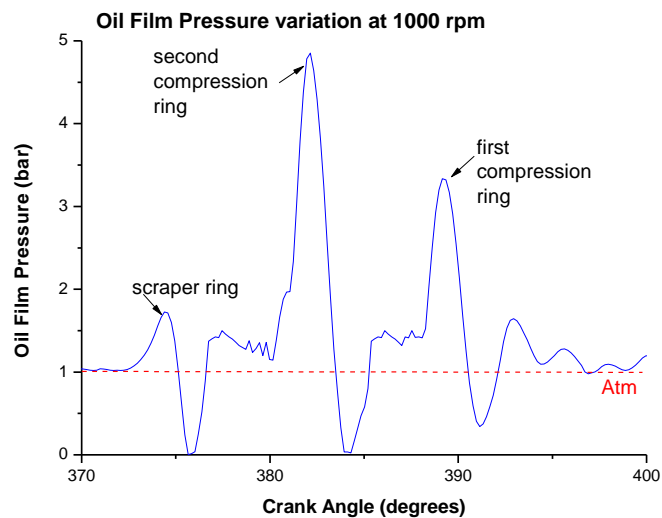
Measurement stations, at TDC, around mid-stroke and BDC, have been installed on the thrust side of the diesel engine to obtain oil film pressure measurements between the piston-rings and liner wall. In the present work the pressure measurements will be used in conjunction with the visualisation experiments to provide supporting evidence for the identification of the cavitation in the oil film. Unfortunately, the only successful pressure readings have been obtained at the mid-stroke station; the other two spark eroded holes, made for the pressure transducer, seem to have been blocked unintentionally. Although at the engine's mid-stroke location it is not possible to perform oil film visualisation, as in the test rig, an attempt has been made to correlate the two set of results. Figure 5.20 illustrates an example of the cyclic variation of the in-cylinder (black line) and oil film pressure (OFT –blue line) at an engine revolution of 1000 rpm. The transducer located at mid-stroke is able to record the oil film pressure readings for the first and second compression rings and the scrapper ring.

Starting from the left hand side of Figure 5.20a (blue line), the rings pass the transducer during the intake but the small hydrodynamic pressure associated with the ring is not measurable. Although the pressure transducer has been designed for detecting the hydrodynamic oil film pressure, it is of course also responsive to the cylinder pressure. As a result of this some of the rise in pressure during the compression stroke can be seen just before the rings pass the transducer. When the rings completely pass through the transducer, the detected pressure is “blocked” from the high cylinder pressure and the transducer only records the lower end pressure. Again as the rings pass through the transducer in the compression stroke no visible hydrodynamic pressure is found. When the piston reverses, in the power stroke, the pressure transducer records in order the hydrodynamic oil film pressure on the scraper, second compression and first compression rings. One possible reason for this is that during the power stroke the piston is more compressed towards the thrust side of the liner which allows more contact between the rings and the wall surface (Nakashima *et al.*, 1995; Tian and Wong, 2000). As the piston passes the pressure transducer, it records the decreasing cylinder pressure as expected. In the exhaust stroke the small hydrodynamic pressure associated with the rings are still undetectable.

Figure 5.20b depicts the pressure recorded on the rings during the power stroke. The first ring to be encountered by the transducer is the scraper ring. A rise in hydrodynamic pressure can be seen before dropping suddenly below atmospheric pressure. Then the pressure rises to the inter-ring pressure between the scraper and the second compression ring. Similar pressure pattern can be seen for the second and first compression rings. It is important to note that the hydrodynamic oil film pressure recorded in the engine is comparable to that obtained in the idealised test rig where normally cavitation inception is accompanied by negative or sub-atmospheric pressures.



(a) 1000 rpm



(b) Oil film pressure variation during power stroke

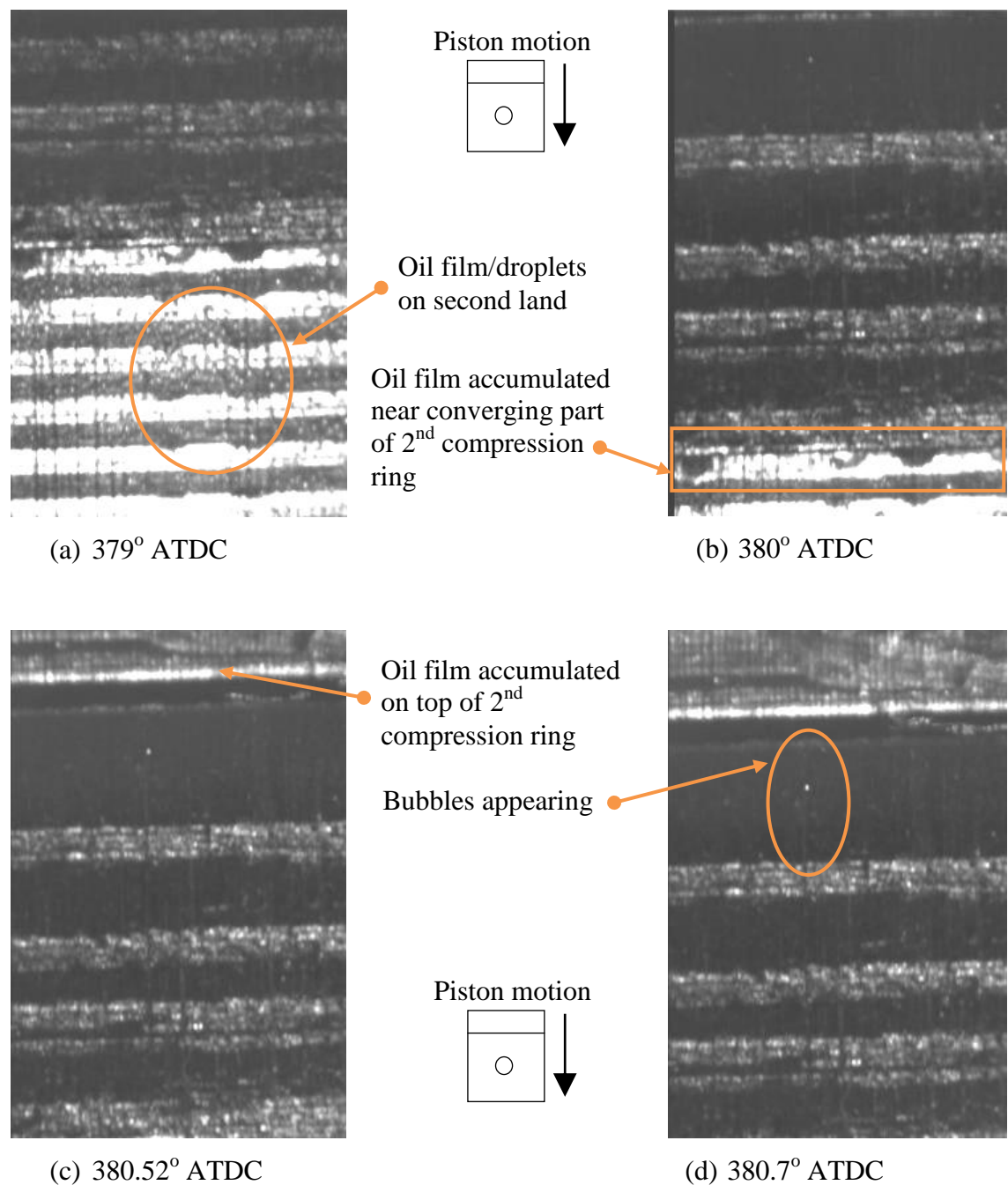
Figure 5.20: Cylinder and oil film pressure distribution in engine

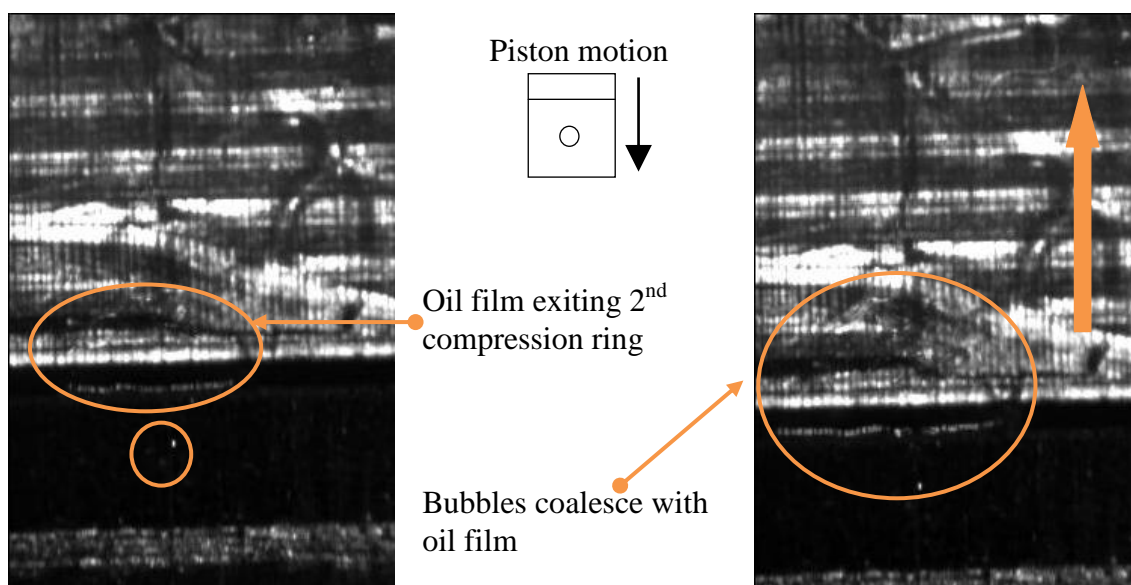
5.2.4 VISUALISATION EXPERIMENTS: CAVITATION INCEPTION

Following the visualisation of cavitation development in the test rig, an investigation into the presence of cavitation structures in the lubricant film between the liner and piston rings of the engine was carried out. To capture the highly transient nature of the cavitation structures, the video camera was set on the highest recording frame rate of 30000 fps. Figure 5.21 shows the recording frames at the top corner of the upper window during the power stroke. These images have a magnification factor of 2 and a view area of 2.2mm x 2.9mm; this setup allows the ring's whole width to be visualised. Unfortunately in the following visualisation, neither fern shape structures nor were cavitation strings were observed as opposed to the test rig. Possible explanations could be that these are real-size engine piston-rings where any cavitation structures that may occur/form in the diverging wedge of the ring are much smaller and possibly short-lived; or alternatively there may be no continuous supply of oil resulting in starved condition. The camera space resolution used here (13.6 frames/mm corresponding about 40 frames for that measurement window) is inferior to that of the test rig (100 frames/mm). The camera spatial resolution used here (13.6 frames/mm corresponding to about 40 frames for that measurement window) is inferior to that of the test rig (100 frames/mm). It can thus be concluded that the transient structure of the cavitation process that have been observed in the test rig may have not been captured by the camera employed in the engine due to its reduced resolution.

However, an interesting pattern has been discovered. Oil film is observed to enter the converging part of the ring and later along the stroke to exit the diverging area as bubbles. Oil on the piston second land is entrained towards the converging part of the second compression ring and then exits on the diverging part (Figure 5.21a-c). A sudden appearance of small bubbles is noted (Figure 5.21d), especially on the diverging section, which move towards the trailing edge of the ring. These bubbles coalesce into an oil "puddle", making it to grow in size and then move forward towards the piston first land (Figure 5.21e-h). Oil accumulated on the first land is driven onto the leading edge of the first compression ring (Figure 5.21i-k). Here, as well, a sudden appearance of bubbles (Figure 5.21l-m) is noted on the diverging section of the ring which are thrust onto the crown land and probably end up into the combustion chamber. The bubbles formed, notably in the diverging sections of both rings, may be due to cavitation. Negative or

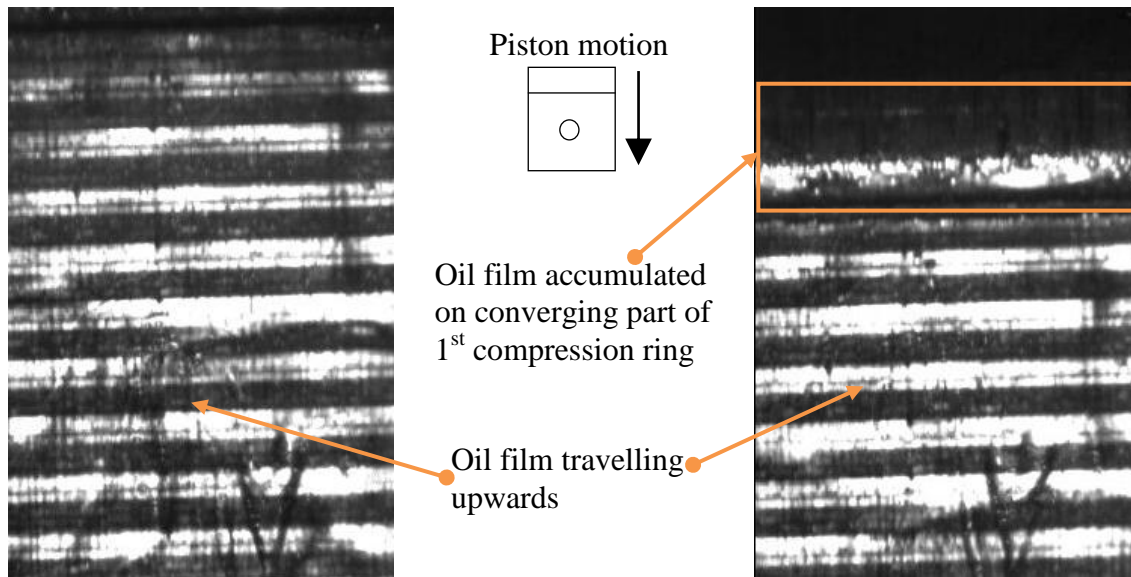
sub-atmospheric pressure readings have also been recorded around that area (Figure 5.20b). This stems from the results in the idealised test rig where cavitation inception has been found to occur in the diverging edge of the ring and to be linked to sub-atmospheric pressures. This suggests that when the oil film enters the diverging section of the engine piston ring, it eventually cavitates and then disintegrates into bubbles as observed in the test rig. Figure 5.22 illustrates schematically most probable oil cavitation development in the engine during the stroke according to the images taken.





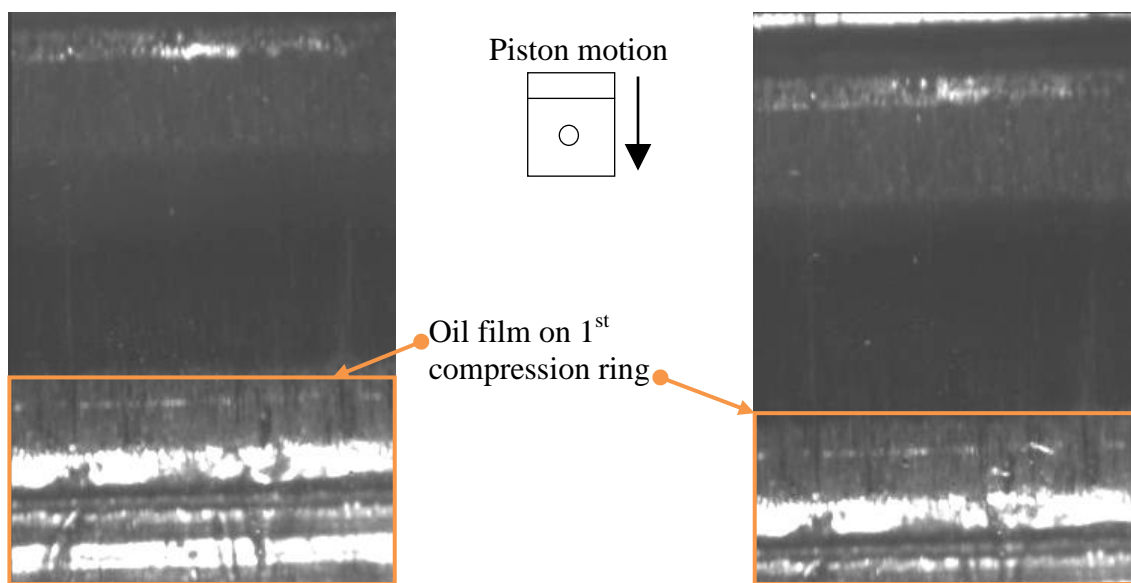
(e) 381.78° ATDC

(f) 381.96° ATDC



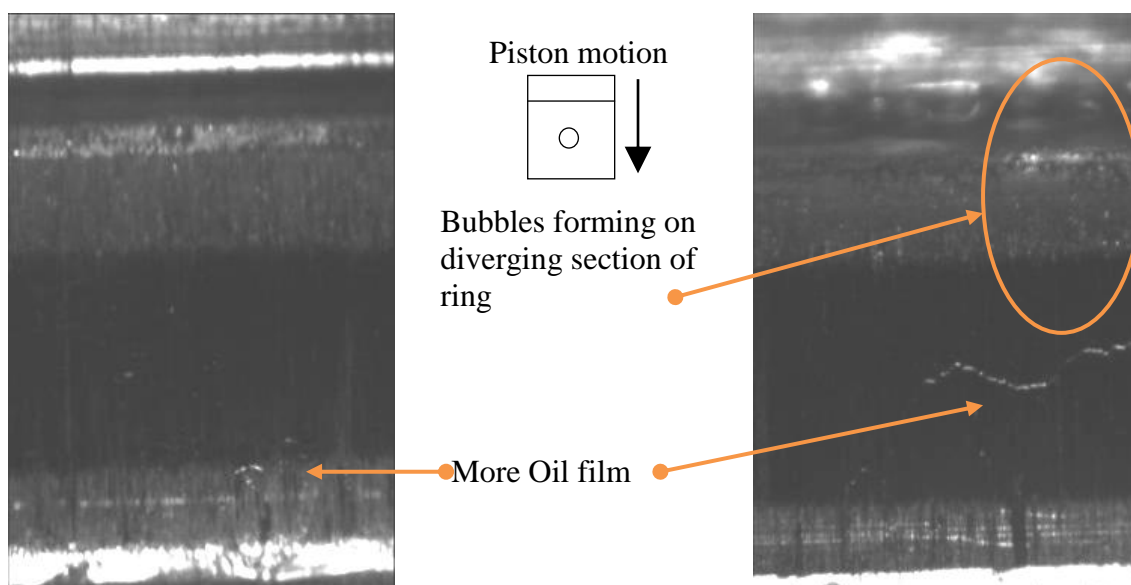
(g) 383.4° ATDC

(h) 384.12° ATDC



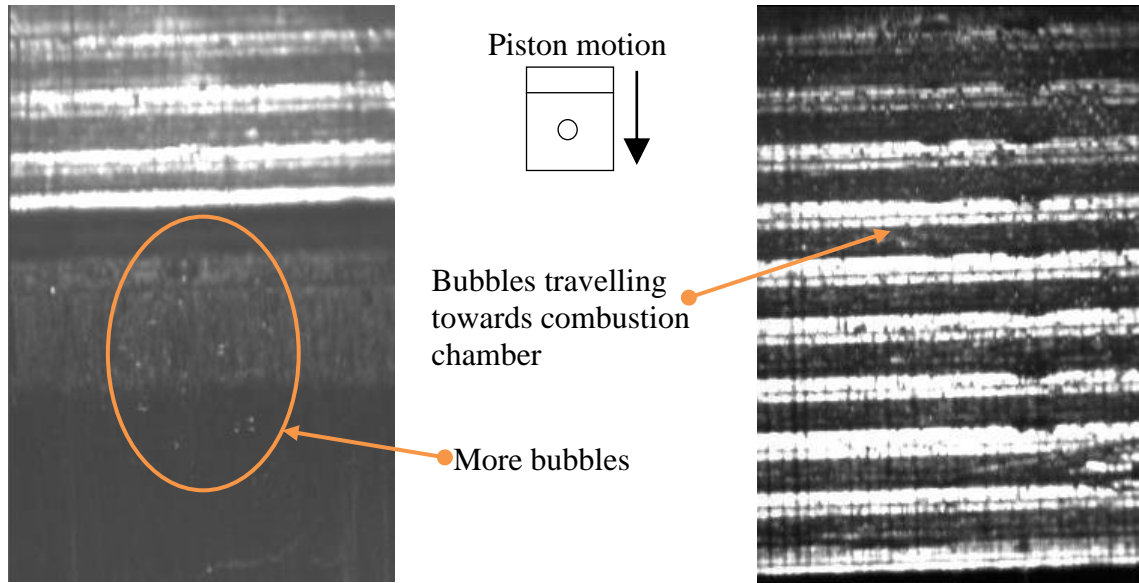
(i) 385.2° ATDC

(j) 385.38° ATDC



(k) 384.12° ATDC

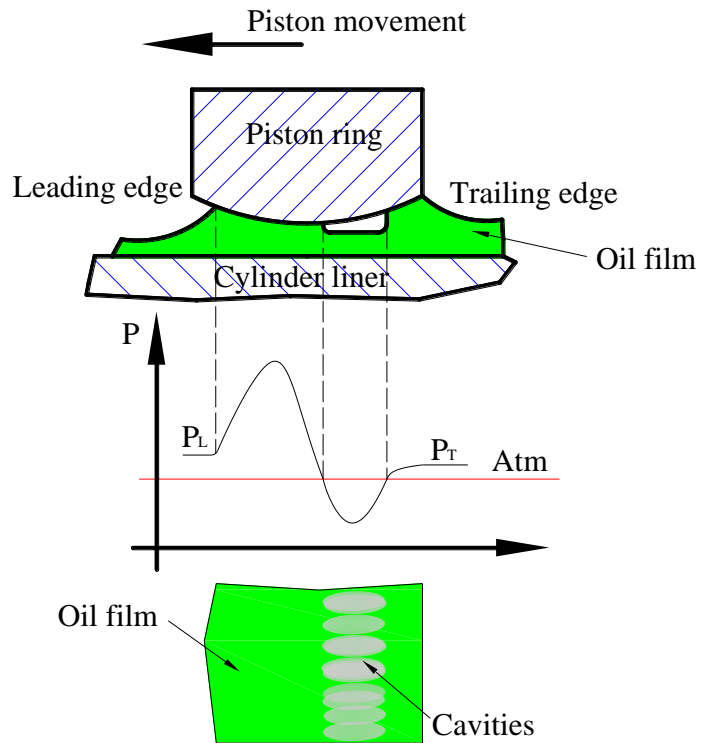
(l) 384.48° ATDC



(m) 384.3° ATDC

(n) 384.12° ATDC

Figure 5.21: Oil film visualisation for compression rings



(a) String cavities

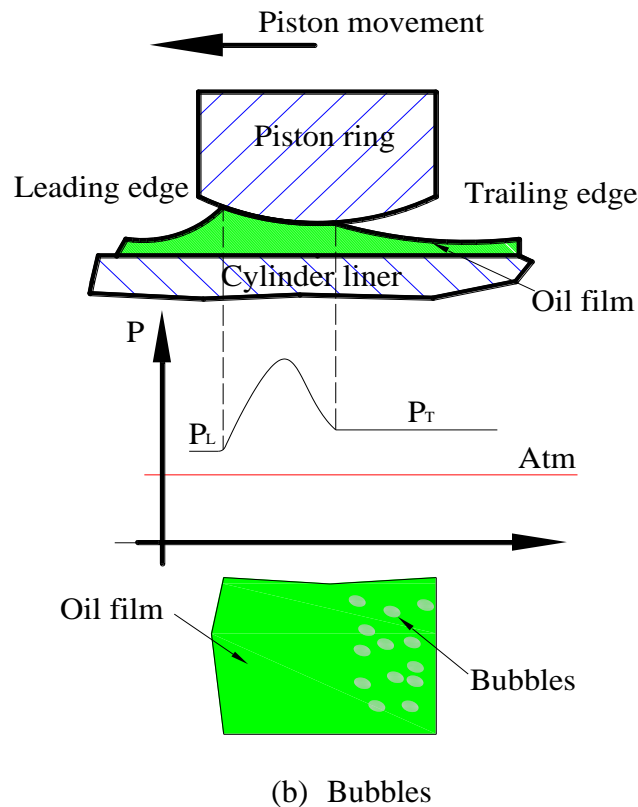


Figure 5.22: Possible cavitation pattern and hydrodynamic pressure in diesel engine

In the above schematic, the possible cavitation stages are shown that point out to the latest cavitation development visualised in these experiments (bubbles). The schematic also presents the anticipated oil film pressure for the oil film. Similarly to the test rig, cavitation inception is being accompanied by negative or sub-atmospheric pressures. In the converging wedge of the piston-ring, the pressure is the leading edge pressure and at the diverging edge the pressure reading would be that of the trailing edge one. Depending on the stroke, these pressures would correspond to that of the combustion/compression or inter-ring pressures. Later on in the stroke as the oil film reaches the diverging area of the ring, the pressure drops below the atmospheric level. As the oil film cannot withstand negative pressures (Cameron, 1971; Castleman, 1936) at the diverging wedge of the piston-ring, it cavitates (Figure 5.22a). The formed cavities later disintegrate into bubbles or break down into oil droplets (Figure 5.22b).

5.2.5 OIL FILM VISUALISATION: LOWER WINDOW

Furthermore, oil film visualisation was carried out through the lower quartz window.

Figure 5.23 shows the recording frames made during the compression stroke at an engine speed of 1000 rpm. Again no fern shapes or string cavities could be visualised but the same pattern observed on the upper window is also found here. The images below show some oil entering the second compression ring and then emerging as droplets and bubbles on the diverging wedge of the ring. Although higher recorded frames could be applied to capture the flow in more detail but the inadequate power of the light source prevented such an investigation.

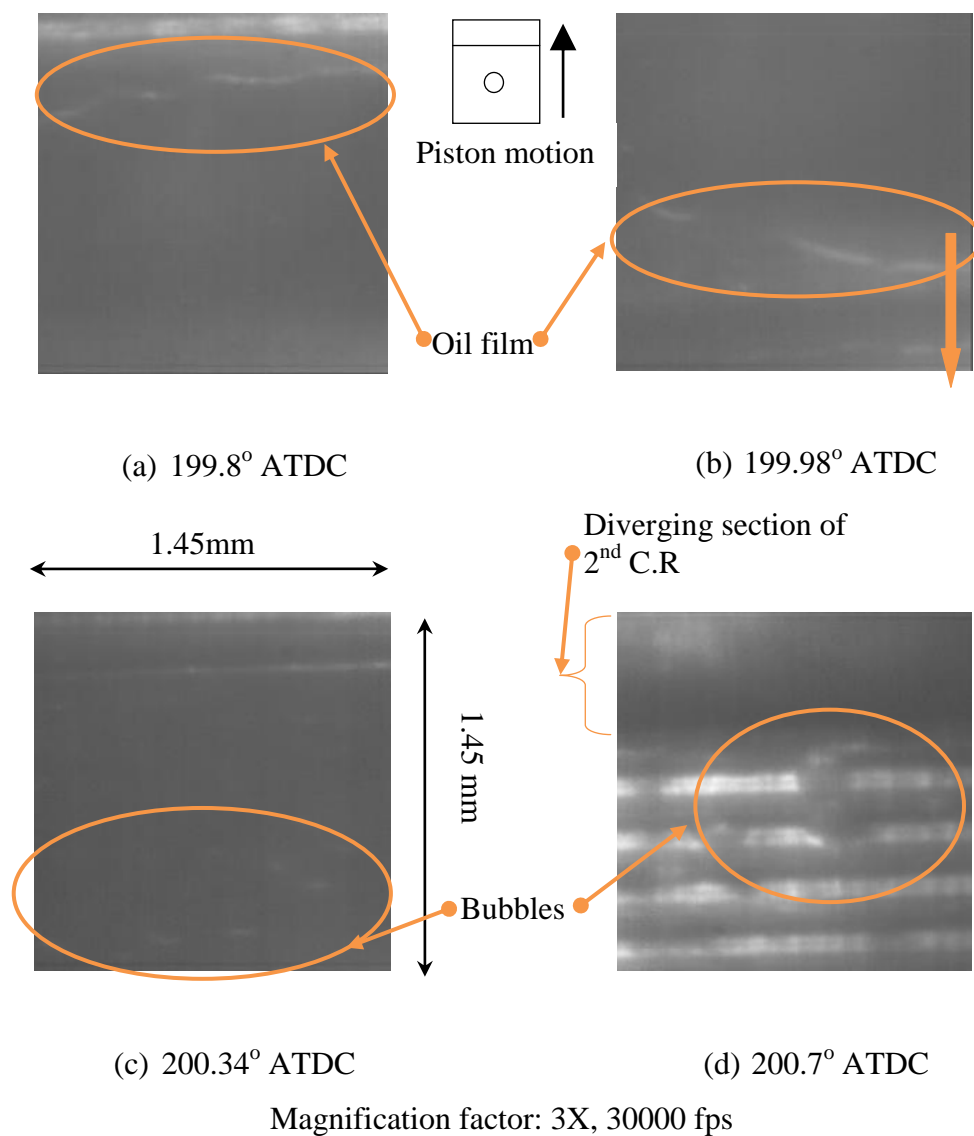


Figure 5.23: Oil film visualisation on lower window

The following images (Figure 5.24) show the capture of the oil mist emerging from the ring groove of the first compression ring during the power stroke. When the oil is inside the ring grooves, its flow is controlled by the gas flow and the pumping effect caused by ring motion. So any film oil film present in the gas is transported to different regions with the gas flow (Yilmaz *et al.*, 2004). Droplet entrainment from the oil film on the cylinder wall to the ring gaps, where the gas velocity is high (Tian *et al.*, 1996; Tian *et al.*, 1998), should also be considered. Inagaki and co-workers (1995) have also observed droplets in their visualisation experiments as well as some oil spouts moving towards the combustion chamber as the piston is going to BDC. The oil mist can initiate a larger oil transport as shown in section 5.2.4; this was identified as one way to transport more oil towards TDC.

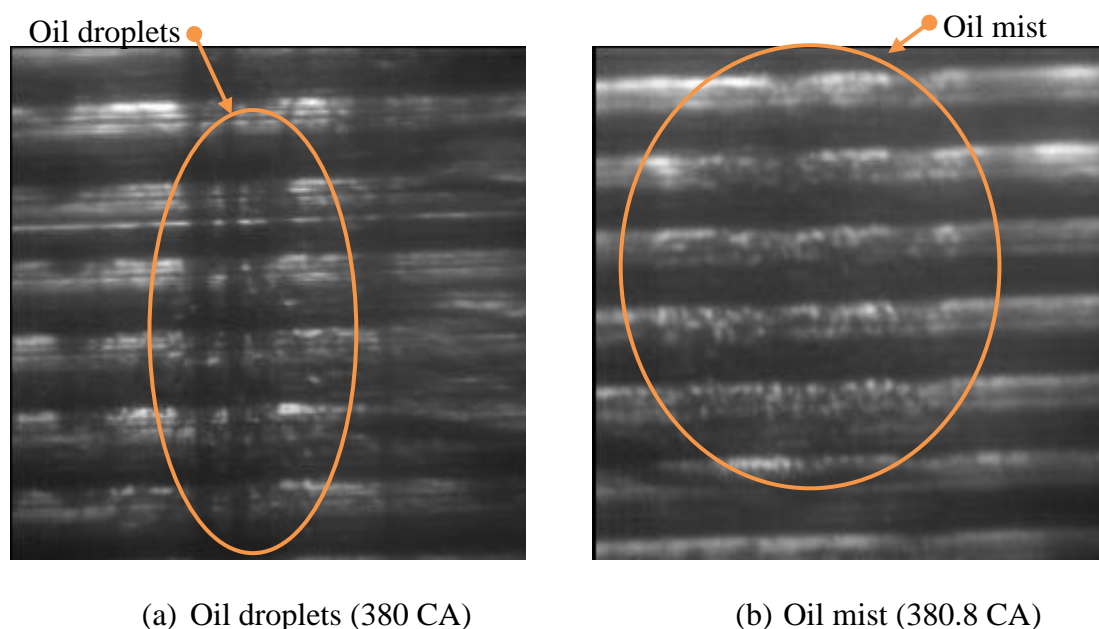


Figure 5.24: Oil mist moving towards combustion chamber in the power stroke

Figure 5.25 illustrates an image of the first compression ring of the Lister Petter diesel engine from the work of Dellis (2005). The author used a still CCD camera combined with a high magnification lens, CF-4, to obtain these images. Dellis has argued that the shapes highlighted in Figure 5.25 are string cavities obtained during the induction stroke. Due to the fact that the flow could not be visualised continuously, in his case, due to the use of the still CCD camera, and the impression that the structures looked like

regular marks on the piston-ring, have made the findings of string cavities by the aforementioned author questionable.

To shed some light on the findings of Dellis (2005), an image of the top compression ring was taken when the piston was still; the whole width of the piston-ring could then be imaged. Similar structures to those found in Figure 5.25 were observed in Figure 5.26. It is likely that these were most probably marks left during manufacturing of this ring. Therefore, the string cavities identified on the piston-ring by Dellis could be merely piston marks rather than true cavitation structures which necessitates further investigation.

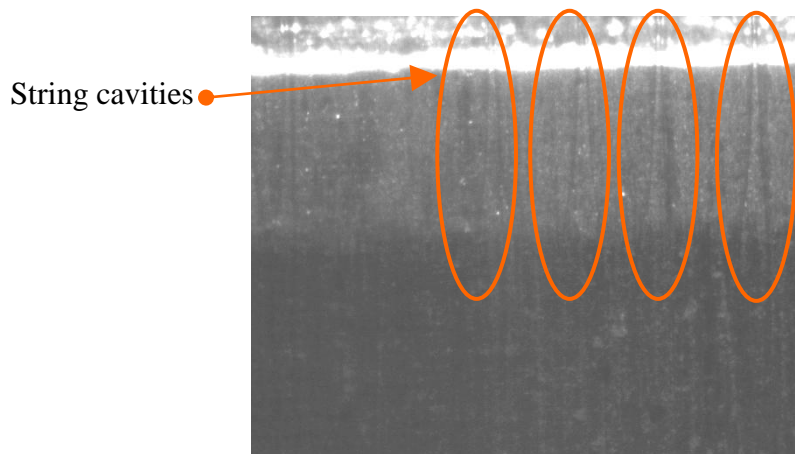


Figure 5.25: String cavities(Dellis, 2005)

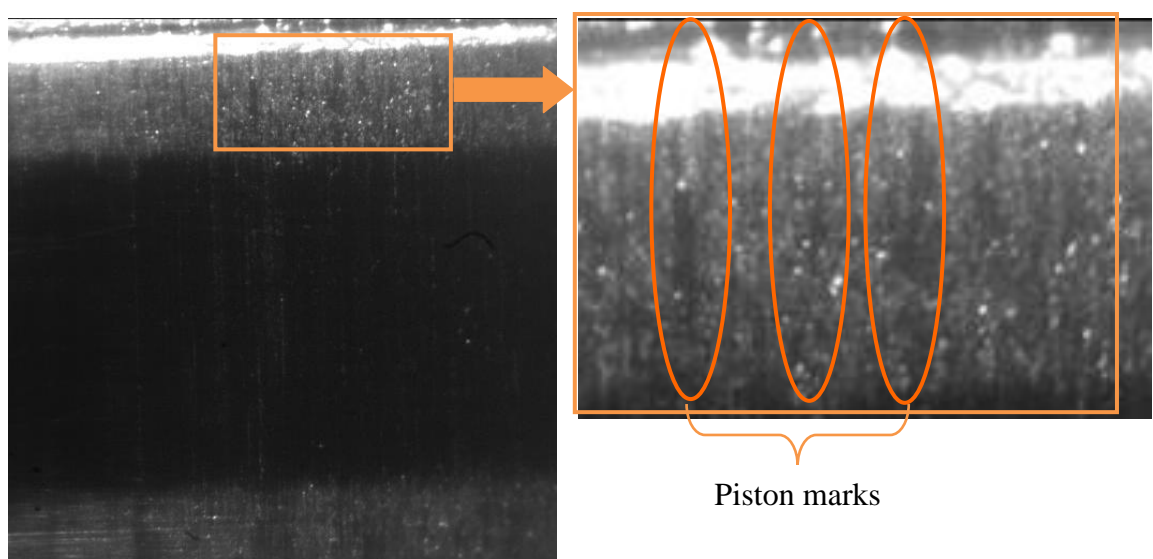


Figure 5.26: Image of first compression ring when piston stationary

5.3 SUMMARY

The implementation of the quartz liner in a single-cylinder diesel engine has allowed the oil film between the piston-ring and the liner to be visualised. It has been confirmed that the cavitation regime between the ring and the liner occurs in the diverging section of the conjunction, when the pressure drops below the atmospheric level. This phenomenon is highly dependent on the localised kinetics within the contact region as well as the dynamics of the ring and piston. The cavitation regime starts as nucleation sites and then rapidly evolves into evolving structures such as ferns, fissures, strings and finally bubbles.

The current research programme has made use of a set of integrated experimental techniques to investigate cavitation onset and development. The oil film pressure was measured, and then compared with the images obtained by a fast speed video camera. The advantage of the high image collection rate of the camera has allowed analysis of the evolution of individual cavitation structures. The parametric investigation included the effect of load, speed, temperature and viscosity on the initiation and growth of cavities to be identified and characterised

The obtained understanding into oil film visualisation in piston cylinder assemblies in the idealised test rig has provided into possible cavitation regimes in the diesel engine. The application of the high speed video camera to the engine has proved very useful in the visualisation of the oil film between the liner and the fast moving piston-rings. Oil was observed to move in the axial direction with an inertia force resulting from the reciprocating motion of the piston being responsible for this occurrence. The visualisation images have shown oil entering the converging side of the ring and then emerging from its diverging wedge. Although the stages of cavitation development found in the test rig have not been confirmed in the engine, the aforementioned observation has been indirectly interpreted as cavitation. Moreover, the pressure measurements obtained at mid-stroke have provided further evidence of sub-atmospheric or negative pressures present in the diverging section of the rings. Oil droplets and mist have also been observed to travel towards the combustion chamber which may contribute towards the oil consumption of the engine and towards the undesirable tail pipe emissions.

Chapter 6

CONCLUSIONS AND FUTURE WORK

6.1 CONCLUSIONS

Optimizing the performance of the piston/ring/liner system is becoming a matter of concern for both the engine manufacturers and the lubricant suppliers. In particular, methods are intensively being sought to reduce both oil and fuel consumption and to provide scope for addressing the intimately related problem of reducing global and local exhaust emissions. In view of the fact that the majority of an engine's oil consumption occurs from losses through the ring packs, attempts to reduce these have been made by component designs which require less oil to maintain sufficient lubrication yet circumvent major wear problems. The development of lubricants for the new advanced engines will require a better understanding of the oil flow and transport phenomena through the ring pack region and their relationship to oil consumption in addition to any need to regulate both friction and wear. These are considered as equally important to the reduction in both friction and wear and are all major contributors to the engine's fuel consumption and overall efficiency.

In this work, the oil transport phenomena in the ring pack have been investigated with particular attention devoted to the formation of cavitation. This work has been broken down into two phases. The first part focussed on the study of piston ring lubrication under controlled conditions in a purpose built test rig. This research has led a better understanding of the complex mechanism of lubrication by isolating the difficult tribological interactions that occur in production engines. The test rig permits the measurement of the oil film thickness, oil film pressure and friction to be done simultaneously. Moreover, the successful calibration approach of the LIF system has allowed the oil film thickness on the surface of the ring to be measured and also to allow identification of cavitation. Initially the measurements of the oil film pressure by

special pressure transducer have proved to be difficult but at the end the installation of the sensor with its good repeatability of oil film pressure was a big success.

Useful results were obtained from the test rig where extensive testing showed good repeatability; these are summarized as follows:

- Oil film thickness as measure by the capacitance probe decreases with increasing load and increases with increasing speed.
- Viscosity of the oils found to be an important factor in the characterisation of the oil films; the more viscous oil gave rise to a higher oil film thickness.
- Oils of similar viscosity exhibited similar oil film thickness at the same operating conditions.
- As increase in oil film temperature decreases friction and reduces the oil film thickness.
- Friction results were found to be repeatable with their symmetry during upstroke and downstroke reflection the design and manufacturing of the test rig.
- Friction results close to the dead centres where peaks were recorded have been validated by the capacitance results.
- The frictional force at the ring/liner contact is mainly attributed to asperity contact and viscous drag; when asperity contact is present, it plays the dominant role.
- For the very viscous oils no asperity interaction was noted and hence the friction measurements have been dominated by viscous drag

A grooved piston-ring specimen was employed in order to enable the study of the lubricant's fluorescence quantum yield at ambient and elevated temperature and to quantify the LIF signal acquired from the fibre optic measuring probe. The results demonstrated that:

- The dynamic calibration based LIF results are comparable to those obtained with the capacitance probe.
- The dynamic calibration coefficient ($\mu\text{m}/\text{V}$) is increasing with temperature as shown by the high temperature tests.

- The LIF results show that cavitation always takes place in the diverging section of the ring and to be independent of load and speed.

A miniature pressure transducer has been used to measure the hydrodynamic film pressure in the test rig; the results showed that:

- Higher oil film pressure occurs on the smaller curvature side of the ring.
- The depletion of the oil film as obtained by the LIF corresponds to the sub-atmospheric pressure measured locally. This lead to the conclusion that cavitation occurs in the sub-atmospheric pressure region within the diverging section of the ring.
- Higher speeds and loads increase the hydrodynamic pressure but the negative pressure remains practically unchanged especially in the larger curvature of the ring.
- Higher viscosity oil gives rise to higher oil film pressure higher oil temperature reduces the oil film pressure; the pressure of the oil film is related to the oil film thickness available between the contacts.

The optical access provided by the quartz liner has enabled the inception and development of cavitation of different lubricants to be visualised by the fast speed video camera. The imaging results revealed that:

- The high frame rate of the video camera has allowed the initial development of cavities up to their disintegration to be captured in one full stroke.
- The cavities appear early in the stroke in the diverging section of the ring.
- The oil flow lags relative to the mechanical movement of the liner which explains the shift in the capacitance and friction peaks around the dead centres.
- The cavities develop in stages: they start as ferns, fissures, strings and finally bubbles.
- The appearance of fern shapes on the surface of the diverging wedge of the ring, is followed by sub-atmospheric or negative pressures which demonstrates that the local pressure either reaches the tensile strength of the lubricant or the lubricant's vapour pressure.

Parametric studies on the oil film visualisation with respect to load, speed, temperature and viscosity have been carried out. The results showed that:

- The higher the load, the earlier in the stroke the fern cavities appear and the smaller their size and the higher the number of strings.
- The higher the speed the later in the stroke the cavities appear, the larger their size and the smaller the number of strings.
- The viscosity of the oil influences the development of the string cavities into ligaments and into bubbles.
- The higher the viscosity, the later in the stroke the cavities appear, the larger their size and the smaller their numbers.
- As temperature rises, the cavities appear earlier in the stroke, the number of string cavities increases and their corresponding width decreases.

The oil film visualisation experiments in the idealised rig were extended to the single cylinder diesel engine where motoring tests were carried out. The following observations were made:

- On the piston rings and land, oil moves in the axial direction. The axial displacement is driven by the inertia force resulting from the piston reciprocating motion.
- Oil is found to be accumulated in the ring grooves.
- The high speed video camera visualisation gave a close insight of the droplets and mist that is generated in the lubricant.
- Oil droplets and mist are transported towards the TDC of the engine and probably end up in the combustion chamber.
- The transient cavitation patterns observed in the test rig have not been identified in the engine. On the other hand, the oil film was found to enter the converging edge of the ring and to emerge as bubbles in the diverging section of the ring. It can be argued that the bubbles formed are considered to be the end product of the cavitation process originating from ferns. Furthermore, the detection of sub-atmospheric pressure by the pressure sensor provides support to the existence of cavitation in the lubricant film between the contacts. Despite this, further investigation is recommended in the engine by employing a camera with higher temporal and spatial resolution in order to capture the highly transient nature of the cavitation process.

6.2 FUTURE WORK

The current research focus has been on lubricant film cavitation where pressure measurements and film visualisation have revealed the onset and development of various cavitation patterns under engine simulated conditions in a reciprocating piston-ring assembly and in a motored diesel engine. The LIF probe used in the tests has provided both quantitative and qualitative information about the film transport. Pressure measurements alongside the LIF probes have been very useful in the engine so as to provide complementary information about the oil film. However, the quartz windows on the engine should be made wider and longer so as to cover a wider circumference of the piston and rings as well as to cover most of the stroke. A range of oils have also to be examined to provide the missing links between lubricant oil formulation, engine operating conditions and cavitation initiation.

To obtain better understanding of the oil transport process between the piston lands, through the grooves and gaps and their interactions, identification and characterization of the mechanisms responsible for the oil flows along the piston have to be made. The driving forces behind axial oil displacements and the circumferential flow should be identified and verified with previous findings. Factors such as inertia-driven oil displacements, ring and piston dynamics, ring/groove relative angle, ring squeeze action, region by region analysis of the piston-ring pack, dragging effect of gases flowing through the ring groove clearances and around the piston circumference, ring and land geometry, ring fluttering, ring instability, flutter induced gas flow, ring pumping, clearance of the ring grooves, land oil distribution, lateral motion of the piston relative to the rings and from the engine side piston speed, engine load and intake manifold pressure should be checked individually and in combination so that the mechanism of oil transport could be evaluated. This can be a major step towards the development of analytical tools for oil consumption reduction and for providing practical guidance for the piston and piston-ring designs. Ideally the oil transport phenomena have to be compared for both diesel and gasoline engines. To take advantage of the very high recording frame rates (250000 fps max) of the high speed video camera the continuous light source, the existing argon-ion laser, will have to be modified to allow the visualisation of the transient oil film transport under various operating conditions.

The single-cylinder diesel engine modification must be done in such a way that will allow measurement of the lubricant oil film thickness, identification of cavitation through direct film visualisation and transfer through piston rings, measurement of the transient pressure in the film and measurement of film temperature through in-situ calibration. In addition to the optical windows, the modified engine should be equipped with pressure transducers and optical fibre probes for pressure and lubricant film thickness measurements. The current visualisation results will continue as the first stage of the proposed work in terms of characterisation of the film thickness and cavitation visualization under a range of engine operating conditions. Tests for various engine speeds, loads and piston ring configurations will be carried out in conjunction to the oil transport. To maximise problem-free operation of the diesel engine, the first tests will be performed under motoring conditions, followed by firing tests. Although the latter tests are more relevant, motored engine operation is equally useful for improving the fundamental understanding of the lubricant distribution and for obtaining experimental data for the development and validation of computer simulations. Modifications will also be made to the crankcase to allow the engine oil to be changed during engine operation. This modification will allow fluorescent dye tracers to be added to the lubricant so that lubricant transport can be monitored through the fluorescence signals from the inserted in key positions fibre probes.

To extend the LIF technique, DWF (Dual Wavelength Fluorescence) will be used to allow the simultaneous monitoring of the film's temperature. The novel temperature sensing technique will first be developed and calibrated in the piston-rig assembly rig, where simultaneous film thickness and temperature measurements will be attempted for a number of preset oil temperatures. This will allow the temperature effect on the film thickness measurement to be identified and corrected. First, the engine lubricant itself will be examined as a fluorescent material and its fluorescence properties, transmission spectra and emission spectra will be characterised. Then a number of fluorescent dyes will be examined and their properties compared to those of the lubricant oil, as means of maximising the accuracy of the temperature measurement. The LIF temperature measurement will be used for optimizing the three parameters which dictate a temperature change:

- (1) change in fluorescence intensity,

(2) change in fluorescence lifetime and

(3) change in fluorescence wavelength.

Intensity-based LIF measurement has the advantage of fast time response and is very suitable for engine applications. Hidrovo and Hart (2000) from MIT have been involved in the development of the two dyes intensity ratio method, the so-called DELIF (Dual Emission Laser Induced Fluorescence) which is considered to be a useful technique. The DELIF preserves the fast time response of the intensity based technique and reduces, if not totally eliminates, the fluorescence intensity dependence on the incident laser energy.

The general objectives of this additional investigation are to use the current expertise obtained in this work to focus on possible ways to:

- Improve understanding of lubricant distribution between a piston ring and cylinder wall as defined by the film thickness, degree of lubricant starvation and the cavitation phenomena
- Identify the correlation between film thickness, cavitation and instantaneous piston friction
- Identify the presence and structure of cavitation in the lubricant film of diesel engines and gasoline engines
- Develop a novel dual wavelength fluorescence (DWF) based temperature sensing system for characterising the temperature variation of the lubricant film during engine operation
- Monitor the pressure variation in the lubricant film during engine operation
- Identify lubricant distribution differences in gasoline and diesel engine
- Establish transient lubricant distribution during cold start in engines
- Study lubricant degradation and transport in the engines
- Study fuel-lubricant synergy in conventional gasoline port injection engines and in gasoline direct injection engines.

Overall, although very interesting results and insight have been obtained on a number of aspects of piston-ring lubrication centred around cavitation, there is an increasing

interest on the subject as means of reducing friction and improving the efficiency of both gasoline and diesel engines. It is widely considered that reduction of friction through design considerations and oil formulation represents one of the most tangible goals in the evolutionary development of reciprocating engines and it is hoped that the work presented in this thesis represents a small step in this direction.

REFERENCE LIST

- Arcoumanis, C., M. Duszynski, H. Flora and P. Ostovar. (1995). Development of a piston-ring lubrication test-rig and investigation of boundary condition for modelling lubricant film properties. *SAE Transactions* 104(4):1433-1451.
- Arcoumanis, C., M. Duszynski, H. Lindenkamp and H. Preston. (1998a). Measurements of lubricant film thickness in the cylinder of a firing diesel engine using LIF. *SAE Transactions* 107(4):898-906.
- Arcoumanis, C., M. Duszynski and H. Preston. (1998b). Cold-start measurements of lubricant film thickness in the cylinder of a firing diesel engine using LIF. *SAE Transactions* 107(4).
- Arcoumanis, C., P. Ostovar and R. Mortier. (1997). Mixed lubrication modelling of Newtonian and shear thinning liquids in a piston-ring configuration. *SAE Transactions*.
- Benchaita, M.T. , S Gonsel and F.E Lockwood. (1990). Wear Behaviour of Base Oil Fractions and Their Mixtures. *Tribology transactions* 33:371-383.
- Boness, R. J. and H. M. Hawthorne. (1995). Acoustic Emission from the Unlubricated Sliding Wear of Steel and Silicon Nitride. *Tribology transactions* 38(2):293-298.
- Boness, R. J., S. L. McBride and M. Sobczyk. (1990). Wear Studies Using Acoustic Emission Techniques. *Tribology International* 23(5):291-295.
- Brennen, Christopher E. (1995) *Cavitation and Bubble Dynamics*. New York: Oxford University Press.
- Brown, M. A., H. McCann and D. M. Thompson. (1993). Characterization of the Oil Film Behavior Between the Liner and Piston of a Heavy-Duty Diesel Engine. *SAE paper* 932784.
- Brown, S. R. and G. M. Hamilton. (1977). The partially lubricated piston ring. *Journal Mechanical Engineering Science* 19(2):81-89.
- Brown, S. R. and G. M. Hamilton. (1978). Negative pressures under a lubricated piston ring. *Journal Mechanical Engineering Science* 20(1):49-57.
- Brown, S. R., G. M. Hamilton and S.L Moore. (1975). Hydrodynamic pressure under a piston ring. *Nature* 253:341-342.

- Burnett, P. J. (1989). Relationship between oil consumption, deposit formation and piston ring motion for single cylinder diesel engines. *SAE paper* 920089.
- Caines, A. J. and R. F. Haycock. (1996) *Automotive lubricants reference book*: Society of Automotive Engineers Warrendale, PA.
- Cameron, A. (1971) *Basic Lubrication Theory*: Longman.
- Casey, S.M. (1998) Effects of engine operating conditions on oil film thickness and distribution along the piston/ring/liner interface in a reciprocating engine. In *1998 Fall Technical Conference of the ASME Internal Combustion Engine Division* 133:47-56. Clymer, New York (ASME)
- Castleman, R. A. (1936). A Hydrodynamical Theory of Piston Ring Lubrication. *Journal of Applied Physics* 7(9):364-367.
- Cooke, V. B. (1990) *Lubrication of Low Emission Diesel Engines*: Society of Automotive Engineers.
- Coyne, J. and H. G. Elrod. (1970a). Conditions for the rupture of a lubricating film, Part 1. *ASME J. Lubrication Technol* 92:451-456.
- Coyne, J. and H. G. Elrod. (1970b). Conditions for the rupture of a lubricating film, Part II: New boundary conditions for Reynolds equation *ASME J. Lubrication Technol* 92:156-167.
- Dellis, P. (2005) "Aspects of Lubrication in Piston Cylinder Assemblies." PhD Thesis, Department of Mechanical Engineering: Imperial College of Science, Technology and Medicine. London.
- Dellis, P. and C. Arcoumanis. (2004). Cavitation development in the lubricant film of a reciprocating piston-ring assembly. *Proceedings of the Institution of Mechanical Engineers, Part J: Journal of Engineering Tribology* 218(3):157-171.
- Didot, F.E., E. Green and R.H. Johnson. (1987). Volatility and oil consumption of SAE 5W-30 engine oil. *SaE paper* 872126.
- Dorinson, A. and K. C. Ludema. (1985) *Mechanics and chemistry in lubrication*: Elsevier.
- Dowson, D, E.H Smith and C.M Taylor. (1980). An experimental study of hydrodynamic film rupture in a steadily-loaded, non-conformal contact. *Journal of Mechanical Engineering Science* 33(2):71-78.
- Dowson, D. (1979) *History of tribology*: Longman New York.

- Dowson, D. (1993). Piston assemblies: Background and lubrication analysis. *TRIBOLOGY SERIES* 26:213-213.
- Dowson, D. and C. M. Taylor. (1979). Cavitation in Bearings. *Annual Reviews in Fluid Mechanics* 11(1):35-65.
- Drinkwater, B., R. Dwyer-Joyce and P. Cawley. (1997). A study of the transmission of ultrasound across solid-rubber interfaces. *The Journal of the Acoustical Society of America* 101:970.
- Duszynski, M. (1999) "Measurement of Lubricant Film Thickness in Reciprocating Engines." PhD Thesis, Department of Mechanical Engineering: Imperial College of Science, Technology and Medicine. London.
- Dwyer-Joyce, R. S., P. Harper and B. W. Drinkwater. (2004). A Method for the Measurement of Hydrodynamic Oil Films Using Ultrasonic Reflection. *Tribology Letters* 17(2):337-348.
- Elrod, H. G. (1979). A general theory for laminar lubrication with Reynolds roughness. *ASME, Transactions, Journal of Lubrication Technology* 101:8-14.
- Floberg, L. (1973). Lubrication of two rotating cylinders at variable lubricant supply with reference to the tensile strength of the liquid lubricant. *Journal of Lubrication Technology, Transactions ASME, Ser F* 95(2):155-165.
- Floberg, L. (1965). On hydrodynamic lubrication with special reference to sub-cavity pressures and number of oil streamers in cavitation regions in cavitation regions. *Acta Polytechnica Scandinavica Mechanical Engineering Series* 19.
- Froelund, K., J. Schramm, T. Tian, V. Wong and S. Hochgreb. (2001). Analysis of the Piston Ring/Liner Oil Film Development During Warm-Up for an SI-Engine. *Journal of Engineering for Gas Turbines and Power* 123:109.
- Frølund, K., J. Schramm, B. Noordzij and T. Tian. (1997). An Investigation of the Cylinder Wall Oil Film Development During Warm-Up of an SI Engine Using Laser Induced Fluorescence. *SAE Transactions* 971699.
- Furuhashi, S. (1959). A Dynamic Theory of Piston-Ring Lubrication (1st report, Calculation). *Bulletin of Japanese Society of Mechanical Engineers* 2(7):423-428.
- Furuhashi, S. (1985) Some Factors on engine oil consumption through a piston. In *Proc JSLE Int Trib Conf.*:301. Tokyo
- Furuhashi, S. (1987). Tribology of reciprocating internal combustion engines. *Jap. Soc. Mech. Engrs Int. J* 30(266):1189-1199.

Furuhama, S. and T. Sumi. (1961). A Dynamic Theory of Piston-Ring Lubrication (3rd report, Measurement of oil film thickness). *Bulletin of Japanese Society of Mechanical Engineers* 4(16):744-752.

Green, D.A., R. Lewis and R. Dwyer-Joyce. (2006) The ultrasonic measurement of automotive component contact pressures. In *Tribology 2006: Surface Engineering and Tribology for Future Engines and Drivelines* London, UK (Institute of Mechanical Engineers)

Greene, A. B. (1969). Initial visual studies of piston-cylinder dynamic oil film behaviour. *Wear* 13:345-360.

Grice, N. and I. Sherrington. (1993). An Experimental Investigation Into the Lubrication of Piston Rings in an Internal Combustion Engine: Oil Film Thickness Trends, Film Stability and Cavitation. *SAE Technical Paper Series 930688*.

Gümbel, L. K. R. (1921). Vergleich der Ergebnisse der rectinerischen Behandlung des Lagerschmierangproblem mit neueren Versuchsergebnissen. *Monatsbl. Berliner Bez. Ver. Dtsch. Ing*:125-128.

Hahn, H. W. (1957). Dynamically loaded journal bearing of finite length. *Conference on Lubrication and Wear Clut*.

Hamilton, D. B., C. M. Allen and J. A. Walowit. (1966a). A theory of lubrication by microirregularities. *ASME, TRANSACTIONS, SERIES D-JOURNAL OF BASIC ENGINEERING* 88:177-185.

Hamilton, D. B., J. A. Walowit and C. M. Allen. (1966b). A Theory of Lubrication by Microirregularities. *Transaction of the ASME, Journal of Basic Engineering, Series D*:177-185.

Hamilton, G. M. and S. L. Moore. (1974). Measurement of the oil-film thickness between the piston rings and liner of a small diesel engine (First Paper). *Proc. Instn Mech. Engrs* 188:253-261.

Hamrock, B. J., S. R. Schmid and B. O. Jacobson. (2004) *Fundamentals of Fluid Film Lubrication*. 2nd Edition. New York: Marcel Dekker Ltd.

Han, D. C. and J. S. Lee. (1998). Analysis of the piston ring lubrication with a new boundary condition. *Tribology International* 31(12):753-760.

Harigaya, Y., M. Ichinose and M. Suzuki. (1996). Effect of temperature on the lubrication characteristics between the piston ring and the cylinder liner of internal combustion engine. *The 1996 18th Annual Fall Technical Conference of the ASME Internal Combustion Engine Division. Part 2(of 5)*:17-24.

Haugland, R. P (1999) Molecular probes. In Handbook of Fluorescent Probes and Research Chemicals. 7th Edition.

Herbst, H. M. and H. H. Priebsch. (2000). Simulation of piston ring dynamics and their effect on oil consumption. *SAE transactions* 109(3):862-873.

Hoult, D. P., J. P. Lux, V.W. Wong and S. A Billian. (1988). Calibration of Laser Fluorescence Measurements of Lubricant Film Thickness in Engines. *SAE paper* 881587.

Hoult, D. P. and M. Takiguchi. (1991). Calibration of the laser fluorescence technique compared with quantum theory. *Tribology transactions* 34:440-444.

Inagaki, H., A. Saito, M. Murakami and T. Konomi. (1995). Development of two-dimensional oil film thickness distribution measuring system. *SAE paper* 952346.

Kim, S., A. Azetsu, M. Yamauchi and T. Someya. (1995). Dynamic Behavior of Oil Film between Piston Ring and Cylinder Liner: Visualization of Oil Film Rupture and Measurement of Oil Film Pressure Using Simulating Rig. *JSME international journal. Series C, Mechanical systems, machine elements and manufacturing* 38(4):783-789.

Klamann, D. and R. R. Rost. (1984) *Lubricants and Related Products: Synthesis, Properties, Applications, International Standards*: Verlag Chemie.

Kustas, F. M., J. N. Schwartzberg, S. H. Carpenter, C. R. Heiple and D. L. Armentrout. (1994). Acoustic emission monitoring of diamond-like carbon coating degradation during sliding wear. *Surf. Coat. Technol.(Switzerland)* 67(1):1-7.

Laurence, R. B., V. W. Wong and A. J. Brown. (1996). Effects of Lubrication System Parameters on Diesel Particulate Emission Characteristic. *SAE Transactions* 105(4):157-164.

Liskiewicz , T. W., A. Morina and A. Neville. (2008). Challenges in Lubricant Additives Technology. *The Triz Journal*.

Luengo, G. , J. Israelachvili and S. Granick. (1996). Generalized effects in confined fluids: New friction map for boundary lubrication. *Wear* 200(1):328-335.

Lux, J. P., D. P. Hoult and M. J. Olechowski. (1990). Lubricant film thickness measurements in a diesel engine piston ring zone. *Lubrication engineering* 47(5):353-364.

Masjuki, H. H., M. A. Maleque, A. Kubo and T. Nonaka. (1999). Palm oil and mineral oil based lubricants—their tribological and emission performance. *Tribology International* 32(6):305-314.

- Meyer, E. (1998) *Nanoscience: Friction and Rheology on the Nanometer Scale*: World Scientific Pub Co Inc.
- Miller, G.M. (1862). On a packing for Pistons of Steam Engines. *Proc Inst Mech. Engrs*.
- Moore, S. L. and G. M. Hamilton. (1978). The Starved Lubrication of Piston Rings in a Diesel Engine. *Journal Mechanical Science* 20(6):345-352.
- Moore, S.L and G. M. Hamilton. (1980). The piston ring at top dead centre. *Proceedings of the Institution of Mechanical Engineers* 194.
- Myers, J. E., G. L. Borman and P. S. Myers. (1990). Measurements of oil film thickness and liner temperature at top ring reversal in a diesel engine. *SAE transactions* 99:339-366.
- Nakashima, K., S. Ishihara and K. Urano. (1995). Influence of Piston Ring Gaps on Lubricating Oil Flow Into the Combustion Chamber. *SAE paper* 952546.
- Ostovar, P. (1996) "Fluid aspects of piston ring lubrication." PhD Thesis, Department of Mechanical Engineering: Imperial College of Science, Technology and Medicine. London.
- Parker, D. A., J. V. Stafford, M. Kendrick and N. A. Graham. (1975) Experimental measurements of the quantities necessary to predict piston ring-cylinder bore oil film thickness, and the oil film thickness itself, in two particular engines. In *Piston Ring Scuffing* conference:79-98. London, UK (Institute of Mechanical Engineers)
- Parks, J. E., J. S. Armfield, T. E. Barber, J. M. E. Storey and E. A. Wachter. (1998). In Situ Measurement of Fuel in the Cylinder Wall Oil Film of a Combustion Engine by LIF Spectroscopy. *Applied Spectroscopy* 52(1):112-118.
- Phen, R. V., D. Richardson and G. Borman. (1993). Measurements of Cylinder Liner Oil Film Thickness in a Motored Diesel Engine. *SAE Transactions Paper* 932789
- Pitts, E. and J. Greiller. (1961). The flow of thin liquid films between rollers. *Journal of Fluid Mechanics* 11(01):33-50.
- Priest, M., D. Dowson and C. M. Taylor. (2000). Theoretical modelling of cavitation in piston ring lubrication. *Proceedings of the Institution of Mechanical Engineers, Part C: Journal of Mechanical Engineering Science* 214(3):435-447.
- Priest, M. and C. M. Taylor. (2000). Automobile engine tribology-approaching the surface. *Wear* 241(2):193-203.

- Pyke, E. A. (2000) "Investigation of piston ring lubrication using laser induced fluorescence." PhD thesis, Department of Mechanical Engineering: Imperial College of Science, Technology and Medicine. London.
- Ramsbottom. (1854). On an improved Piston for steam Engines. *Proc Inst Mech. Engrs*:70-74.
- Ramsbottom. (1855). On the construction of Packing Rings for Piston. *Proc Inst Mech. Engrs*:206-208.
- Richardson, D. E. and G. L. Borman. (1992). Theoretical and experimental investigations of oil films for application to piston ring lubrication. SAE, WARRENDALE, PA(USA). 1992.
- Ruddy, B. L., D. Dowson and P. N. Economou. (1982). A review of studies of piston ring lubrication. *Proceedings of 9th Leeds-Lyon Symposium on Tribology: Tribology of Reciprocating Engines*:109-121.
- Sanda, S. (1998). Measurement of oil film thickness: The Fluorescence Method and Others. *Japanese Journal of Tribology* 43(7):893-902.
- Sanda, S., A. Saito, T. Konomi and H. Nohira. (1993). Development of Scanning Laser-Induced-Fluorescence Method for Analyzing Piston Oil Film Behavior. *Proceedings of IMechE, C* 465:155-164.
- Sanda, S. and T. Someya. (1987) The Effect of Surface Roughness on Lubrication Between a Piston Ring and a Cylinder Liner. In *Tribology - Friction, Lubrication and Wear: Fifty Years On* 1:135-143. (Proceedings of the Institution of Mechanical Engineers, International Conference)
- Savage, M. D. (1977). Cavitation in lubrication. Part 1. On boundary conditions and cavity—fluid interfaces. *Journal of Fluid Mechanics* 80(04):743-755.
- Sawicki, J. T. and T. V. Rao. (2004). Cavitation Effects on the Stability of a Submerged Journal Bearing. *The International Journal of Rotating Machinery* 10(3):227-232.
- Schiemann, L. F., C. A. Andrews, V. A. Carrick and B. K. Humphrey. (1995). Developing Heavy Duty Diesel Lubricants to meet the extended Service Interval Challenge. *SAE Paper SP-1121*:159-172.
- Seki, T., K. Nakayama, T. Yamada, A. Yoshida and M. Takiguchi. (2000). A study on variation in oil film thickness of a piston ring package: variation of oil film thickness in piston sliding direction. *Journal of Society of Automotive Engineers of Japan* 21(3):315-320.

- Shaw, B. T., D. P. Hoult and V. W. Wong. (1992). Development of Engine Lubricant Film Thickness Diagnostics Using Fiber Optics and Laser Fluorescence. *SAE paper* 920651.
- Shenghua, L., L. Jijun, A. Longbao and W. Rong. (1996). An Experimental Investigation of the Oil Film Lubricating Piston Rings. *SAE Transactions* 961912:32-37.
- Sherrington, I. and E. H. Smith. (1985). Experimental methods for measuring the oil-film thickness between the piston-rings and cylinder-wall of internal combustion engines. *Tribology International* 18(6):315-320.
- Sherrington, I. and S. Söchting. (2006) An experimental study of variability in the thickness of the hydrodynamic lubricant film between the piston-rings and cylinder bore of an internal combustion engine under steady operating conditions. In *Tribology 2006: Surface Engineering and Tribology for Future Engines and Drivelines* London, UK (Institute of Mechanical Engineers)
- Shuster, M., D. Combs, K. Karrip and D. Burke. (2000). Piston Ring Cylinder Liner Scuffing Phenomenon Studies Using Acoustic Emission Technique. *SAE Transactions*.
- Skinner, S. (1903). On the Occurrence of Cavitation in Lubrication. *Proceedings of the Physical Society of London* 19:73-81.
- Smart, A. E. and R. A. J. Ford. (1974). Measurement of Thin Liquid Films by a Fluorescence Technique. *Wear* 29(1):41-47.
- Stachowiak, G. and A. W. Batchelor. (2000) *Engineering Tribology*: Butterworth-Heinemann.
- Stieber, W. (1933). Das Schwimmlager. *Ver. Dtsch. Ing.*
- Sun, J., R.J.K. Wood, Wang. L., I. Care and H.E.G. Powrie. (2006) Wear monitoring of lubricated sliding contacts by acoustic emission and electrostatic technologies. In *Tribology 2006: Surface Engineering and Tribology for Future Engines and Drivelines* London, UK (Institute of Mechanical Engineers)
- Swales, P. D. (1974) A review of cavitation phenomena in engineering situations. In *Tribology, Cavitation and Related Phenomena in Lubrication, Proceedings of the 1st Leeds-Lyon Symposium* (Eds. D. Dowson, M. Godet and C. M. Taylor) Paper 1(i):3-9. The University of Leeds, England (Institute of Mechanical Engineers)
- Swift, H. W. (1932). The Stability of Lubricating Film in Journal Bearings. *Proceedings Institute Civil Engineers (London)* 233:267-288.

- Takiguchi, M., K. Nakayama, S. Furuhashi and H. Yoshida. (1998). Variation of Piston Ring Oil Film Thickness in An Internal Combustion Engine--Comparison Between Thrust and Anti-Thrust Sides. *SAE Transactions* 107(3):816-824.
- Takiguchi, M., R. Sasaki, I. Takahashi, F. Ishibashi, S. Furuhashi, R. Kai and M. Sato. (2000) Oil Film Thickness Measurement and Analysis of a Three Ring Pack in An Operating Diesel Engine. In *Advances in Powertrain Tribology 2000* (CEC/SAE)
- Taylor, G. I. (1963). Cavitation of a viscous fluid in narrow passages. *Journal of Fluid Mechanics Digital Archive* 16(04):595-619.
- Thirouard, B. (2001) "Characterization and modeling of the fundamental aspects of oil transport in the piston ring pack of internal combustion engines." PhD Thesis, Department of Mechanical Engineering: Massachusetts Institute of Technology, Massachusetts, Cambridge.
- Thirouard, B. P., T. Tian and D. P. Hart. (1998). Investigation of Oil Transport Mechanisms in the Piston Ring Pack of a Single-Cylinder Diesel Engine, Using Two-Dimensional, Laser-Induced Fluorescence. *SAE paper* 982658.
- Tian, T., L. B. Noordzij, V. W. Wong and J. B. Heywood. (1996). Modeling piston-ring dynamics, blowby, and ring-twist effects. *The 1996 18 th Annual Fall Technical Conference of the ASME Internal Combustion Engine Division. Part 2(of 5)* 2:67-80.
- Tian, T. and V. W. Wong. (2000). Modeling the lubrication, dynamics, and effects of piston dynamic tilt of twin-land oil control rings in internal combustion engines. *Journal of Engineering for Gas Turbines and Power (Transactions of the ASME)* 122:119-131.
- Tian, T., V. W. Wong and J. B. Heywood. (1998). Modeling the dynamics and lubrication of three piece oil control rings in internal combustion engines. *SAE transactions* 107(4):1989-2006.
- Ting, L. L. (1993a). Development of a Reciprocating Test Rig for Tribological Studies of Piston Engine Moving Components--Part II: Measurement of Piston Ring Friction Coefficients and Rig Test Confirmation. *SAE paper* 930686.
- Ting, L. L. (1993b). Development of a Reciprocating Test Rig for Tribological Studies of Piston Engine Moving Components - Part I: Rig Design and Piston Ring Friction Coefficients Measuring Method. *SAE paper* 930685.
- Van Dam, W. and W.M. Klelser. (1995). Lubricant Related Factors Controlling Oil Consumption in Diesel Engines. *SAE paper* 952547.
- Vijay, H. and V. H. Arakeri. (1973). Viscous effects on the position of cavitation separation from smooth bodies. *J Fluid Mech* 68(4):779-799.

- Wakuri, Y, S Ono, M Soejima and N Noguchi. (1979). Oil-film behaviour of reciprocating slider with circular profile (Observation of film by means by thin film interferometry). *Bulletin of JSME* 22(167):755-762.
- Wakuri, Y., S. Ono, M. Soejima and K. Masuda. (1981). Oil-film Behaviour of Reciprocating Slider with Circular Profile: Optical Measurement of Oil-film Separation Boundary. *Bulletin of JSME* 24(194):1462-1469.
- Wakuri, Y., M. Soejima, Y. Ejima, T. Hamatake and T. Kitahara. (1995). Studies on Friction Characteristics of Reciprocating Engine. *SAE transactions* 104(4):1463-1477.
- Washio, S., S. Takahashi and S. Yoshimori. (2003). Study on cavitation starting at the point of separation on a smooth wall in hydraulic oil flow. *Proceedings of the Institution of Mechanical Engineers, Part C: Journal of Mechanical Engineering Science* 217(6):619-630.
- Wing, R. D. and O. A. Saunders. (1972). Oil film temperature and thickness measurements on the piston rings of a diesel engine. *Proc. Instn Mech. Engrs* 186:1-9.
- Wong, V. W. and D. P. Hoult. (1991). Experimental Survey of Lubricant-Film Characteristics and Oil Consumption in a Small Diesel Engine. *SAE paper* 910741.
- Wong, V.W., S.M. Casey and G Tamai. (1999) Lubricant film characteristics in power cylinder and dependence on location, oil properties, and engine operation conditions. In *Proceedings of the 15th International Combustion Engine Symposium (International)* 30:161-166. Seoul, Korea (SAE International)
- Woods, H.A. and H.M. Trowbridge. (1955). Shell Roll Test for Evaluating Mechanical Stability. *NLGI Spokesman* 19:26-27 and 30-31.
- Yilmaz, E., T. Tian, V. Wong and J. B. Heywood. (2004). The contribution of different oil consumption sources to total oil consumption in a spark ignition engine. *S A E Transactions* 2004-01-2909.
- Yu, S. and K. Min. (2002). Effects of the oil and liquid fuel film on hydrocarbon emissions in spark ignition engines. *Proceedings of the Institution of Mechanical Engineers, Part D: Journal of Automobile Engineering* 216(9):759-771.

APPENDIX: THEORY OF FLUORESCENCE

To estimate the intensity of the emitted fluorescence, the amount of photons absorbed must be evaluated first. The Beer-Lambert law expresses the amount of transmitted light as a function of the absorbing medium thickness.

$$I_a = I_o(1 - 10^{-\epsilon x h}) \quad (1)$$

where I_a is the intensity of the absorbed light, I_o the intensity of the incident light source, ϵ the molar absorptivity, h the path length (lubricant film thickness) and x the molar concentration of the fluorescing species. Both the molar absorptivity and the molar concentration of the fluorescing species may vary with temperature and also with the lubricant composition, which changes in the top ring zone due to lubricant degradation by the extreme conditions associated with combustion.

The quantum yield of fluorescence (Φ_L) is defined as the ratio of quanta emitted to absorbed and is normally less than 100% ($0 \leq \Phi_L \leq 1$). The spectral fluorescence power yield P_{VL} over a frequency band $\nu + d\nu$ is defined as the ratio of the radiant power of fluorescence, measured over that frequency interval, to the radiant power of absorbed

energy, i.e. $P_{VL} = \frac{\Phi_{VL}}{\Phi_A} \quad (2)$

The fluorescence power yield will normally decrease with an increase in the excitation frequency as a greater fraction of the absorbed energy will be converted to heat.

Because internal conversion is much more likely than emission directly from electronic states higher than the lowest one, fluorescence emission typically occurs from the singlet excited state S^* . This is the reason why fluorescence quantum yield is related to absorption and emission from the first excited state and strongly depends on the number of molecules with fluorescent properties (fluorophores). The fluorescence quantum efficiency is thus defined as the ratio of fluorescent radiant power to the absorbed radiant power:

$$\phi_F = \frac{\Phi_F}{\Phi_A} \quad (3)$$

The rate of change of the number of molecules populating the first excited singlet state can be expressed by the following equation:

$$\frac{dn_{S_1}}{dt} = k_A n_{S_0} - (k_F + k_{NR}) n_{S_1} \quad (4)$$

where n_{S_0} and n_{S_1} are the densities of the ground and first excited state in molecules/mm³ and k_A , k_F and k_{NR} are constants of absorption, fluorescence and non radiative deactivation respectively. If a sample of a fluorophore is irradiated with light of constant intensity, a steady state population of the first excited singlet state will be achieved almost instantaneously. Applying this condition to the above equation gives

$$n_{S_1} = \frac{k_A n_{S_0}}{k_F + k_{NR}} \quad (5)$$

This population density of the first excited state is directly proportional to the rate of absorption and fluorescence emission can be expressed by:

$$\Phi_A = k_A n_{S_0} V \quad (6)$$

$$\Phi_F = k_F n_{S_1} V \quad (7)$$

Where V is a sample volume. In the case of the multi-mode fibre-optic probes mounted inside the cylinder liner, this volume is equal to the volume of the frustum of the cone formed by the 50 μm core of the fibre, the circular area on a piston ring or the piston itself illuminated by the laser beam diverging from the fibre and the side surface of the truncated cone at an angle equal to the fibre acceptance angle. The fibre acceptance angle is defined as:

$$A_{\max} = \arcsin\left(\frac{NA}{n_o}\right) \quad (8)$$

where NA the numerical aperture of the fibre and n_o is the refractive index of the external medium-the lubricant present between the cylinder wall and the piston and piston rings. Combining equations 3, 5, 6 and 7 gives another expression of the fluorescence efficiency:

$$\Phi_F = \frac{k_F}{k_F + k_{NR}} \quad (9)$$

which shows the effect of non-radiative deactivation of fluorescence quantum yield. Using this equation together with the substitution of equation 5 for the density n_{s_1} in equation 7 results in the following expression for fluorescence emission

$$\Phi_F = n_{s_0} k_A \phi_F V \quad (10)$$

The above expression shows that fluorescence intensity is a function of the density of the fluorescence species present in the ground electronic state, the coefficient of absorption, the fluorescence quantum yield and the volume of a sample. Assuming that the lubricant present inside the cone of laser light between the tip of the fibre and the piston is continuously replenished and the rate of absorption is the same, the intensity of the emitted fluorescence is proportional to the thickness of the oil film. The volume of the frustum of a cone of oil is not a linear function of the oil film thickness, but, due to the divergent laser beam, it is governed by a cubic relationship.

The fluorescent quantum yield of engine oils is predominantly caused by the presence of polycyclic aromatic hydrocarbons (PAH). The intense fluorescence of these molecules is attributed to the low energy levels of their excited singlet state. Because PAH's require a relatively small amount of absorbed energy for the electronic transitions to occur, the rate of band disruption is low. High excitation energy is one of the reasons for bond rupturing occurring after absorption (dissociation) causing fluorescence quenching.

Environmental factors such as temperature can bring about significant changes in the viscosity of engine oils and their fluorescence spectra. The main condition for fluorescence to occur is the stability of the excited electronic state. In liquid oils, where the probability of collisional quenching is high, an increase of temperature will normally disturb the stability of molecules in the excited state and will have a marked effect on the characteristics of fluorescence emission. A higher temperature of the fluorophore encourages conversion to the triplet state or other energy transfer reactions in which electrons from non-fluorescent molecules fill the ground electronic state thus blocking the return of the original electron whose energy, in turn, is deactivated through a radiationless transition such as dynamic quenching. Aromatic hydrocarbons present in engine oils will normally undergo increased dynamic quenching with increasing temperature, or decreasing viscosity. These intermolecular quenching mechanisms are

controlled by the rate of diffusion in the oil and thus the fluorescence quantum yield will depend on viscosity and temperature.

As a consequence, increasing the temperature decreases fluorescence emission. This statement, however, is a very general one as there might exist circumstances in which the effect of temperature could be found to be quite the opposite; increased temperature could bring about increased molecular fluorescence quantum yield. The specific conditions under which such phenomena could take place are related to both the type of fluorescent oil molecules populating the ground electronic state and the configuration of the experimental apparatus used for quantitative fluorescence studies. Amongst the possible circumstances conducive to increasing the fluorescence emission of engine oils with increasing temperature are:

- Dimmer formation
- Indirect excitation
- Spectral shift

The complex mixture of molecules in engine oils will almost certainly undergo dimerization. Dimers can be defined as molecular structures of two similar molecules combined by forces other than chemical bonds (electrostatic interactions, van der Waals bonding enhanced by electronic transitions) or very weak chemical bonds, such as hydrogen bonds. Dimers can be formed between one molecule in the ground electronic state and another molecule in an excited state. Since the excitation energy is always divided equally between the two molecules forming a dimer, dimerization will lead to deactivation of the absorbed energy through internal conversion and reduction of fluorescence quantum yield. With the increase in temperature, the level of dimer formation will be lower and, thus, dynamic quenching of fluorescence reduces. Disrupted dimer formation by increased diffusion at elevated temperatures results in monomer fluorescence of higher intensity.

In the process of indirect excitation, the reverse singlet transition is brought about by thermal energy. The temperature assisted populating of the first electronic excited state can give rise to delayed fluorescence.

The receiving optics of the LIF experimental system could also be held responsible for detecting a higher level of fluorescence intensity with increasing temperature of engine oils. A slight increase in the fluorescence signal could occur. This apparent increase may not necessarily be the result of higher fluorescent intensity, but may simply be the result of a spectral shift of the fluorescence peak. The phenomenon of blue shift in the fluorescence emission maxima could occur with an increase in temperature. The phenomenon can be associated with a Franck-Condon excited state at lower temperatures. This effect, however, could be compensated for either by the bandwidth of the interference filter or by employing a monochromator in the receiving optics of the LIF system.